Closed-Loop Regulation of Internal Brain States using Wearable Brain Machine Interface Architectures with Real-World Experimental Implementation

by
Hamid Fekri Azgomi

A dissertation submitted to the Department of Electrical and Computer Engineering,

Cullen College of Engineering

in partial fulfillment of the requirements for the degree of

Doctor of Philosophy
in Electrical Engineering

Chair of Committee: Rose T. Faghih, PhD

Committee Member: Jose Luis Contreras-Vidal, PhD

Committee Member: Joe Francis, PhD

Committee Member: David Mayerich, PhD

Committee Member: Marzia Cescon, PhD

University of Houston
December 2021

DEDICATION/EPIGRAPH

This dissertation is lovingly dedicated to the beautiful soul of my mom, Mahnaz Khodaverdi. Thank you for always believing in me. I love you Maman!

Hamid Fekri Azgomi

December 2021

ACKNOWLEDGMENTS

I would love to express my sincere gratitude to my advisor, Dr. Rose Faghih for providing me with the opportunity to conduct my dissertation under her supervision. This dissertation would not have been possible without her guidance, expertise, enthusiastic encouragement, patience, and valuable feedback. Dr. Faghih has been extremely supportive, understanding, and a great source of inspiration. I would like to also thank our collaborators, Dr. Jin-Oh Hahn and Dr. Iahn Cajigas for their valuable advice and feedback. I would like to also thank the committee members, Dr. Jose Luis Contreras-Vidal, Dr. Joe Francis, Dr. David Mayerich, and Dr. Marzia Cescon for their time, guidance, and insightful feedback.

I would also like to acknowledge the support given by my lab mates at computational medicine lab; Dilranjan Wickramasuriya, Md. Rafiul Amin, Anan Yaghmour, Michelle Patrick-Krueger, Samiul Alam, Srinidhi Parshi, Divesh Pednekar, Luciano Branco, Sankalp Parekh, Saman Khazaei, Jon Genty, and Samantha Havens. I enjoyed every moment of working with you and learned a lot from all of you.

I would like to thank my parents, Mahnaz and Iraj, for their support, patience and encouraging me to pursue my dream. To my siblings, I am truly grateful for having all in my life. You have always been the source of love and fun in my entire life. Thank you for always extending your helpful hands when I needed. I also feel very fortunate to have lots of friends to whom I know I can count on.

Above all I would like to thank my lovely wife, Mojdeh, for her love and constant support, for all the late nights and early mornings, and for keeping me sane over the past few months. Thank you for being my inspiration and motivation through my study. But most of all, thank you for being my best friend.

ABSTRACT

The brain is a control system with a strong impact on all human functions. Inspired by the recent advances in wearable technologies, we design wearable-machine interface (WMI) architectures for controlling brain responses. The WMI architecture encompasses collecting physiological data using wearable devices, inferring neural stimuli underlying pulsatile signals, estimating an unobserved state based on the underlying stimuli, designing the control, and closing the loop. In this thesis, we design WMI architectures for regulating human's cognitive stress state and controlling energy levels in patients with hypercortisolism.

Hypercortisolism, which corresponds to the excessive levels of cortisol hormone, is associated with tiredness and fatigue during the day and disturbed sleep at night. Automating the use of medications that are effective by either elevating or lowering the energy levels might help patients with hypercortisolism to experience more balanced energy cycles required for their daily activities and better sleep patterns at night. Keeping cognitive stress at a healthy range can improve the overall quality of life by helping the subjects to decrease their high levels of arousal to relax them and elevate their low levels of arousal to increase the engagement. Skin conductance data provides us with valuable information regarding one's cognitive stress-related state. We propose to use this physiological data collected via wearable devices to infer individuals' arousal state.

In the first part of this research, we simulate multi-day cortisol profile data for multiple subjects both in healthy conditions and with Cushing's disease. Then, we present a state-space model to relate an internal hidden cognitive energy state to subject's cortisol secretion patterns. Particularly, we consider circadian upper and lower bound envelopes on cortisol levels, and timings of hypothalamic pulsatile activity underlying cortisol secretions as continuous and binary observations, respectively. By estimating the hidden energy state and incorporating the simulated hypothetical medication dynamics, we design a knowledge-based control system and close the loop. In the second part of this research, we design a simulation environment to control a cognitive stress-related state in a closed-loop manner. Hence, using the state-space approach, we relate internal cognitive stress state to the changes in skin conductance. Then, we estimate the hidden stress state and close

the loop by designing a fuzzy controller. Next, we propose supervised control architectures to enhance the closed-loop performance in cognitive stress regulation. To further enhance the closed-loop design, we consider adaptive and robust control systems to handle model uncertainty and additional disturbance input.

Finally, we design and perform multiple human-subject experiments to further explore safe actuation to regulate internal hidden brain states in real-world. In these novel experiments, we employ wearable technologies and publish data sets that could be further investigated to model the dynamics of proposed safe actuation. These studies are the first steps toward the goal of treating similar mental and hormone-related disorders in real-world situations. Analyzing the human subjects' responses to the effective safe actuation would further enhance the efficiency of proposed approaches and lead us to a practical automated personalized closed-loop architecture.

Table of Contents

List of Tables

List of Figures

1 Introduction

1.1 Motivation and Objective

The brain is a complex control system with a strong impact on all human functions, such as adjusting autonomic nervous system and hormone-release patterns in response to internal or external stimuli. In recent years, stress-related health issues and hormone-related diseases have attracted massive attention [1, 2, 3, 4, 5, 6, 7]. According to the American Institute of Stress, 77% of individuals experience high levels of stress that affects their physical health and 73% suffer from stress that influences their mental health [8]. Despite recent advances in technology, handling cognitive stress-related disorders is still a major problem around the globe and impacts quality of life in general [9]. Furthermore, any dysregulation in hormonal release could also affect the individuals in multiple ways. For instance, abnormal secretion of cortisol, which is a glucocorticoid hormone and isreleased in a pulsatile manner, can lead to irregular daily energy patterns such as feeling fatigued, mood irregularities, and sleep disorders [10, 11]. While there have been growing advances in medical fields, there still exist gaps for mental health enhancement and addressing hormone-related disorders [12, 13].

In this dissertation, inspired by the recent advances in wearable technologies, we propose wearable machine interface (WMI) architectures. Hence, we design closed-loop WMI architectures for controlling brain responses. As presented in Figure 1, the WMI architecture encompasses collecting physiological data using wearable devices, inferring neural stimuli underlying pulsatile signals, estimating an unobserved state based on the underlying stimuli, designing the control, and closing the loop in real-time. To close the loop, we propose to use safe actuation such as hypothetical medication, listening to music, drinking beverages, or smelling fragrances (Figure 1). Compared to the existing open-loop approaches, which aim to employ actuation without any feedback from the human body, we propose to regulate internal states by monitoring physiological measurements that could be collected using wearable devices [5, 6]. In this dissertation, we aim to employ WMI architectures to (1) build a novel architecture for energy management in patients with hypercortisolism and

(2) investigate different approaches for internal cognitive stress state regulation.

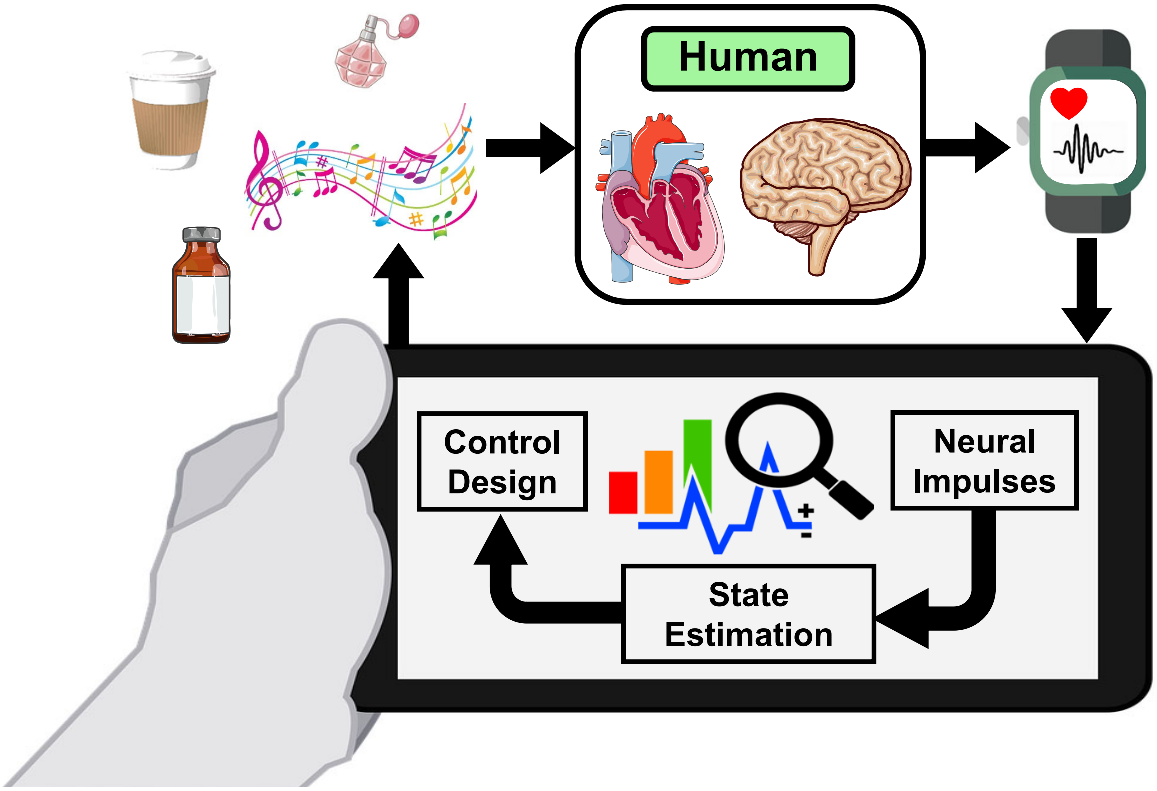

Figure 1: **Overview of wearable machine interface architectures.**

1.2 Prior Studies and Existing Challenges

Hypercortisolism, or Cushing's disease, which corresponds to the excessive levels of cortisol hormone, is associated with fatigue during the day and disturbed sleep at night [14]. Cushing's disease is a rare disorder and affects individuals between 25 to 40 years old. It also targets females five times more frequently than males [15]. While the initial treatment option for Cushing's disease is a surgery with a 78% success rate, evidence shows that relapse happens in almost 13% of patients [16]. For the patients in whom the surgery is not successful or feasible, medical therapy is unavoidable [17]. As patients with hypercortisolism suffer from lack of energy for their daily life and balanced sleep cycles at night [18], we propose a closed-loop architecture to automate medications' intake effective in regulating energy state. While the proposed approach is one of the very first to manage energy imbalance in patients with cortisol-related disorders, real implementation needs further advancement in wearable technologies to monitor cortisol levels in real-time. To further explore real-world implementation of the proposed WMI architectures, we intend to handle internal cognitive stress in a closed-loop manner.

Keeping cognitive stress at a healthy range can improve the overall quality of life: helping subjects to decrease their high levels of arousal, which will make them relaxed, and elevate their low levels of arousal, which could increase their engagement. Experiencing high levels of cognitive stress while performing routines, or low cognitive engagement with the environment, may seriously affect an individual's life [19]. While there exist methods for managing stress, there is still a lack of reliable systems that continuously track the stress levels in individuals and automatically regulate them by suggesting appropriate safe solutions during daily activities [20, 21]. To this end, we propose a novel architecture to infer internal stress state by monitoring electrodermal activity. Next, we design and implement multiple control algorithms to close the loop. We then propose novel supervised control architectures to combine knowledge-based and model-based control techniques to regulate the internal arousal state in a more efficient way. Considering model uncertainty in the model dynamics and additional disturbance input caused by potential inter- and intra-subject variations, we also design adaptive and robust control systems.

To implement the proposed WMI architectures in real-world, we design and perform multiple human-subject experiments to further investigate effects of potential safe actuation for closing the loop. To this end, we propose to employ safe actuation such as listening to music, drinking coffee, smelling fragrances, and diaphragmatic breathing to regulate internal brain states. We perform three sets of closed-loop human-subject experiments. In experiment 1, we aim to analyze the effectiveness of listening to different kinds of music while under cognitive load. In experiment 2, we propose to explore the effects of drinking coffee and smelling fragrances as safe actuation in closing the loop. We hypothesize that taking this actuation would influence the cognitive stress state and affect the cognitive performance. In experiment 3, we design procedures to expose the subjects with an existing degree of acrophobia to face their fear conditioning. To investigate how safe actuation would affect their fear, we propose to use music and diaphragmatic breathing to close the loop. To measure changes in cognitive arousal, we employ wearable devices. The collected data further validates our hypothesis in including these safe actuation while utilizing WMI architectures and closing the loop in a real-world setting. Investigating the effects of the proposed actuation in individuals' responses would further enable us to model their dynamics and incorporate them while closing the loop.

1.3 Thesis Outline

In this research, we employ WMI architectures in closed-loop brain state regulation. This thesis is conducted in five chapters:

- Chapter 2 is dedicated to regulating energy state in patients with hypercortisolism and designing a closed-loop control system for automating hypothetical medications.
- Chapter 3 is focused on establishing a simulation system based on experimental data for exploring control systems techniques in closing the loop and regulating internal brain cognitive stress-related state.
- Chapter 4 addresses developing supervised control architectures in enhancing the performance of the closed-loop cognitive stress regulation.
- Chapter 5 is arranged to design adaptive and robust control systems to consider model uncertainty and additional disturbance input while modeling cognitive stress state.
- In chapter 6, we present our novel human-subject experiments to further explore the effects of safe actuation in closed-loop brain state regulation in real-world.

1.4 Scientific Significance

These studies are the first steps toward the ultimate goal of treating similar mental and hormone-related disorders in real-world situations. This thesis includes transformative system-theoretic toolsets for regulating brain internal states in a personalized framework that is robust and adaptive to the inter- and intra-subject variabilities. Results of this research produce control-theoretic tools for different physiological observations. While the initial focus is on two aspects of brain function, namely internal arousal and energy states, the proposed architectures open up the opportunity to investigate broader questions in computational neuroscience. In a similar manner, one may explore other physiological signals that correspond to different diseases or malfunctions and track the latent state(s) that could not be measured directly. Consequently, the proposed architectures could be further expanded to close the loop and regulate other hidden brain state(s).

2 Closed-loop Energy Regulation in Patients with Hypercortisolism

2.1 An Overview of Closed-Loop Energy Regulation by Monitoring Cortisol Data

The cortisol hormone is the main stress hormone in an individual's body which is secreted in a pulsatile process [5, 22, 23, 24]. Cortisol secretion patterns, which are mainly controlled by the hypothalamus, are critical in assessing various functionalities such as regulating blood pressure and adjusting blood glucose levels. So, investigating changes in cortisol secretion would shed some light on one's internal energy state variations [22, 23, 25]. Adrenocorticotrophic hormone (ACTH) (i.e. a tropic hormone) causes the adrenal cortex to release cortisol in a pulsatile manner [26, 10, 27]. The hypothalamus employs corticotrophin-releasing hormone (CRH) to stimulate the anterior pituitary to produce ACTH [28, 29]. Any irregular patterns in cortisol secretions (e.g. too much cortisol release, which is called hypercortisolism, or not providing a sufficient amount of cortisol, which is called hypocortisolism) may cause the imbalance in internal energy variations [30, 31, 32]. These irregularities, which are common among the Cushing's patients who are exposed to the hypercortisolism, lead them to feel fatigue during the daytime and sleep problems at night [33, 34]. Insufficient release of cortisol early in the morning may result in feeling fatigue during the day. On the other hand, high levels of cortisol in the evening might cause sleep disturbances at night [35].

While the initial treatment option for Cushing's disease is a surgery with a 78% success rate, evidence shows that the relapse happens in almost 13% of patients [16]. For the patients in whom the surgery is not successful or feasible, medical therapy is unavoidable [17]. Due to recent advances in employing novel compounds that can regulate cortisol secretions, medical therapy has attracted more attention [36]. Nowadays, medical therapy

Chapter two was first presented in part at the proceedings of the 2019 Asilomar Conference on Signals, Systems, and Computers [5]. Chapter two has been mainly adopted from Fekri Azgomi, Hamid, Jin-Oh Hahn, and Rose T. Faghih. "Closed-Loop Fuzzy Energy Regulation in Patients With Hypercortisolism via Inhibitory and Excitatory Intermittent Actuation." Frontiers in Neuroscience (2021): 909 [4].

is being suggested in different ways: pre-surgical treatment, post-surgical options for the patients that fail the surgical option, and the primary remedy for those in whom the surgery is not considered as an option [17].

The clinical observations in Cushing's syndrome patients clearly demonstrate a role for the HPA axis in the regulation of energy balance [37, 38, 23]. While there exist multiple factors to understand one's energy variations, there is not any specific method to directly infer internal energy state. Hence, it is not possible to present the evidence to show the correlation between energy state and cortisol variations. However, there is evidence that patients with irregular cortisol patterns experience fatigue during day time and disturbed sleep cycles at night. For example, authors in [27, 10] have shown that the patients with fibromyalgia syndrome, which is also associated with the irregular patterns in cortisol secretions, experience fatigue during the day and sleep disorders at night. Researchers in [39] identified lower cortisol levels in the patients with chronic fatigue syndrome. This evidence verifies the potential correlation between cortisol measurements and internal energy state.

As it is discussed, patients with Cushing's syndrome have disturbed circadian rhythm in their sleep cycles. In this regard, medications with inhibitory effects to lower the energy state and help the subjects with more balanced sleep cycles could be helpful. An example of these types of medications could be Melatonin. In the literature, it has been indicated that excessive cortisol secretions associated with Cushing's disease may lead to an irregular Melatonin rhythm [40, 41]. So, taking the advantages of Melatonin in improving sleep cycles, we can suggest using this medication for inhibitory effects. Although patients with hypercortisolism usually experience high levels of energy during the evening, they may suffer a lack of sufficient energy levels during the daytime [10, 27]. As a result, the need for medications to elevate the energy levels is unavoidable. Medications with excitatory effects to enhance energy state and prevent the subjects to feel fatigue during the daytime would be helpful in this regard. An example of these types of medications could be Methylphenidate. As patients with hypercortisolism suffer from not having enough energy levels in the daytime, medications like Methylphenidate could be suggested while implementing the proposed approach in the real world. In literature, it has been validated that taking two doses of Methylphenidate is significantly effective in relieving fatigue [42, 43].

Due to the potential medications' side-effects, tolerance, and resistance that a person shows against the use of specific medications, it is highly important to establish a supervision layer that enables automated regulation of medication usage [44]. We propose our approach by taking the advantages of wearable-type devices capable of monitoring blood cortisol in a non-invasive way as a feedback modality for such supervision. The proposed approach is the first attempt to automate the regulation of medications required to manage the energy levels in patients with hypercortisolism in a closed-loop manner.

Recently, there has been an increased interest in employing control theory in advancing modern medication therapies such as goal-directed fluid therapy [45], cardiopulmonary management [46], fluid resuscitation [47], and medically induced coma [48, 49]. In a similar way, and considering how irregular cortisol secretion patterns affect energy state in patients with hypercortisolism, we leverage control theory in regulating energy variations in these patients. While there exist medications effective in managing energy levels, there is still a lack of closed-loop and automated architecture for making the decisions on the time and dosage of the medications in real-time. Hence, we construct a virtual patient environment based on the experimental cortisol data for further analysis. Then, we design the control algorithm that can determine the time and dosage of hypothetical simulated medications in a real-time automated fashion.

As someone's energy variations are influenced by changes in their cortisol levels, the objective of this research is to regulate the energy state by monitoring the cortisol secretion patterns. To model the internal energy state and relate it to the cortisol variations, we utilize the state-space model presented in [23]. To close the loop, we simulate hypothetical medication dynamics and develop a control system. In the present simulation study, we apply hypothetical medication dynamics as the actuation in a real-time closed-loop brain machine interface architecture [5, 6]. As presented in Figure 1, a wearable device measures the cortisol data in a non-invasive manner. We infer the CRH secretion times via a deconvolution algorithm [10, 27, 29, 28, 50, 51, 52, 53]. We use the state-space approach [23, 54] to link the CRH secretion times, which cause the fluctuations in cortisol levels [5, 23, 55, 56], to the internal energy state. This state-space representation tracks the internal energy state continuously and provides the capability of utilizing the control systems theory to close the loop. To estimate the hidden cognitive energy-related state in real-time, we employ Bayesian filtering method [23]. By incorporating hypothetical dynamical system model of medications effective in both decreasing and increasing energy levels [42, 41], and designing a fuzzy controller, we close the loop to regulate the energy state in patients with hypercortisolism in a simulation environment.

In section 2.2, we explain the steps required for creating the virtual patient environment. We also discuss the state-space model along with the real-time estimation process. We then incorporate the hypothetical medication dynamics and propose a knowledge-based control system to close the loop in real-time. In Section 2.3, we present the outcome of implementing the proposed approach in regulating the energy state in patients with hypercortisolism. More particularly, we present the results on two classes of patients: (1) who do not have the circadian rhythm in their cortisol profiles, and (2) who have the circadian rhythm in their cortisol profiles. The final results demonstrate that our proposed real-time architecture can not only track one's energy state, but also regulate the energy variations in patients with hypercortisolism utilizing the simulated medication dynamics. Section 2.4 points out the implications of our findings. This simulation study based on the experimental data is the first step toward treating other hormone-related disorders.

2.2 Methodologies

Figure 2 illustrates an overview of the proposed closed-loop architecture. The present study consists of two main parts: the offline process and the real-time closed-loop simulation environment. In the offline part, we first generate multi-day cortisol data for multiple

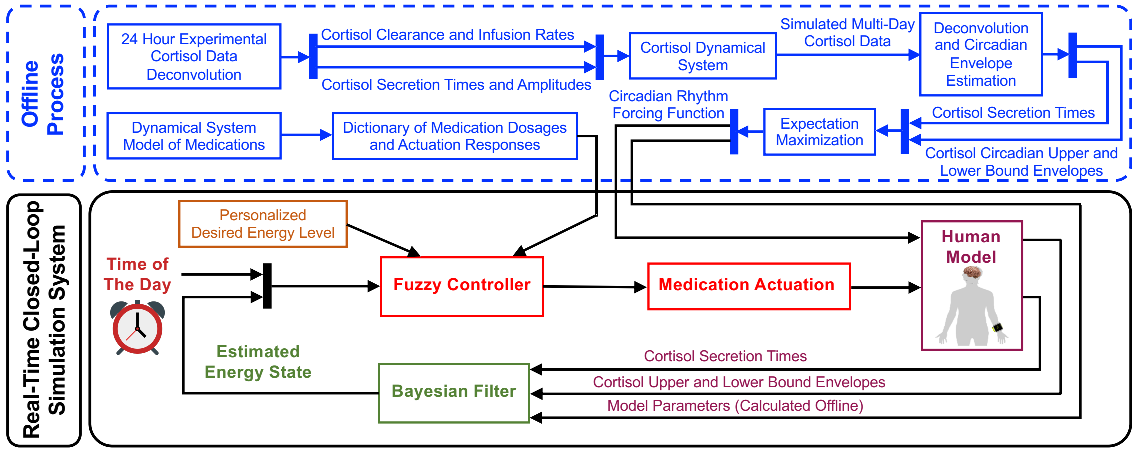

Figure 2: **Overview of closed-loop energy regulation.**

subjects based on their experimental data collected over 24 hours. Although there are recent advances in monitoring cortisol levels using wearable devices [57, 58, 59], there is still a lack of technologies for real-time multi-day cortisol data collection. Hence, to design a virtual patient environment, we first follow the results from [23, 54, 60] to simulate cortisol profiles in both healthy subjects and Cushing's patients. To extend our preliminary results presented in [5], we simulate data for ten subjects [29]. This offline process enables us to examine the performance of the proposed architecture in multiple cases. By performing deconvolution algorithm, we infer the cortisol secretion times and the circadian upper and lower envelopes. Utilizing Expectation Maximization (EM) approach, we estimate the circadian rhythm forcing function along with model parameters. In the offline stage, we also model dynamical systems for hypothetical medications with both inhibitory (i.e. medications to lower the cortisol levels) and excitatory (i.e. medications to elevate the cortisol levels) effects.

As depicted in the bottom section of Figure 2, we take the circadian rhythm forcing function in the real-time simulation system and relate the internal energy state to the cortisol secretion times and cortisol upper and lower bound envelopes using the state-space approach. Employing the Bayesian filtering, which uses the estimated model parameters calculated with the offline EM algorithm, we estimate the hidden energy-related state in real-time. Incorporating the dynamical system model of medications and the personalized desired levels of energy, we design a fuzzy controller to close the loop. The deigned control system will take the energy state estimate and determine the time and dosage of each medication as the actuation in the loop. Hence, it controls cortisol variations which will result in energy regulation.

2.2.1 Data Simulation

Due to the lack of multi-day experimental measurements of healthy subjects and the patients with Cushing's disease, we first simulate multi-day cortisol data profiles [23, 29, 54, 60]. Following [28, 54], cortisol secretion process could be assumed to follow a second-order stochastic differential equation

$$\frac{dCort_1(t)}{dt} = -\zeta_1 Cort_1(t) + n(t) \tag{1}$$

$$\text{and} \quad \frac{dCort_2(t)}{dt} = \zeta_1 Cort_1(t) - \zeta_2 Cort_2(t), \tag{2}$$

where $Cort_1(t)$ and $Cort_2(t)$ are cortisol concentration in adrenal glands and plasma space at time t, respectively [29]. Moreover, ζ_1 stands for cortisol infusion rate from adrenal gland to the blood, ζ_2 corresponds to the cortisol clearance rate by the liver [28, 54]. In addition, $n(t)$ represents secretory events (pulses) underlying cortisol release. The output equation $y_k = Cort_2(k) + \psi_k$, where $Cort_2(k)$ is the discretized cortisol concentration in plasma with $\psi_k \sim \mathcal{N}(0, \sigma_\psi^2)$ as the measurement noise with variance σ_ψ^2. We employ estimated model parameters ζ_1 and ζ_2 derived in [28]. The details of this information are presented in Table 1.

To model cortisol secretory events $n(t)$, we follow the approach presented in [54].

- Healthy Profiles: We use the gamma distribution for pulse inter-arrival times and Gaussian distribution for pulse amplitudes [54]. The corresponding parameters for gamma distribution are $\alpha = 54$ and $\beta = 39$. The pulse amplitude follows a Gaussian distribution $H_k \sim \mathcal{N}(\mu_k, k_k^2)$, where $\mu_k = 6.1 + 3.93\sin(\frac{2\pi k}{1440}) - 4.75\cos(\frac{2\pi k}{1440}) - 2.53\sin(\frac{4\pi k}{1440}) - 3.76\cos(\frac{4\pi k}{1440})$ and $k_k = 0.1\sqrt{\mu_k}$ [5, 23].

Table 1: Infusion and clearance rates associated with the ten simulated cortisol profiles.

Subject number	$\zeta_1(min^{-1})$	$\zeta_2(min^{-1})$
1	0.0739	0.0067
2	0.0762	0.0057
3	0.0921	0.0082
4	0.1248	0.0061
5	0.0585	0.0122
6	0.0726	0.0095
7	0.0799	0.0107
8	0.0365	0.0091
9	0.0361	0.0090
10	0.0864	0.0073

To simulate the data for patients with Cushing's disease, we consider two cases: (1) Cushing's patients without circadian rhythms in their cortisol profiles, and (2) Cushing's patients with circadian rhythms in their cortisol profiles. While cortisol variations in patients with Cushing's disease do not follow normal circadian rhythms, at the very early stages of the disease, the circadian rhythms might be slightly dysregulated [23, 61].

- Cushing's patients without circadian rhythm: We follow [60, 61] and consider the inter-arrival times following a gamma distribution that belong to the range of 59 ± 11 min. Regarding the pulse amplitudes, we assume they are within the range of 38 ± 2.5 μgdL^{-1} min^{-1}, following a Gaussian distribution [5, 23],
- Cushing's patients with circadian rhythm: We employ $\mu_k = 38.5 + 1.93\sin(\frac{2\pi k}{1440}) - 1.6\cos(\frac{2\pi k}{1440}) - 1.5\sin(\frac{4\pi k}{1440}) - 3.5\cos(\frac{4\pi k}{1440})$, $k_k = \frac{2.5}{\sqrt{38\mu_k}}$ as the Gaussian distribution parameters in the pulse amplitudes and the same gamma inter-arrival time distribution as described previously for the Cushing's patients with circadian rhythm.

Employing the model parameters ζ_1 and ζ_2 provided in supplementary information and a vector input of pulse timings and amplitudes $n(t)$ presented above, we simulate the cortisol profiles. We employ coupled differential equations (1) and (2), and add measurement noise to generate cortisol profile data for different subjects in three different situations. More particularly, we simulate the cortisol profiles associated with healthy subjects, Cushing's patients with circadian rhythm in their cortisol profiles and Cushing's patients without circadian rhythm in their cortisol profiles over five days for further analysis [25, 29, 54].

The resulting multi-day cortisol profiles are presented in Figures 3–4. In Figures 3–4, panel **(A)** displays the healthy profile, panel **(B)** shows the profile associated with the Cushing's patients without circadian rhythm, and panel **(C)** depicts the profiles associated with the Cushing's patients with circadian rhythm. Each panel displays cortisol levels (black curve), upper bound envelopes (orange curve), and lower bound envelopes (green curve).

2.2.2 State-space Modeling

Cortisol dynamical system explained above will generate the cortisol observations for our virtual patient environment. We employ the state-space approach presented in [27, 29] to relate the hidden cognitive energy-related state to cortisol variations. The state-space approach lets us systematically track internal energy state and control it in real-time [62]. We model the cognitive energy-related state as a first-order state-space representation

$$x_{k+1} = \rho x_k + u_k + \epsilon_k + I_k, \tag{3}$$

where x_k is the hidden internal energy-related state, ρ is a person-specific parameter, u_k is the control input, $\epsilon_k \sim \mathcal{N}(0, \sigma_\epsilon^2)$ is the process noise, and I_k is being considered as the forcing function that keeps the energy variations during wakefulness and sleep in 24 hour periods. By analyzing the simulated cortisol profiles [23], we design the harmonic forcing function as

$$I_k = \sum_{i=1}^{2} \alpha_i \sin\left(\frac{2\pi ik}{1440}\right) + \beta_i \cos\left(\frac{2\pi ik}{1440}\right), \tag{4}$$

where the coefficients α_i and β_i along with parameter ρ in (61) for each subject/case are derived using the EM algorithm explained in [23] (Table 2).

Analyzing the discretized cortisol data at a one minute time resolution, we observe that the presence or absence of the cortisol pulses builds a binary point process [23]. Hence, we assume the probability of receiving pulses associated with CRH secretion times that results

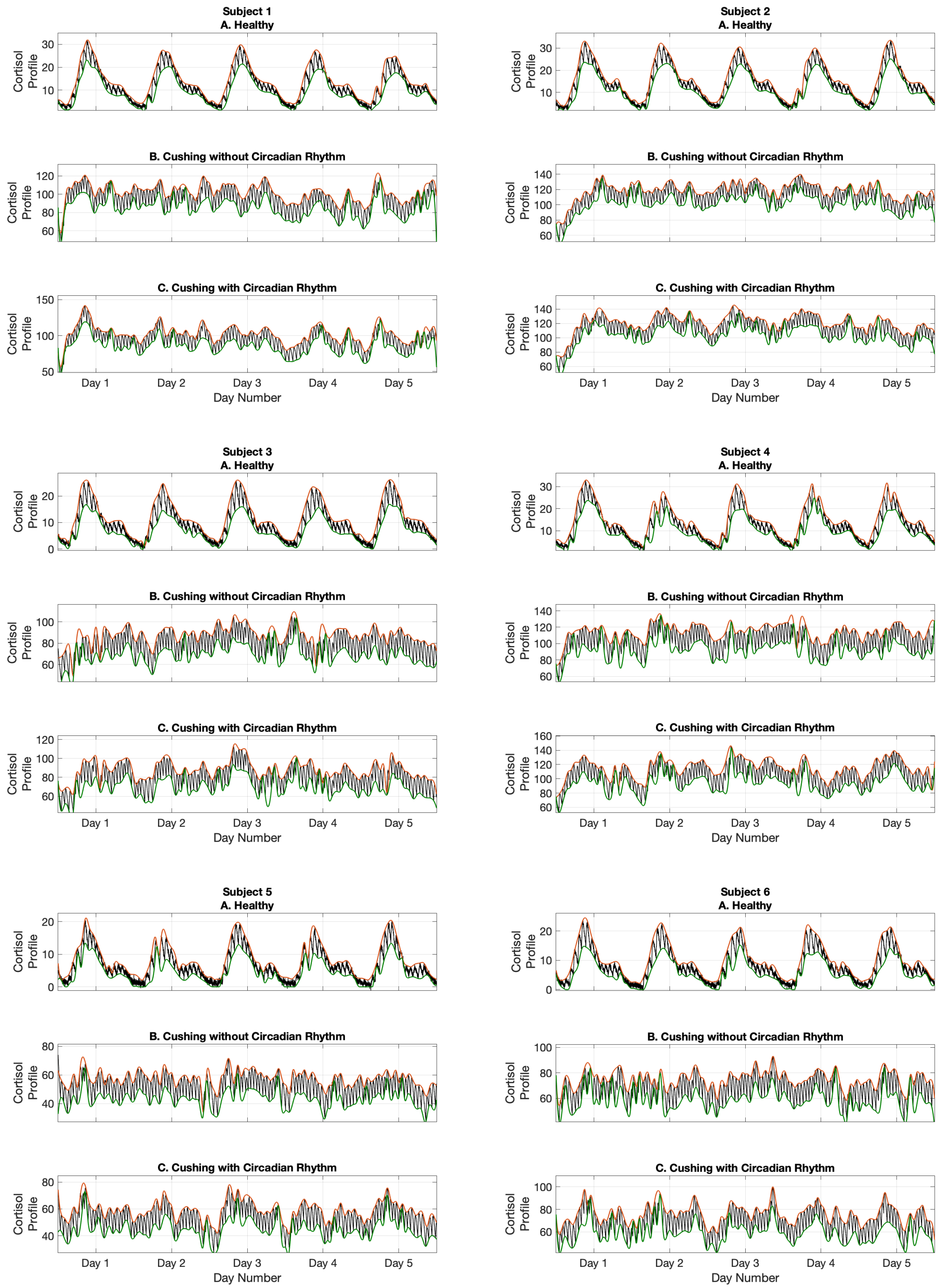

Figure 3: **Simulated multi-day cortisol profile - Subjects 1-6.**

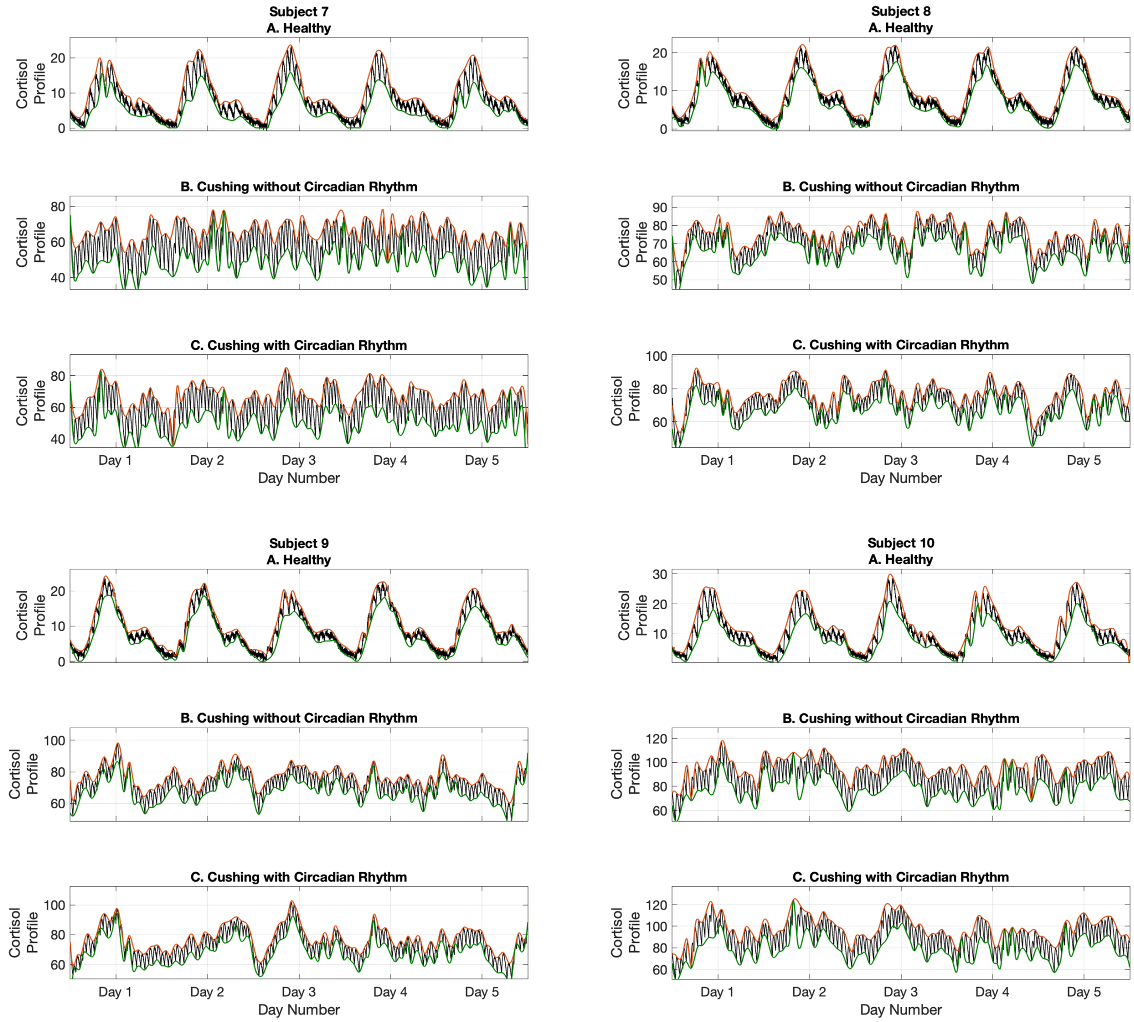

Figure 4: **Simulated multi-day cortisol profile - Subjects 7-10.**

in cortisol secretion, c_k, follows a Bernoulli distribution

$$P(c_k|p_k) = p_k^{c_k}(1-p_k)^{1-c_k}, \tag{5}$$

where the probability p_k is connected to the energy state x_k by the Sigmoid function:

$$p_k = \frac{1}{1+e^{-(\gamma_0+\gamma_1 x_k)}}. \tag{6}$$

This model relates the probability p_k of observing a CRH pulse event c_k to the energy state x_k through person-specific baseline parameters γ_0 and γ_1 calculated by the offline EM.

Table 2: Parameters used to generate forcing function (I_k).

Subject number	Case	α_1	β_1	α_2	β_2
1	A	0.00565	0.00108	−0.00046	−0.00585
	B	0.00104	0.000003	0.00370	−0.00186
	C	0.00280	0.00129	0.00286	−0.000546
2	A	0.00577	0.00100	−0.00062	−0.00533
	B	0.00048	−0.00100	0.000011	−0.000006
	C	0.00300	−0.00035	−0.00017	−0.00376
3	A	0.00538	−0.000013	−0.00087	−0.00657
	B	−0.000002	0.000002	0.000009	−0.000002
	C	0.00267	−0.00007	−0.00073	−0.00530
4	A	0.00566	0.00101	−0.00051	−0.00626
	B	0.00125	0.000006	0.000001	−0.00236
	C	0.00285	0.00203	0.00085	−0.00595
5	A	0.00522	0.00191	−0.000014	−0.00693
	B	0.00284	0.00069	−0.000006	−0.00099
	C	0.00393	0.00080	0.00334	−0.00659
6	A	0.00534	0.00190	0.00105	−0.00672
	B	0.00163	−0.00233	−0.00064	−0.00453
	C	−0.00295	−0.00095	0.00238	−0.00911
7	A	0.00516	0.00220	0.00017	−0.00659
	B	−0.00079	−0.00235	−0.00031	−0.00381
	C	0.00241	−0.00082	0.00245	−0.00895
8	A	0.00560	0.00003	−0.00064	−0.00613
	B	0.00023	0.00063	0.00190	0.00060
	C	0.00186	−0.000032	−0.00001	−0.00613
9	A	0.00543	0.00114	−0.00117	−0.00637
	B	0.00104	0.00188	−0.00152	0.00095
	C	0.00267	0.00286	−0.00140	−0.00306
10	A	0.00559	0.00124	−0.00049	−0.00632
	B	0.00283	−0.00052	0.00002	0.00288
	C	0.00445	−0.00003	−0.00054	−0.00416

In addition to the cortisol secretion times as binary observations, we use the upper and the lower bound envelopes of the blood cortisol measurements as continuous observations to estimate the energy state x_k [23]. We label these two upper and lower envelopes as R_k and S_k, respectively. Assuming there exists a linear relationship between these envelopes and the corresponding state x_k:

$$R_k = r_0 + r_1 x_k + v_k \tag{7}$$

$$\text{and} \quad S_k = s_0 + s_1 x_k + w_k, \tag{8}$$

where $v_k \sim \mathcal{N}(0,\, \sigma_v^2)$, $w_k \sim \mathcal{N}(0,\, \sigma_w^2)$, and r_0, r_1, s_0, s_1 are regression coefficients obtained by offline EM algorithm [23, 63, 56].

It is worth mentioning that while there exist recent advances in performing deconvolution methods, there is still lack of real-time deconvolution algorithm. With real-time deconvolution tool, we directly infer the cortisol impulses $n(t)$ in (1) and employ it in further analysis.

2.2.3 Energy State Estimation

We employ two continuous and one binary observations in the estimation process [64, 65, 66]. Taking the CRH pulse events c_k and the upper and lower envelopes R_k and S_k as observations, we perform Bayesian filtering [64, 63] to estimate the hidden cognitive energy-related state mean x_k and its variance σ_k in two prediction and update steps.

Prediction step:

$$x_{k|k-1} = \rho x_{k-1|k-1} + I_k + u_k \tag{9}$$

$$\text{and} \quad \sigma^2_{k|k-1} = \rho^2 \sigma^2_{k-1|k-1} + \sigma^2_\epsilon. \tag{10}$$

Update step:

$$A_k = \frac{\sigma^2_{k|k-1}}{\sigma_v^2 \sigma_w^2 + \sigma^2_{k|k-1}(r_1^2 \sigma_w^2 + s_1^2 \sigma_v^2)}, \tag{11}$$

$$\hat{x}_k = x_{k|k} = x_{k|k-1} + \\ A_k\Big(\gamma_1\sigma_v^2(c_k - p_k) + r_1^2\sigma_w^2(R_k - r_0 - r_1 x_{k|k-1}) + s_1^2\sigma_v^2(S_k - s_0 - s_1 x_{k|k-1})\Big), \tag{12}$$

$$\text{and} \quad \hat{\sigma}_k^2 = \sigma_{k|k}^2 = \left(\frac{1}{\sigma_{k|k-1}^2} + \gamma_1^2 p_k(1-p_k) + \frac{r_1^2}{\sigma_v^2} + \frac{s_1^2}{\sigma_w^2}\right)^{-1}. \tag{13}$$

The p_k presented in (12) is related to the $\hat{x}_k$ by (6). Consequently, the $\hat{x}_k$ is present on both sides of (12) and we employ Newton's method to solve the update equations.

2.2.4 Dynamic System Model of Medications

The next step in closing the loop and regulating energy-related state is to model the dynamical system of hypothetical medications and include them in control design process. In this research, we focus on the medications that can lead the subjects to reach their desired energy levels [42, 41]. In this regard, we consider two classes of medications: (1) for elevating the energy levels required for daily activity (i.e. excitation effect), and (2) for helping the subjects to lower their energy levels in the evening which may help them experience well-ordered sleep cycles at nights (i.e. inhibition effect). To analyze how a specific medication affects one's energy levels and incorporate them in the control design process, we model their dynamics by a second-order state-space representation

$$\begin{pmatrix} \dot{z}_1(t) \\ \dot{z}_2(t) \end{pmatrix} = \begin{pmatrix} -\theta_{i1} & 0 \\ \theta_{i1} & -\theta_{i2} \end{pmatrix} \begin{pmatrix} z_1(t) \\ z_2(t) \end{pmatrix} + \begin{pmatrix} \eta \\ 0 \end{pmatrix} q(t), \tag{14}$$

where $i = 1, 2$ denotes the type of medications. $y(t) = z_2(t)$ is the estimated energy level and θ_{i1}, θ_{i2} correspond the infusion rate and the clearance rate of each corresponding medication i, respectively. We assume $\theta_{\mathbf{i}} = \begin{pmatrix} \theta_{i1} & \theta_{i2} \end{pmatrix}$. In the state-space representation (14), $q(t) = q_i^* \, \delta(t - \tau_i^*)$ is the actuation input impulses where parameters τ_i^* and q_i^* stand for time and dosage of the corresponding medication i [29, 67]. The η term also determines if the actuation should be excitation (i.e. $\eta = +1$ for elevating the energy level) or inhibition (i.e. $\eta = -1$ for lowering the energy level). With this representation, we analyze how using a specific dosage q_i^* of medication i at time τ_i^* will affect the internal energy levels $z_2(t)$

dynamically. Solving the state-space equation (14) and considering the output equation $y(t) = z_2(t)$, we compute the output at each time step j as

$$y_j = a_j y_0 + \boldsymbol{b_j}\mathbf{q} + e_j, \tag{15}$$

where $a_j = e^{-\theta_{i2}j}$ and $\boldsymbol{b_j} = \frac{\theta_{i1}}{\theta_{i1}-\theta_{i2}}\big[(e^{-\theta_{i2}j} - e^{-\theta_{i1}j}) \quad (e^{-\theta_{i2}(j-1)} - e^{-\theta_{i1}(j-1)}) \quad \cdots \quad (e^{-\theta_{i2}} - e^{-\theta_{i1}}) \quad \underbrace{0 \quad \cdots \quad 0}_{N-j}\big]'$. The vector input $\mathbf{q}$ consists of one non-zero element (i.e. $\mathbf{q} = [q_1 \cdots q_N]$, where $q_j = 0, \forall j$ except the one element q_i^* at time τ_i^*) and error term $e_j \sim \mathcal{N}(0,\, \sigma_e^2)$. Forming the output for the whole time horizon N, we generate the vector representation $\mathbf{y}$ as

$$\mathbf{y} = \mathbf{A}_\theta y_0 + \mathbf{B}_\theta \mathbf{q} + \mathbf{e}, \tag{16}$$

where $\mathbf{y} = \begin{bmatrix} y_1 & y_2 & \cdots & y_N \end{bmatrix}'$, $\mathbf{A}_\theta = \begin{bmatrix} a_1 & a_2 & \cdots & a_N \end{bmatrix}'$, $\mathbf{B}_\theta = \begin{bmatrix} \boldsymbol{b_1} & \boldsymbol{b_2} & \cdots & \boldsymbol{b_N} \end{bmatrix}'$, and $\mathbf{e} = \begin{bmatrix} e_1 & e_2 & \cdots & e_N \end{bmatrix}'$. To complete the system identification task, we impose the constraint $||\mathbf{q}||_0 = 1$ in the corresponding parameter estimation problem [68]. To find the optimum parameters, we solve the following optimization problem to optimize the error term $J = \mathbf{e}'\mathbf{e}$ as

$$\min_{\substack{\theta_{\mathbf{i}}, \mathbf{q} \\ ||\mathbf{q}||_0 = 1}} \; J = \frac{1}{2}||\mathbf{y} - \mathbf{A}_\theta y_0 - \mathbf{B}_\theta \mathbf{q}||_2^2. \tag{17}$$

Given $\mathbf{y}$, we can estimate $\mathbf{A}_\theta$, $\mathbf{B}_\theta$ (i.e. include $\theta_{\mathbf{i}}$), and $\mathbf{q}$ to obtain the actuation dynamics [55]. As a result of this process, we simulate the way that a specific medication affects the energy levels. In the following part, we explain the control approach and close the loop.

In this *in silico* study, incorporating the hypothetical medication dynamics (14), we design the control strategy to determine the time and the dosage of each medication to regulate the estimated energy state. In the practical case, this system identification step is recommended to be performed in parallel to update the dynamical model parameters in real-time.

2.2.5 Fuzzy Control System

Fuzzy control, which is known as a knowledge-based control approach, employs the insights about the system, performs the corresponding inference, and makes the control decisions [69, 70, 71]. As an intelligent approach, it is a powerful bridge from the expertise inference to the real world [6, 72]. Any fuzzy controller includes four main parts: rule base, fuzzifier, inference engine, and defuzzifier. In the rule base, we define the rules to achieve our control objective [73]. These IF-THEN rules are derived employing expert knowledge of the system and the corresponding constraints.

In the present study, the estimated cognitive energy-related state and the time of the day are the inputs of the fuzzy controller, and the control output is the time and dosage of the required simulated medications [5]. To design the fuzzy system, we employ information about the personalized levels of energy state and the dictionary of medication dosages and actuation responses (Figure 2). We also use two classes of actuation: exciting medications which increase the energy levels, and inhibiting medications which lower the estimated energy levels. The purpose of applying medications with exciting and inhibiting effects is to provide the required energy for daily activity [10] and lowering the energy-related state to result in a better sleep cycle at nights [74], respectively. Based on the literature and nature of the medications [42, 41], we consider the constraint of applying maximum two medications (i.e. control inputs) per day: one in the morning which increases energy levels, and one in the evening to lower the energy levels. The rule base of the proposed fuzzy controller is presented in Table 3.

As an example, to clarify the structure of rules presented in Table 3, rule number 1 denotes:

- If the estimated energy state is *High*, and the time is *early in the morning* then the actuation is *positive small*.

To quantify the linguistic variables presented in the rule base, we employ membership functions as the fuzzifiers [75]. Investigating the simulated environment including estimated

Table 3: Fuzzy Rule Base.

Rule #	Time *(Input 1)*	Energy State *(Input 2)*	Actuation *(Output)*
1	Early Morning	High	Positive Small
2	Early Morning	Low	Positive Big
3	Early Morning	Medium	Positive Medium
4	Late Morning	High	Zero
5	Late Morning	Low	Positive Medium
6	Late Morning	Medium	Positive Small
7	Early Evening	High	Negative Medium
8	Early Evening	Low	Zero
9	Early Evening	Medium	Negative Small
10	Late Evening	High	Negative Big
11	Late Evening	Low	Negative Small
12	Late Evening	Medium	Negative Medium

energy state, hypothetical medication dynamics, personalized levels of energy state, and the rule base, we utilize the appropriate number of relevant membership functions presented in Figure 14. As observed in Figure 14, we employ six membership functions for time of the day (input 1), three membership functions for estimated energy values (input 2), and seven membership functions for the control output to cover all cases in the rule base (Table 3). In Figure 14, top panel shows the first input membership functions describing time of the day. Middle panel shows the input membership functions associated with the estimated energy-related state. In Figure 14, bottom panel shows the membership functions for the actuation output (i.e. control signal u_k). The abbreviations P, N, Z, S, M, and B stand for "Positive," "Negative," "Zero," "Small," "Medium," and "Big", respectively.

We use *Mamdani* inference engine to execute the inference and produce fuzzy outputs [76]. We employ *minimum* method for both *AND* operation in the fuzzy inputs and implication process for fuzzy output generation. We also use *Maximum* method for rule output

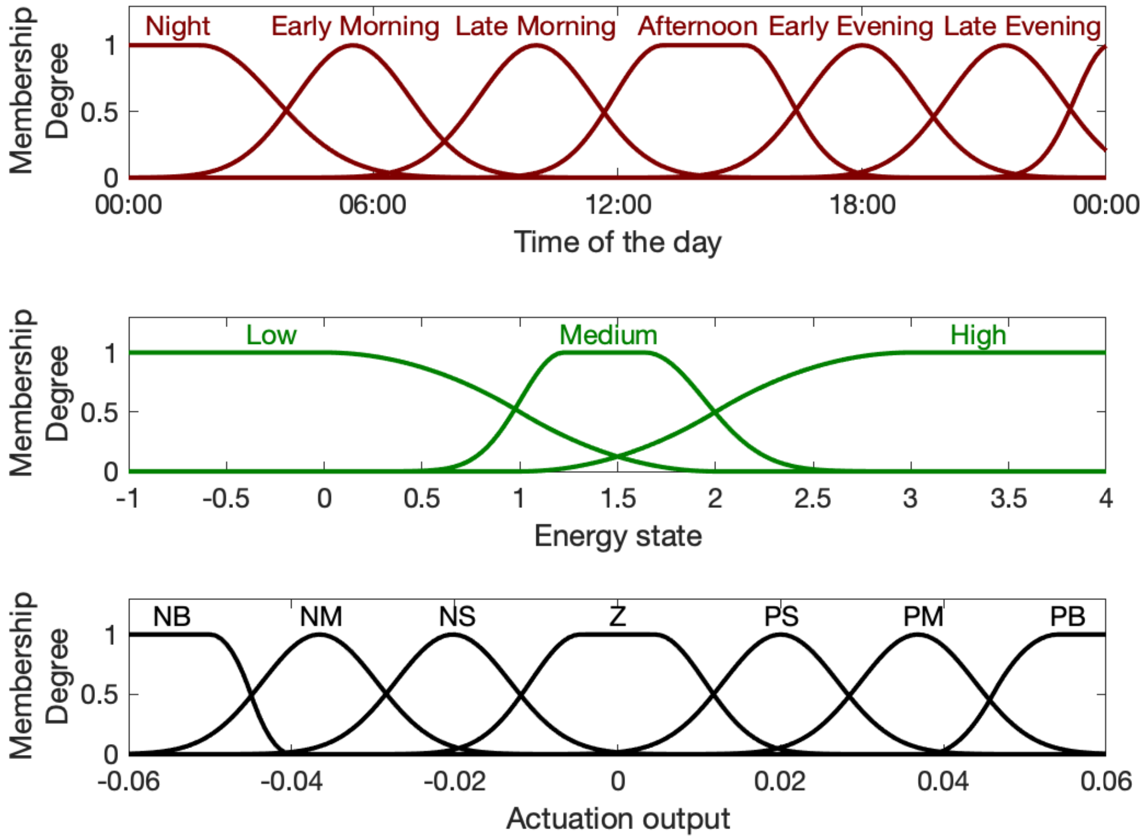

Figure 5: **Input and output membership functions.**

aggregation. Consequently, the final fuzzy output will be resulted as

$$\mu_{mamdani}(q) = \mu_m(q) = \max_j [\mu_j(q)] = \max_j [min(min(\mu_{time}(t), \mu_{state}(x)), \mu_{actuation}(c))] = \max_j [min(\mu_{time}(t), \mu_{state}(x), \mu_{actuation}(c))], \tag{18}$$

where j denotes the effective rules at each time step and $\mu_j(q)$ is the resulted fuzzy set. $\mu_{time}(t)$, $\mu_{state}(x)$, and $\mu_{actuation}(c)$ also stand for the membership functions presented in Figure 14. To demonstrate the way that this inference engine works, we explain the proposed fuzzy system (18). At each time step, the fuzzy system monitors all the rules presented in Table 3 and finds the effective rules according to the input membership functions (Figure 14). By extracting the corresponding membership degree and executing *AND* operation in each applied rule, it then performs implication between the resulted input fuzzy sets (time and the estimated energy state) and the corresponding output fuzzy membership function (medication actuation). By aggregating results from all applied rules, it generates the final fuzzy output. To produce crisp output out of the generated fuzzy outputs and applying it into the system in real-time, we employ *centroid* defuzzification method

$$q^* = \frac{\int \mu_m(q) q \, dq}{\int \mu_m(q) \, dq}. \tag{19}$$

At any time step where either the rules with *Zero* actuation output (Table 3) are effective, or the output q^* in (19) equals zero, the fuzzy system would determine no need for applied control. At the time t that the fuzzy system results a nonzero output ($q^* \neq 0$), time of actuation would be derived ($\tau^* = t$). Considering the resulted crisp output and constraint to apply maximum two medications per day, the designed control will determine the time and the amplitudes of each medication. Hence, by taking the decisions about the dosage and the desired time of the hypothetical medications (i.e., q^* and τ^* in (14)), the resulted control signal (i.e., u_k in (61)) will be applied to regulate the internal energy state.

2.3 Results

In this section, first we present the open-loop results. Then, we present our real-time closed-loop results for two categories of Cushing's diseases: one without circadian rhythm in their cortisol profiles, and another with circadian rhythm in their cortisol profiles. The results associated with ten simulated subjects are presented in Figures 6–7.

For each subject, panel **(A)** displays the open-loop results. Panel **(B)** shows closed-loop results for the Cushing's patients without circadian rhythm. Panel **(C)** shows closed-loop results for the Cushing's patients with circadian rhythm. In each panel: the top sub-panel shows the estimated cognitive energy-related state, the middle sub-panel displays the control input, and the bottom sub-panel depicts the medication injections. Red pulses are related to excitation and the blue pulses are related to inhibition. The white and grey backgrounds indicate open-loop (i.e. $u = 0$) and closed-loop results, respectively.

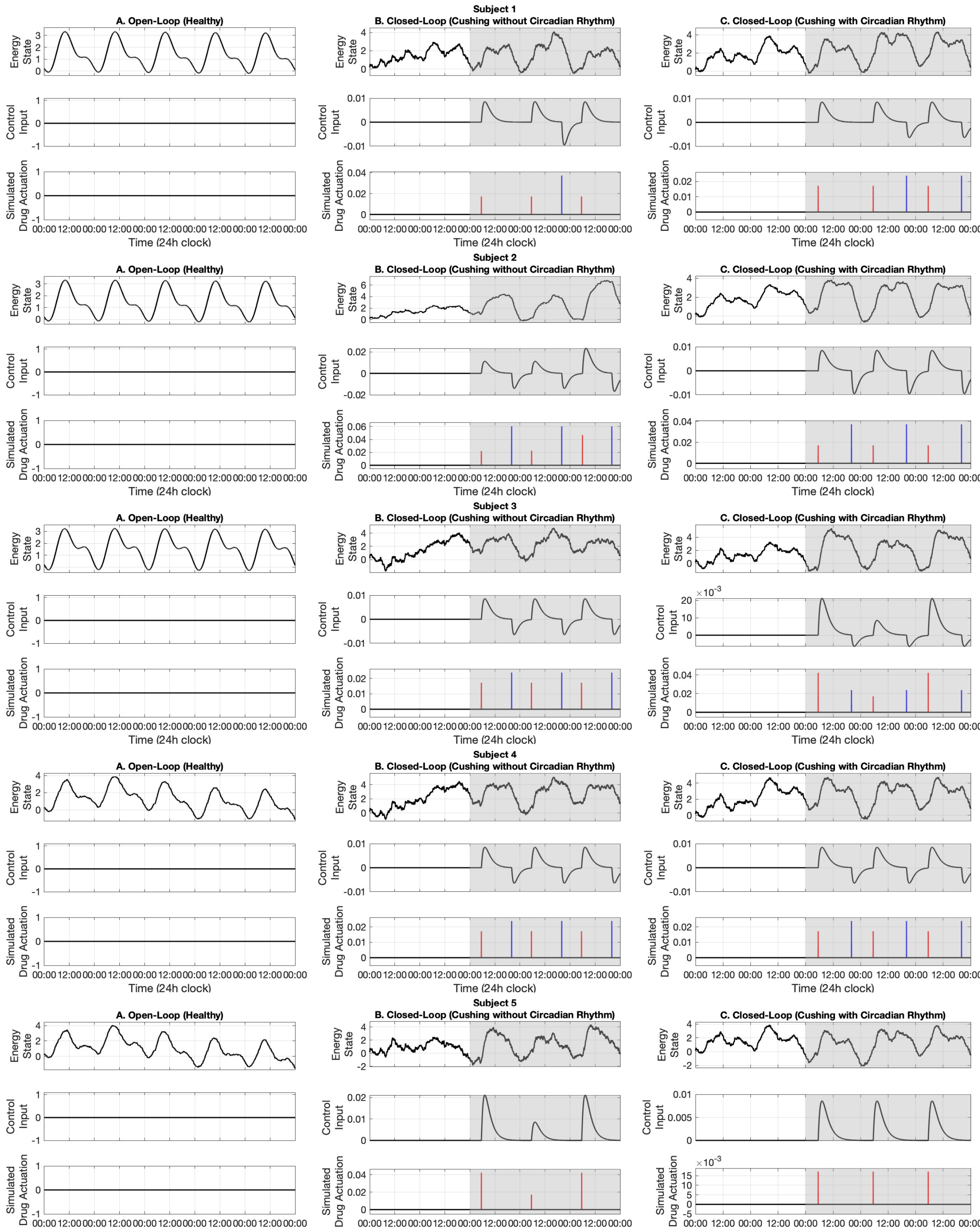

Figure 6: **Open-loop and closed-loop energy regulation results (Subjects 1-5).**

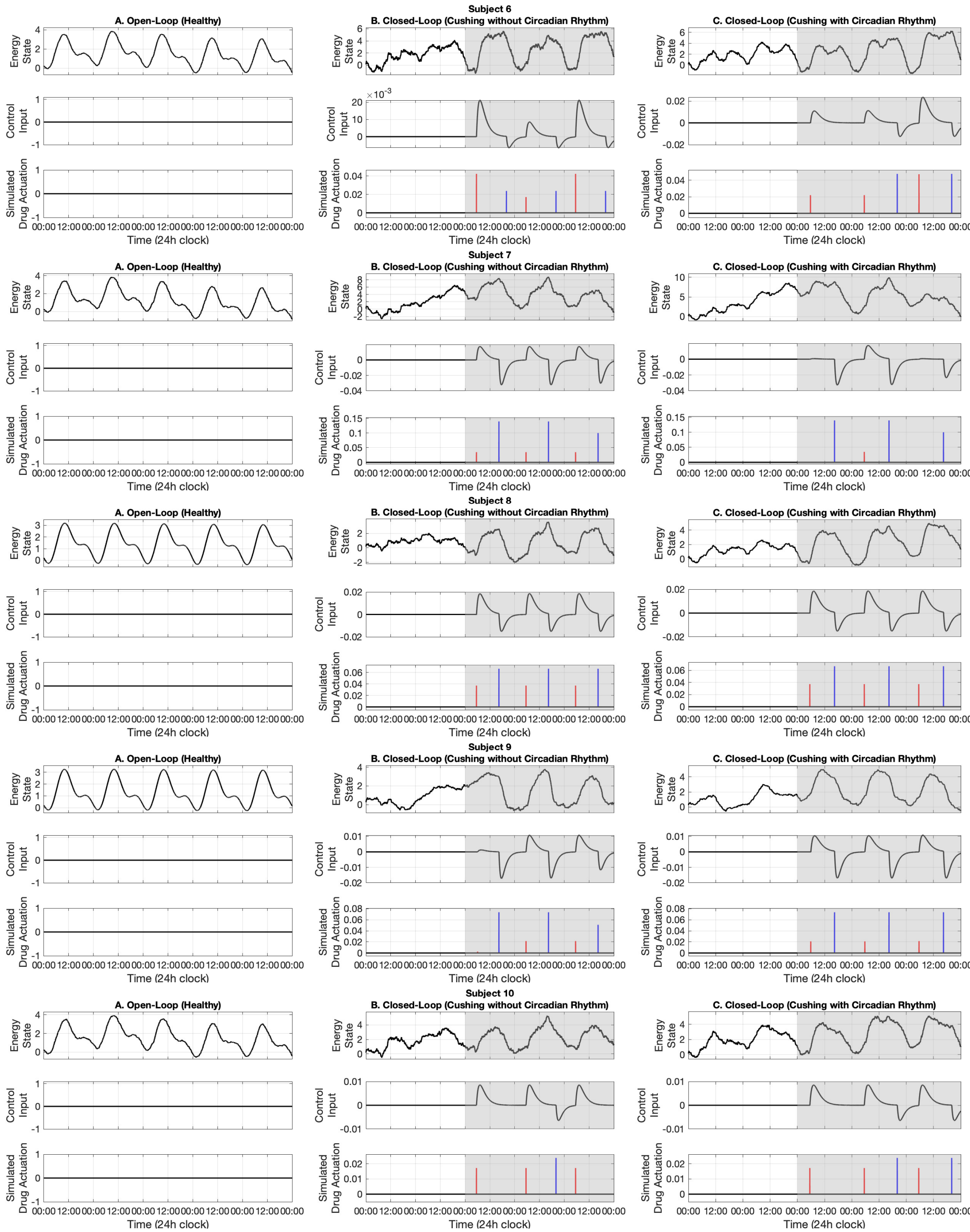

Figure 7: **Open-loop and closed-loop energy regulation results (Subjects 6-10).**

2.3.1 Open-loop (Healthy subject)

In the first part, we use data associated with healthy subjects to show the tracking performance. As depicted in the left panels of Figures 6–7, the system tracks the energy state in an open-loop manner. In the middle sub-panel, it is observed that there is not any control in this stage ($u_k = 0$). Top sub-panels show that the estimated energy state has its peak during the daytime (06:00 - 16:00) and it drops in the evening. It verifies that we successfully track the energy state in the simulated healthy profiles.

2.3.2 Closed-loop (Cushing's patients without circadian rhythm)

In this part, we employ the simulated cortisol data associated with Cushing's patients without circadian rhythm in their cortisol profiles. The results are observed in the middle panels of Figures 6–7. The white and grey backgrounds correspond to the open-loop and the closed-loop periods, respectively. After day two, the control is activated and the closed-loop system detects an imbalanced energy state (top sub-panel in the middle panels of Figures 6–7). Then, the time and dosage of the required simulated medications are produced by the control system (bottom sub-panel in the middle panels of Figures 6–7). The red pulses stand for the simulated medications with excitation effects, while the blue pulses are associated with the simulated medications with inhibitory effects. Employing the suggested hypothetical medications will lead the generated control input to follow the curves presented in the middle sub-panel of Figures 6–7. Thereafter, starting day three of simulation (once the loop gets closed), the energy state is being regulated.

2.3.3 Closed-loop (Cushing's patients with circadian rhythm)

Similar to the previous case, here we investigate the performance of the proposed closed-loop architecture by making use of simulated Cushing's patients' data together with existing circadian rhythm in their cortisol profiles. The results are presented in the right panels of Figures 6–7. Similarly, the system detects the irregular energy patterns and regulates the energy state variations by designing the corresponding control signals in a closed-loop manner.

2.4 Discussion

Inspired by the fact that CRH plays an undeniable role in internal energy regulation, we proposed our novel approach for regulating the energy-related state using a wearable brain machine interface architecture. In the proposed architecture, we infer one's energy variations by monitoring cortisol data which can be collected using wearable devices in real time [59]. We implemented the control algorithm on ten simulated data profiles in healthy subjects and Cushing's patients.

In the offline stage of this research, we simulated the cortisol data for multiple subjects. As it is validated in the literature, we employ stochastic models to simulate multi-day cortisol secretion patterns. Following [54, 29, 60, 23], we consider different gamma distributions for inter-arrival times associated with cortisol secretion impulses. We also assume the pulse amplitudes follow Gaussian distributions. Employing the model parameters that are presented in the manuscript, we simulate cortisol profiles which have day-by-day variability. The stochastic variability existing in model parameters would be viewed as a realistic multi-day case in this *in silico* study. Employing the state-space approach along with EM algorithm, we estimated the model parameters and the forcing circadian function. Using the virtual patient environment, we aimed to track the energy state based on the changes in cortisol secretion times and cortisol upper and lower envelopes (See Figure 2).

With the goal of tracking the energy state in the proposed architecture, we first simulated a real-time open-loop case. In this part, we used the data associated with healthy subjects. In the present study, due to the lack of real-time deconvolution algorithm, we assume the presence or absence of cortisol secretion forms a binary point process and follows a Bernoulli distribution. Besides, we take the cortisol upper and lower bound envelopes as the continuous observations. Utilizing the EM algorithm, we estimated the hidden energy state. As it can be seen in the left panels, with no control implemented (i.e. $u_k = 0$), the energy state variations in simulated healthy profiles are as desired. It is observed that the energy state is at its peak during the daytime and it drops in the evening. It leads to providing enough energy for daily activity and having well-ordered sleep cycles at evening. In fact, this normal condition is because of the well-balanced cortisol secretion patterns in healthy subjects.

In this research, we assumed that including the hypothetical medications would impact the energy state. Hence, we incorporated the simulated medication dynamics as the actuation while closing the loop. In this regard, we first presented the system identification required to design the control system. To incorporate the corresponding medications in real-world implementation of the proposed closed-loop architectures, it is important to pay appropriate attention to medications' half-lives. In the present design, we assumed that the hypothetical medications have prompt effects on one's energy levels. In the case of utilizing long-acting agents, the rules and membership functions should be revised accordingly. While this step is performed in the offline stage of this research, in the practical case, it is recommended to execute it in real-time to update the medication dynamics according to the subject's response. To design the control, we proposed a knowledge-based fuzzy controller. Employing the estimated energy state, personalized desired levels of energy state, and hypothetical medication dynamics we built the rule base, membership functions, and inference engine (See Figure 2).

Next, we presented the results of the closed-loop system. In this regard, we employed the cortisol data profiles associated with the Cushing's patients. To depict the performance of the closed-loop system, we assumed the control system gets activated starting day three, which means the system is open-loop (i.e. $u_k = 0$) in the first two days of the simulation. During the open-loop period, we observe that the energy variations do not follow the ideal circadian rhythm. In other words, the patients with hypercortisolism do not have normal cortisol secretion patterns which will cause them to have insufficient energy levels in the day time and experience disturbed sleep cycles at night [10]. Starting day three, the feedback control system (i.e. $u_k \neq 0$) closes the loop (grey background in Figures 6–7). In the closed-loop period, the implemented control system detects undesired energy variations and tries to infer the right time and dosage of the simulated medications in real-time. That is to say, the fuzzy structure receives the estimated energy state, employs the rule base (Table 3) and membership functions (Figure 14), and generates the appropriate control signal. This intermittent control signal is depicted in the bottom sub-panels of Figures 6–7. When low levels of energy are detected, the red pulses would be generated to adjust the dosage of the required medications with excitation effect to provide required energy levels. On the other hand, once undesired high levels of energy are detected in the evening, the medications with the energy lowering effect, i.e. blue pulses, would be suggested to provide the inhibition effect. The required time and dosage of these hypothetical medications are produced by the fuzzy structure. The control actuation signal, which is result of applying these simulated medications, is presented in the middle sub-panels of Figures 6–7. Considering the constraint of using maximum two medications per day [77], the energy state is regulated in real-time. It is worth mentioning that in the real-world case, the only needed signal for closing the loop is the time and dosage of required medications. Since this simulation study is the first step to show the feasibility of our proposed approach, we simulated hypothetical medication dynamics to include actuation in the virtual patient environment.

In the final part of our results, we presented the outcomes of our proposed structure on simulated cortisol data profiles associated with the Cushing's patients with circadian rhythm in their profiles. While Cushing's patients do not generally have the required circadian rhythm in their cortisol profiles, there exist some patients with some circadian rhythm in their blood cortisol profiles [60]. This slight circadian rhythm could be assumed to be available in the patients in their early stages of Cushing's disease. Similar to the results of the Cushing's patients without circadian rhythm, our proposed closed-loop architecture successfully detects the energy irregularities and makes the control decisions in real time.

Analyzing the results of multiple subjects, we observe some interesting outcomes. In the results associated with subjects 1, 5, 6,7 and 10, we see that for some days no blue pulses (i.e. simulated medications with the inhibition effects) are necessary. It might be because energy levels are already low and would not affect their sleep cycles. In these cases, employing only the medications with excitation effects in the morning may lead to energy regulation in the evening too. These results are shreds of evidence of an intrinsic advantage of our proposed closed-loop architectures which is handling the energy regulation in an automated way and suggesting the medications as needed.

To further depict the efficiency of the proposed closed-loop architecture, we define corresponding metrics (Figures 8–9). Panel **(A)** shows the difference between average levels of energy in the day and night. Panel **(B)** shows the internal energy growth required for the wake-up time balance. Panel **(C)** shows the decrease in internal energy levels required for sleep time balance. The empty circles and the filled green circles show the results of the open-loop and closed-loop cases, respectively. The left and right sub-panels show the data corresponding to the Cushing patients without and with circadian rhythm in their cortisol profiles, respectively.

As the first criteria, we analyze the effect of closed-loop system in increasing the difference between average levels of energy in the day and night (top panel of Figure 8). As presented, the difference between the average levels of energy in day and night has been increased for all ten simulated subjects in both Cushing's classes (filled green circles compared to the empty circles). As the second criteria, we analyzed the growth of internal energy state in the morning, which will ultimately lead the subjects to wake up with higher levels of energy. To do this task, we compared the growth of energy before the start of the day in both open-loop and closed-loop cases (middle panel of Figure 8). The observed growth of energy in all simulated subjects will help them to wake up with having more energy required for their daily activities. As the final criteria, we compared the drop of energy levels late at evening (bottom panel of Figure 8). It demonstrates how the proposed closed-loop architecture resulted in decreasing the energy levels required for a better sleep cycle. As presented in the bottom panel of Figure 8, the internal energy state in patients with Cushing's disease are not decreased sufficiently in the evenings (empty circles). However, in the closed-loop case, by applying the required medications, the simulated energy state has been dropped more efficiently which will further help the subjects to experience

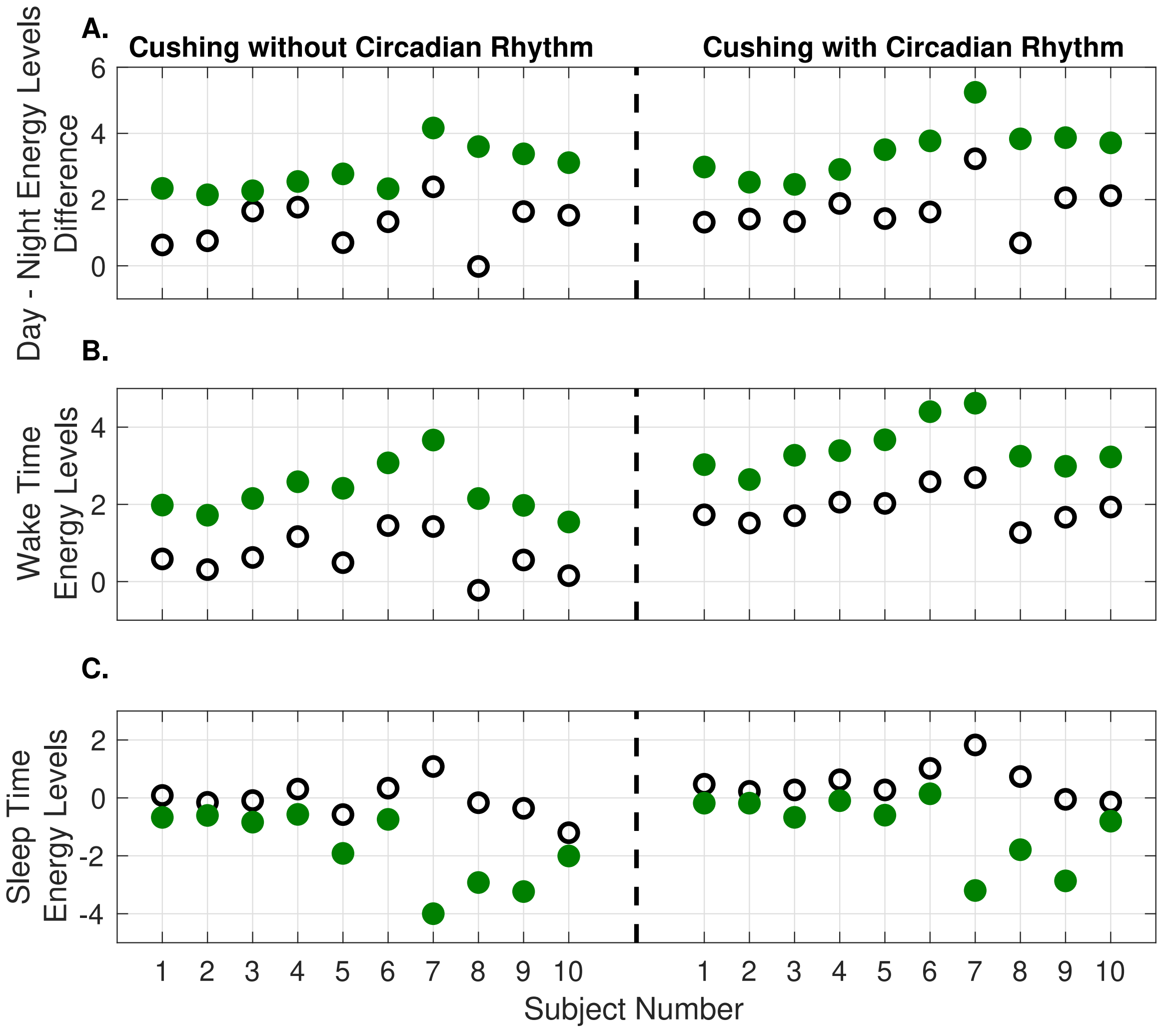

Figure 8: **Open-loop and closed-loop results analysis.**

more balanced sleep cycle at night.

In Figure 9, the lower- and upper-bounds of the of each box represents the 25th and 75th percentiles of the distribution of each metric for all ten simulated profiles, and the middle line in each box displays the median. Panels **(A)** and **(B)** show the data corresponding to the Cushing patients without and with circadian rhythm in their cortisol profiles, respectively.

Analyzing the results on all the simulated subjects, the difference between the average energy levels in day and night in Cushing's patients without and with circadian rhythm in their cortisol profiles is improved by 140% and 97%, respectively (left sub-panels in Figure 9). The growth in the energy levels before the wake time in both classes of Cushing's

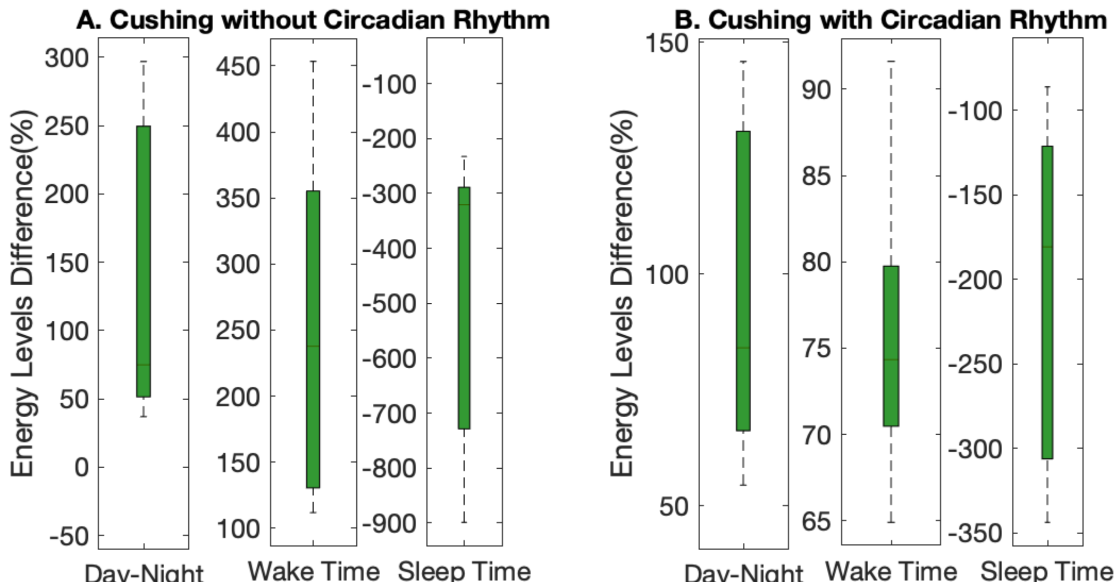

Figure 9: **Overall closed-loop results analysis.**

patients is improved by 245% and 75%, respectively (middle sub-panels in Figure 9). Similarly, the average drop in the energy levels required for sleep time regulation is improved by 473% and 208% in simulated Cushing's patients without and with circadian rhythm in their profiles has been, respectively (right sub-panels in Figure 9). This analysis verify how our proposed architecture is effective in regulating energy levels in a virtual patient environment.

In the offline stage of this research, we simulated multi-day data profiles for healthy subjects and subjects with Cushing's disease. It is worth mentioning that this stage of simulating multi-day data profiles is because of the lack of technology for real-time cortisol measurements. Future advances in wearable technologies would provide the opportunity to continuously monitor the cortisol data and design a system that could take care of inter- and intra-subjects fluctuations. In the present study, we assumed that the suggested medications could be successful in lowering or increasing energy levels. In practical implementation, there exist multiple factors that might cause the proposed architectures (i.e., using suggested medications to regulate internal energy state) to fail and result in less efficiency.

- Diverse sensitivity to glucocorticoid hormones among individuals might prevent to observe similar energy adjustments in response to the medications [78].

- Sever dysregulation of the HPA axis, which happens in some endogenous Cushing's syndrome cases, could only be treated by removing the pituitary or adrenal tumor(s) [79].

3 Closed-Loop Cognitive Stress Regulation

3.1 An Overview of Cognitive Stress Regulation in Wearable-Machine Interface Architectures

Stress-related health issues attract massive attention in the modern world [6, 7]. Despite recent advances in technology, handling cognitive stress-related disorders is still a major problem around the globe and impacts quality of life in general [9]. Additionally, low levels of eustress, or positive cognitive stress, could negatively affects work productivity [2]. Experiencing high levels of cognitive stress while performing routines, or low cognitive engagement with the environment, may seriously affect an individual's life [19]. Over 60% of Americans feel that stress negatively affects their work performance [80]. Considering the fact that the brain performs better when internal cognitive stress state is within a moderate range [81], stress regulation has recently received a lot of attention. Figure 10 depicts the relationship between performance and the amount of stress that a person encounters. As depicted in Figure 10, the performance is at its peak when the stress level is within a normal range [2]. While high amount of arousal (stress) may cause nervousness, too little amount of arousal (stress) may negatively affects productivity and bring the person about feeling bored and inactive. Eustress or good type of stress will cause the person to be focused, more productive, and better engaged with the environment. While there exist methods for managing stress, there is still a lack of reliable systems that continuously track the stress levels in individuals and automatically regulate stress levels by suggesting appropriate non-invasive solutions during daily activities [20, 21].

The human brain detects and mediates the physiologic response to environmental stimuli including cognitive stress tasks [23]. Traditional approaches that try to directly monitor brain activity (e.g., using electroencephalogram (EEG) signal[82]) are neither comfortable nor practical in daily life [83]. Thanks to the recent advances in wrist-worn wearable device

Chapter three was first presented in part at the proceedings of the 2019 IEEE Engineering in Medicine and Biology Society Conference [6]. Chapter three has been mainly adopted from Azgomi, Hamid Fekri, Iahn Cajigas, and Rose T. Faghih. "Closed-Loop Cognitive Stress Regulation Using Fuzzy Control in Wearable-Machine Interface Architectures." IEEE Access 9 (2021): 106202-106219 [3].

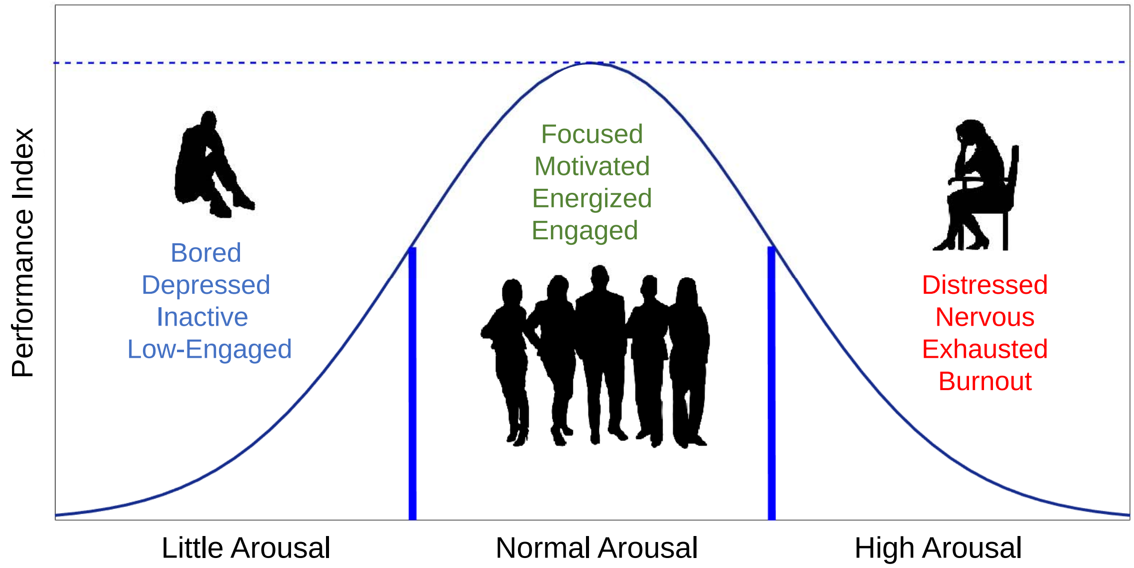

Figure 10: **Arousal-performance relationship.**

technologies, we now have the opportunity to easily monitor various physiological signals and understand brain activity [84, 85, 86, 87]. To infer internal stress state, rather than monitoring the brain activity directly, one might be able to collect measurements that correspond to the hidden stress state using the wearable devices [51, 53, 88, 89, 50, 90, 91].

Among the data that can be collected via wearable devices, skin conductance data carries important information about the brain's cognitive stress [92, 93, 94, 95, 52]. Cognitive stress can be inferred from the tone of the sympathetic nervous system (or "fight or flight" response system). The sympathetic nervous system is a branch of the automatic nervous system (ANS) [96]. Since Electrodermal activity (EDA) does not include any representation of the parasympathetic nervous system (i.e., another branch of ANS), it is a suitable representative for cognitive stress analysis [97, 98]. While heart rate also provides insight about the internal arousal state, it carries information associated with cardiac activity [96, 99]. As skin conductance signal provides information about sympathetic nervous system, we focus on this physiological signal for further analysis [100]. In the presence of external (e.g., environmental) or internal (e.g., mental) stimulus, there are small variations in the activity of the sweat glands [101]. Consequently, electrical characteristics of the skin will change. Such fluctuations are indicated in the skin conductance response (SCR), which can be measured using wearable devices [50, 53, 52].

That the SCR rate encodes stress-related information (i.e., more stress is associated with the increased SCR and vice versa) has been validated in experimental studies [50, 94, 102]. In addition to the studies related to inferring brain activity using skin conductance signal [52, 103, 101], there exist research that employ this biomarker as a reference signal [104, 105, 106]. For instance, Lee *et al.* use motion sensors to classify the stress level and employ skin conductance as a reference for stress detection [107]. Perry *et al.* designed a wearable device that can determine stress levels by monitoring the amount of cortisol that is present in human's sweat [108]. In this research, we relate the internal cognitive stress state to the changes in skin conductance signal.

Compared to available methods that try to detect stress and send an alert to the person [109, 110], our goal here is to track stress levels in a continuous manner and design a control strategy to regulate the cognitive stress by a non-invasive approach in a simulation environment. Rachakonda *et al.* used physiological data such as respiration, heart rate and skin conductance, and then, by incorporating machine learning algorithms, they performed a classification method on the stress levels [111]. The results demonstrate classifications for particular stress ranges. Similarly, Sano *et al.* have employed machine learning tools on the collected physiological signals (i.e., accelerometer and skin conductance data), mobile data such as text and call, and the surveys completed by the subjects to perform stress range classification [112]. Compared to the majority of research being done in this area, which employ machine learning approaches to classify the stress levels [113, 114, 115], the proposed state-space method would lead us to track stress severity as a continuous value in real-time. This will further provide the chance to better design the actuation policy for closing the loop and keeping the stress state within a desired range. Moreover, continuously tracking of cognitive stress might help the person to increase eustress [116]. Hence, following the proposed architecture, we would be able to track subject's cognitive stress as a continuous state and design the control mechanism to keep this hidden state within a desired range.

In recent years, there have been several studies dealing with closed-loop approaches

[117, 118, 119, 120, 121, 122]. Walter *et al.* classified workload in an adaptive learning environment [122]. They proposed to track mental workload using the EEG signal and design the course material to close the loop and increase the efficiency. Utilizing our proposed approach, one would be able to track the internal stress state continuously and design the required actuation accordingly. This actuation could be any changes in the workload, changing light colors and frequencies in workplaces, listening to music, drinking excitatory or relaxing beverages, or designing the break time based on internal stress levels to keep them within desired range. In this research, we propose to use wearable-machine interface (WMI) architectures to control the cognitive stress-related state in a simulation environment. As presented in Figure 1, the architecture includes collecting physiological signals using a wearable device, inferring neural stimuli underlying pulsatile SCR events, estimating an unobserved stress-related state from underlying neural stimuli, designing the control, and closing the loop to regulate subject's cognitive stress state and keep it within a desired range in a real-time manner [6].

Taking advantage of the real-time simulation model, we present our approach in designing the control algorithm and closing the loop in a systematic way. We employ fuzzy logic, as a knowledge-based control approach, to control cognitive stress state in a simulation environment [123, 124]. The knowledge-based control approaches make inference and design the control action using the insight achieved from system dynamics. The fuzzy logic controller employs insights about the system, performs inference, and derives the actuation policy [75, 125]. Researchers in [123] assume that all the states are available while designing the control system. Zhang *et al.* employ a fuzzy adaptive state observer to estimate the hidden state and design a fuzzy controller to close the loop [125]. Their proposed approach is effective when dealing with unknown control directions [125].

In this regard, we present a simulation setting to show how an automated control action will result in regulation of both modeled SCR events and the estimated cognitive stress-related state. Toward this aim, we relate the internal stress state to the changes in SCR events. By estimating the hidden stress-related state and designing the control action, we close the loop in real-time. More specifically, we consider one open-loop, one closed-loop inhibitory, and one closed-loop excitatory examples to demonstrate the performance of our proposed WMI architecture in different simulation scenarios. The final results verify that the proposed architecture not only can successfully track one's cognitive stress state, but also that the control mechanism is effective in both excitation and inhibition applications in real-time. The present *in silico* study based on experimental data is one of the very first attempts to build a real-time environment to further investigate the effects of modern control techniques in regulating internal arousal state. The main contributions of this research are summarized as follows.

- Building a simulation environment based on experimental data from wearable devices to relate the changes in skin conductance signal to one's internal arousal state.
- Simulating the required environmental stimuli functions for both high and low arousal sessions.
- Real-time and continuous tracking of the internal arousal state in response to the changes in the environmental stimuli via state-space methods and Bayesian estimation in the simulation framework.
- Estimating an internal arousal state based on peripheral physiological data that are collected using wearable devices, rather than directly monitoring of brain activity.
- Presenting a novel framework suitable to investigate the effects of various noninvasive strategies to regulate the internal stress-related state.
- Implementing a straightforward fuzzy controller to take advantage of the open-loop simulation results and regulating the estimated arousal state in both inhibitory and excitatory class of closed-loop systems.

3.2 Methodologies

Figure 11 illustrates an overview of the present research paradigm. The dashed box implies the offline process (A) and the solid box depicts the real-time closed-loop system

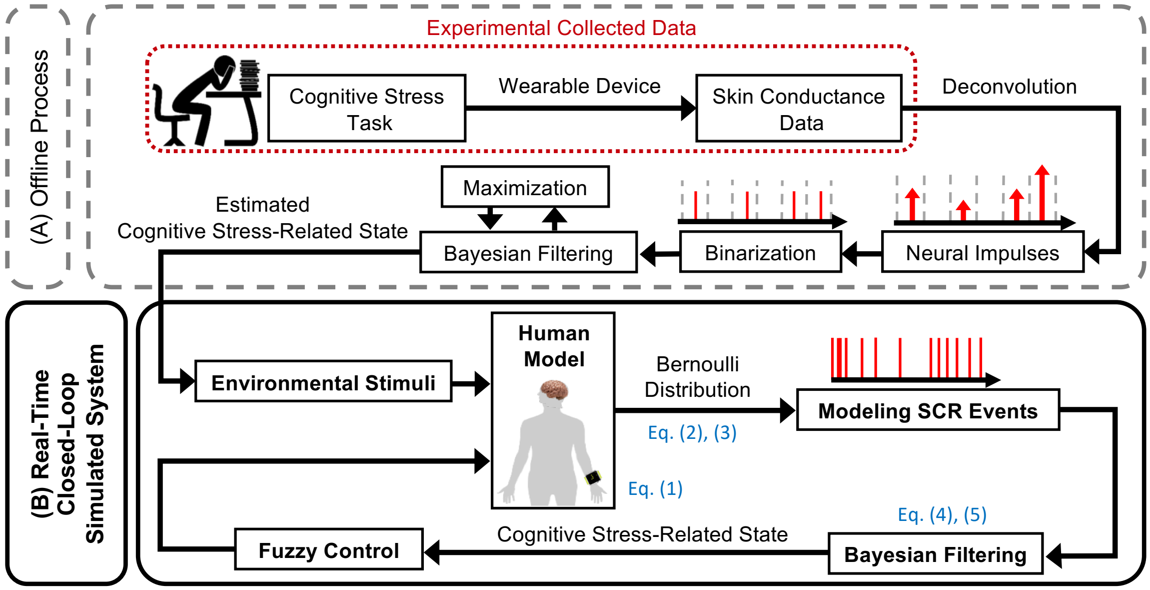

Figure 11: **Overview of closed-loop cognitive stress regulation.**

(B). In the offline process prior to the real-time implementation, we aim to build a simulation environment based on the experimental measurements [83] (red box in panel (A) of Figure 11). To this end, we focus on the collected skin conductance data from subjects during a cognitive stress task followed by a relaxation period. Performing deconvolution on skin conductance data, we take the information regarding the number, timings, and amplitudes of underlying neural stimuli associated with SCR [50, 94]. By binarizing the neural impulses, and employing a state-space approach, we follow the methods presented in [94, 95, 126] to relate the internal cognitive stress-related state to the changes in underlying neural impulses. Incorporating Bayesian filtering with an Expectation Maximization (EM) algorithm, we estimate the hidden cognitive stress-related state in an offline manner.

To design the real-time simulation environment, we take the estimated cognitive stress state as the output of the offline process and model the required environmental stimuli responsible for the changes in estimated state trajectory. Then, we generate two different sets of stimuli: one for causing low arousal (relaxation), and one for inducing high arousal (cognitive stress). Next, in a real-time simulation environment, we relate a cognitive stress-related state to the simulated SCR events using a state-space approach. In a state-space representation, human model simulates the skin conductance response (SCR) events by a

Bernoulli distribution. We estimate the hidden stress-related state using Bayesian filtering. To close the loop and regulate the estimated cognitive stress-related state in the simulation environment, we design a fuzzy control algorithm to derive essential control signals in real-time. Fuzzy controller takes the estimated stress state and regulates it with the derived control action in a closed-loop manner.

3.2.1 Experimental Collected Data Description

In this study, we focus on the Non-EEG Dataset for Assessment of Neurological Status [83] which is publicly available in the PhysioNet database [127]. In this experiment, twenty college students were subjected to different tasks: physical stress, cognitive stress, emotional stress followed by a relaxation period [83]. With the goal of investigating human responses to different types of stress, they have collected skin conductance, body temperature, and 3D accelerometer signals using the Affectiva Q Curve wearable device [83]. In addition, they have collected heart rate and blood oxygenation by the Nonin Wireless WristOx2 oximeter [83]. Among all of the collected physiological signals, it has been shown that SCR, which reflects changes in the sweat gland activities, carry important information regarding sympathetic nervous system arousal [105, 51, 50, 94, 52, 66]. Toward the goal of creating a closed-loop simulation environment for cognitive stress regulation, we extract skin conductance data that corresponds to the cognitive stress task and the relaxation periods [83, 94, 95].

The cognitive stress task in this experiment consists of an arithmetic task (i.e., counting backward by sevens, starting with 2485) for three minutes and the Stroop test (i.e., reading words including a color's name written in a different color ink and indicating the color ink) for two minutes. This arithmetic stress task is a good representative for the cognitive stressor [128]. In the relaxation task, subjects are asked to sit and listen to relaxing music. In the relaxation period, subjects have listened to a portion of *Binaural*, (i.e, a soothing music used in meditation [129, 130]). As the arithmetic task and the relaxation period are considered as the most representative cases, we select on these two parts to show the feasibility on

Table 4: Selected Subjects' Information.

Participants	Subjects ID	Gender	Age	Height [cm]	Weight [kg]
1	1	M	30	177	94
2	5	M	30	182	82
3	8	M	27	182	64
4	9	M	25	177	68
5	12	F	32	162	53
6	16	M	24	180	54

the most extreme arousal scenarios (i.e., high arousal vs low arousal [6]). In other words, we investigate these two parts of data to get insight about how the brain will respond during extreme cases. Skin conductance signal can be contaminated by measurement noise sources such as motion artifacts, range saturation and amplification factor changes [131]. The present work builds on a previously published dataset [50, 94, 95, 52]. So, highly noisy data was discarded prior to further processing. Selected subjects' information is presented in Table 4.

3.2.2 Deconvolution Algorithm

In the offline process, we perform a deconvolution algorithm to infer underlying neural stimuli. While we followed the approaches presented in [94, 50], in what follows we present a brief description of the deconvolution method.

Skin conductance signal $y_{SC}(t)$ contains two parts; tonic and phasic parts [94, 50]. The tonic which is slow varying in nature is highly related to thermoregulation and is a function of ambient temperature and humidity. The phasic part which includes faster changes is generated by sympathetic nerve fibers stimulating the sweat glands

$$y_{SC}(t) = y_P(t) + y_T(t), \tag{20}$$

where $y_P(t)$ and $y_T(t)$ stand for the phasic and tonic components, respectively. The phasic part $y_P(t)$ is extracted from the skin conductance signal by an algorithm such as cvxEDA [132]. The physiology behind the formation of the phasic component could be found in detail in [94, 50, 133, 134, 131] and will result in the following state-space model:

$$\dot{z}_1(t) = -\frac{1}{\theta_r} z_1(t) + \frac{1}{\theta_r} u(t) \qquad \text{(diffusion)} \tag{21}$$

$$\text{and} \quad \dot{z}_2(t) = \frac{1}{\theta_d} z_1(t) - \frac{1}{\theta_d} z_2(t) \qquad \text{(evaporation),} \tag{22}$$

where $z_1(t)$ and $z_2(t)$ are internal state and the phasic component, respectively. $u(t)$ represents the neural stimuli to the sweat glands to cause skin conductance responses (SCR). θ_r and θ_d are the rise and decay times of a single SCR. As the number of underlying neural impulses, which causing the SCRs, is also small, it leads us to employ a sparsity constraint when solving for $u(t)$. We model $u(t)$ as a finite summation of weighted, shifted delta functions

$$u(t) = \sum_{i=1}^{N} u_i \delta(t - \Delta_i), \tag{23}$$

where u_i represents the SCR's amplitude at time Δ_i, and N is the total number of samples in the neural stimuli signal and is proportional to the recording duration T_d and the input sampling frequency f_u ($N = T_d \cdot f_u$). We consider the phasic part $z_2(t)$ as the output in the state-space model

$$y_P(t) = z_2(t) + \mu(t), \tag{24}$$

where $\mu(t)$ is Gaussian measurement noise. If the signal is periodically sampled at T_y intervals to yield a total of M measurements, we can define the equivalent discrete-time observation y_k as

$$y_k = x_2(kT_y) + \mu_k. \tag{25}$$

Given all the discrete measurements $y_k = y_P(k)$ for $k = 1, 2, \ldots, M$, we aim to find $u(t)$ and estimate θ_r and θ_d. We take $z_1(0) = 0$ as an initial condition assuming that the sweat duct is empty at the beginning. The state-space solution for $z_2(kT_y)$ leads us to [92]

$$y_k = a_k y_0 + \mathbf{b}_k \mathbf{u} + \mu_k, \tag{26}$$

where $a_k = e^{-\frac{kT_y}{\theta_d}}$, $\mathbf{b}_k = \big[\frac{1}{(\theta_r-\theta_d)}(e^{-\frac{kT_y}{\theta_r}} - e^{-\frac{kT_y}{\theta_d}}) \quad \frac{1}{(\theta_r-\theta_d)}(e^{-\frac{kT_y-T_u}{\theta_r}} - e^{-\frac{kT_y-T_u}{\theta_d}}) \quad \frac{1}{(\theta_r-\tau_d)} (e^{-\frac{kT_y-2T_u}{\theta_r}} - e^{-\frac{kT_y-2T_u}{\theta_d}}) \quad \cdots \quad \frac{1}{(\theta_r-\theta_d)}(e^{-\frac{T_u}{\theta_r}} - e^{-\frac{T_u}{\theta_d}}) \quad \underbrace{0 \quad \cdots \quad 0}_{N-\frac{kT_y}{T_u}}\big]$, and $\mathbf{u} = [u_1 \quad u_2 \quad \cdots \quad u_N]^\top$ represents a sparse vector containing all the neural stimuli over the entire signal duration (i.e., very few of the u_i's are non-zero). Concatenating all the measurements into a single vector $\mathbf{y} = [y_1 \quad y_2 \quad \cdots \quad y_M]^\top$ we derive

$$\mathbf{y} = \mathbf{A}_\theta y_0 + \mathbf{B}_\theta \mathbf{u} + \boldsymbol{\mu}, \tag{27}$$

where $\mathbf{A}_\theta = [a_1 \quad a_2 \quad \cdots \quad a_M]^\top$, $\mathbf{B}_\theta = [\mathbf{b}_1^\top \quad \mathbf{b}_2^\top \quad \cdots \quad \mathbf{b}_M^\top]^\top$, $\boldsymbol{\mu} = [\mu_1 \quad \mu_2 \quad \cdots \quad \mu_M]^\top$, and y_0 is the initial condition of the phasic skin conductance signal. Here, T_y is an integer multiple of T_u. Letting $\boldsymbol{\theta} = [\theta_r \quad \theta_d]^\top$, to derive the SCR events $\mathbf{u}$, we aim to solve the optimization problem

$$\underset{\substack{\boldsymbol{\theta},\, \mathbf{u} \\ C\theta \leq b,\, \mathbf{u} \geq 0}}{\operatorname{argmin}} \; J(\boldsymbol{\theta}, \mathbf{u}) = \frac{1}{2}||\mathbf{y} - \mathbf{A}_\theta y_0 - \mathbf{B}_\theta \mathbf{u}||_2^2 + \lambda ||\mathbf{u}||_p^p, \tag{28}$$

where $C = \begin{bmatrix} -1 & 1 & 0 & 0 \\ 0 & 0 & -1 & 1 \end{bmatrix}^\top$, $b = [-0.1 \quad 1.4 \quad -1.5 \quad 6]^\top$ and λ is the l_p-norm regularization parameter determining the sparsity level on $\mathbf{u}$. Due to the unavoidable challenges in solving this optimization problem, we follow the approaches presented in [95, 92, 28, 25] and break it into two sub-problems. A desired coordinate descent approach can be formulated as

1. $\mathbf{u}^{(l+1)} = \underset{\substack{\mathbf{u} \\ \text{s.t. } \mathbf{u} \geq 0}}{\operatorname{argmin}} J_\lambda(\boldsymbol{\theta}^{(l)}, \mathbf{u})$
2. $\boldsymbol{\theta}^{(l+1)} = \underset{\substack{\boldsymbol{\theta} \\ \text{s.t. } C\boldsymbol{\theta} \leq b}}{\operatorname{argmin}} J(\boldsymbol{\theta}, \mathbf{u}^{(l+1)})$

To derive the final results, we iteratively solve the above sub-problems (for $l = 0, 1, 2, \cdots$) until convergence.

3.2.3 Human Brain Stimulus-Response Model

To model human brain responses, we use the state-space approach and assume that the hidden cognitive stress-related state is affected by the environmental stimuli

$$x_{k+1} = x_k + u_k + \eta_k, \tag{29}$$

where x_k is the hidden cognitive stress-related state, u_k is the control signal, $\eta_k = s_k + \nu_k$ is the environmental input, s_k is the environmental stimuli with the process noise $\nu_k \sim \mathcal{N}(0, \sigma_\nu^2)$ at kth time step. [95, 66]. Similar to [94, 95], we assume the probability of receiving SCR events follows a Bernoulli distribution

$$P(n_k|x_k) = q_k^{n_k}(1 - q_k)^{1-n_k}. \tag{30}$$

To relate probability q_k of observing a SCR event n_k to the stress state x_k, we employ a Sigmoid function

$$q_k = \frac{1}{1 + e^{-(\beta + x_k)}}, \tag{31}$$

where β is the person-specific baseline parameter. To derive β, we define the baseline state of the subject as zero ($x_0 = 0$) and look at changes from this baseline state. Then, we calculate β based on the average probability of an SCR occurring in the whole data $\big(\beta = log(\frac{q_0}{1-q_0}) - x_0\big)$ [94].

3.2.4 Cognitive Stress State Estimation

To estimate the hidden cognitive stress-related state, we follow the state estimation framework presented in [94, 95]. For the sake of completeness, we briefly review the methodology and employ it for further analysis. Given the simulated SCR events n_k, we estimate hidden state x_k and its corresponding variance term σ_k^2. At this stage of the offline process,

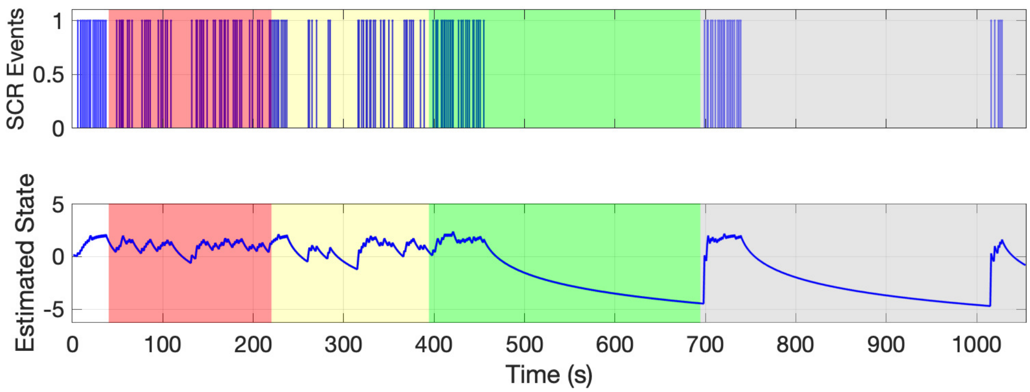

Figure 12: **Cognitive arousal state estimation in multiple tasks.**

we ignore environmental stimuli term, η_k, in (61):

$$\hat{x}_k = \hat{x}_{k-1} + (\hat{\sigma}^2_{k-1} + \sigma^2_\nu)\Big(n_k - \frac{1}{1+e^{-(\beta+\hat{x}_k)}}\Big) \tag{32}$$

$$\text{and} \quad \hat{\sigma}^2_k = \Big(\frac{1}{\hat{\sigma}^2_{k-1} + \sigma^2_\nu} + \frac{e^{(\beta+\hat{x}_k)}}{(1+e^{(\beta+\hat{x}_k)})^2}\Big)^{-1}. \tag{33}$$

where $\hat{x}_k$ and $\hat{\sigma}^2_k$ are the estimated hidden cognitive stress-related state and its variance, respectively. We use the EM algorithm presented in [94, 95], to find the σ^2_ν in (61) and initial values (i.e., x_0 and σ^2_0). The details of EM algorithm can be found in [126, 135]. It should be noted that $\hat{x}_k$ observed on both sides of (32) results in a nonlinear equation. Hence, Newton's method is employed to solve update equations. While for control design we only focus on cognitive stress (as the high arousal representative) and relaxation (as the low arousal representative) periods, we present the results of implementing the same modeling and estimation algorithms on the whole experiment in [83] to show the accuracy and the adequacy of proposed approach (see Figure 12) [94, 95]. The top panel and the bottom panel show the SCR events and the estimated arousal state, respectively. The shaded backgrounds correspond in turn to the instruction for cognitive stress task (white), arithmetic task (red), Stroop test (yellow), relaxation (green), and emotional stress (grey). Both arithmetic task and Stroop test are associated with the cognitive stress period.

As discussed, we perform EM algorithm to estimate the initial values (i.e., x_0 and σ^2_0)

Table 5: EM Algorithm Initialization.

Participant	Reference session	x_0	σ_0^2
1	High arousal	0.9134	0.00049
	Low arousal	0.8312	0.00032
	Combined sessions	0.8817	0.00041
2	High arousal	0.4473	0.00087
	Low arousal	0.3501	0.00071
	Combined sessions	0.4112	0.00080
3	High arousal	0.4334	0.00047
	Low arousal	0.3815	0.00032
	Combined sessions	0.4209	0.00041
4	High arousal	0.4501	0.00036
	Low arousal	0.3318	0.00024
	Combined sessions	0.4017	0.00031
5	High arousal	0.5333	0.00044
	Low arousal	0.4321	0.00039
	Combined sessions	0.4983	0.00042
6	High arousal	0.7434	0.00022
	Low arousal	0.7102	0.00015
	Combined sessions	0.7321	0.00019

[94, 126, 135]. This step is important in designing the real-time filter to estimate the state. Hence, we estimate these initial values in three different scenarios and compare the outcome. We derive the initial values using EM algorithm employing: (1) high arousal session, (2) low arousal session, and (3) combined sessions. The resulted initial values are presented in Table 5. To show the outcome in response to these different initializations, we present the open-loop results for participant 1 in Figure 13. In Figure 13, the top panel shows the results while the filter is initialized based on the high arousal session. The middle panel shows the results while the filter is initialized based on the low arousal session. The bottom panel shows the results while the filter is initialized using both high and low arousal sessions. In each panel, the top sub-panel displays the SCR events, while the bottom sub-panel displays the estimated cognitive stress-related state. The grey and white backgrounds belong to the high arousal (i.e., the cognitive stress task) and low arousal (i.e., the relaxation task) environmental stimuli, respectively.

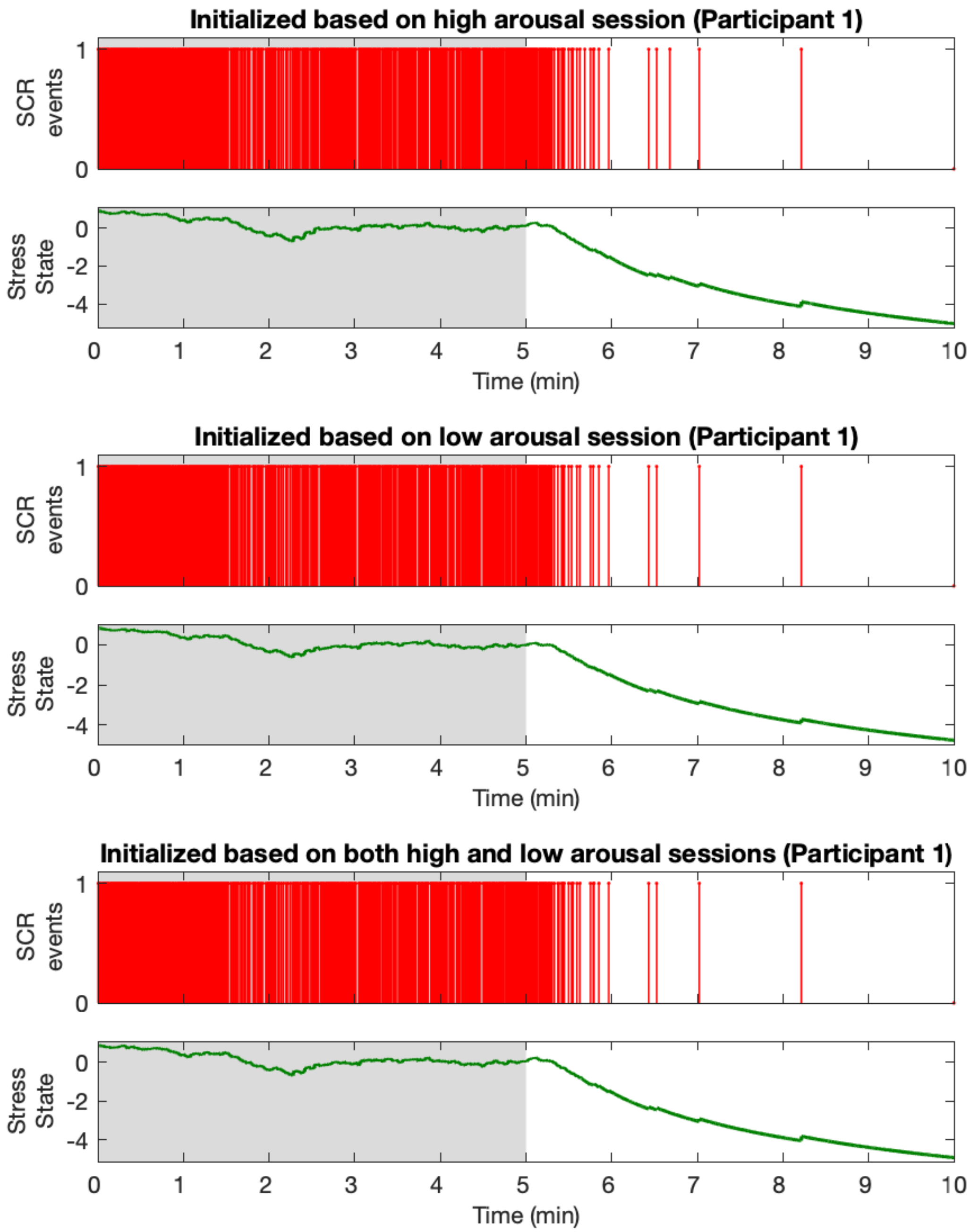

Figure 13: **Open-loop results based on different EM initialization.**

As presented in Figure 13, different initial values, which are derived based on different sessions, do not significantly affect the state estimation performance. The open-loop results presented in Figure 13 verify that the implemented Bayesian filter is sufficiently robust to the offline EM initialization process.

3.2.5 Environmental Stimuli Model

As presented in Figure 11, to design the real-time simulation environment, we model the environmental stimuli which is responsible for the fluctuations in estimated stress state. It is worth mentioning that in case of real-world settings, SCR events are obtained via deconvolving measured skin conductance signal [50, 52, 53] in a real-time manner. Analyzing the estimated stress-related state in both cognitive stress and relaxation tasks in the offline process, we aim to find the required environmental stimuli for both sessions. Examining the open-loop system and considering there is no control in (61) (i.e., $u_k = 0$), we derive $\eta_k = s_k + \nu_k = x_k - x_{k-1}$. Where x_k is the estimated cognitive stress-related state in the offline stage. By ignoring the process noise in this stage, we find time series for environmental stimuli s_k

$$\begin{pmatrix} s_1 \\ s_2 \\ \vdots \\ s_T \end{pmatrix} = \begin{pmatrix} x_1 - x_0 \\ x_2 - x_1 \\ \vdots \\ x_T - x_{T-1} \end{pmatrix}. \tag{34}$$

Investigating the offline open-loop results on all selected subjects, we analyze the general trend in s_k. To simulate a general environmental stimuli function s_k responsible for the changes in cognitive stress session, we consider the summation of sinusoidal harmonic functions. We also assume the behaviour of s_k in the relaxation period follows an exponential decay [6]. These assumptions are made to simplify solving the optimization problems and generating the environmental stimuli. Hence, we consider two environmental stimuli models: one for the cognitive stress task s_k^c, and one for the relaxation period s_k^r. We assume $s_k^c = \sum_{n=1}^{N} \alpha_n \cos(\omega_n k + \gamma_n)$, where N is the number of the harmonics, and α_n, ω_n, and

γ_n for $n = 1, .., N$ are the amplitude, frequency, and phase shift of each of the harmonics, respectively. Performing spectral analysis on each participant, we find the optimal number of harmonics N needed for estimating the high arousal stimuli. The regression parameters are estimated using a least square approach [136]. Similarly, for relaxation period, we assume an exponential decay as the environmental forcing function. More specifically, we let $s_k^r = ae^{bk}$ where the regression parameters a and b are being derived using least square regression method.

It should also pointed out that any changes to these assumptions (i.e., sinusoidal harmonics for high arousal, and exponential decay for low arousal) would change the resulted environmental stimuli functions. However, in real-world implementation of the proposed approach, by monitoring the skin conductance signal and performing the deconvolution algorithm on the captured signal, there is no need to apply these simulated environment functions.

By extracting the environmental stimuli associated with both high and low arousal, and including the process noise, ν_k, we incorporate them in the state-space model (61) and build the simulation environment. Consequently, we run the whole simulation system in both open-loop (i.e., $u_k = 0$) and closed-loop (i.e., $u_k \neq 0$) scenarios.

3.2.6 Control Design

Analyzing the system's open-loop behaviour in the simulation environment leads us to design the fuzzy structure including the membership functions, defuzzification, and inference engine [137]. We use the simulated environmental stimuli for both high and low arousal sessions and obtain the required knowledge about the system behavior in an open-loop manner. In the simulation environment, the human brain model generates SCR events in response to the various environmental stimuli. As a result, we see how the estimated stress state will fluctuate in response the changes in external environmental stimuli. This feature of incorporating insights about the system while designing the control structure is the main reason for choosing the fuzzy control.

In the proposed architecture, the real-time estimated cognitive stress-related state x_k is the input and the control signal u_k in (61) is the output of the fuzzy system. The heart of any fuzzy system, is its rule base. These rules are based on the constraints and insight about the system dynamics. To build a rule base applicable for multiple subjects, we form the rules as follows:

- If the estimated cognitive state is *low arousal*, then control is *excitatory*.
- If the estimated cognitive state is *neutral*, then control is *neutral*.
- If the estimated cognitive state is *high arousal*, then control is *inhibitory*.

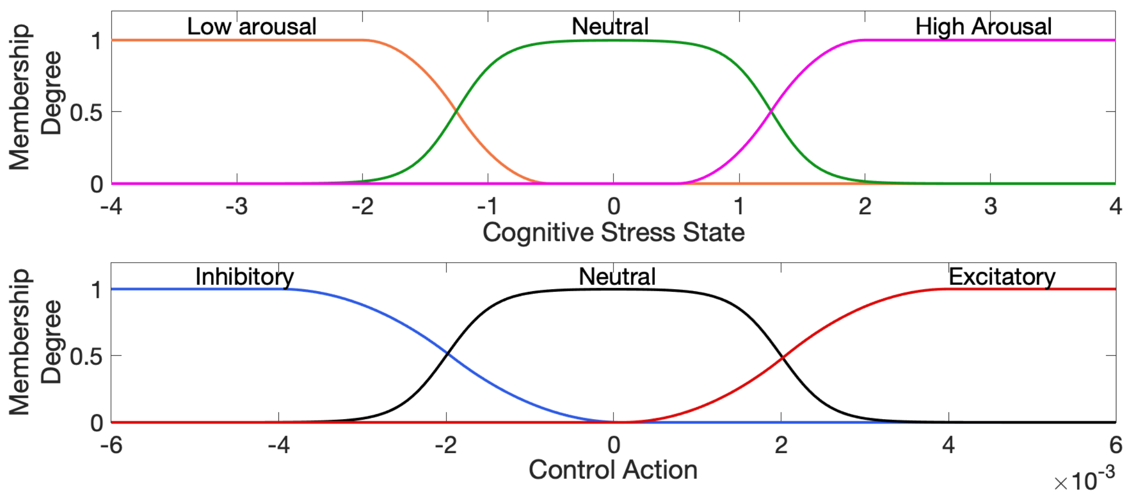

Figure 14: **Input and output membership functions.**

To convert the linguistic variables presented in the rule base to the crisp values, we impose the membership functions. These membership functions for both input and output values are depicted in Figure 14. In Figure 14, the top-panel shows the membership functions for the input (i.e., estimated cognitive stress-related state x_k). The bottom-panel shows the membership functions for the output (i.e., control signal u_k). As presented in top-panel of Figure 14, the input membership functions of the fuzzy system, which are related to the stress state, include three sets of functions; low arousal, neutral, and high arousal. The output of the fuzzy system, which is the control signal, consists of three sets; inhibitory, neutral, and excitatory (bottom-panel of Figure 14). The membership functions

Table 6: Input and Output Membership Functions (Figure 14).

Variable	Membership Function	Category
$\mu(x_k)$	$zmf(x_k, -2, 0.5)$	Low arousal
	$psigmf(x_k, 5.6, -1.2, -5.6, 1.2)$	Neutral
	$smf(x_k, 0.5, 2)$	High arousal
$\mu(u_k)$	$zmf(u_k, -0.004, 0.0001)$	Inhibitory
	$psigmf(u_k, 3500, -0.002, -3500, 0.002)$	Neutral
	$smf(u_k, 0.0001, 0.004)$	Excitatory

presented in Figure 14 are described in Table 6.

According to the rule base, once the system detects the high arousal, we need to have inhibitory control to decrease the number of SCR events and lower the stress state. On the other hand, when we deal with the low levels of cognitive stress state, we need excitation control to increase the number of SCR events and elevate the stress-related state. Similar to [6], we use *Mamdani engine* and *centroid* method for inference and defuzzification, respectively [124, 125].

3.2.7 Stability Analysis

According to the state-space model (61) and nonlinear stochastic observation (62), similar to any control technique, global stability could not be guaranteed within the proposed control approach [138]. However, by following the recent approaches that handle the stability analysis for control of probabilistic models [139], we aim to calculate a stability region. It will ensure that the state trajectory will be converged to the target levels in a finite time horizon [140]. In this approach, taking advantage of the simulation environment, as well as the real-time estimate of state mean, $\hat{x}_k$, we analyze the performance of the closed-loop system in response to multiple initial starting point, x_0, and derive the stability region [139].

According to Lyapunov's stability theory, the target point x^d is stable, if for any $\epsilon > 0$, there exists $\delta > 0$, such that $||x_k - x^d|| < \epsilon$ and $||x_0 - x^d|| < \delta$. A stability region, X^s, denotes to a subset in which $||x_k - x^d|| \to 0$ for all $x_0 \in X^s$ as $k \to \infty$. Here, we aim to obtain such a region which would guarantee that the difference between the current state and the target levels would be decreased as time evolves. So,

$$||x_k - x^d|| < \zeta ||x_{k-1} - x^d||, \tag{35}$$

for a fixed $\zeta < 1$. According to the positively invariant sets[139, 141], once the state transition starts within the calculated region (i.e., $x_0 \in X^s$) and (35) holds, it will never leave it.

3.3 Results

Implementing the proposed WMI architecture on selected subjects' simulated profiles (Table 4), we present the results in this section. Particularly, we illustrate the results in three different cases: (A) open-loop cognitive stress tracking, (B) closed-loop inhibitory, and (C) closed-loop excitatory. For each case, we consider two environmental stimuli models in the simulation: (1) cognitive stress stimuli, and (2) relaxing stimuli. Following the offline process presented in Figure 11, we simulate the environmental stimuli and run the simulation system in real-time. The final results are presented in Figure 15–17. In each case, we consider the environmental stimuli associated with the high arousal (cognitive stress) and low arousal (relaxation period) in the first and second half of the simulation, respectively.

3.3.1 Open-Loop

The main objective of presenting the open-loop case is to show how we could track the cognitive stress-related state without any control implemented (i.e., $u_k = 0$) in the developed simulation environment. In each panel of Figure 15, the top sub-panel shows the SCR events from the human model, the bottom sub-panel displays the estimated cognitive stress-related state. The grey background belongs to the high arousal environmental stimuli (i.e., the cognitive stress task), while the white background implies the low arousal environmental stimuli (i.e., the relaxation task). As observed in the top sub-panels of Figure 15, the number of SCR events significantly decreased in the second half of the simulation (i.e., relaxation period) because of the decreased sympathetic firing rate compared to the first half of the simulation (i.e., cognitive stress task). This variation in the number of SCR events results in a lower level of the estimated cognitive stress-related state (bottom sub-panels) in the relaxation period compared to the high arousal (cognitive stress) period. This open-loop case shows that our proposed algorithm is successful in tracking internal cognitive stress state in the real-time simulation environment.

3.3.2 Closed-Loop Inhibitory

In this case, we examine the performance of the proposed WMI architecture in lowering high levels of cognitive stress-related state caused by an high arousal environmental stimuli. By detecting high levels of cognitive stress state, the control systems attempts to regulate it in real-time. In each panel of Figure 16, the top sub-panel shows the SCR events from the human model, the middle sub-panel displays the estimated cognitive stress-related state, and the bottom sub-panel depicts the control signal. The grey background belongs to the high arousal environmental stimuli (i.e., the cognitive stress task), while the white background implies the low arousal environmental stimuli (i.e., the relaxation task).

As presented in the Figure 16, the high number of SCR events and the higher levels of estimated cognitive stress-related state (top and middle sub-panels) are detected by the system and control becomes active (bottom sub-panel). Then, employing the derived control actions results in fewer number of SCR events and a lower levels of estimated stress state in the first half of the simulation (i.e., cognitive stress period). This closed-loop inhibitory case validates the performance of proposed WMI architecture in lowering the estimated cognitive stress-related state levels in a real-time manner.

3.3.3 Closed-Loop Excitatory

As discussed earlier, it is important to keep one's cognitive stress levels within a desired range. Meaning, the cognitive stress state is sometimes considered as the cognitive engagement which is a positive stress (or eustress). In each panel of Figure 17, the top

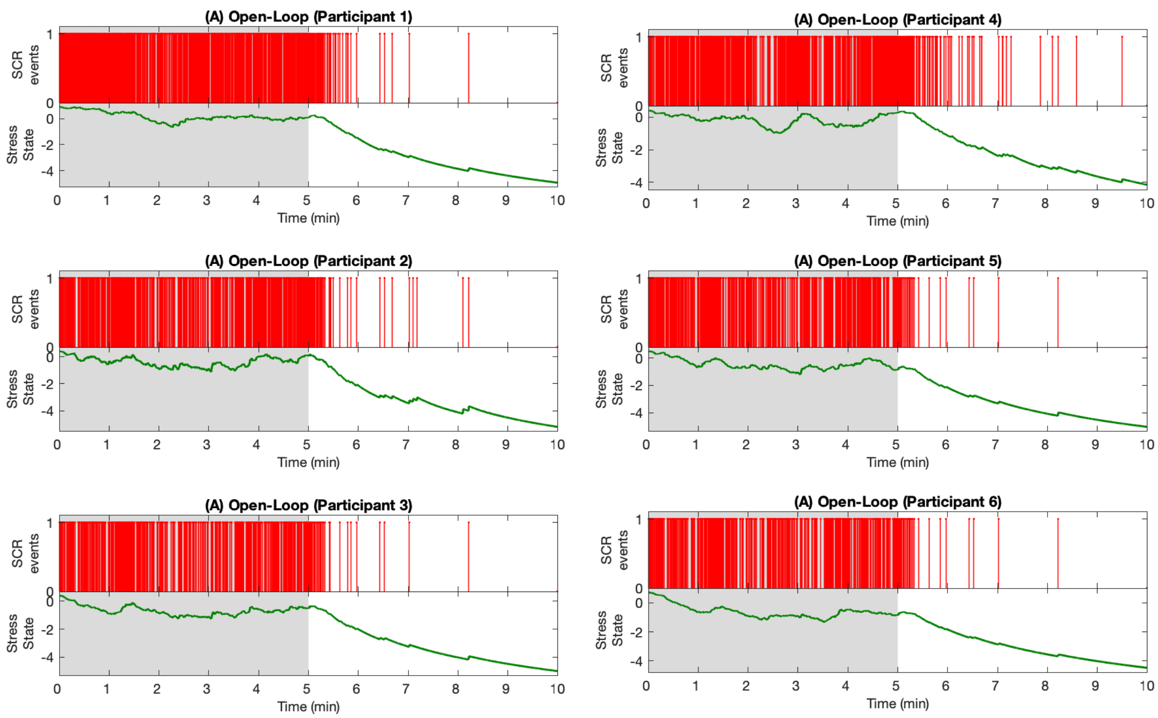

Figure 15: **Open-loop results of cognitive arousal estimation.**

sub-panel shows the SCR events from the human model, the middle sub-panel displays the estimated cognitive stress-related state, and the bottom sub-panel depicts the control signal. The grey background belongs to the high arousal environmental stimuli (i.e., the cognitive stress task), while the white background implies the low arousal environmental stimuli (i.e., the relaxation task). The main goal in this case is to prevent cognitive disengagement. More particularly, as observed in Figure 17, the small number of SCR events and the lower levels of estimated cognitive stress-related state (top and middle sub-panels) in the second half of the simulation (i.e., low cognitive engagement period) are detected by the system. Then, employing the control signals (bottom sub-panel) results in more SCR events and a higher estimated cognitive-related state levels in this period of low cognitive engagement. This closed-loop excitatory case illustrates how the proposed WMI approach is effective in elevating the cognitive stress-related state in a real-time manner.

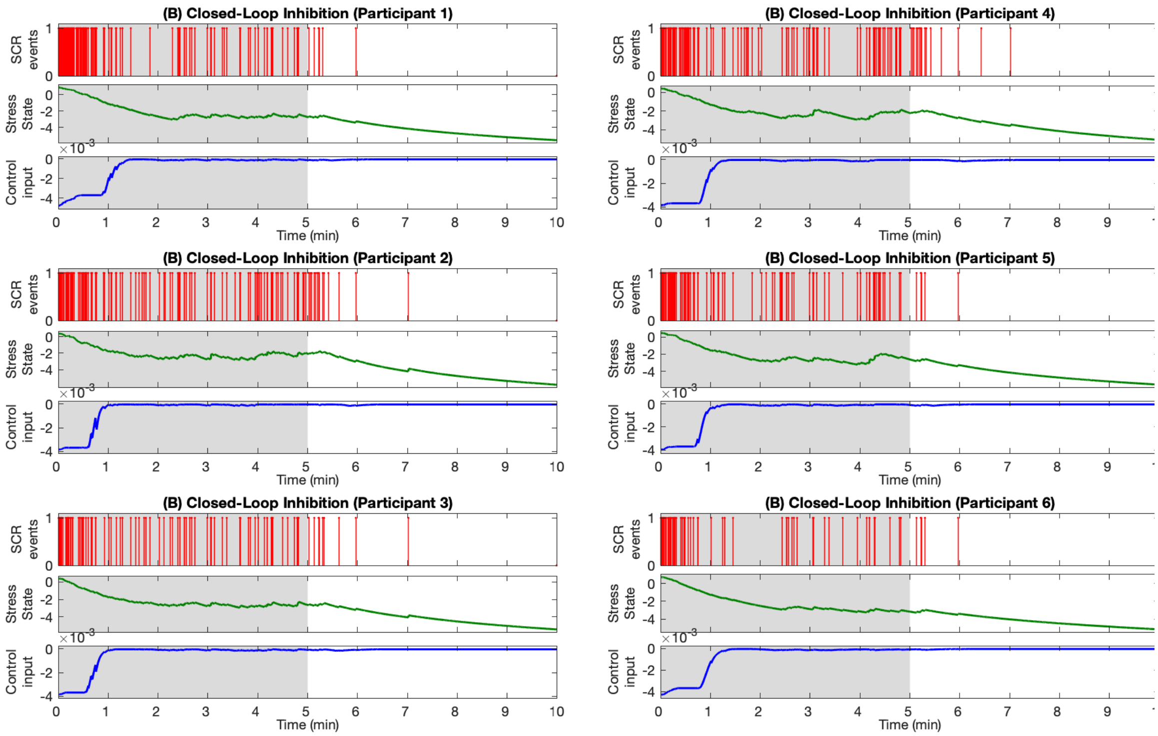

Figure 16: **Closed-Loop inhibition results in WMI architecture.**

3.4 Discussion

To design a simulation system for tracking and control internal cognitive stress state based on SCR events, we analyzed recorded data on multiple subjects in an offline process (Figure 11). Next, we presented two different models for environmental stimuli: one for cognitive stress (high arousal) and one for relaxation (low arousal). Taking advantage of simulated environmental stimuli, we designed the real-time system for further analysis. By modelling SCR events, we employed the state-space approach to relate the internal cognitive stress state to the changes in SCR events. Using Bayesian filtering, we estimated the hidden cognitive stress-related state in real-time. To close the loop and regulate the estimated stress state, we designed a fuzzy control system in the proposed WMI architecture.

To the best of our knowledge, this research is one of the very first to relate the cognitive stress state to the changes in SCR events and designing the control mechanism to close the loop in a real-time simulation system. In particular, we accomplished the task of closed-loop cognitive stress regulation in a simulation study based on experimental data. The

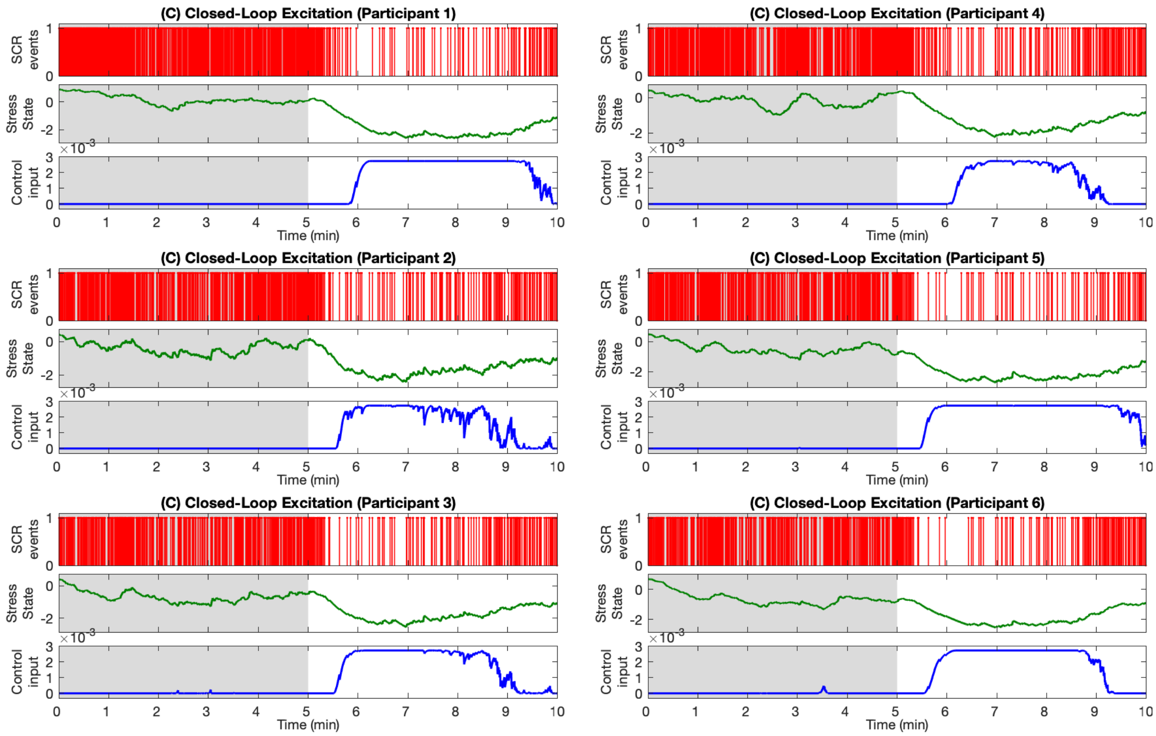

Figure 17: **Closed-Loop inhibition results in WMI architecture.**

final results verify that the proposed architecture has great potential to be implemented in a wrist-worn wearable device and used in daily life. To illustrate this idea, we presented three cases. In the first case (Figure 15), open-loop results demonstrated how the proposed architecture is successful in tracking internal stress state in both high and low arousal periods.

In the second case (Figure 16), we investigated the performance of the proposed approach in cognitive stress inhibition. Here, we assumed that the first half of the simulation (first 5 min in Figure 16) is associated with the undesired cognitive stress, which is due to an unpleasant stressful environment. The goal of lowering the estimated cognitive stress state is achieved by detecting the high arousal levels and applying the appropriate control action in the real-time system. Hence, the number of SCR events and the estimated cognitive stress levels have significantly dropped in the first half of the simulation compared to the same period of time in the open-loop case (Figure 15). Furthermore, since the main goal in this case was to inhibit cognitive stress-related state, and as the second half of the simulation is associated with the low arousal session, the control input goes to zero during this time span. The simulated human brain responses in the second half of the simulation, which is related to low arousal (relaxation) environment, is affected by the inhibitory control applied in the first half of the simulation. For example, in an experiment with a cognitive task followed by a relaxation task, if a subject listens to relaxing music during the cognitive stress task to decrease his/her stress levels, he/she will be even more calmed during the relaxation period compared to a subject who did not listen to relaxing music during the cognitive stress task. So, the more calmed response in the second half of the simulation is due to the applied inhibitory control in the first half of the simulation. In other words, for the closed-loop inhibition case, while we do not observe any control action during the second half of the simulation, the number of SCR events and estimated stress levels are lower in this period of simulation compared to the open-loop case.

The final case is related to the condition in which we assume the simulated subject is not cognitively engaged with the environment. Here, we aimed to increase the arousal state which is useful for concentration and productivity [2]. Implementing the proposed excitatory WMI architecture, the number of SCR events and the estimated cognitive stress-related state have been elevated remarkably in the second half of the simulation compared to the same period of time in the open-loop case (Figure 15). As a result, the proposed approach could be used to detect this low arousal state and increase it in real-time. It should be pointed out that, since the objective in this case was to excite cognitive stress-related state, and as the first half of the simulation is associated with the high arousal environmental stimuli, the control input will remain zero during this time period. From medical perspective, modulating the levels of cognitive stress and increasing eustress are potentially beneficial in individuals with anxiety and depression. In particular, patients with traumatic brain injury who suffer from both disorders could benefit from increased eustress to enhance their engagement during rehabilitation treatments [142].

To further analyze the performance of the closed-loop system, we present the following Figure 18 on achieved closed-loop results. Analyzing the final results on all simulated subjects, we present the effect of the real-time closed-loop system in decreasing (increasing) the number of SCR events and lowering (elevating) the levels of estimated stress state in Figure 18. As depicted in Figure 18, each row belongs to one subject. In each row, left panel (big green box) and right panel (big red box) are related to the inhibitory and excitatory closed-loop cases, respectively. In each colored box, the left sub-panel is related to the total number of observed SCR events in each high/low arousal session, while the right sub-panel depicts the difference in the average levels of stress state in each session. Red bars are associated with the first half of the simulation (i.e., high arousal or cognitive stress period), while the green bars are related to the second half of the simulation (i.e., low arousal or relaxation period).

By running the closed-loop system and observing the results, we analyze the performance of the proposed closed-loop system for both inhibitory (big green box in each row) and excitatory (big red box in each row) controllers. To better show the performance, we present the results of the implemented control system on both simulated SCR events (left sub-panels) and estimated stress levels (right sub-panels). In both closed-loop cases, we summed the number of SCR events in both high arousal (red bars) and low arousal (green bars) periods of the simulations. To analyze the performance of the closed-loop system on the estimated stress levels, we averaged the levels of estimated stress state over both high arousal (red bars) and low arousal (green bars) sessions (right sub-panels).

The decline in the total number of SCR events and the average levels of estimated stress state in the first half of the simulation (red bars) is due to the applied inhibitory controller in the high arousal session. Similarly, the increase in the total number of SCR events and the average levels of estimated stress state in the second half of the simulation (green bars) is due to the applied excitatory controller in the low arousal session.

To illustrate the performance of our proposed closed-loop architecture, we perform the t-test analysis on all six participants' results. To this end, we analyze the performance of the proposed closed-loop system for both inhibitory and excitatory controllers (See Figure 18). Hence, we investigate the results of implemented control system on both simulated SCR

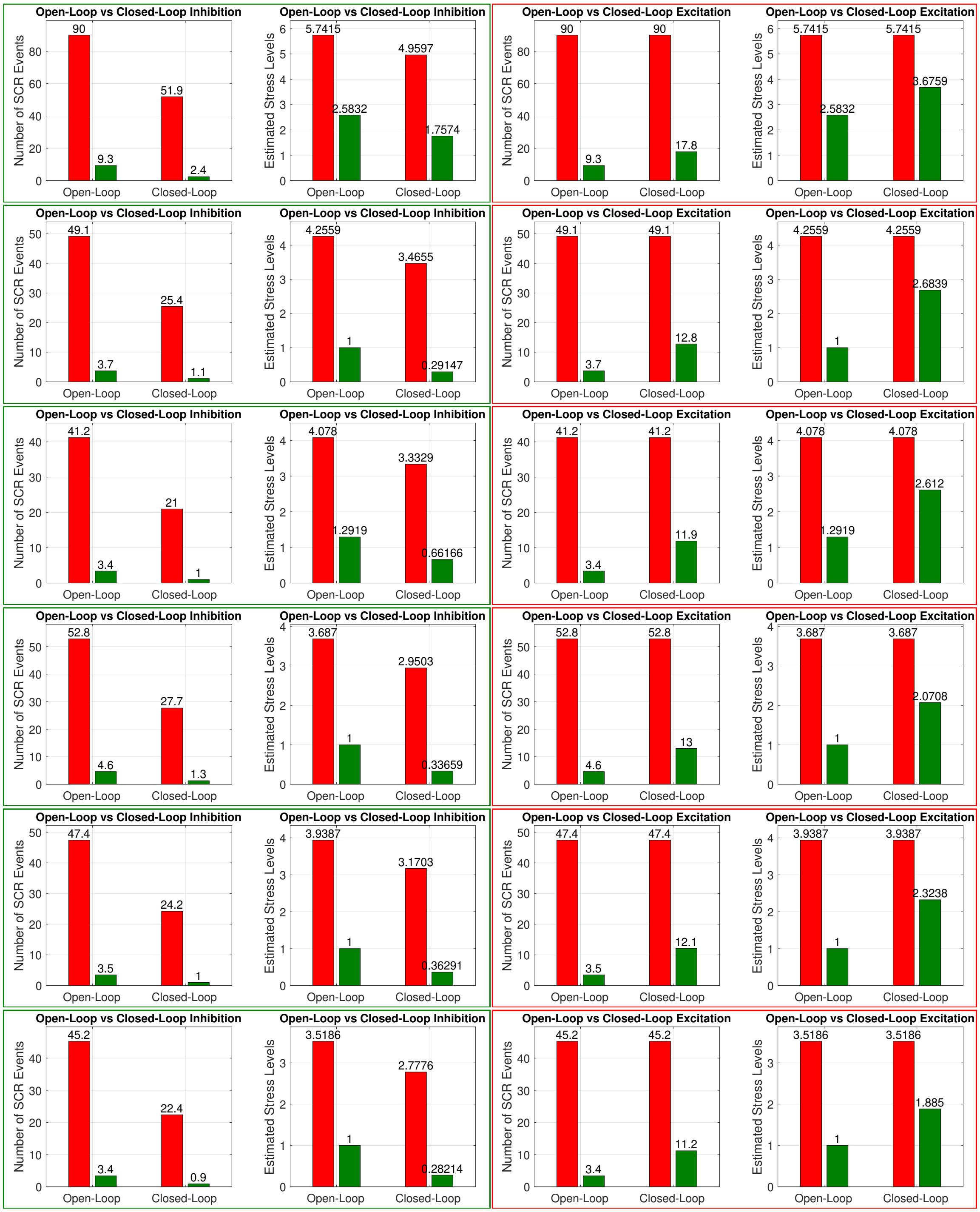

Figure 18: **Closed-loop performance evaluation for all participants.**

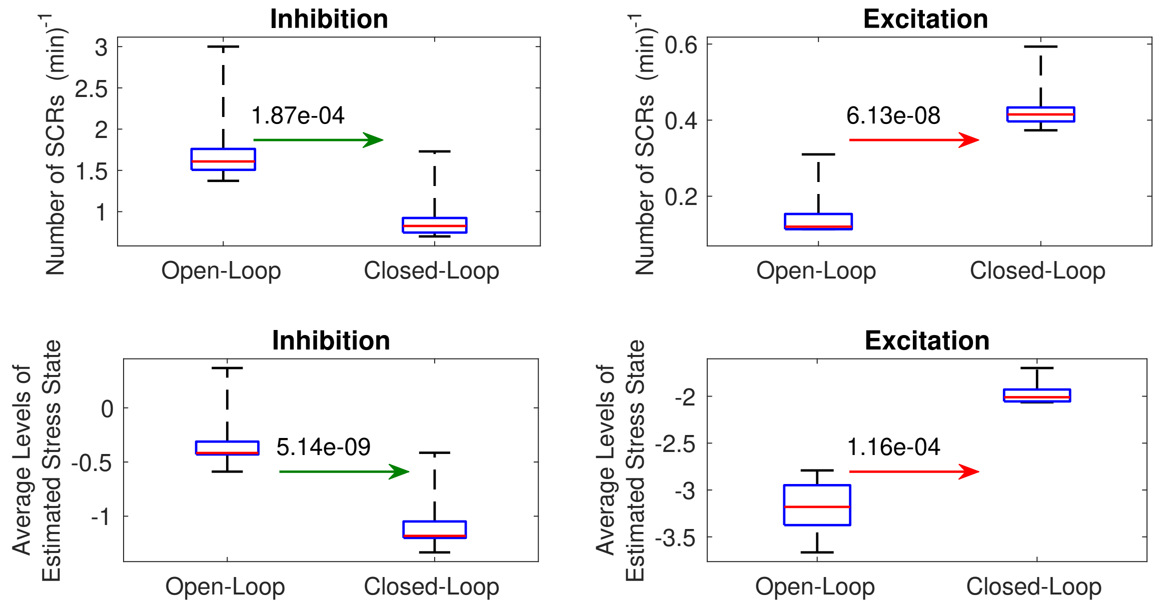

Figure 19: **Closed-loop performance analysis on all participants.**

events and estimates stress levels. We compute the number of observed SCR events per minute in both open-loop and closed-loop sessions for both high and low arousal periods (i.e., five minutes in each case). Moreover, to examine the effect of proposed architecture on the estimated stress state, we averaged the values associated with the estimated stress state in both open-loop and closed-loop sessions. The results of performing the t-test analysis on all simulated profiles are depicted in Figure 19. In Figure 18, the left panels show the performance of the inhibitory closed-loop system. The right panels are associated with the results of the excitatory closed-loop system. The top panels depict the performance of the closed-loop system in regulating the number of SCR events per minute. The bottom panels show the performance of the closed-loop system in regulating the estimated stress levels. The numbers on top of the arrows stand for the corresponding p-values.

The decrease in the number of SCR events and average levels of estimated stress state presented in left sub-panels of Figure 19 are due to the implemented inhibitory control system. Conversely, the increase in the number of SCR events and average levels of estimated stress state observed in right sub-panels of Figure 19 are because of applying excitatory control system. In each t-test analysis, the resultant p-values presented on top of the arrows confirm the efficiency of the proposed closed-loop architecture in both inhibitory and excitatory classes.

It should also be highlighted that different experimental environments would influence the results. In fact, this *in silico* study is based on the experiment in [83], in which the high and low arousal sessions are designed accordingly. In [83], the cognitive stress session is designed to ask the subjects to perform the Stroop and arithmetic tests, while the low arousal is derived by asking them to listen to relaxing music. While the performance of the proposed algorithm is validated by implementing it on multiple subjects' profiles, any changes in the reference experiment would further affect the subjects' skin conductance response and estimated stress state, accordingly.

In comparison to other available efforts that attempt to infer brain activity by directly monitoring it [82, 122, 143, 144], our proposed approach aims to detect the cognitive stress indirectly by collecting physiological signals from wearable devices and inferring the arousal state. Compared to the existing approaches, which classify the stress levels based on the physiological data and provide different classes of stress levels, the proposed approach tracks the stress state in a systematic way and in a continuous manner. The state-space model and Bayesian filter are in good agreement with the physiology underlying the sympathetic arousal activities [63, 145]. An increase in sympathetic arousal, which is a natural response to certain external stimuli, causes rise to measurable bio-signal such as skin conductance. The applied filter in this research takes the information presented in SCR changes and relates it to the hidden cognitive stress state.

Although scientists and engineers have performed research in the field of emotion regulation [117, 118, 119, 146, 147, 148], the present work is one of the first to present a simulation environment for designing closed-loop control algorithms based on the inferred arousal state. In the proposed architecture, the arousal decoder only requires a skin conductance signal that can be collected using wrist-worn wearable devices. Indeed, instead of using the raw skin conductance signal, we infer the underlying neural responses (i.e., the increase or decrease in sympathetic tone termed the skin conductance events rate) and use that information to decode the hidden arousal state. Then, we design the controller to close the loop. In this research, we demonstrated how the fuzzy control is successful in closing the loop and managing internal stress state. One of the main advantages of a fuzzy control structure is its expandability. This knowledge-based approach can be modified to cover different types of stress. The results on all simulated subjects' profiles verify the performance of the proposed architecture and show its feasibility to be implemented in the real world. Although the steps presented in section 3.2.7 provide the local stability condition in the proposed fuzzy controller in a finite time horizon window, it should be noted that finding the stability region in a closed form, and for an infinite time horizon, is not yet a tractable problem and needs further investigation [149]. Applying uncertainty-based control techniques is an alternative approach to establish a stable control system. While the proposed approach in this study employs point process analysis for state-space modeling and Bayesian filtering for the state estimation process, Li *et al.* proposed a novel adaptive fuzzy tracking and control system to handle the system nonlinearities both in the filter design and tracking procedures [150]. Another possible approach for closing the loop is to consider the model nonlinearities, which are present in the observations, while tracking the state and designing the control system [150].

In this *in silico* study, we made use of a publicly available dataset to create a virtual environment for real-time tracking and regulation of internal cognitive stress state. In what follows, we present some of the main challenges we faced in the design process. We used the skin conductance signal as a biomarker that carries valuable information about the autonomic nervous system and could be collected using wearable devices. Selecting clean profiles with fewer artifacts was one of the very first challenges addressed. Performing a deconvolution algorithm and Bayesian filtering to estimate the hidden cognitive stress-related state are the next important steps. To design the virtual environment, we successfully simulated environmental stimuli functions. This challenging step led us to evaluate the efficiency of the proposed architectures in stress tracking and closing the loop in real-time. The next challenging task is to design an appropriate control strategy for closing the loop and regulating the stress state. To this end, we employed fuzzy control as a powerful knowledge-based approach to enhance the closed-loop system with some expertise inference. Developing a unified fuzzy structure to efficiently regulate stress state in all simulated profiles is the next important step. By analyzing the open-loop results, we designed appropriate rule base, membership functions, and defuzzification methods to ensure handling inter-subject variability in the proposed architecture and closed the loop.

The present research is the first attempt to design a virtual environment based on the experimental data and relate the internal cognitive stress state to the changes in skin conductance. Taking advantage of the developed system, we track cognitive stress state in real-time. By designing the control algorithm, we demonstrated the feasibility of the proposed closed-loop architectures to inhibit and excite the estimated stress state in real world.

4 Enhancement of Closed-Loop Cognitive Stress Regulation using Supervised Control Architectures

4.1 An Overview of Supervised Control Architectures

In the modern world, any challenge might be a source of cognitive stress [151]. The fast-paced life has the potential to induce emotional and cognitive stress [152]. Feeling overwhelmed, anxiety, and agitation are among the symptoms associated with the high levels of cognitive stress [153]. Conversely, loss of cognitive engagement might also prevent individuals from following their goals [154]. A low level of positive stress, which is also called eustress, might cause memory problems, lack of motivation, and poor concentration [155]. It can also negatively affect persons' productivity in work places. While it is important to track internal stress levels [94], it is also critical to establish a mechanism for keeping internal cognitive stress state within a favorable range [6]. In this research, we aim to track the internal cognitive stress and propose novel control architectures to maintain it within the pleasant range. Advances in the fields of control and automation have opened avenues of applications in various area such as autonomous vehicles, robotics, and financial systems [156]. Recently, there has been much interest in investigating the use of modern control techniques in physiological systems [157]. Researchers are actively working on automating multiple clinical processes such as: artificial pancreas for regulating blood glucose levels [158, 159], feedback control mechanism in neuroprosthesis [160], internal energy regulation in patients with cortisol-related disorders [4, 23, 5], anesthesia delivery system for medically induced coma [48, 161, 162], and deep brain stimulation for treating neurodegenerative disorders [163]. Hence, we propose to employ control methods in internal cognitive stress regulation.

As internal cognitive stress state is a hidden state and can not be measured, we approach this problem indirectly [66]. In human body, the autonomic nervous system (ANS) is

Chapter four is mainly adopted from the accepted manuscript Fekri Azgomi, Hamid and Rose T. Faghih. "Enhancement of Closed-Loop Cognitive Stress Regulation using Supervised Control Architectures." IEEE Open Journal of Engineering in Medicine and Biology (2021).

responsible for a vast number of functions in response to the mental stress [53]. Changes in the arousal of the sympathetic nervous system (SNS) and parasympathetic nervous systems (PSNS), as branches of ANS, are presented in different physiological signals [164, 165]. In fact, the human brain employs SNS and PSNS to react to environmental stimuli. As a result of SNS and PSNS activation, we observe changes in physiological signals such as heart rate, respiration, and skin conductivity [166]. In response to internal/external stress stimuli, brain changes the sweat gland activation via SNS [167, 168, 169]. Consequently variations in sweat glands activation could be reflected in skin conductance signal monitored by sensors located in wrist-worn devices [170]. Skin conductance signal or electrodermal activity has been shown to be an indicator of mental arousal and cognitive stress [94, 171, 50, 95]. Therefore, we follow the approaches presented in [3] for further analysis. In the simulation system presented in [3], the hidden cognitive stress state is connected to the changes in skin conductance response (SCR) events via a state-space approach. Employing experimentally collected data, a real-time simulation system is developed to investigate the control design algorithm for closing the loop [3].

In the system presented in [3, 6], we took SCR events as the binary observation and estimated the hidden stress state in real time. While SCR time events carry important information about internal arousal state [94, 95], focusing on only the events' time as the binary observations and ignoring their amplitudes may cause loss of valuable details. As reported in several articles [50, 53], SCR amplitudes includes information about internal arousal state. In [66], a modified version of the filtering approach, which incorporates continuous-valued information from the SCR amplitudes (i.e., phasic amplitude and tonic levels) is presented. In their proposed approach, they have reported overfitting to the continuous values [66]. To solve this issue, authors in [56] proposed the marked point process (MPP) filtering approach. The MPP filter is applied to estimate internal arousal state from SCR events and their corresponding amplitudes to address the overfitting problem [56]. Compared to our previous approach [3], which we only included SCR time events as binary observations, here we enhance the state estimation process by incorporating the event amplitudes and estimate the internal state with MPP approach.

Exploiting the state-space representation which will lead us to track internal arousal state in a systematic way, we aim to invest in control system techniques to regulate the estimated arousal state and close the loop. In recent years, there exists a growing interest in employing control methods to automate various procedures [172, 173]. Researchers in [174] developed a novel boundary control scheme to regulate a rigid-flexible wing system and close the loop. He *et al.* considered distributed disturbances and designed a robust control strategy to reject them [175]. Similarly, in present research, we propose novel control approaches to close the loop, regulate the estimated stress state, and keep it within the desired range. The state-space model and the real-time estimation enable us to handle this physiological system as a control-theoretic problem. Hence, we propose to employ well-established model-based optimal control techniques, including linear quadratic regulator (LQR) and model predictive control (MPC) to close the loop. In both LQR and MPC, by optimizing corresponding objective functions, the optimal control would be derived in a real-time manner. The performance of both LQR and MPC depends on the selection of the objective functions [176]. Additionally, due to the nature of this physiological system, the inter- and intra-subject variability make the objective function selection process a challenging task. Among available approaches that address the challenges associated with the objective function selection, research in [177] proposed to use genetic algorithm for optimal tuning of MPC weights. Ramasamy *et al.* have established a mechanism to update the cost functions based on the system performance as well as the operator input in an offline manner [177]. In their proposed approach, they use an interactive decision tree to get feedback from the operator and infer the optimal gain weights. Researchers in [178] proposed a multi-scenario approach for designing a robust MPC system. They evaluated the operational system for each scenario and considered them while tuning the MPC. Van *et al.* also proposed to combine the genetic algorithm with a multi objective fuzzy decision making system for MPC tuning [179]. In their proposed approach, they rank the predefined objective functions based on the fuzzy systems [179]. Zhao *et al.* in [180] implemented a real-time system for adjusting the MPC tuning parameters in an adaptive cruise control system. The expert system proposed in [180] adjusts the tune parameters based on if-then rules. The corresponding cost functions are regulated based on the changes in sign of error terms [180]. To address the need for creating a system to dynamically update the control tune parameters, we propose to establish a supervised layer on top of the implemented model-based control systems. In the proposed architectures, a knowledge-based fuzzy system would supervise the LQR and MPC and adjusts the objective functions in real-time.

The combination of fuzzy systems and model-based control techniques have been explored in the literature [181, 182, 183]. The researchers in [181] have used fuzzy logic methodology to address the output constraints while designing the MPC. Researchers in [182] use the fuzzy system to decouple the modeling process and use LQR approach to control the power plant. In a similar approach, researchers in [183] apply fuzzy system to model building heating system and implemented the MPC for the process control. However, the present work is the first attempt to use a fuzzy system as the supervised layer to adjust tuning parameters in model-based control structures. Moreover, the proposed supervised control architectures provide a setting to include the relevant medical expertise to enhance the closed-loop system. These novel supervised control approaches could be further expanded to deliver adaptive and robust closed-loop characteristics. The key contributions of the present research include (i) implementing real-time MPP Bayesian-type filter to estimate the hidden arousal state from amplitude and timings of skin conductance response events, (ii) taking advantage of state-space representation of internal arousal state and utilizing model-based LQR and MPC structures to regulate the hidden state, and (iii) presenting novel supervised fuzzy-LQR and fuzzy-MPC architectures to adjust control tuning parameters in real-time.

4.2 Methodologies

An overview of the proposed closed-loop supervised control architectures is presented in Figure 20. We utilize the simulation system presented in [3]. The idea presented in

[3] is associated with employing experimental data [83] and simulating the environmental stimuli for two scenarios: cognitive stress and relaxation. In Figure 20, the orange dashed box displays the open-loop system (A). The solid green box, shows the supervised control architectures (D). We take the SCR events generated by human brain model and utilize the MPP Bayesian filter to estimate the cognitive stress state. To close the loop, we use the optimal control and model predictive control structures (B). We establish a knowledge-based fuzzy system, as a supervised layer (C), and apply expertise knowledge for updating the control tune parameters in a real-time manner (D).

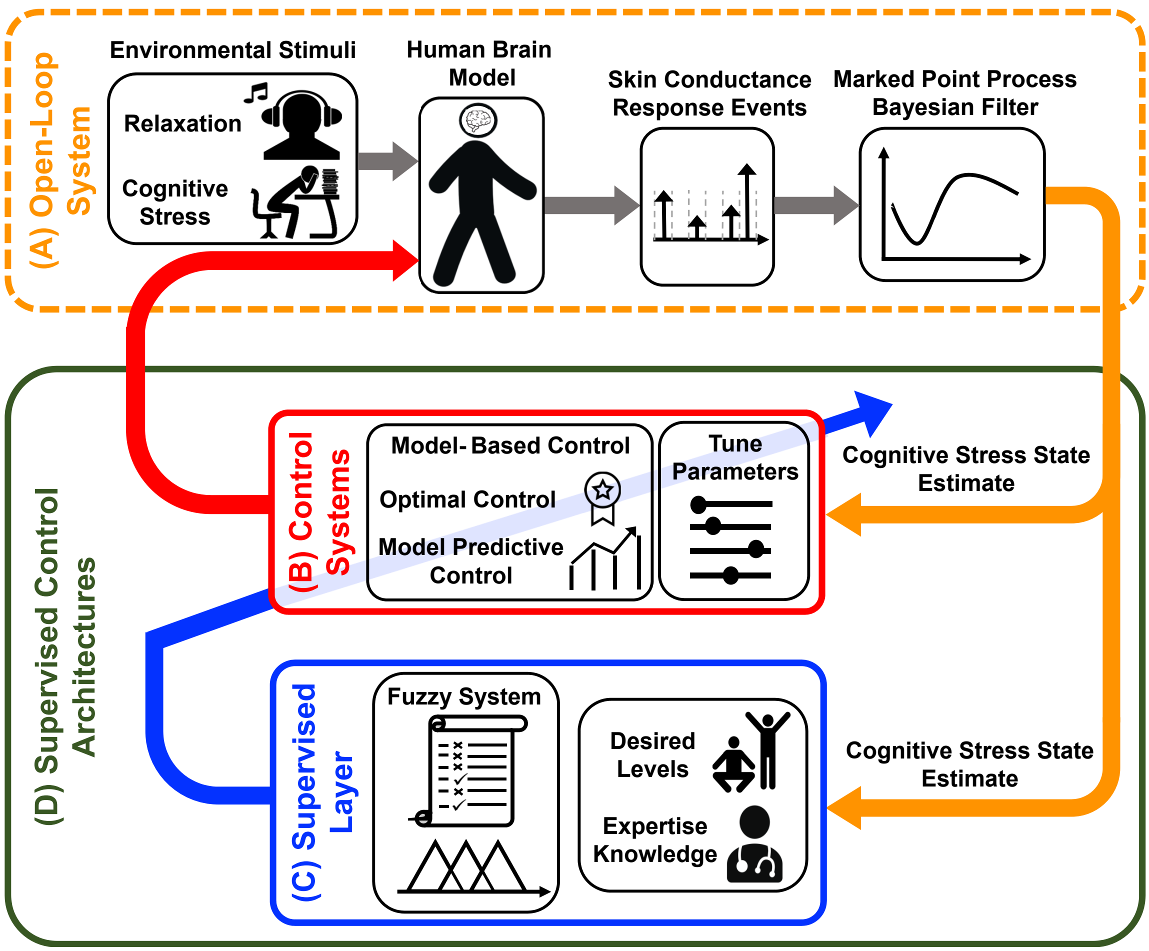

Figure 20: **Overview of supervised control architectures.**

In a state-space representation, we take simulated SCR events and estimate the hidden cognitive stress state in real-time. To this end, we employ the MPP Bayesian-type filtering ((A) in Figure 20). To design the control signal and close the open-loop system, we use the model-based approaches LQR and MPC ((B) in Figure 20). We establish a supervised fuzzy system on top of the LQR and MPC structures to automatically update the control tune parameters ((C) in Figure 20). The supervised layer executes this task based on feedback from the estimated cognitive stress state, desired state levels, and expertise knowledge.

4.2.1 Human Brain Stimulus-Response Model

We use the simulation model that is based on the experimental data [83] and presented in [3]. Non-EEG Dataset for Assessment of Neurological Status [83] is publicly available through the PhysioNet database [83, 127]. This study contains multiple experiments that induce different types of the stress to the subjects. The simulation model is based on two sessions: cognitive stress and relaxation, as the most representative cases [3]. In the original study [83], multiple physiological data were collected (i.e., skin conductance, body temperature, 3D accelerometer signals, heart rate, and blood oxygenation levels). In this research, we aim to track and regulate internal stress state by monitoring skin conductance measurements which were collected using Affectiva Q Curve wearable device to build the simulation environment. Similar to [94, 3], we analyze profiles associated with six selected participants whose data were clean and reliable. More information regarding this experiments and simulation system could be found in [83, 94, 3].

In the simulation system presented in [3], to model individual's brain responses, we relate the internal cognitive stress-related state to the changes in skin conductance signal by employing a first-order state-space model [94, 95]

$$x_{k+1} = x_k + s_k + \nu_k + u_k, \tag{36}$$

where x_k stands for the hidden stress-related state, s_k reflects the environmental stimuli, and $\nu_k \sim \mathcal{N}(0, \sigma_\nu^2)$ represents the process noise [66, 95]. u_k denotes the control input signal designed and applied in real-time to regulate the simulated stress-related state. It is worth mentioning that we include the s_k in (61) for the simulation purpose. In a real-world scenario, the human's internal cognitive stress state is affected by real environmental stimuli.

The details of modeling the environmental stimuli is presented in [3]. We also assume the occurrence of SCR events, n_k, follows a Bernoulli distribution with the probability function

$$P(n_k|x_k) = q_k^{n_k}(1 - q_k)^{1-n_k}, \tag{37}$$

where the probability q_k is connected to the stress state x_k, via a Sigmoid function [184]:

$$q_k = \frac{1}{1 + e^{-(\gamma + x_k)}}, \tag{38}$$

where γ is the person-specific baseline parameter that should be determined. Similar to [3], we first assume x_0 approximately equals to zero. We then calculate the γ based on the average probability of an SCR occurring in the whole data. According to (38), with increase in the levels of the cognitive stress state, the probability of receiving the SCR events also increases.

To incorporate all the information included in SCR events, we extend our previous research [3], which only employs the SCR events' time, to comprise the amplitudes associated with the SCR events. To this end, we assume there exists a linear relationship between the internal cognitive stress state x_k and the SCR amplitudes

$$r_k = \rho_0 + \rho_1 x_k + \omega_k, \tag{39}$$

where r_k is assumed to be the log transformation of the continuous-valued associated with each SCR event's amplitude. ρ_0 and ρ_1 are constant values derived by the offline expectation maximization algorithm [56, 3]. $\omega_k \sim \mathcal{N}(0, \sigma_\omega^2)$ is measurement noise with variance σ_ω^2. Accordingly, the joint density function on the probability of receiving the SCR event n_k with the corresponding amplitude r_k is

$$p(n_k \cap r_k|x_k) = \begin{cases} q_k \frac{1}{\sqrt{2\pi\sigma_\omega^2}} e^{\frac{-(r_k - \rho_0 - \rho_1 x_k)^2}{2\sigma_\omega^2}} & \text{if } n_k = 1, \\ 1 - q_k & \text{if } n_k = 0. \end{cases} \tag{40}$$

As presented in (40), the amplitude information will not be included when there is no impulse ($n_k = 0$) [56].

It is worth mentioning that the log transformation, discussed in r_k modeling (64), is only considered in this *in silico* study [66]. In real-world implementation of the proposed algorithm, we take amplitude and timing of SCR events to model and estimate cognitive arousal state [56].

4.2.2 Cognitive Stress State Estimation via Marked Point Process Filtering

Taking the SCR events time and their corresponding amplitudes (n_k, r_k), as the binary and continuous observations, we follow the MPP-based Bayesian filtering approach to estimate the hidden cognitive stress state x_k [56]. While the estimation process includes the forward filter and a backward smoother, we only implement the forward part of the filter for further *real-time* analysis. At each time step, a Gaussian approximation is applied to the posterior density. Combining the prediction and the update steps in the forward filter [56], we estimate the stress state and its variance using the recursive equations

$$\hat{x}_k = \hat{x}_{k-1} \ + \ n_k C_k \ + (\hat{\sigma}^2_{k-1} + \sigma^2_\nu)(n_k - q_k)\left(\frac{(1-n_k)\rho_1^2(\hat{\sigma}^2_{k-1} + \sigma^2_\nu) + \sigma^2_\omega}{\rho_1^2(\hat{\sigma}^2_{k-1} + \sigma^2_\nu) + \sigma^2_\omega}\right) \tag{41}$$

$$\text{and} \quad \hat{\sigma}^2_k = \left(\frac{1}{\hat{\sigma}^2_{k-1} + \sigma^2_\nu} + q_k(1 - q_k) + n_k D_k\right)^{-1}, \tag{42}$$

where,

$$C_k = \frac{\rho_1(\hat{\sigma}^2_{k-1} + \sigma^2_\nu)(r_k - \rho_0 - \rho_1 \hat{x}_{k-1})}{\rho_1^2(\hat{\sigma}^2_{k-1} + \sigma^2_\nu) + \sigma^2_\omega} \quad \text{and} \quad D_k = \frac{\rho_1^2}{\sigma^2_\omega}, \tag{43}$$

when there exists a SCR event ($n_k \neq 0$). Otherwise (i.e., $n_k = 0$), C_k and D_k equal zero ($C_k = D_k = 0$). In fact, the terms C_k and D_k presented in (41) and (42) incorporate the continuous-valued information (r_k in (64)) associated with the observed SCR event n_k at time step k. So, these terms are applied only when there exists a SCR event ($n_k \neq 0$). The probability q_k presented in (41) and (42) is being related to the state x_k via (63). So, it will results in a nonlinear problem that should be solved by employing numerical methods such as Newton-Raphson [56]. Consequently, we estimate the cognitive stress-related state $\hat{x}_k$ and its corresponding variance parameter $\hat{\sigma}_k$ in a real-time manner.

4.2.3 Control Design

In this part, we follow the goal of establishing a knowledge-based fuzzy system ((C) in Figure 1) as a supervised layer in model-based control approaches ((B) in Figure 1) to close the loop and regulate the estimated cognitive stress state. Particularly, we implement the fuzzy control structure as a supervised layer in LQR and MPC structures. In the supervised architectures, the fuzzy system will automatically adjust the control tune parameters in real-time. In what follows, we discuss both model-based control approaches.

LQR

Taking advantage of the state-space model and estimates of cognitive stress state, in LQR framework, we find the optimal solution of a predefined cost function. Hence, the obtained control signal u_k will minimize the objective function

$$J = \sum_{k=1}^{K} (\hat{x}_k - x_d)'_k Q(\hat{x}_k - x_d) + u'_k R u_k, \tag{44}$$

where K is the ultimate time of the process. Q and R are positive definite weight matrices to penalize the state deviations and the input efforts, respectively. x_d in (44) also stands for the desired levels of estimated stress state. Solving this optimization problem, the optimal control signal u_k is derived as a linear state feedback controller

$$u_k = -G_k \hat{x}_k, \tag{45}$$

where, the feedback gain G_k is derived recursively

$$G_k = (R + P_{k+1})^{-1} P_{k+1}, \tag{46}$$

where P_k is the discrete solution of the algebraic Riccati equation

$$P_k = Q + \Big(P_{k+1} - P_{k+1}(R + P_{k+1})^{-1}P_{k+1}\Big), \tag{47}$$

with the $P_K = Q$ initial condition.

MPC

To advance the optimal control LQR, we propose to use MPC structure as the second model-based control technique. In MPC framework, we first project the state values for whole time-window horizon [185]. Then, we derive the control input for all future prediction window and apply the first control action. To this end, we form a quadratic function that needs to be minimized

$$J_{\mathbf{u}_k} = \sum_{l=1}^{N_p} \hat{x}'_{k+l|k} Q \hat{x}_{k+l|k} + \Delta u'_{k+l|k} R \Delta u_{k+l|k}, \tag{48}$$

where N_p is the prediction horizon, $\hat{x}_{k+l|k}$ denotes to the state estimate prediction, and $\Delta u_{k+l|k} = u_{k+l+1|k} - u_{k+l|k}$ is the predicted variation of control input at each time step. Similar to LQR, Q and R are positive definite weight matrices to penalize the predicted state deviations and control efforts. To find the control signal, we aim to derive $\mathbf{u}_k = [u_{k|k} \quad u_{k+1|k} \quad \dots \quad u_{k+N_p-1|k}]'$ which is the control input for whole time horizon window prediction. To this end, we first define $\Delta\hat{x}_k = \hat{x}_k - \hat{x}_{k-1}$ and $\Delta u_k = u_k - u_{k-1}$. Using these terminologies, general state-space model (61) would be simply transferred to $\Delta\hat{x}_{k+1} = \Delta\hat{x}_k + \Delta u_k$. By considering the estimated state as the output equation ($y_k = \hat{x}_k$), and defining a new augmented variable, we build

$$x_a(k) = \begin{pmatrix} \Delta\hat{x}_k \\ y_k \end{pmatrix}. \tag{49}$$

So, the augmented system dynamics would be derived as

$$x_a(k+1) = A_a x_a(k) + B_a \Delta u(k) \tag{50}$$

$$\text{and} \quad y(k) = C_a x_a(k), \tag{51}$$

where the augmented system matrices in (50) and (51) are

$$A_a = \begin{pmatrix} 1 & 0 \\ 1 & 1 \end{pmatrix}, \ B_a = \begin{pmatrix} 1 \\ 1 \end{pmatrix}, \text{and} \quad C_a = \begin{pmatrix} 0 & 1 \end{pmatrix}. \tag{52}$$

Employing the output equation in the augmented system (51), we build the predicted future observation for whole prediction horizon N_p as

$$Y = W x_a(k) + Z\Delta U, \tag{53}$$

where:

$$Y = \begin{pmatrix} y(k+1|k) \\ y(k+2|k) \\ \vdots \\ y(k+N_p|k) \end{pmatrix}, W = C_a \begin{pmatrix} A_a \\ A_a^2 \\ \vdots \\ A_a^{N_p} \end{pmatrix}, \text{and} \ \ Z = C_a \begin{pmatrix} B_a & & & \\ A_a B_a & B_a & & \\ \vdots & & \ddots & \\ A_a^{N_p-1} B_a & \dots & A_a B_a & B_a \end{pmatrix}. \tag{54}$$

Now, the goal of finding control action u_k is converted to calculating the sequence of $\Delta U = \begin{pmatrix} \Delta u(k) & \Delta u(k+1) & \dots & \Delta u(k+N_p-1) \end{pmatrix}$. Consequently, this sequence will provide the predicted state variables $\begin{pmatrix} x_a(k+1|k) & x_a(k+2|k) & \dots & x_a(k+N_p|k) \end{pmatrix}$.

To find the sequence ΔU in (53), by knowing Y, W, Z and $x_a(k)$, minimizing the cost function presented in (48) would be equal to minimizing the objective function

$$J_{\Delta U} = Y' Q_T Y + \Delta U' R_T \Delta U, \tag{55}$$

where $R_T = R I_{N_p \times N_p}$ and $Q_T = Q I_{N_p \times N_p}$ are diagonal matrices for penalizing the control effort and deviations in the estimated state, respectively. Assuming there is no constraint, by setting $\frac{\partial J}{\partial \Delta U} = 0$, we derive the optimal solution

$$\Delta U^* = (R_T + Z^T Q_T Z)^{-1} Z^T Q_T W x_a. \tag{56}$$

It is also worth mentioning that positive definite matrices R_T and Q_T (i.e., $R \succ 0$, $Q \succ 0$) will guarantee the second order necessary condition in the computed ΔU^*. Finally, the first element in ΔU^*, which is $\Delta u(k)$, includes required control action signal for each time step (i.e., $u_k = u_{k-1} + \Delta u(k)$).

It should be also noted that by any selections of positive definite weight matrices Q and R, finding the optimal control would be equal to solving a quadratic program optimization problem (55). Solution ΔU^* in (56) only relies on the current state, past control input, and the desired level. Consequently, it will result in a closed-loop well-posed system that always has a unique solution [186].

In MPC design, while there exist methods for ensuring stability in infinite time horizon cases, utilizing a straightforward method for delivering rigorous stable property with finite time horizon remains challenging. In this research, to invest the stability, we evaluate prediction tail and consider terminal constraint [187]. Assuming terminal constraint $\hat{x}_{k+N_p} = x_d$ in (48) also provides with recursive feasibility. To this end, we consider the general form of optimal control input as Lyapunov function

$$V(k) = min \sum_{i=1}^{N_p} l(\hat{x}_k, \Delta u_k), \tag{57}$$

where $l(\hat{x}_k, \Delta u_k) = \hat{x}_k' Q \hat{x}_k + \Delta u_k' R \Delta u_k$. In $(k+1)$ time instant, the first component of $V(k+1)$ has been occurred and is no longer prediction. This unused part is called prediction tail (i.e., $[\Delta u_{k+1} \quad \dots \quad \Delta u_{k+N_p-1}]$) [187, 188]. For the sake of simplicity, we assume zero terminal constraint at this stage (i.e., $\hat{x}_{k+N_p} = 0$). Next, we follow the steps presented in [189] and derive $V(k+1)$

$$V(k+1) = V(k) - l(\hat{x}_k, \Delta u_0) + l(0, 0), \tag{58}$$

where initial cost $l(\hat{x}_k, \Delta u_0)$ is subtracted and corresponding cost for staying at terminal state is added (i.e, $l(0,0)$) [187]. Hence,

$$V(k+1) - V(k) \leq -l(\hat{x}_k, \Delta u_0). \tag{59}$$

Since $l(\hat{x}_k, \Delta u_0) \geq 0$, we may conclude that $V(k+1) - V(k) \leq 0$ and the Lyapunov function candidate is stable.

4.2.4 Supervised Control Architectures

As illustrated, in both LQR and MPC approaches, the selection of weight matrices Q and R plays an important role in the control design process. In fact, derived control gain in these model-based approaches highly depends on the weight matrices presented in (44) and (48). To update the weight matrices in real-time, we consider a knowledge-based system as a supervised layer in the design process. Therefore, we establish a fuzzy system on top of the pure LQR and MPC structures to (i) take the intrinsic advantages of the modeled dynamics employed in LQR and MPC, (ii) enhance the performance of the conventional architectures by adjusting the tune-parameters in real-time, and (iii) overcome the heuristic nature of the pure fuzzy control design (i.e., presented in [3]). To this end, we define the corresponding rule-base and fuzzy structure to change the tune-parameters (i.e., Q and R matrices) in real-time. On the basis of LQR and MPC, the larger Q and R values are, the more we penalize state deviations and control effort, respectively. Therefore, we set to use higher values for Q while the error between the estimated state and target state levels is large and decrease it once the estimated stress state is within a predefined range. Following a similar logic, while the error term between the estimated state and the desired value is large, we set not to penalize the control input and let it minimize the error. Once the estimated state tends to a predefined range of the target level, we set to increase the R and penalize the control effort to minimize it. Hence, we build the fuzzy rule base as presented in Table 7.

Table 7: Supervised Fuzzy Rule Base.

Rule number	IF	Then	
	e error	Q parameter	R parameter
Rule[1]	Large	Strong	Weak
Rule[2]	Moderate	Moderate	Moderate
Rule[3]	Small	Weak	Strong

To quantify the linguistic variables presented in Table 7, we employ the membership functions depicted in Figure 21. According to the rule base (Table 7), three sets of membership function for each input and output variables (i.e., error between the estimated state and the target level, Q parameter, and R parameter) are considered. For each error input e and the tune parameters Q and R, three membership functions are employed to quantify the linguistic variables presented in Table 7. Blue notations are for the error input and the green notations associated with the output tune parameters.

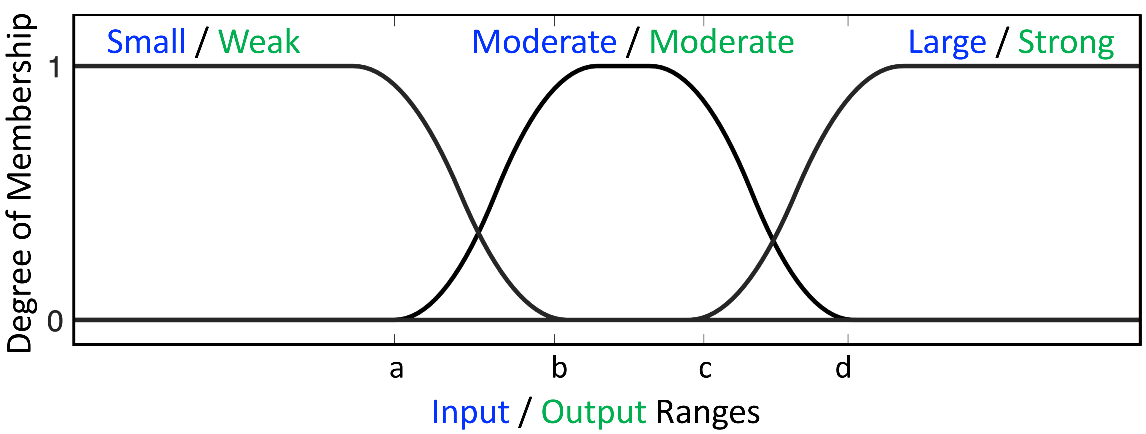

Figure 21: **Input and output membership functions in supervised architectures.**

For each sets of input and outputs in Figure 21, the middle functions belong to π-shaped membership functions with parameters a, b, c and d. The left one and the right ones are z-shape function with the parameter a and b and s-shape function with parameters c and d, respectively. To illustrate the shape of the membership function presented in Figure 21, we present the middle π-functions as:

$$\mu(x;a,b,c,d)=\begin{cases}0 & \text{if } x\leq a,\\ 2\left(\frac{x-a}{b-a}\right)^2 & \text{if } a\leq x\leq \frac{a+b}{2},\\ 1-2\left(\frac{x-b}{b-a}\right)^2 & \text{if } \frac{a+b}{2}\leq x\leq b,\\ 1 & \text{if } b\leq x\leq c,\\ 1-2\left(\frac{x-c}{d-c}\right)^2 & \text{if } c\leq x\leq \frac{c+d}{2},\\ 2\left(\frac{x-c}{d-c}\right)^2 & \text{if } \frac{c+d}{2}\leq x\leq d,\\ 0 & \text{if } x\geq d.\end{cases} \tag{60}$$

The s-shaped and z-shaped functions are spacial cases of the π-shaped function. The values associated with variables a, b, c and d for each input and output are presented in Table 8. We also use the *Mamdani* inference engine and *centroid* defuzzification to execute the fuzzy system in the proposed supervised control architectures.

Table 8: Membership Function Values in Supervised Layer (60).

Membership Function	Variable	a	b	c	d
Input **Error**	e value	0.1	0.3	0.5	0.7
Output **Fuzzy-LQR**	Q parameter	100	300	500	800
	R parameter	5	20	30	45
Output **Fuzzy-MPC**	Q parameter	1000	1500	2000	2500
	R parameter	3	6	9	12

4.3 Results

Implementing the model-based LQR and MPC methods in addition to the proposed supervised fuzzy-LQR and fuzzy-MPC approaches, we present the results. To show the performance of MPP filter in tracking cognitive stress state and demonstrate the efficiency of implementing the proposed supervised architectures, we present open-loop and closed-loop results. We follow the developed simulation environment in the order of first inducing cognitive stress and then causing the relaxation [3]. To analyze the accuracy of proposed control architectures, we present two closed-loop scenarios: inhibition for reducing the cognitive stress levels in the first half, and excitation to increase the levels of cognitive stress estimates in the second half of the simulation. Figures 22–27 depict the results associated with the Participants 1-6. In each figure, the top four panels show the closed-loop inhibition results. The bottom four panels show the closed-loop excitatory results. In each panel, the top two sub-panels show the SCR events along with their amplitudes in open-loop (orange color) and closed-loop (blue color) cases. In open-loop case, there is no control applied (i.e., $u_k = 0$ in (61)). The third sub-panel shows the estimated cognitive stress-related state. The bottom sub-panel shows the designed control implemented in real-time to close the loop and either inhibit or excite the estimated stress levels. The grey and white backgrounds correspond to the high and low arousal environmental stimuli, respectively (i.e., cognitive stress condition vs relaxing condition).

4.3.1 Closed-Loop Inhibition

The main goal in inhibitory closed-loop case is to design the control action to reduce the levels of the estimated cognitive stress state in the first half of the simulation. To investigate the effects of supervised layer, we present each model-based LQR and MPC methods along with their fuzzy supervised pairs (top four panels of Figures 22–27). As presented in Figures 22–27, control system detects high arousal levels and, by deriving the appropriate action, reduces the high levels of cognitive stress state in the first half of the simulation. As the second half is related to the low arousal period (or relaxation), there is no need to apply any control (i.e., $u = 0$). The left panels in Figures 22–27 present the results of applying LQR and supervised fuzzy-LQR controllers. The right panels in Figures 22–27 present the results of applying MPC and supervised fuzzy-MPC controllers.

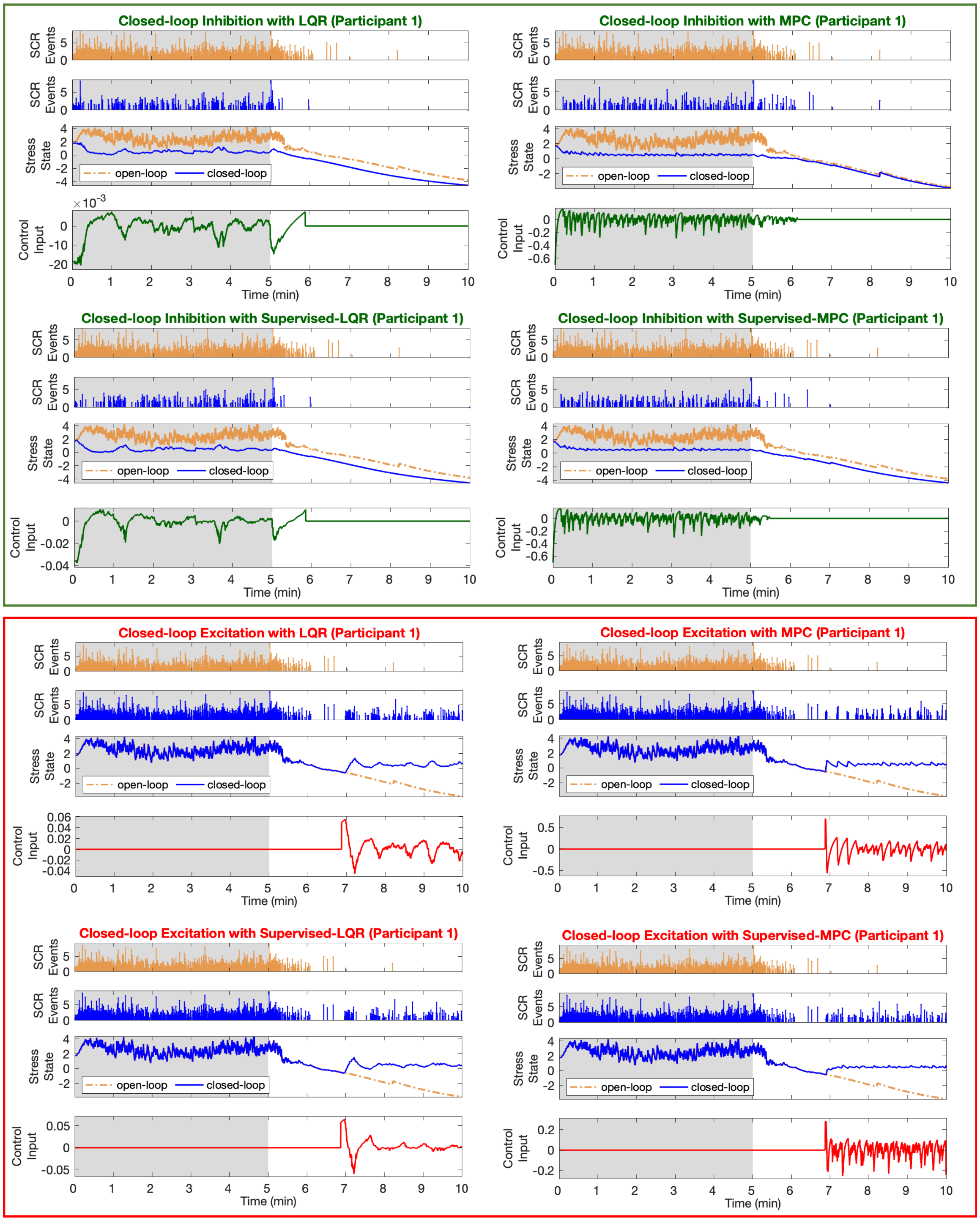

Figure 22: **Supervised inhibition and excitation results (Participant 1).**

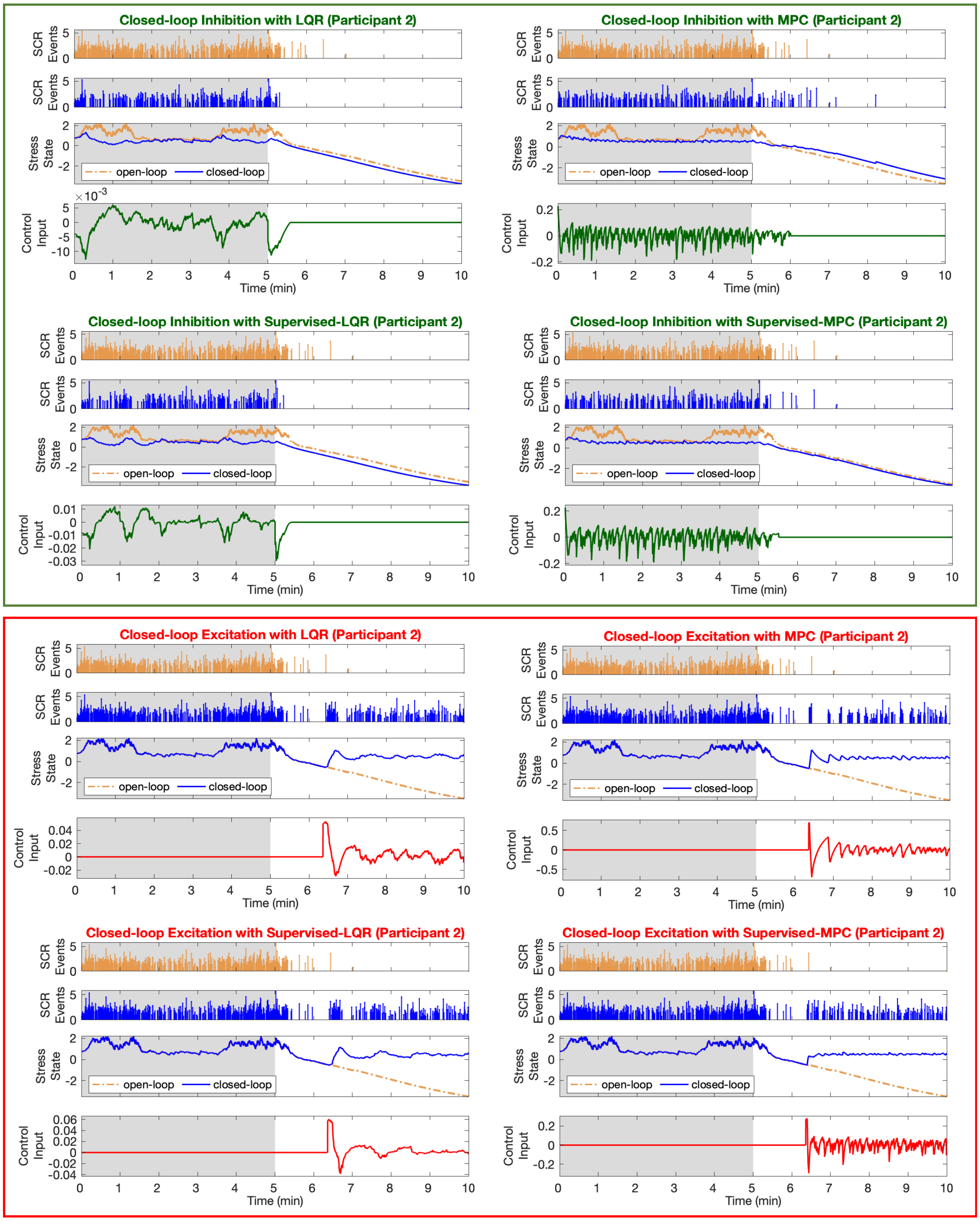

Figure 23: **Supervised inhibition and excitation results (Participant 2).**

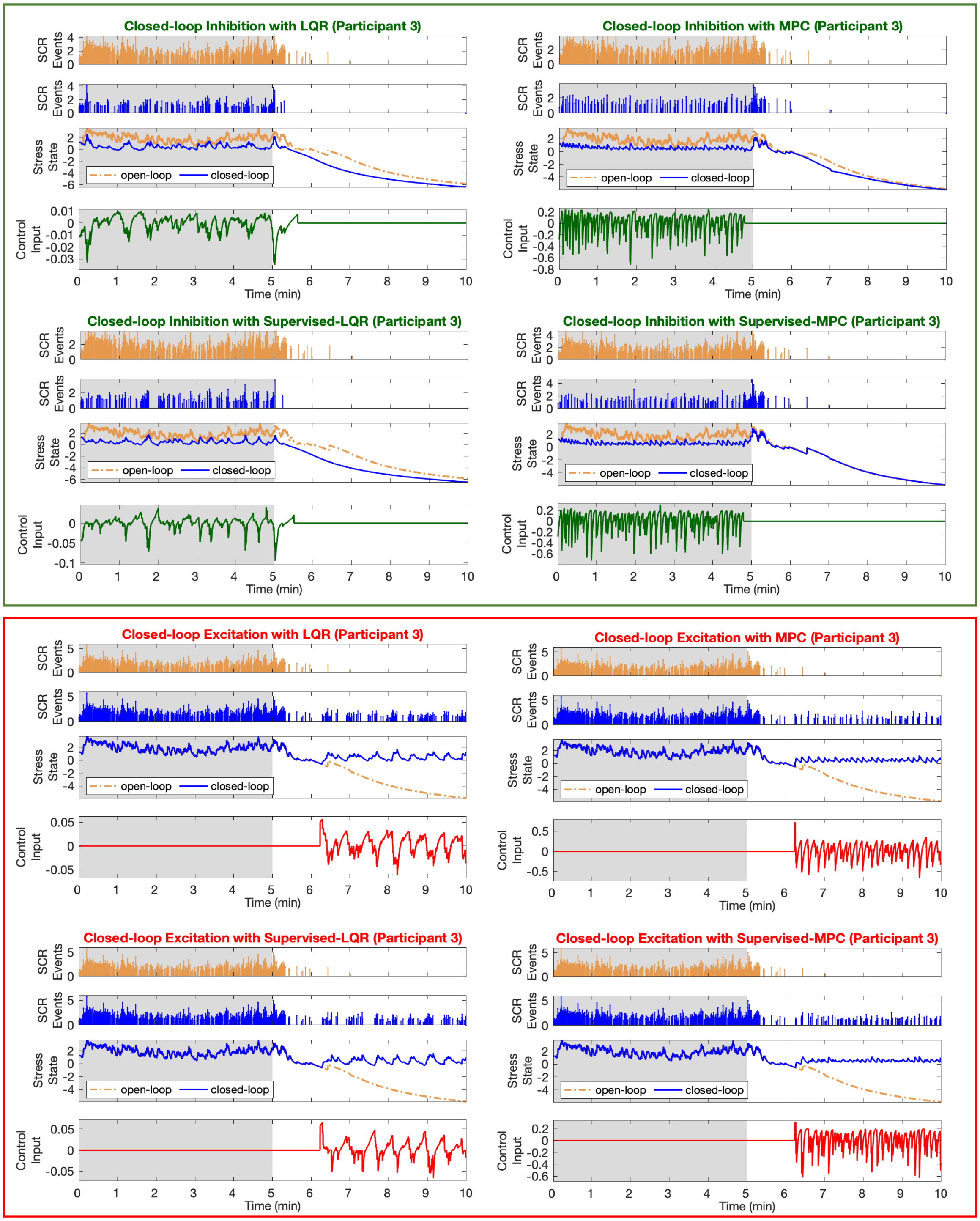

Figure 24: **Supervised inhibition and excitation results (Participant 3).**

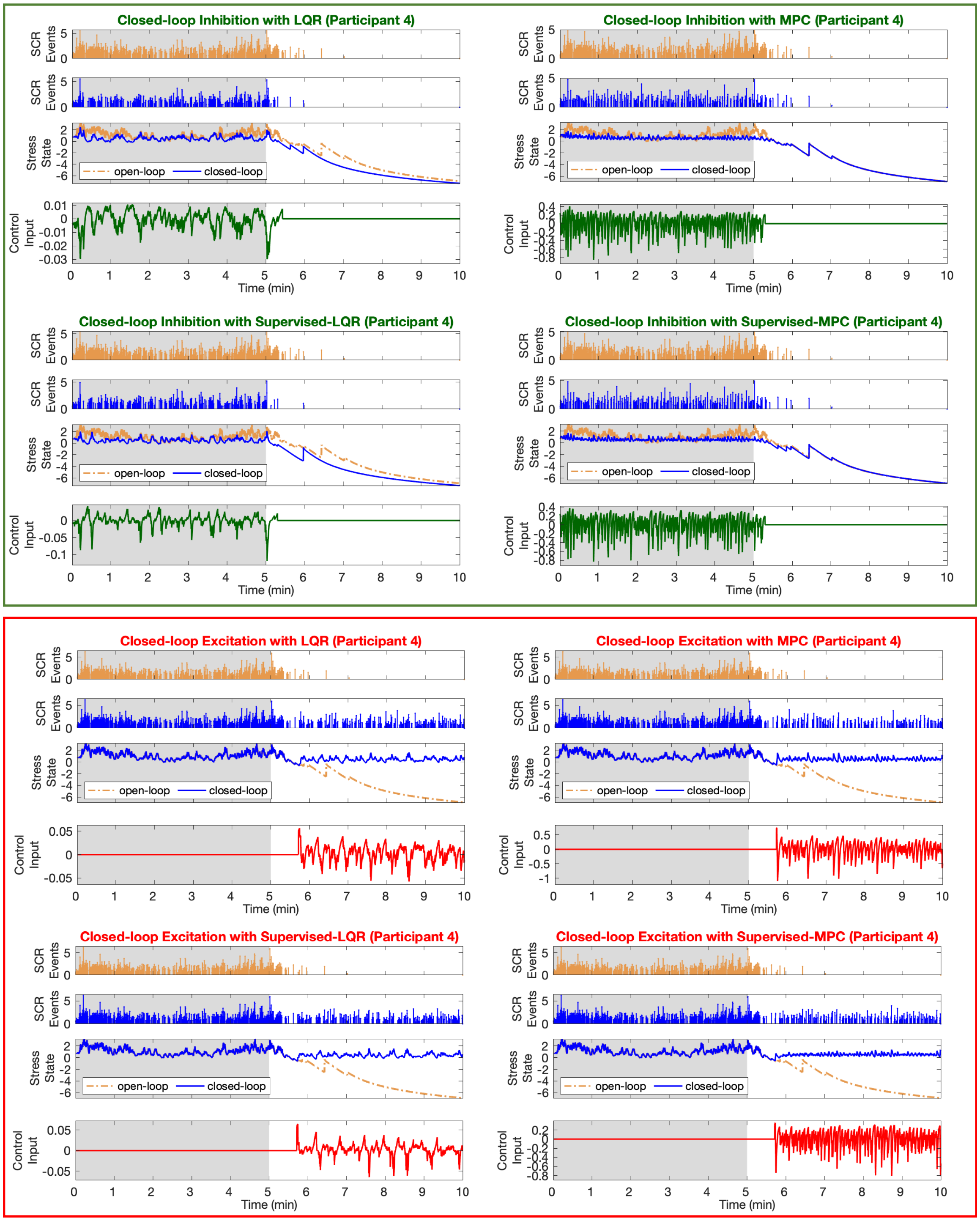

Figure 25: **Supervised inhibition and excitation results (Participant 4).**

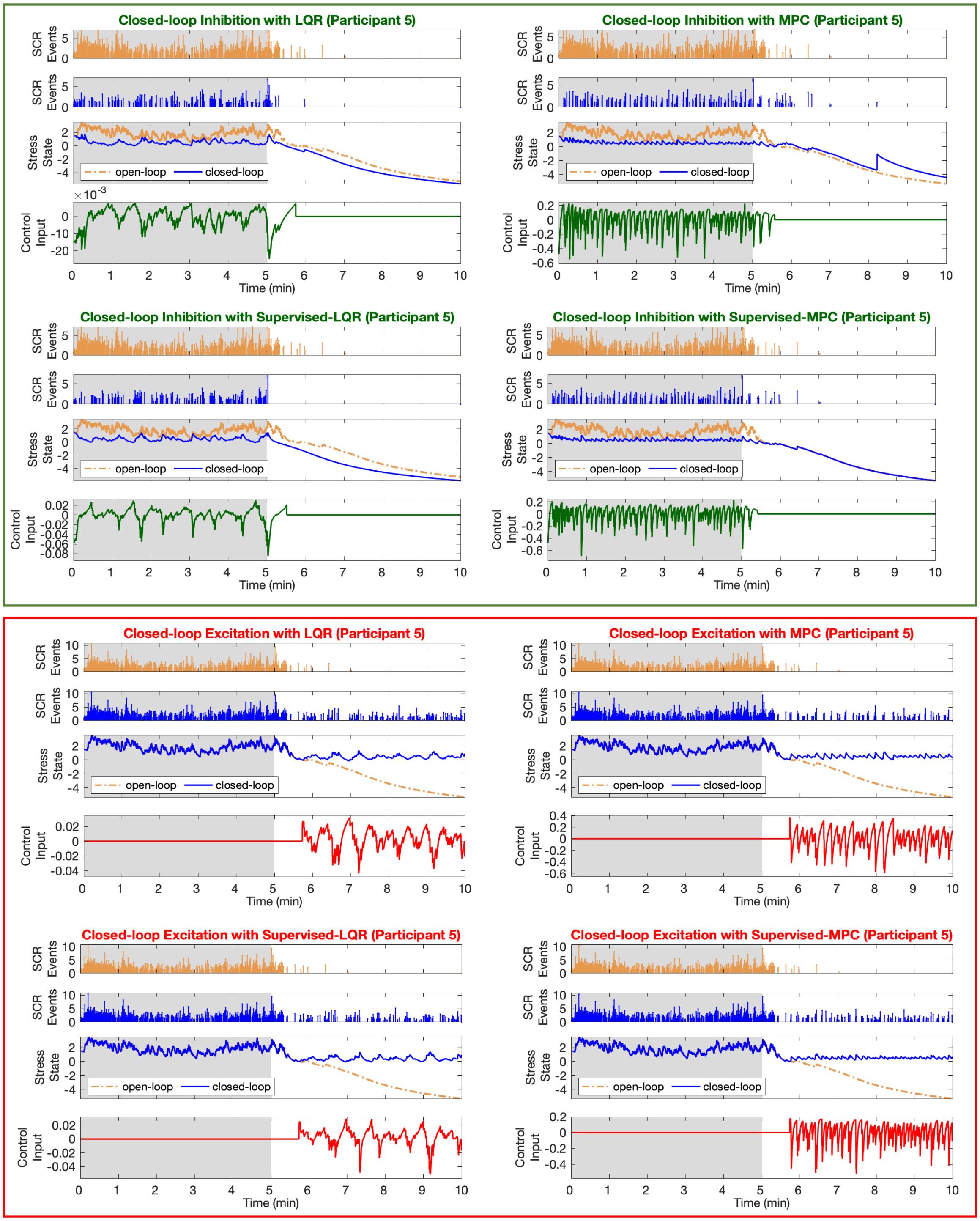

Figure 26: **Supervised inhibition and excitation results (Participant 5).**

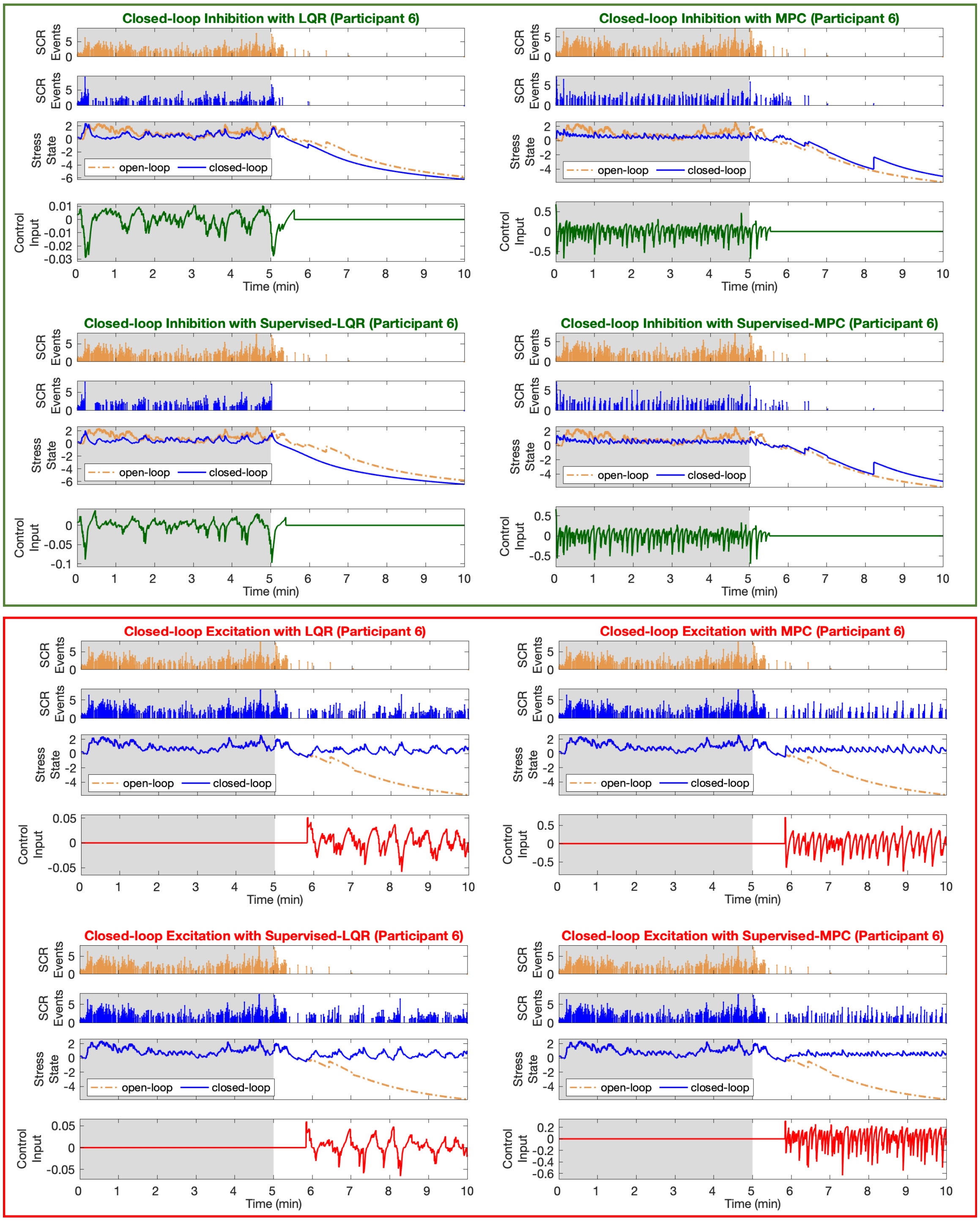

Figure 27: **Supervised inhibition and excitation results (Participant 6).**

4.3.2 Closed-Loop Excitation

The main objective in excitatory closed-loop case is to design the control action for increasing the levels of the estimated cognitive stress state in the second half of the simulation (with low arousal environmental stimuli). The results of applying each model-based LQR and MPC method along with their fuzzy supervised pairs are presented in bottom four panels of Figures 22–27. The excitatory control aims to detect the low levels of estimated cognitive stress state in the second half of the simulation and derive the appropriate control action to enhance it. As the first half is related to the high arousal (or cognitive stress stimuli), there is no need to apply any control action in this period (i.e., $u = 0$). The left panels in Figures 22–27 present the results of applying LQR and supervised fuzzy-LQR controllers. The right panels in Figures 22–27 present the results of applying MPC and supervised fuzzy-MPC controllers.

4.4 Discussion

In this research, as one of the very first in the context of closed-loop cognitive stress regulation, we proposed to use MPP filtering along with novel supervised control approaches to enhance the closed-loop control performance. In this regard, we utilized a simulation environment [3] based on the experimental data [83] to investigate the proposed methodologies in tracking and regulating internal cognitive stress state. To this end, we investigated skin conductance signal measurements and related them to the hidden stress state. To estimate the hidden state in real-time, we employed the MPP Bayesian-type filter and incorporated the information regarding the time and the amplitudes of SCR events.

The open-loop results, presented in Figures 22–27, illustrate the sufficiency of internal stress state tracking in response to the changes in simulated environmental stimuli. The higher numbers/values of SCR events (i.e., orange spikes in the first sub-panel) and levels of estimated stress state (i.e. orange graph in the third sub-panel) in the first half of the simulation is because of the applied high arousal environmental stimuli. Moving toward the low arousal session (white background in Figures 22–27), both the numbers/values of

SCR events and the estimated stress levels drop significantly, which is due to the induced relaxing environmental stimuli in the second half of the simulation. These changes in the estimated stress state are in good agreement with the changes in SCR events: higher levels of the estimated stress state in the first half of the simulation (i.e., cognitive stress), and lower levels for the second half of the simulation (i.e., relaxation). These results verify the efficiency of the state-space approach along with the MPP filter in tracking the cognitive stress state in real-time.

To regulate the estimated stress levels in a closed-loop manner, we proposed novel supervised control approaches. Taking advantage of the state-space model as well as the real-time state estimation, we first presented the results of applying model-based system-theoretic control approaches: LQR and MPC. As the performance in these controllers highly depends on adjusting tune-parameters (i.e., weight matrices), we proposed a novel knowledge-based fuzzy supervised layer to enhance the control systems and update the control tuning parameters in real-time. The fuzzy system performs this task based on the insights into the system and changes in the control design criteria. The results of the proposed supervised control approaches in both inhibition and excitation cases are presented in Figures 22–27.

In the closed-loop inhibition task (top four panels of Figures 22–27), the goal is to reduce the levels of the estimated stress state in the stress session (i.e., first half of the simulation). During this period, we assume that the environmental stimuli cause the subject to feel stressed. As a result, SNS would activate the sweat glands and skin conductivity would be increased. Consequently, more activation on SCRs would be observed (top sub-panels of Figures 22–27). By tracking the estimated stress state, the designed control system derives the required action for inhibition task. The control signal, presented in third sub-panel, is mainly active in the first half and results in lowering the stress state. The results of implementing supervised fuzzy-LQR approach is presented in the bottom left panel of Figures 22–27. Establishing a supervised layer on top of the LQR approach results in achieving the control goal more precisely (second sup-panel) with more optimized control efforts. The results of applying MPC and supervised fuzzy-MPC approaches to inhibit the cognitive stress state are depicted in the right panels of Figures 22–27. The control signal, presented in third sub-panel, is active in the first half of the simulation and tries to lower the estimated stress state. The results of implementing the supervised fuzzy system on top of the MPC system are presented in the bottom right panel of Figures 22–27. This supervised architecture has improved the state tracking accuracy. Besides, the supervised layer has resulted in achieving the control goal with a more optimal control effort.

Compared to the inhibition task, the goal of implementing excitation class of controllers is to excite the low levels of arousal state. It is also important to keep the positive stress (i.e., eustress) in a desired range. The second half of the simulation in the presented environment is assumed to induce low cognitive stress condition on the person. We assume that the similar condition might happen while the subject is supposed to concentrate on the task, but due to multiple possible reasons, the cognitive engagement would be lost. The goal of elevating the estimated stress-related state has been followed by both designing the LQR and MPC approaches. The results of closed-loop excitation task are presented in the bottom four panels of Figures 22–27.

First, by implementing the pure LQR method, the control action is active in the second half of the simulation, which is associated with the low arousal environmental stimuli. The LQR control action results in more activation in the simulated SCRs (first sub-panel), and leads to a higher level of estimated cognitive stress state (middle sub-panel). Enhancing the LQR closed-loop system by considering the supervised layer and updating the control tune-parameters in real-time, improves the results on both state tracking and control effort criteria. As presented in the bottom left panel of Figures 22–27, the supervised fuzzy-LQR has led to a more precise state tracking with more optimal control efforts. As the second model-based approach, we implemented MPC method. First, by applying the pure MPC, the control action (third sub-panel) has elevated the levels of estimated stress state (second sub-panel). By enhancing the pure MPC structure with supervised fuzzy layer, we derive the results presented in the bottom right panel of Figures 22–27. Similar to fuzzy-LQR,

Table 9: Closed-Loop Performance Analysis (Participant 1).

Closed-Loop Class	Controller	$\frac{1}{K_T}\sum_{k=1}^{K_T} e_k^2$	$\frac{1}{K_T}\sum_{k=1}^{K_T} \|u_k\|$
Inhibition	LQR	0.1642	0.0045
	Supervised LQR	0.1260	0.0052
	MPC	0.0658	0.0662
	Supervised MPC	0.0592	0.0590
Excitation	LQR	0.0664	0.0074
	Supervised LQR	0.0640	0.0054
	MPC	0.0181	0.0621
	Supervised MPC	0.0154	0.0338

Table 10: Closed-Loop Performance Analysis (Participant 2).

Closed-Loop Class	Controller	$\frac{1}{K_T}\sum_{k=1}^{K_T} e_k^2$	$\frac{1}{K_T}\sum_{k=1}^{K_T} \|u_k\|$
Inhibition	LQR	0.0630	0.0038
	Supervised LQR	0.0434	0.0047
	MPC	0.0394	0.0415
	Supervised MPC	0.0261	0.0402
Excitation	LQR	0.0744	0.0047
	Supervised LQR	0.0599	0.0051
	MPC	0.0123	0.0444
	Supervised MPC	0.0149	0.0294

the supervised fuzzy-MPC architecture has improved the performance of the closed-loop excitation in both tracking accuracy and control effort minimization. To better evaluate the results of establishing supervised fuzzy system on top of model-based LQR and MPC approaches, we analyze the closed-loop results. Hence, we consider two criteria: (1) the effectiveness in reducing error term and improving the state tracking, and (2) achieving the closed-loop goal with optimized control efforts (see Tables 9–14).

Table 11: Closed-Loop Performance Analysis (Participant 3).

Closed-Loop Class	Controller	$\frac{1}{K_T}\sum_{k=1}^{K_T} e_k^2$	$\frac{1}{K_T}\sum_{k=1}^{K_T} \|u_k\|$
Inhibition	LQR	0.2356	0.0076
	Supervised LQR	0.1841	0.0138
	MPC	0.1059	0.1385
	Supervised MPC	0.0611	0.1249
Excitation	LQR	0.1416	0.0107
	Supervised LQR	0.1381	0.0113
	MPC	0.0580	0.1489
	Supervised MPC	0.0372	0.0931

Table 12: Closed-Loop Performance Analysis (Participant 4).

Closed-Loop Class	Controller	$\frac{1}{K_T}\sum_{k=1}^{K_T} e_k^2$	$\frac{1}{K_T}\sum_{k=1}^{K_T} \lvert u_k \rvert$
Inhibition	LQR	0.1429	0.0059
	Supervised LQR	0.1119	0.0102
	MPC	0.3438	0.1390
	Supervised MPC	0.2780	0.1235
Excitation	LQR	0.0967	0.0115
	Supervised LQR	0.0954	0.0085
	MPC	0.0736	0.1699
	Supervised MPC	0.0494	0.1309

Table 13: Closed-Loop Performance Analysis (Participant 5).

Closed-Loop Class	Controller	$\frac{1}{K_T}\sum_{k=1}^{K_T} e_k^2$	$\frac{1}{K_T}\sum_{k=1}^{K_T} \lvert u_k \rvert$
Inhibition	LQR	0.1584	0.0093
	Supervised LQR	0.1225	0.0107
	MPC	0.1110	0.1214
	Supervised MPC	0.0859	0.1093
Excitation	LQR	0.0823	0.0151
	Supervised LQR	0.0868	0.0081
	MPC	0.0348	0.1162
	Supervised MPC	0.0221	0.0810

Table 14: Closed-Loop Performance Analysis (Participant 6).

Closed-Loop Class	Controller	$\frac{1}{K_T}\sum_{k=1}^{K_T} e_k^2$	$\frac{1}{K_T}\sum_{k=1}^{K_T} \lvert u_k \rvert$
Inhibition	LQR	0.2751	0.0145
	Supervised LQR	0.2334	0.0154
	MPC	0.3458	0.1401
	Supervised MPC	0.3087	0.1391
Excitation	LQR	0.1542	0.0058
	Supervised LQR	0.1261	0.0108
	MPC	0.0471	0.1330
	Supervised MPC	0.0362	0.0961

Table 15: Overall Closed-Loop Performance Analysis.

Closed-Loop Class	Criteria	Controller	Improvement
Inhibition	Average Error	*Supervised* LQR	+22.6%
		Supervised MPC	+23.0%
	Control Effort	*Supervised* LQR	-35.4%
		Supervised MPC	+7.6%
Excitation	Average Error	*Supervised* LQR	+5.4%
		Supervised MPC	+20.4%
	Control Effort	*Supervised* LQR	-0.0%
		Supervised MPC	+32.9%

In Tables 9–14, e_k and u_k represent the tracking error and the control input, respectively. K_T is the total time that the control is active in the loop. For example, as presented in Table 9, the supervised layer in LQR structure has decreased the tracking error e_k in inhibition task (0.1260 compared to 0.1642). Supervised fuzzy-LQR approach has improved state tracking accuracy by 23% with a 14% increase in the control efforts. In the excitation class, establishing supervised layer on top of the LQR system has resulted in a small improvement in state tracking accuracy (0.0640 compared to 0.0664) with a 27% decrease in total control efforts (0.0054 compared to 0.0074). Implementing the supervised fuzzy-MPC approach has resulted in more promising results. In comparison to the pure MPC, the supervised fuzzy-MPC system has reduced the tracking error by 10% and 15% in inhibition and excitation tasks, respectively. The supervised fuzzy-MPC architecture has also lead to applying less control efforts. It has reduced the total control effort by 10% and 45% in inhibition and excitation closed-loop tasks, respectively. We also analyzed the results of implementing supervised approaches on all six simulated profiles [3, 94]. A summary of overall closed-loop performance analysis for all simulated profiles are presented in Table 15.

As presented in Table 15, establishing supervised fuzzy system has significantly improved the MPC performance in both inhibition and excitation closed-loop systems. The proposed supervised fuzzy-MPC architecture has resulted in an enhanced tracking accuracy with more optimized control efforts. These analyses verify how the proposed supervised control architectures result in a more accurate state tracking with more optimal control efforts in MPC design. While the supervised fuzzy layer has also improved the tracking accuracy in LQR design, it has not been effective in accomplishing this task by reducing the control efforts. Supervised fuzzy-LQR system has decreased the tracking error on all six simulated profiles by average of 22.6% and 5.4% in inhibition and excitatory closed-loop classes, respectively. However, these improvements are not achieved by reducing the control efforts. Instead, in inhibition task, supervised LQR resulted in an average of 35% increase in control efforts. These analysis show that the proposed supervised architecture has great potential in improving state tracking accuracy in LQR design. The results in this *in silico* study confirm that the proposed supervised architectures have great potentials to be implemented in real-world.

5 Adaptive and Robust Control Systems for Closed-loop Cognitive Stress Regulation

5.1 An Overview of Adaptive and Robust Control Design

Concerned by inter- and intra subject variation presented in different individuals' physiological responses, we aim to design adaptive and robust control architectures in this chapter. To further enhance the control methodologies presented in chapters 3 and 4, we expand the main state-space equation by incorporating model uncertainty and additional disturbance input [3, 6].

To model inter-subject variations, we include model uncertainty in the proposed state-space representation. To model intra-subject variations, we propose to include additional disturbance input to handle potential model mismatch within the subjects. To handle the uncertainty in model parameter and additional disturbance input, we explore adaptive and robust design methodologies. Bolus *et al.* proposed an optimal feedback control to establish robust control design in a system with optogenetically driven neural activity [190]. In their proposed approach, they utilize an extended Kalman filter to re-estimate the augmented state that consists of the latent state and additional disturbance term. Yang *et al.* developed an adaptive latent state estimation algorithm to model brain network dynamics [191]. In their proposed algorithm, a rate-optimized adaptive linear state-space model is utilized to enable adaptation [191]. In a similar manner, we propose to employ a linear quadratic regulator (LQR) to estimate (1) time varying coefficient in an adaptive framework and (2) additional disturbance input to make the closed-loop system robust to these changes.

5.2 Methodologies

5.2.1 Human Brain Stimulus-Response Model

We utilize the simulation model that is generated based on the experimental data [83] and presented in [3]. The original dataset (i.e., Non-EEG Dataset for Assessment of Neurological Status) is publicly available through the PhysioNet database [83, 127]. This study includes several experiments that induce different types of stress to the participants. The simulation model presented in [3] is based on two sessions: cognitive stress and relaxation, as the most representative cases [3]. Similar to what is discussed in chapter 4, we track and manage internal stress state by monitoring skin conductance measurements which were collected using Affectiva Q Curve wearable device. Similar to [94, 3], we analyze six profiles associated with selected participants whose data were clean and reliable. Further information regarding these experiments are available in [83, 94, 3].

As presented in [3], in a nominal case without any uncertainty in model parameter and in the absence of disturbance input, we model the internal cognitive stress-related state to the changes in skin conductance signal by employing a first-order state-space model [94, 95]:

$$x_{k+1} = x_k + s_k + \nu_k + u_k, \tag{61}$$

where x_k corresponds to the hidden stress-related state, s_k stands for the environmental stimuli, and $\nu_k \sim \mathcal{N}(0, \sigma_\nu^2)$ represents the process noise [66, 95]. u_k is the control signal to regulate the simulated stress-related state. It should be noted that incorporated s_k in (61) is only for the simulation purpose. In experimental implementation, the human's internal cognitive stress state is influenced by actual environment. Additional details of modeling the environmental stimuli is presented in [3]. To derive the observations, we assume the occurrence of SCR events, n_k, follows a Bernoulli distribution with the probability function

$$P(n_k|x_k) = q_k^{n_k}(1 - q_k)^{1-n_k}, \tag{62}$$

where the probability q_k is connected to the stress state x_k, via the Sigmoid function [184]

$$q_k = \frac{1}{1 + e^{-(\gamma + x_k)}}, \tag{63}$$

where γ is the person-specific baseline parameter that should be determined. Similar to [3], we first assume x_0 approximately equals to zero. We then calculate γ based on the average probability of receiving SCR in the whole data. According to (63), with increase in the levels of the cognitive stress state, the probability of receiving the SCR events is also increased. To incorporate additional information presented in skin conductance signal, similar to chapter 4, we employ continuous feature as well. Hence, we assume there is a linear relationship between the internal cognitive stress state x_k and the tonic component of skin conductance signal

$$r_k = \rho_0 + \rho_1 x_k + \zeta_k, \tag{64}$$

where r_k is assumed to be the log transformation of the continuous-valued observation associated with the tonic component of skin conductance signal. ρ_0 and ρ_1 are constant values derived by the offline expectation maximization algorithm [56, 3]. $\zeta_k \sim \mathcal{N}(0, \sigma_\zeta^2)$ is measurement noise with variance σ_ζ^2.

In the literature, the dynamics of hidden neural states are frequently modeled as random walks and first-order auto-regressive with extra input (ARX) models [64, 192]. We utilize the same family of models to capture the evolution of cognitive stress-related state through time. Hence, we extend the state-space model (61) and consider two different cases: uncertainty in model parameters and disturbance input. In the first representation, we aim to design adaptive control system to handle the variations. In the second case, we wish to establish a robust control method to handle undesired disturbance input in modeled dynamics.

5.2.2 State-Space Modeling in Presence of Time-Varying Model Uncertainty

To incorporate model uncertainty in state-space formulation (61) [193], we relax the imposed time-invariant condition as

$$x_{k+1} = \rho_k x_k + u_k + s_k + \nu_k, \tag{65}$$

where uncertainty in model parameter ρ_k is modeled as a random walk process

$$\rho_k = \rho_{k-1} + \epsilon_k \qquad \text{and} \qquad \epsilon_k \sim \mathcal{N}(0, \sigma_\epsilon^2). \tag{66}$$

To design adaptive control and close the loop, we first purse developing an estimation algorithm to estimate ρ_k and x_k simultaneously. To this end, we employ a recursive Bayesian estimator that jointly estimates these variables based on the observation $\mathbf{Y}_k = \begin{pmatrix} n_k \\ r_k \end{pmatrix}$. We derive the two-dimensional augmented state vector

$$\mathbf{x}_{a,k} = \begin{pmatrix} \mathbf{x}_{a,k}^{(1)} \\ \mathbf{x}_{a,k}^{(2)} \end{pmatrix} = \begin{pmatrix} x_k \\ \rho_k \end{pmatrix}. \tag{67}$$

Therefore, the augmented system's dynamic is

$$\mathbf{x}_{a,k+1} = \begin{pmatrix} \mathbf{x}_{a,k}^{(2)} & 0 \\ 0 & 1 \end{pmatrix} \mathbf{x}_{a,k} + \begin{pmatrix} 1 \\ 0 \end{pmatrix} u_k + \mathbf{w}_{a,k} = f_a(\mathbf{x}_{a,k}, u_k) + \mathbf{w}_{a,k}, \tag{68}$$

where $\mathbf{w}_{a,k} = \begin{pmatrix} \nu_k \\ \epsilon_k \end{pmatrix}$, is a Gaussian random vector with zero mean vector, and covariance matrix $\mathbf{K}_a = \begin{pmatrix} \sigma_\nu^2 & 0 \\ 0 & \sigma_\epsilon^2 \end{pmatrix}$. The proposed recursive Bayesian estimator consists of the prediction and update steps. The prediction step relays on a recursive probabilistic model for the time evolution of the augmented states. The update step, utilizes a probabilistic observation model relating the hidden cognitive stress-related arousal state to the SCR events time and continuous feature.

Prediction step:

$$\mathbf{x}_{a,k|k-1} = f_a(\mathbf{x}_{a,k-1|k-1}, u_k) \tag{69}$$

$$\text{and} \quad \mathbf{\Sigma}_{a,k|k-1} = \mathbf{F}_{a,k-1}\mathbf{\Sigma}_{a,k-1|k-1}\mathbf{F}'_{a,k-1} + \mathbf{K}_a, \tag{70}$$

where $\mathbf{x}_{a,k|k-1}$, $\mathbf{\Sigma}_{a,k|k-1}$ are the mean and the coveriance of $\mathbf{x}_{a,k}$ and are derived using all the previous $k-1$ observations, $\mathbf{Y}_{1:k-1}$ at each time step k. Moreover, $\mathbf{F}_{a,k-1} = \left[\frac{\partial f_a}{\partial \mathbf{x}_a}\right]_{\mathbf{x}_{a,k-1|k-1}}$.

Update step:

$$g_{a,k} = \left[\frac{\partial \log(p(\mathbf{Y}_k|\mathbf{x}_{a,k}^{(1)}))}{\partial \mathbf{x}_{a,k}^{(1)}}\right]_{\mathbf{x}_{a,k}^{(1)}=\mathbf{x}_{a,k|k-1}^{(1)}}, \tag{71}$$

$$\mathbf{x}_{a,k|k} = \mathbf{x}_{a,k|k-1} + \mathbf{\Sigma}_{a,k|k} \begin{pmatrix} g_{a,k} \\ 0 \end{pmatrix}, \tag{72}$$

$$\text{and} \quad \mathbf{\Sigma}^{-1}_{a,k|k} = \mathbf{\Sigma}^{-1}_{a,k|k-1} + \begin{pmatrix} \left[\frac{\partial g_{a,k}}{\partial \mathbf{x}^{(1)}_{a,k}}\right]_{\mathbf{x}^{(1)}_{a,k} = \mathbf{x}^{(1)}_{a,k|k-1}} & 0 \\ 0 & 0 \end{pmatrix}. \tag{73}$$

5.2.3 Adaptive Feedback Controller Design

We follow the goal of designing an adaptive feedback-controller to derive on the control input u_k. The adaptive controller will utilize the real-time estimate of the hidden states and model parameter as feedback to "optimally" solve for u_k. Satisfying the optimality criterion implies defining a cost function and finding u_k to minimize it. We formulate a quadratic cost function given as

$$\mathbf{J}_a = \sum_{k=0}^{\infty} Q_a(x_k - x^*)^2 + R_a(u_k - u^*_k)^2, \tag{74}$$

where Q_a, R_a are positive weight matrices. By fixing the time-varying parameter at its current estimate (i.e., $\rho_k = \mathbf{x}^{(2)}_{a,k|k}$), ignoring environmental stimuli, and given the system reaches the steady state, we derive a single linear equation described in (65). Solving it for u^*_k, we derive

$$u^*_k = x^*(1 - \mathbf{x}^{(2)}_{a,k|k}). \tag{75}$$

Fixing the cognitive stress-related arousal state dynamics parameters at their current estimate, both formulas lead to a non-zero set-point LQR problem [194, 195]. To convert it to a traditional LQR formulation, where the control goal is to derive the state close to the origin, we let $\tilde{x}_k = x_k - x^*$, $\tilde{u}_k = u_k - u^*_k$. The optimal $\tilde{u}_k$ for the classical LQR problem is simply a linear feedback control as

$$\tilde{u}_k = -l_k \tilde{x}_k, \tag{76}$$

where $\overset{a}{l}_k$ is a scalar feedback gain derived as

$$l_k = \frac{\rho_k p_{a,k}}{p_{a,k} + R_a}, \tag{77}$$

where $p_{a,k}$ is the solution of the algebraic Riccati equation in the discrete form [194]

$$\rho_k^2 p_{a,k} + \frac{\rho_k^2 p_{r,k}^2}{p_{a,k} + R_a} + Q_a = p_{a,k}. \tag{78}$$

Consequently, the optimal control signal u_k will be equal to $u_k = u_k^* - l_k(x_k - x^*)$.

5.2.4 State-Space Modeling in Presence of Disturbance Input

In this part, we add an additional input to nominal dynamical system to model disturbances. The nominal system expands as

$$x_{k+1} = x_k + u_k + s_k + \nu_k + d_k, \tag{79}$$

where d_k is defined as

$$d_k = d_{k-1} + \omega_k \qquad \text{and} \qquad \omega_k \sim \mathcal{N}(0, \sigma_{\omega_k}^2). \tag{80}$$

To estimate the added parameter along with the hidden state, we follow an approach similar to adaptive counterpart, with the only change in the system dynamics. Concatenating x_k and d_k into an augmented two-dimensional state vector

$$\mathbf{x}_{r,k} = \begin{pmatrix} \mathbf{x}_{r,k}^{(1)} \\ \mathbf{x}_{r,k}^{(2)} \end{pmatrix} = \begin{pmatrix} x_k \\ d_k \end{pmatrix}. \tag{81}$$

We derive dynamics of augmented system as

$$\mathbf{x}_{r,k+1} = \begin{pmatrix} 1 & 1 \\ 0 & 1 \end{pmatrix} \mathbf{x}_{r,k} + \begin{pmatrix} 1 \\ 0 \end{pmatrix} u_k + \mathbf{w}_{r,k} = f_r(\mathbf{x}_{r,k}, u_k) + \mathbf{w}_{r,k}, \tag{82}$$

where $\mathbf{w}_{r,k} = \begin{pmatrix} \nu_k \\ \omega_k \end{pmatrix}$, is a Gaussian random vector with zero mean vector, and covariance matrix $K_r = \begin{pmatrix} \sigma_\nu^2 & 0 \\ 0 & \sigma_\omega^2 \end{pmatrix}$. In what follows, we derive prediction and update steps to estimate variable in augmented system.

Prediction step:

$$\mathbf{x}_{r,k|k-1} = f_r(\mathbf{x}_{r,k-1|k-1}, u_k) \tag{83}$$

$$\text{and} \quad \mathbf{\Sigma}_{r,k|k-1} = \mathbf{F}_{r,k-1}\mathbf{\Sigma}_{r,k-1|k-1}\mathbf{F}'_{r,k-1} + \mathbf{K}_r, \tag{84}$$

where $\mathbf{x}_{r,k|k-1}$, $\mathbf{\Sigma}_{r,k|k-1}$ are the mean and the coveriance of $\mathbf{x}_{r,k}$ and being estimated using observation $\mathbf{Y}_{1:k}$. Moreover, $\mathbf{F}_{r,k-1} = \left[\frac{\partial f_r}{\partial \mathbf{x}_r}\right]_{\mathbf{x}_{r,k-1|k-1}}$.

Update step:

$$g_{r,k} = \left[\frac{\partial \log(p(\mathbf{Y}_k|\mathbf{x}^{(1)}_{r,k}))}{\partial \mathbf{x}^{(1)}_{r,k}}\right]_{\mathbf{x}^{(1)}_{r,k}=\mathbf{x}^{(1)}_{r,k|k-1}}, \tag{85}$$

$$\mathbf{x}_{r,k|k} = \mathbf{x}_{r,k|k-1} + \mathbf{\Sigma}_{r,k|k}\begin{pmatrix} g_{r,k} \\ 0 \end{pmatrix}, \tag{86}$$

$$\text{and} \quad \mathbf{\Sigma}^{-1}_{r,k|k} = \mathbf{\Sigma}^{-1}_{r,k|k-1} + \begin{pmatrix} \left[\frac{\partial g_{r,k}}{\partial \mathbf{x}^{(1)}_{r,k}}\right]_{\mathbf{x}^{(1)}_{r,k}=\mathbf{x}^{(1)}_{r,k|k-1}} & 0 \\ 0 & 0 \end{pmatrix}. \tag{87}$$

5.2.5 Robust Feedback Controller Design

In this part, we design a robust feedback-controller to derive the control action u_k [190]. Similar to adaptive control design, we formulate a quadratic cost function as

$$\mathbf{J}_r = \sum_{k=0}^{\infty} Q_r(x_k - x^*)^2 + R_r(u_k - u_k^*)^2, \tag{88}$$

where Q_r and R_r are positive weight matrices. By fixing the time-varying parameter at its current estimate (i.e., $d_k = \mathbf{x}^{(2)}_{r,k|k}$), ignoring environmental stimuli, and given the system reaches the steady state, we derive a single linear equation described in (79). Solving it for

u_k^*, we derive

$$u_k^* = -\mathbf{x}_{r,k|k}^{(2)}. \tag{89}$$

Fixing the cognitive stress-related arousal state dynamics parameters at their current estimate, both formulas lead to a non-zero set-point LQR problem [194, 195]. To convert it to a traditional LQR formulation, where the control goal is to derive the state close to the origin, we let $\tilde{x}_k = x_k - x^*$, $\tilde{u}_k = u_k - u_k^*$. The optimal $\tilde{u}_k$ for the classical LQR problem is simply a linear feedback of the form given

$$\tilde{u}_k = -l_k \tilde{x}_k, \tag{90}$$

where $\overset{a}{l_k}$ is a scalar feedback gain derived as

$$l_k = \frac{p_{r,k}}{p_{r,k} + R_a}, \tag{91}$$

where $p_{r,k}$ is the solution of the algebraic Riccati equation in the discrete form [194]

$$p_{r,k} + \frac{p_{r,k}^2}{p_{r,k} + R_a} + Q_a = p_{r,k}. \tag{92}$$

Consequently, the optimal control signal u_k will be equal to $u_k = u_k^* - l_k(x_k - x^*)$.

5.3 Results

We utilize the developed simulation environment presented in [3] in the order of first inducing cognitive stress and then causing relaxation [3]. We present the closed-loop results in both adaptive and robust frameworks.

5.3.1 Adaptive Closed-Loop Results

The main goal of designing an adaptive closed-loop system is to establish a control system for handling model uncertainty in state-space representation. The results associated with both adaptive inhibitory and robust excitatory classes are presented in Figures 28–33. In Figures 28–33, the top and bottom panels show the results associated with closed-loop inhibition and excitation, respectively. In each panel, the top two sub-panels show the SCR events along with their amplitudes in open-loop (orange color) and closed-loop (blue color) cases. The third sub-panel shows the estimated cognitive stress-related state. The bottom sub-panel shows the designed control implemented in real-time to close the loop and either inhibit or excite the estimated stress levels. The grey and white backgrounds correspond to the high and low arousal environmental stimuli, respectively (i.e., cognitive stress condition vs relaxing condition).

5.3.2 Robust Closed-Loop Results

The main goal of designing robust closed-loop system is to utilize a control system to handle additional disturbance input in state-space representation. The results associated with both adaptive inhibitory and robust excitatory classes are presented in Figures 34–39. In Figures 34–39, the top and bottom panels show the results associated with closed-loop inhibition and excitation, respectively. In each panel, the top two sub-panels show the SCR events along with their amplitudes in open-loop (orange color) and closed-loop (blue color) cases. The third sub-panel shows the estimated cognitive stress-related state. The bottom sub-panel shows the designed control implemented in real-time to close the loop and either inhibit or excite the estimated stress levels. The grey and white backgrounds correspond to the high and low arousal environmental stimuli, respectively (i.e., cognitive stress condition vs relaxing condition).

5.4 Discussion

As inter- and intra-subject variations in human-in-the-loop problems are unavoidable, we implemented adaptive and robust control systems to handle them. To this end, we employed a simulation environment [3] based on the experimental data [83]. To model inter- and intra-subject variations, we extended the state-space representation and included

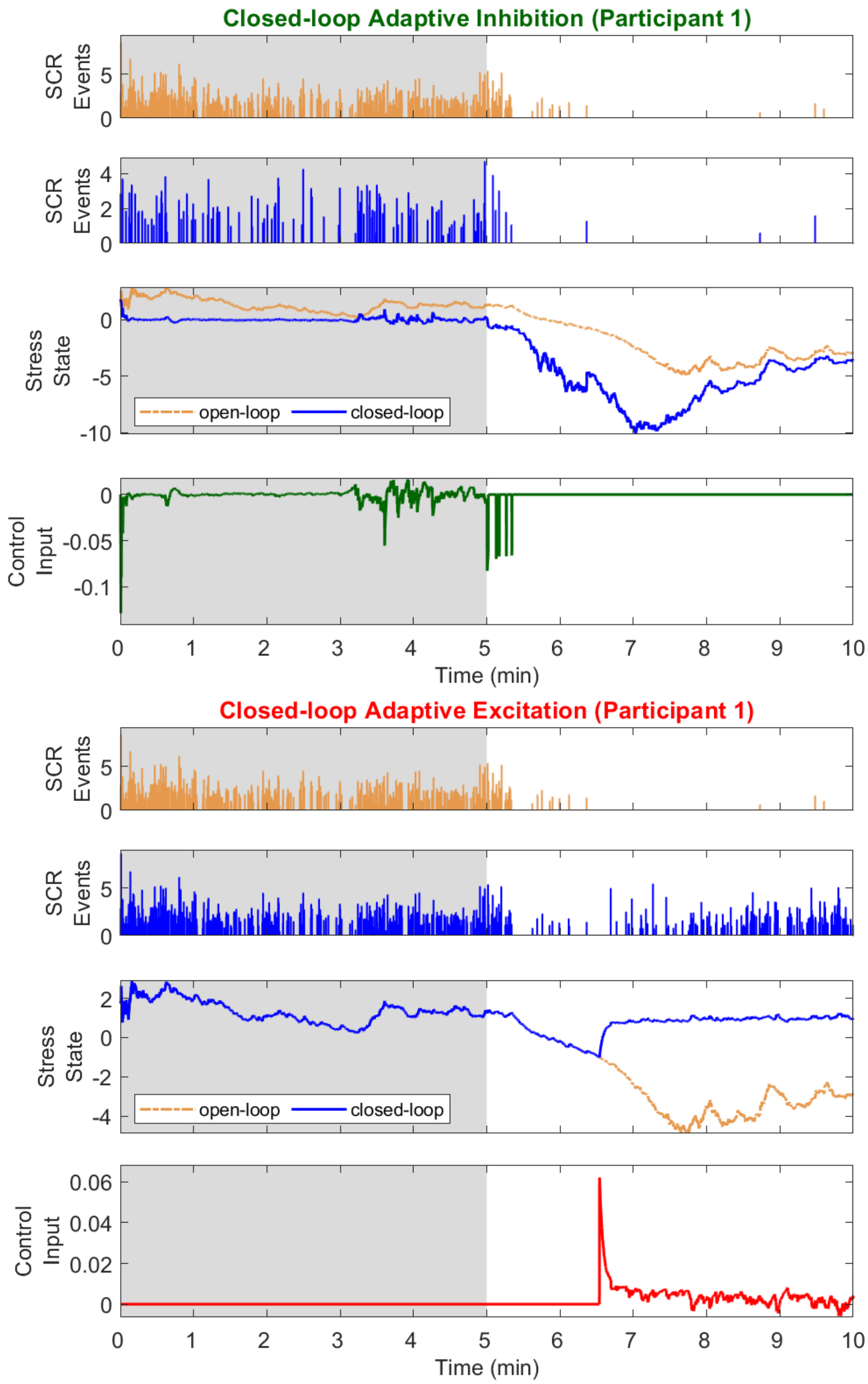

Figure 28: **Adaptive inhibition and excitation results (Participant 1).**

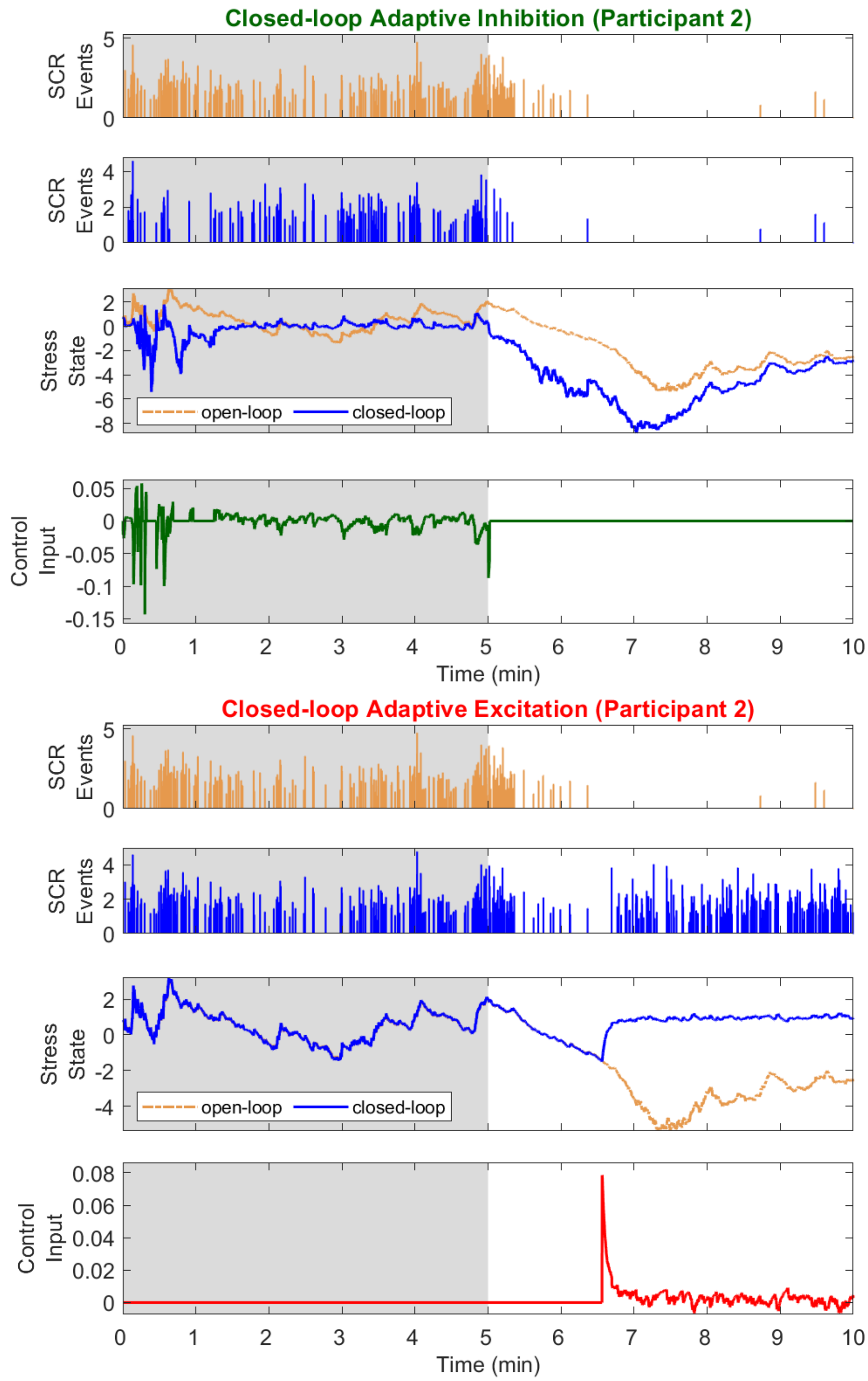

Figure 29: **Adaptive inhibition and excitation results (Participant 2).**

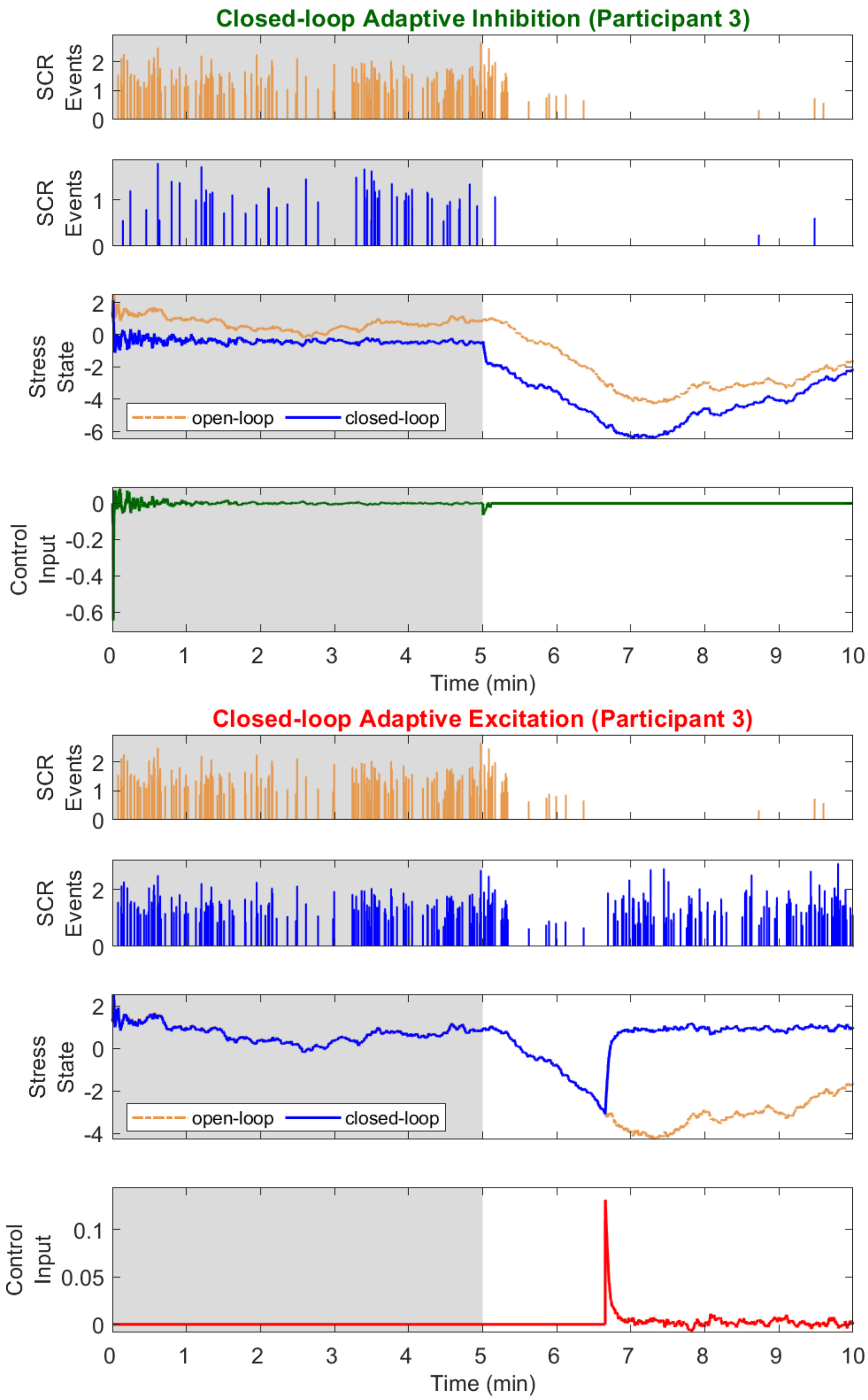

Figure 30: **Adaptive inhibition and excitation results (Participant 3).**

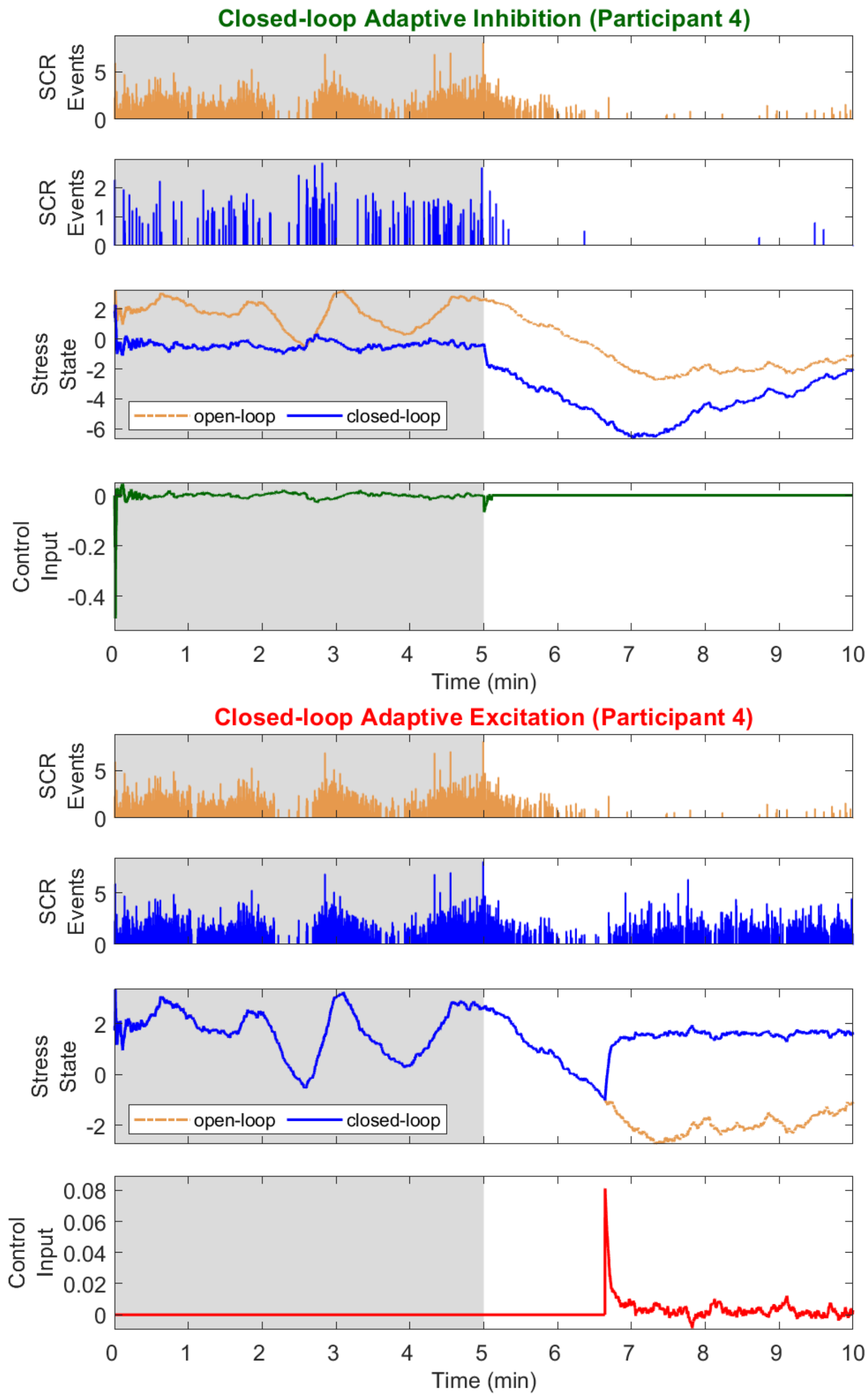

Figure 31: **Adaptive inhibition and excitation results (Participant 4).**

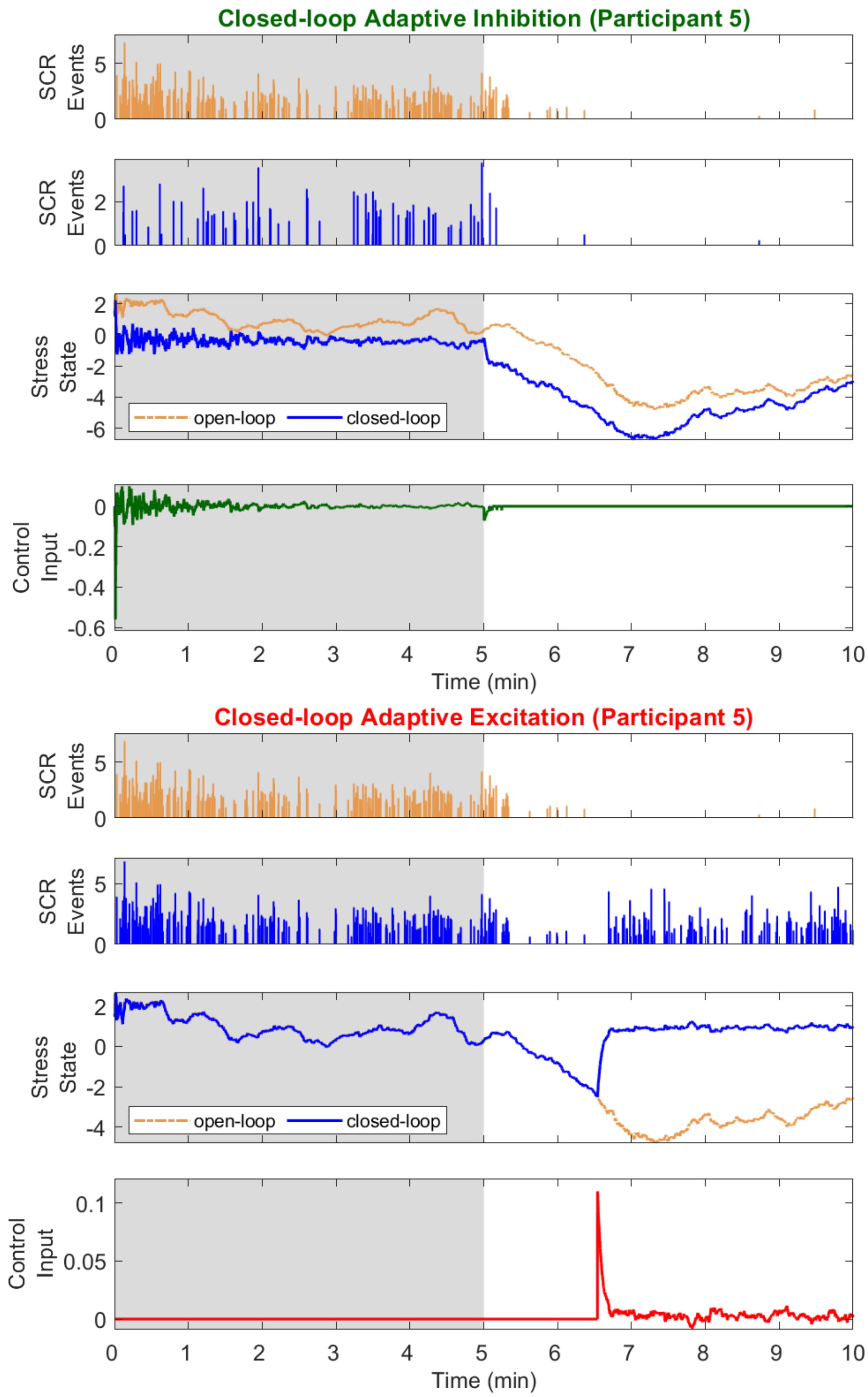

Figure 32: **Adaptive inhibition and excitation results (Participant 5).**

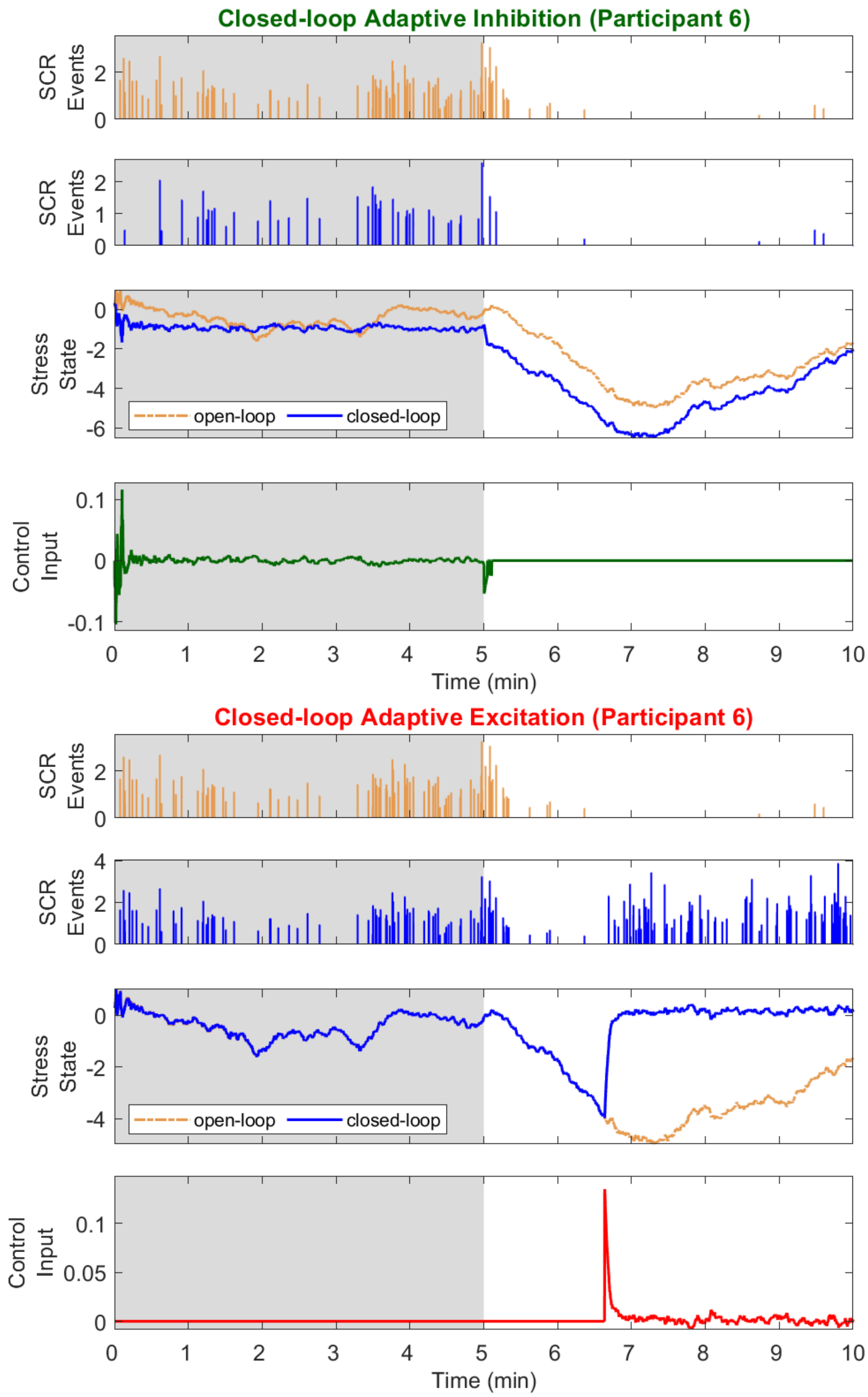

Figure 33: **Adaptive inhibition and excitation results (Participant 6).**

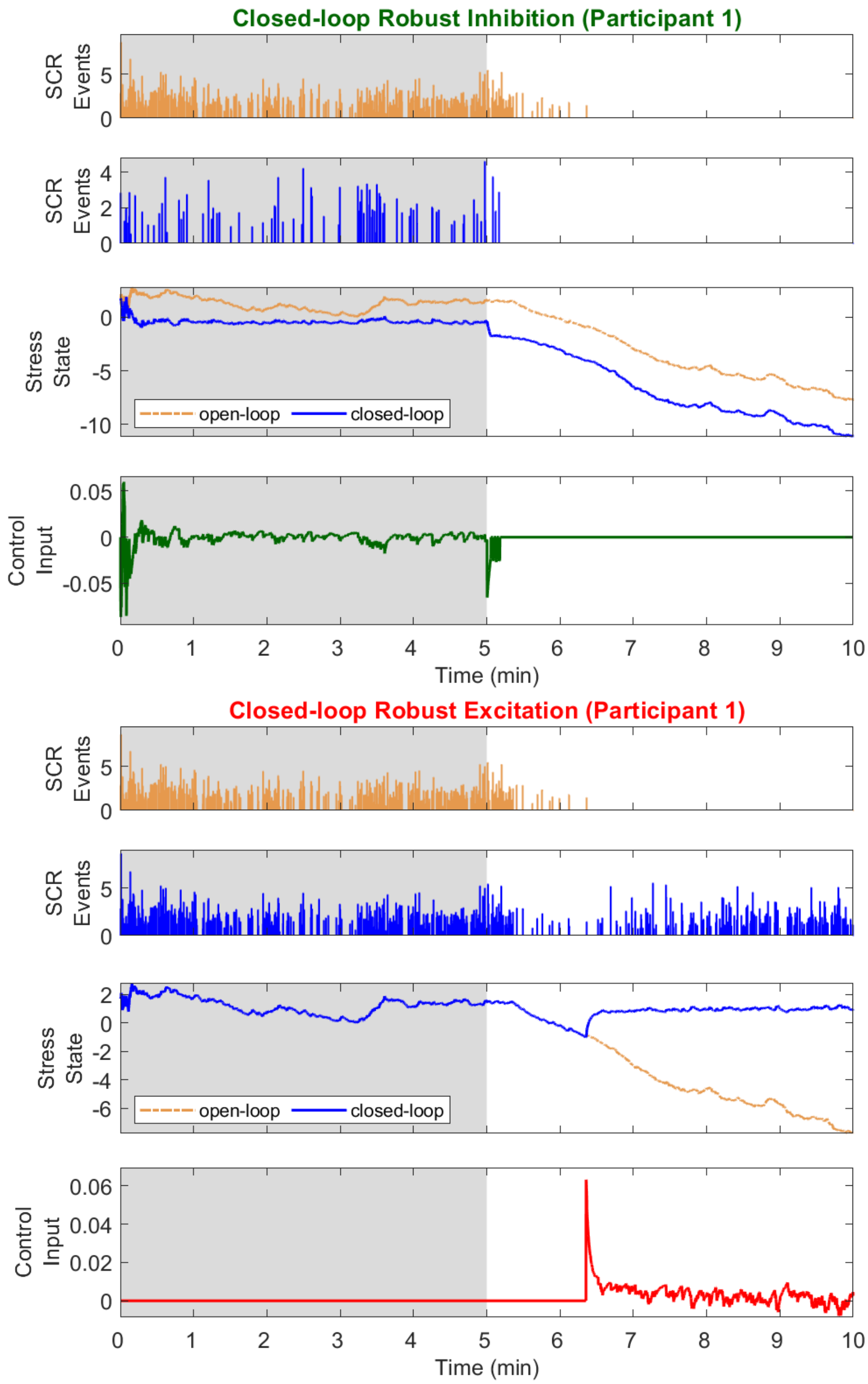

Figure 34: **Robust inhibition and excitation results (Participant 1).**

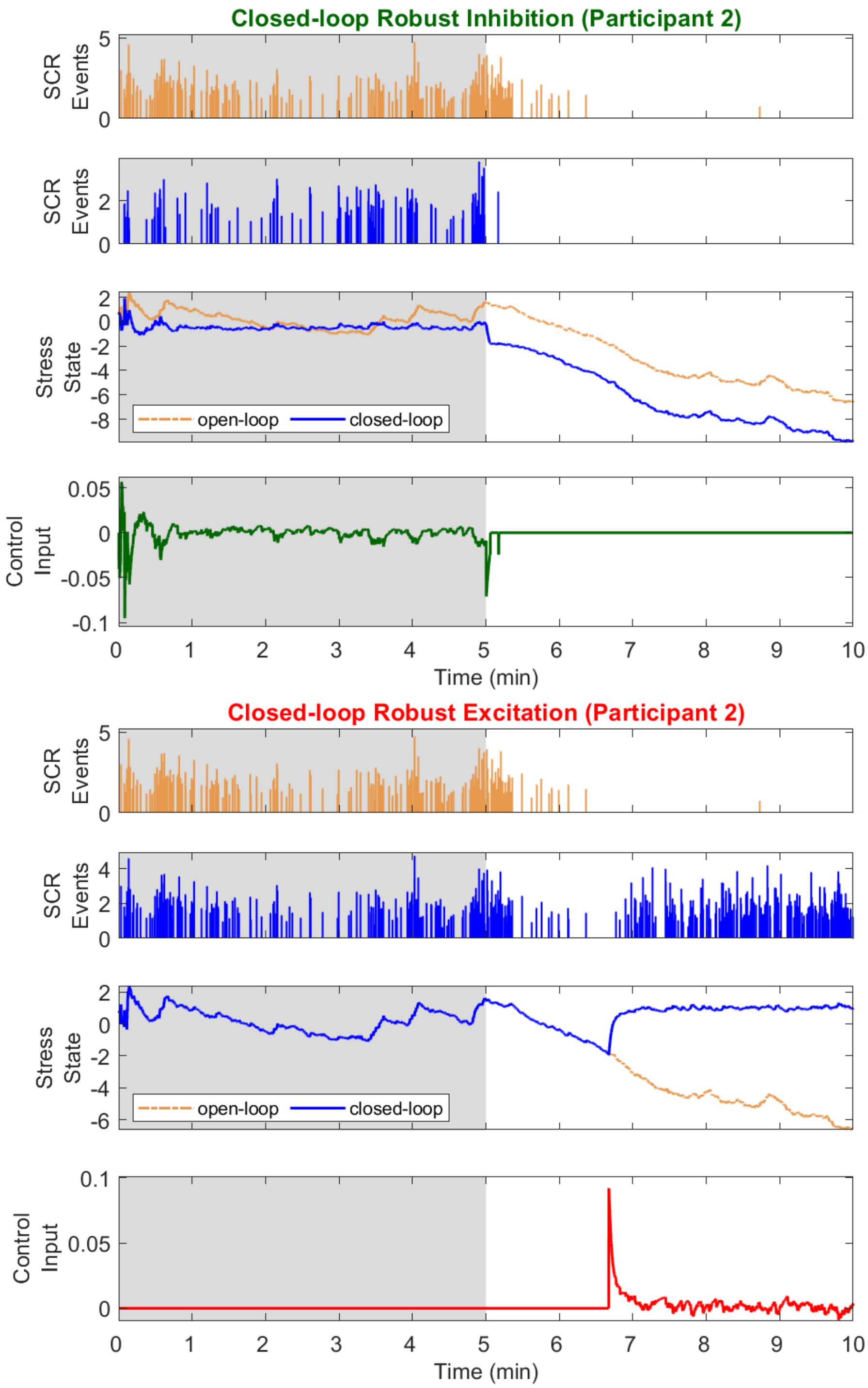

Figure 35: **Robust inhibition and excitation results (Participant 2).**

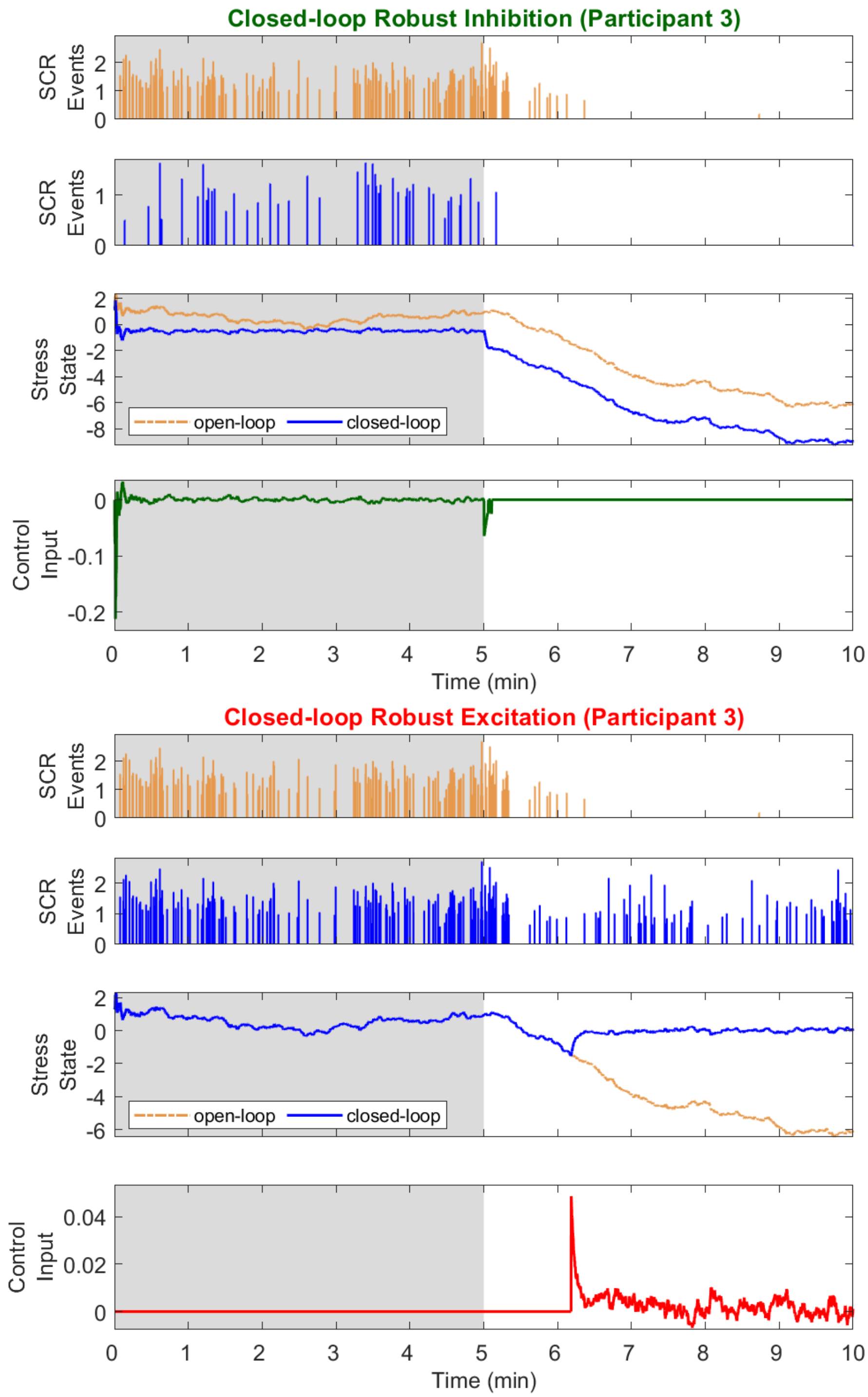

Figure 36: **Robust inhibition and excitation results (Participant 3).**

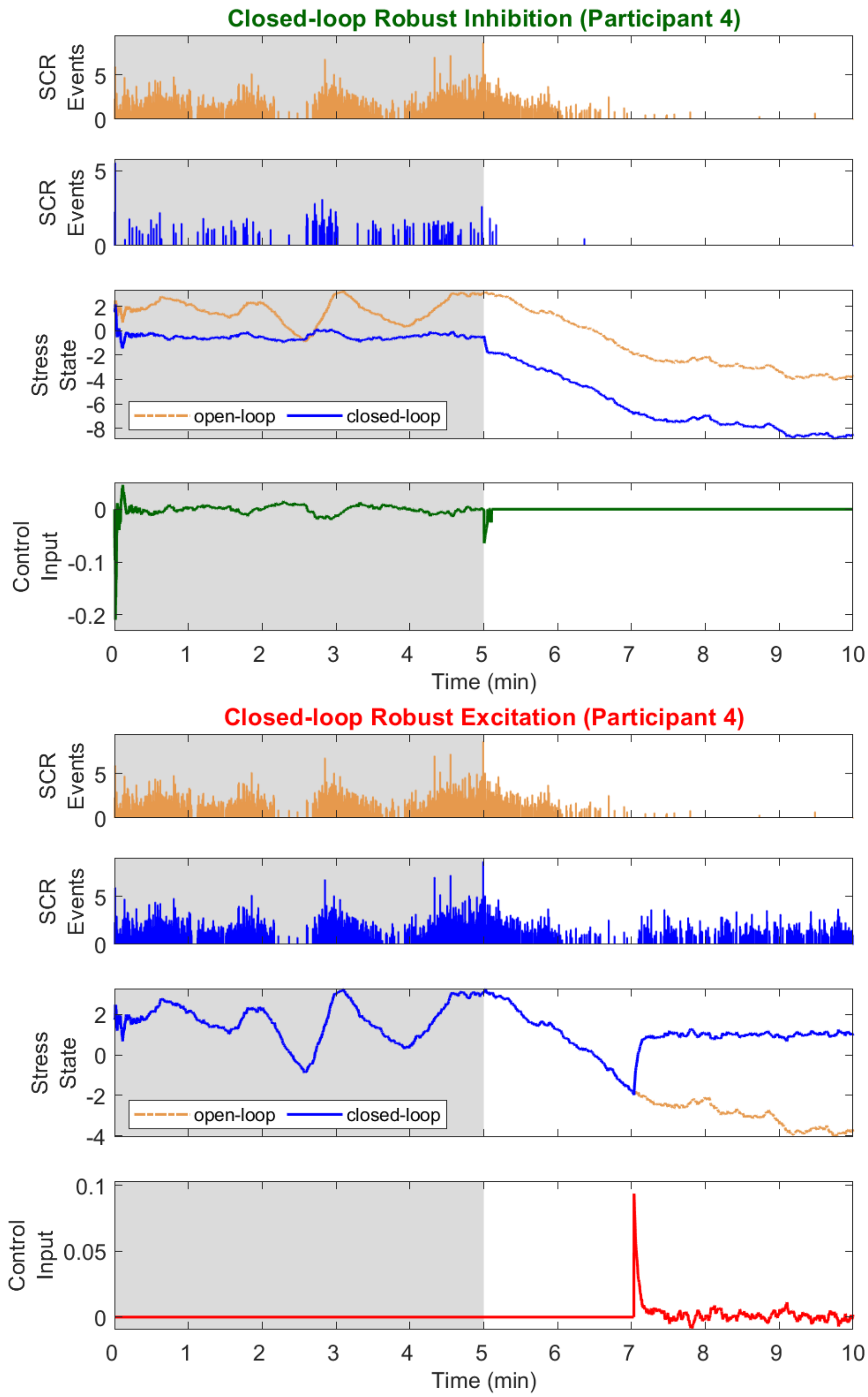

Figure 37: **Robust inhibition and excitation results (Participant 4).**

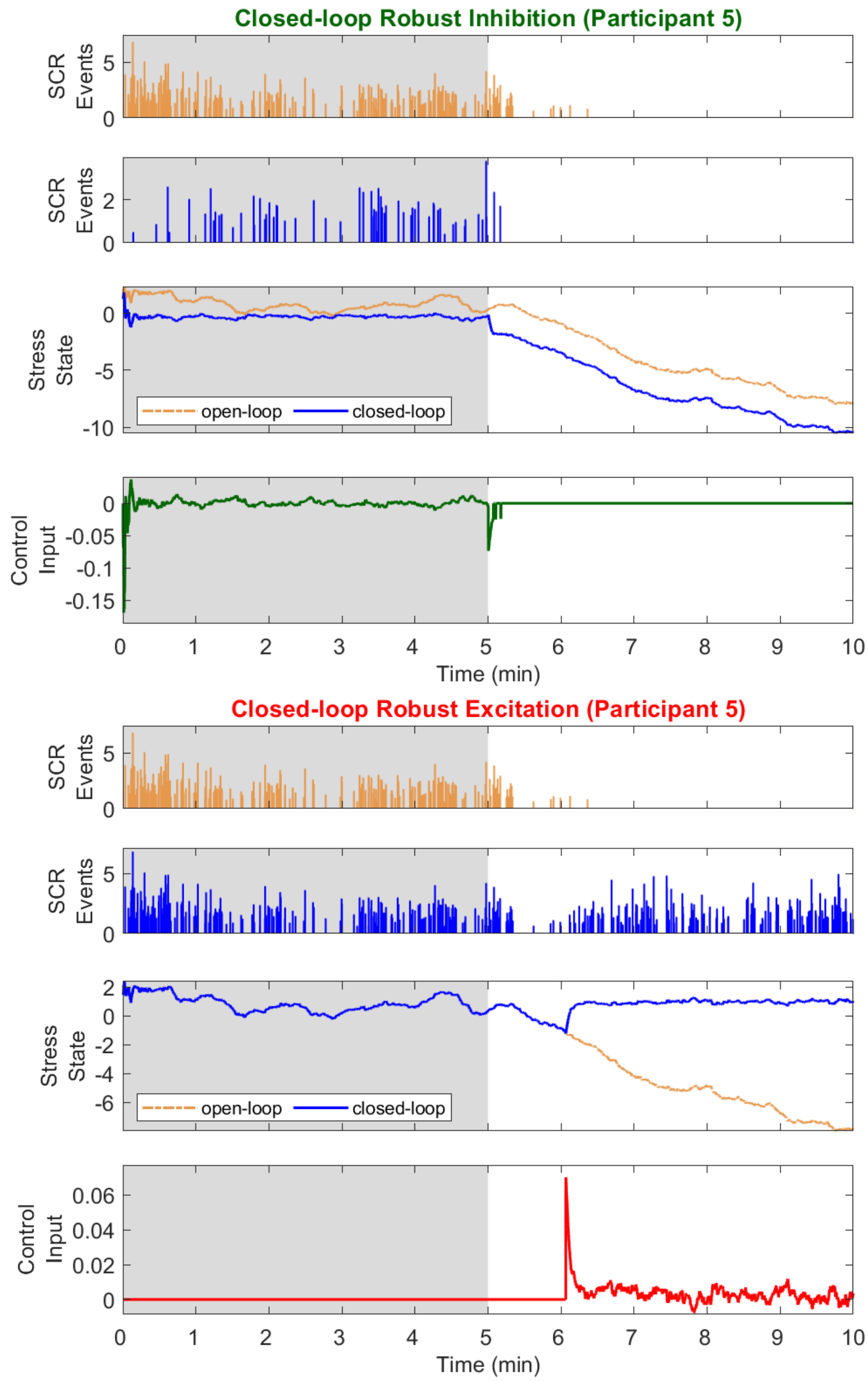

Figure 38: **Robust inhibition and excitation results (Participant 5).**

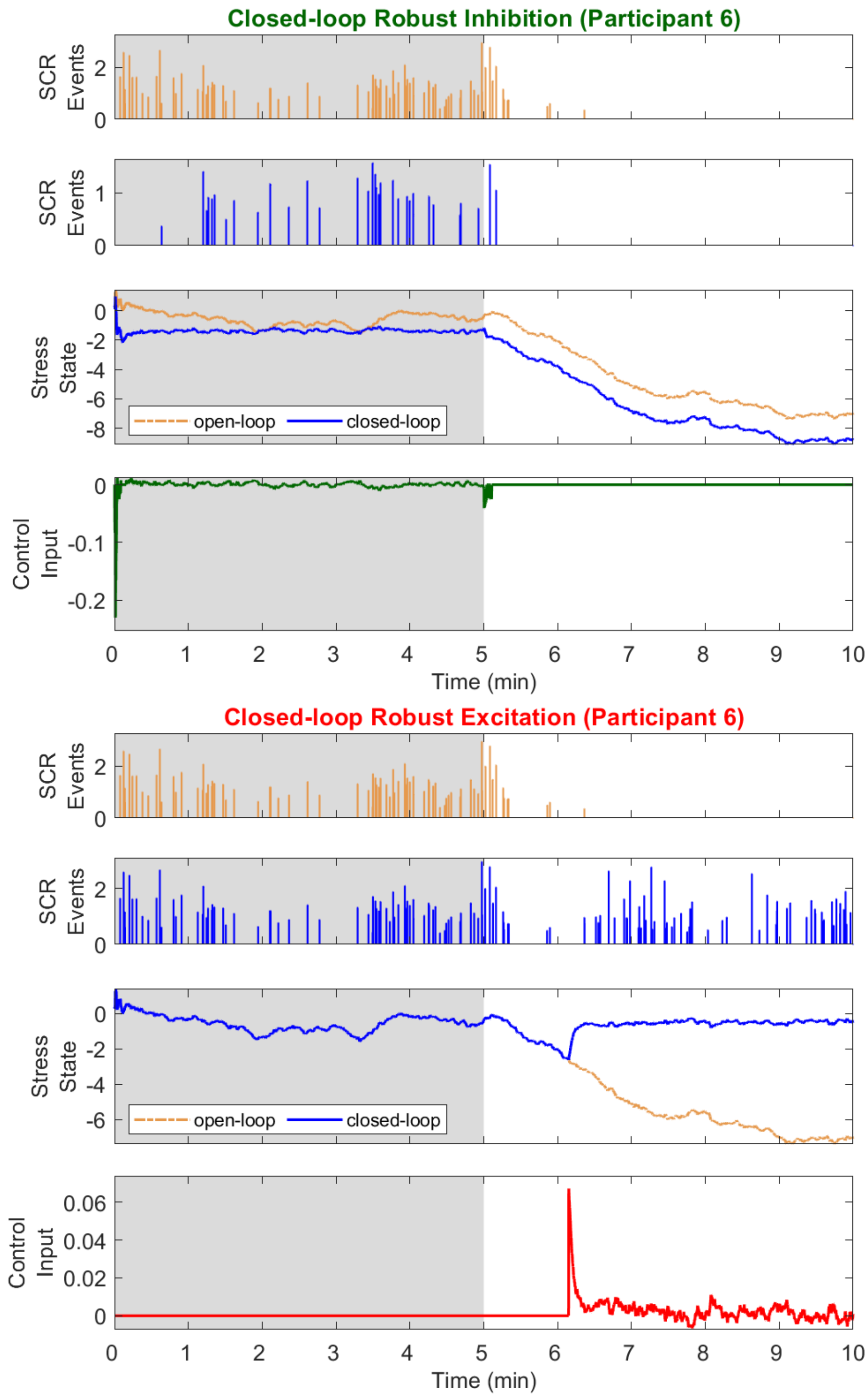

Figure 39: **Robust inhibition and excitation results (Participant 6).**

uncertainty in model parameters and disturbance input. To simultaneously estimate the hidden cognitive arousal state along with added unknown parameter, we defined augmented states. To close the loop, we designed and implemented an optimal controller. Applying adaptive and robust control approaches, we enhanced the closed-loop performance by handling model uncertainty and disturbance input. The results on all six simulated profiles [3] further validate our proposed algorithms in regulating the hidden cognitive stress state while considering time varying model parameters and additional disturbance input in the state-space representation.

The open-loop results, presented in Figures 28–39, illustrate the sufficiency of internal stress state tracking in the presence of uncertainty in model parameters and disturbance input. The higher numbers/values of SCR events (i.e., orange spikes in the first sub-panel) and levels of estimated stress state (i.e. orange graph in the third sub-panel) in the first half of the simulation is because of the applied high arousal environmental stimuli. Moving toward the low arousal session (white background in Figures 28–39), both the numbers/values of SCR events and the estimated stress levels drop significantly, which is due to the induced relaxing environmental stimuli in the second half of the simulation. These changes in the estimated stress state are in good agreement with the changes in SCR events: higher levels of the estimated stress state in the first half of the simulation (i.e., cognitive stress), and lower levels for the second half of the simulation (i.e., relaxation).

To regulate the estimated stress levels in a closed-loop manner, we first presented the adaptive control design to handle model uncertainty presented in state-space representation. To close the loop, we considered inhibition and excitation classes of controllers. In the closed-loop inhibition task, the goal is to reduce the levels of the estimated stress state in high arousal session (i.e., first half of the simulation) (Top panels of Figures 28–33). During this period, we assume that the environmental stimuli cause the subject to feel stressed. As a result, SNS would activate the sweat glands and skin conductivity would be increased. Consequently, more activation on SCRs would be observed (Top panels of Figures 28–33). By tracking the hidden stress state in the presence of model uncertainty, the designed adaptive optimal control signal derives the required action for inhibition task (Top panels of Figures 28–33). The control signal, presented in third sub-panel, is mainly active in the first half and results in lowering the stress state.

Compared to the inhibition task, the goal of implementing excitation class of controllers is to excite the low levels of arousal state. The second half of the simulation in the simulated environment is assumed to induce low cognitive stress condition on the person. The goal of elevating the estimated stress-related state has been followed by designing adaptive optimal control signal. The results of closed-loop excitation task are presented in the bottom panels of Figures 28–33.

Next, we developed a robust control system to handle disturbance input presented in state-space representation. Similar to the adaptive control design, we considered inhibition and excitation classes of controllers for closing the loop (Figures 34–39). The closed-loop results further validate the effectiveness of designed robust control systems by either inhibiting the estimated arousal state (Top panels of Figures 34–39) or exciting it (Bottom panels of Figures 34–39) in the presence of additional disturbance input. The proposed adaptive and robust control designs would lead us one step closer to implementing the proposed WMI architectures in real-world settings.

6 Closed-loop Human-Subject Experiments for Internal Brain State Regulation with Wearable Technologies

6.1 An Overview of Closed-Loop Human-Subject Experiments

Any activity might be a source of cognitive stress. Stress in workplaces [196] and cognitive load while learning at schools [197] are reported as examples of condition that might cause cognitive stress on humans. Additionally, to reach enhanced productivity and retain it, it is beneficial to elevate internal cognitive arousal levels and prevent low engagement [3, 198, 199]. According to the Yerkes–Dodson law, there exists an inverse-U relationship between the internal arousal state and cognitive performance [199]. Therefore, the performance is maximized once the internal arousal state is regulated and lies in a normal optimal range [200, 201]. Hence, it is highly crucial to regulate the arousal state and keep it within the optimal range [202]. Over the last few years, a growing interest in human emotion regulation arises in various areas such as education [203, 204], neural rehabilitation [205, 206], and brain computer interfaces [207]. In this study, we aim to analyze the internal arousal state in individuals while performing cognitive stress tasks and taking safe actuation for the purpose of closed-loop arousal regulation. With respect to the recent enhancement in ubiquity of wearable technologies, we focus on employing wearable devices for monitoring brain responses.

To this end, we propose three sets of human-subject experiments. In the first two experiments, to induce cognitive stress, we propose to employ well-explored memory-related n-back tasks [208]. We design and perform n-back experiments to investigate the brain responses while under cognitive load [209, 210, 110]. In n-back tasks, the system represents a sequence of stimuli, each followed by a consistent fixation [211]. The subjects are asked to recall if the stimulus they observe is the same as the one they were shown during the n-th step before. It is obvious that higher values for n will result in more difficult tasks. This study also seeks to explore effects of using safe actuation in influencing physiological responses and enhancing cognitive performance in a closed-loop manner. To close the loop in these experiments, we propose to incorporate safe actuation such as listening to music, smelling perfumes, and drinking coffee while performing cognitive stress tasks.

To further investigate the relationship between the cognitive performance and internal arousal state, we aim to analyze the changes in internal cognitive arousal state while under cognitive load [94, 6]. As internal arousal state is a hidden state, we approach this problem indirectly. In response to the cognitive stress stimuli, similar to any other internal or external stimuli, the brain starts to react in multiple ways. Monitoring brain signals with Electroencephalography (EEG) [212, 213, 214, 215] or functional Near-Infrared Spectroscopy (fNIRS) [216] would shed light on how the brain would respond to those environmental stimuli. From a physiological signals perspective, there are also changes in heart rate, blood volume pulses, and electrodermal activity [217] that carry important information about an individual's internal arousal state. With recent advances in wearable technologies, there exist fascinating and unique opportunities to investigate human brain responses in a more applicable way. Compared to research-grade technologies that are more expensive and precise in sensing, wearable devices are designed to deliver more practical properties [218, 219, 220, 217, 221]. Low-cost and portability features are the most remarkable characteristics that make the wearable technologies more attractive in the field of emotion recognition [222, 223, 224]. Hence, we propose to use Empatica E4 wristbands [225] and a muse headband [226] to collect data from human subjects while exposing them to cognitive stress tasks. The Empatica E4 wristband employs noninvasive sensors to collect multiple physiological signals (i.e., electrodermal activity (EDA), blood volume pulse (BVP), photoplethysmography (PPG), 3-axis accelerometer data, and skin temperature). Additionally, we employ a muse headband to directly record brain electrical activity with a noninvasive EEG method [227, 228]. Compared to other research-grade devices that are not applicable in daily life, a muse headband collects EEG signals from a limited number of channels [229].

6.1.1 Experiment 1: Brain Cognitive States Regulation in Memory Experiments by means of Listening to Music

To regulate cognitive performance and cognitive arousal states, we propose to use music as the safe actuation in experiment 1. There are multiple studies showing how listening to different kinds of music might affect humans' internal states [230, 231, 232]. Researchers in [233] performed an experiment to show the efficiency of listening to music in improving imagery in the context of sport skills. By collecting physiological data such as skin conductance and heart rate, they have demonstrated the effectiveness of listening to music in enhancing the performance index. Lehmann *et al.* examined effectiveness of background music in enhancing learning outcome [234]. They asked half of the subjects to perform a memory task in silence and the second half while listening to two pop songs [234]. The results further prove their hypothesis about positive role of music in improving working memory capabilities [235]. In a similar study, Du *et al.* analyzed the effects of high and low arousal music on neural responses. They collected 64-channel EEG signal and inferred the arousal state using eye blinks extracted from the recorded EEG data [235].

6.1.2 Experiment 2: Brain Cognitive State Regulation in Memory Experiments by means of Smelling Perfume and Drinking Coffee

In experiment 2, we aim to explore the effects of drinking coffee and smelling perfumes on cognitive performance and arousal states. There also exists extensive research showing how caffeine drinks influence individuals' performance in positive ways [236, 237, 238, 239, 240]. McLellan *et al.* performed a comprehensive review of multiple studies verifying the effects of caffeine in enhancing alertness, attention, and reaction time [241]. Souissi *et al.* demonstrated how caffeine ingestion is effective in enhancing cognitive and physical performance [242]. They used reaction time and the number cancellation test to analyze cognitive performance [242]. Researchers in [243] designed an experiment and analyzed the effects of coffee intake in the brain electrical activity. To this end, Saifudinova *et al.* collect EEG signal before and after taking coffee. In a recent study by Sargent *et al.*, they performed experiments and collected EEG and EDA data from subjects while performing daily tasks in a naturalistic work environment [244]. While participants are in an office-type environment, they were provided with hot beverages. In a similar study, researchers in [245] designed and performed experiments to investigate the effects of hot tea and coffee on cognitive performance. During the experiment, they collected EDA and fNIRS data from the subjects. To explore the effects of coffee in brain computer interfaces, Meng *et al.* performed an experiment and analyzed EEG signal from the subjects who are asked to drink coffee [246]. In a separate study, Fine *et al.* verified the effects of caffeine in improving cognitive performance and reducing fatigue.

In experiment 2, to further explore the effects of safe actuation, we use favorite fragrances for closing the loop. In past decades, the effects of olfactory stimulation have been explored by multiple researchers [247]. Examples of these studies are analyzing effects of smelling perfumes in lung function and exercise performance [248], pain management [249, 250], and alleviating psychological effects in women's menopausal symptoms [251]. Porcherot *et al.* designed and performed experiments to investigate changes in emotions in response to smelling fragrances [252]. Similar to any stimulation, to analyze the effects of olfactory stimulation, researchers proposed to collect multiple physiological signals such as cardiac and electrodermal activity [253], EEG recording [254], galvanic skin response [255], heartbeat [256], and fNIRS [257]. Saeki *et al.* investigated effects of inhaling favorite fragrances for relieving pricking pain. [258]. They used electrical stimulation to cause pain and measured skin conductance levels as the corresponding biomarkers [258]. The results verify their hypothesis about the influence of fragrances to alleviate the pain. They also discuss the possibility of the effectiveness of aromatherapy in chronic pain relief [259]. Onuma *et al.* conducted similar research and recorded brain activity from the frontal region and explored how smelling fragrances would affect it [260]. They concluded a positive relationship between activity associated with the right region of brain and induced impression [260]. Moss *et al.* performed experiments for evaluating the effects of different aromas in modulating cognitive performance [261]. They showed that peppermint has great potential in enhancing cognitive mood. The results of these studies validate the effects of smelling fragrances on changes in individuals' psychological and physiological conditions.

6.1.3 Experiment 3: Closed-Loop Experiments to Help Subjects with Acrophobia by means of Music and Diaphragmatic Breathing

In experiment 3, we design and perform closed-loop human-subject experiments to investigate how safe actuation such as listening to music and breathing exercises could affect the participants with high levels of acrophobia. According to [262], acrophobia is knows as irrational fear of heights, resulting in the prevention of such occasions with substantial high levels of stress. While exposing to acrophobia, there exist evidences of changes in physiological signals such as heart rate, skin conductance signal, and salivary cortisol levels [263]. Researchers in [264] employed machine learning and deep learning-based methods and multimodal sensory data (i.e., EEG, HR, and SCR) as well as self-reported emotion assessment to detect fear levels. Kritikos *et al.* develop an architecture to collect EDA signals while exposing the subjects to different virtual reality environments [265]. In this experiment, we ask the participants to watch the clips that might induce fear of heights condition. To analyze their physiological signals, we propose to use Empatica E4 and muse headband. To close the loop and alleviate internal arousal states, we propose to use safe actuation (i.e., listening to music and practice diaphragmatic breathing). In the literature, the efficiency of listening to music in relaxing the participants have been explored [266]. As the first actuation, we wish to play relaxing music and analyze how this safe actuation could help them with lowering arousal and engagement levels. In the second session, we play newly generated relaxing music. As the final actuation, the subjects are asked to practice diaphragmatic breathing while watching the clips. Diaphragmatic breathing is an influential self-administered, cost-free, and non-pharmacologic intervention [267]. Researchers in [268] investigated the efficiency of diaphragmatic breathing to relax the human subjects while are exposed to their fear condition in virtual reality. They collected HR, SCR, and their self-assessment to explore the influence of diaphragmatic breathing while taking the

VR treatment exposure. The results demonstrate that the group of subjects who practice diaphragmatic breathing show better progress in their fear of heights treatment. Shiban *et al.* analyze raw skin conductance levels to evaluate the effectiveness of diaphragmatic breathing [268]. The research by Hopper *et al.* also verifies the impacts of diaphragmatic breathing in reducing physiological and psychological stress [267]. In a similar study, Ma *et al.* investigate effects of this breathing exercises in stress relieving and improving mental health function.

6.1.4 Summary of Closed-Loop Experiments

In what follows, we summarize the experiments in this research. In experiment 1, we analyze the effectiveness of listening to different kinds of music while under cognitive load. In experiment 2, we propose to explore the effects of drinking coffee and smelling fragrances as safe actuation in closing the loop. To analyze the performance index, and explore effects of safe actuation in regulating it, we record the correct/incorrect responses as well as their reaction time. Next, we employ a Bayesian filter to estimate the cognitive performance index based on these observations. We hypothesize that taking this actuation would influence the cognitive stress state and affect the cognitive performance. In experiment 3, we design procedures to expose the subjects with degree of acrophobia to face their fear conditioning. To this end, we asked the participants to watch the clips in which the individuals jump between tall buildings without caring facilities. Watching these clips would lead the participants to assume themselves in similar situations and could arouse them. To measure changes in cognitive arousal, we employ the same wearable devices (i.e., Empatica E4 and muse headband) to collect their physiological data while watching the clips. To investigate how safe actuation would affect them, we propose to use music and diaphragmatic breathing to overcome their fear of heights.

To infer an individual's internal arousal state, we aim to model and estimate the hidden state by utilizing well-established computational tools. Hence, we analyze EDA data measured by the Empatica E4. While the main function of sweat gland activation is body thermoregulation, it also carries important information regarding an individual's internal arousal state [94, 51]. In response to internal and external stimuli, the human brain employs the autonomic nervous system to adjust sweat gland secretions [269]. Accordingly, skin surface conductivity, which is measured by electrodes placed on the Empatica wristbands, provides information about brain peripheral signal. By performing deconvolution algorithms and inferring underlying neural impulses [50], we employ state-space representations and point process-based algorithms to model and estimate internal arousal state [56, 66]. Scholars have shown that the state-space representation is a suitable tool for capturing internal arousal state in response to the changes in skin conductance signal [168, 63]. As another measure, we also propose to collect EEG signal to directly explore brain activity. We further evaluate the relationship between the cognitive arousal and performance state in all participants. The acquired data in these experiments will give us the insight required to confirm our hypothesis in effectiveness of safe actuation while closing the loop [212].

While there exist multiple studies verifying the impacts of safe actuation in regulating the human brain states, there is still lack of a systematic approach required for implementing them in real-world environments. The experiments in this study are the first attempts to systematically explore closed-loop cognitive stress regulation using safe actuation with wearable technologies. Employing commercially available wearable devices (i.e., Empatica and muse headband) along with safe actuation make this research applicable in real world settings. The goal is to demonstrate how safe actuation along with practical wearable technologies could be effective in enhancing cognitive performance state and regulating cognitive stress state. The insight resulted from this study would shed light on future closed-loop regulation of internal brain states in a more applicable way. As a result of this research, we aim to publish comprehensive physiological data and their detailed responses in memory-related n-back experiments. Consequently, future research teams could analyze these data sets within different perspective and further investigate these closed-loop human-in-the-loop experiments.

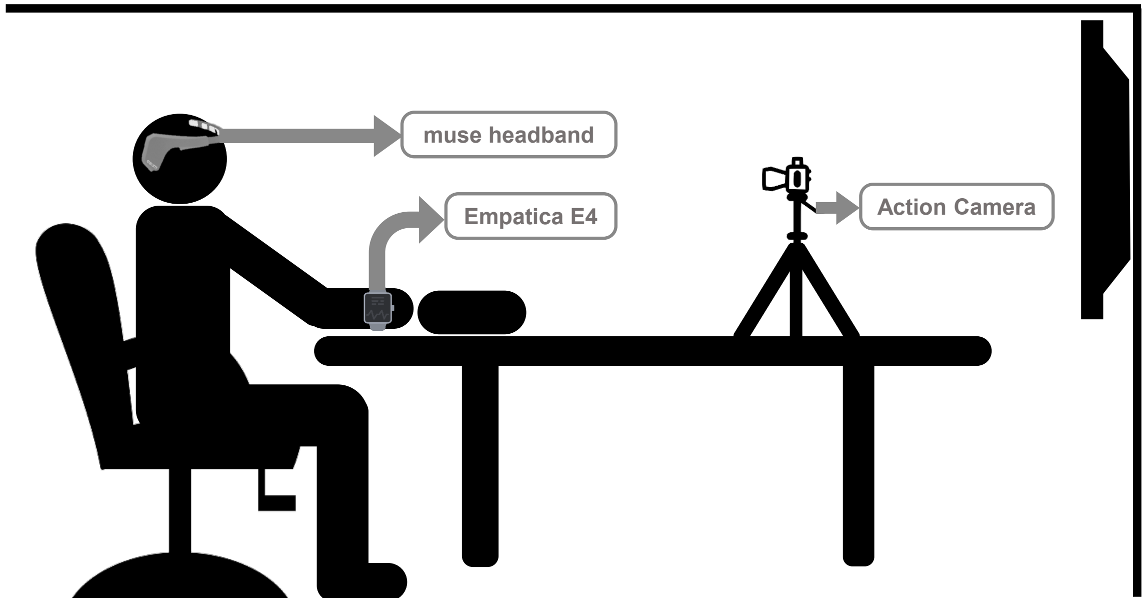

Figure 40: **Human-subject experiments setup.**

6.2 Methods and Materials

All experiments were performed in the computational medicine lab (CML) at the University of Houston (see Figure 40). During the experiment, subject is seated comfortably on an armchair and wears muse headband and Empatica E4 wristbands on both hands. During the experiment, subject looks at the screen to perform n-back memory-related tasks or watching inducing "fear of heights" clips. We also record facial activity with an action camera.

6.2.1 Participants

This pilot study includes three closed-loop experiments. Subjects from the University of Houston population participated in these experiments. In Experiment 1, 17 subjects (11 males, 6 females), with a mean age of 28.5 (SD=4.7), involved in total. In Experiment 2, 13 subjects (10 males, 3 females), with a mean age of 28.4 (SD=3.8), involved in total. In Experiment 3, overall 18 subjects participated (10 males, 7 females with a mean age of 28.3 (SD=4.3)). Participants were required to be at least 18 years old. All subjects read and signed an informed consent document. In analyzing subjects' data, four subjects were excluded due to program crashes ($N = 1$) or skin conductance issues ($N = 3$) in experiment 1. In experiments 2 and 3, one subject was excluded due to program crashes and skin conductance issues. Subjects received gift cards as incentive compensation. They all received a base amount plus additional incentive to further encourage them to fully focus on the tasks. All the experimental procedures and corresponding documents were approved by the institutional review board at the University of Houston, TX, USA (STUDY 00002490).

6.2.2 Equipment

We used two wearable Empatica E4 wristbands and a portable muse headband for EEG recording. Using the Empatica E4 wristbands, we collected electrodermal activity (EDA) (or skin conductance) that tracks the changes in skin conductivity using two metal electrodes, blood volume pulse (BVP), from which heart rate variability can be measured, using a photoplethysmography sensor, motion-based activity using a 3-axis accelerometer sensor, and skin temperature using infrared thermopile. Using the 2016 edition muse headband, we collected brain activity using four EEG sensors.

6.2.3 Procedure

In this study, we propose to perform three sets of closed-loop experiments. As presented in Figure 41, in the first experiment we aim to analyze effects of listening to music in enhancing brain states. As presented in Figure 42, in the second experiment we aim to evaluate the effects of drinking coffee and smelling perfume in a closed-loop manner. In experiments 1 and 2, we ask the subjects to perform memory-related n-back tasks (see Figure 43). In experiment 3, we investigate the effects of safe actuation (i.e., listening to relaxing music and practicing diaphragmatic breathing) while the subjects are exposed to the fear of heights (see Figure 44). Prior to their participation, they are asked to answer behavioral questionnaire and they were recruited only if they show specific levels of acrophobia. To induce fear of heights emotion, we ask the subjects to watch the clips in which humans jump between the tall buildings and run on the edge of them.

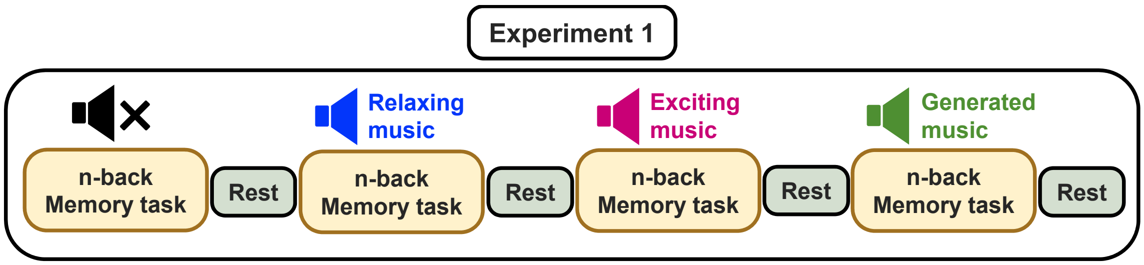

Figure 41: **Experiment 1 procedures.**

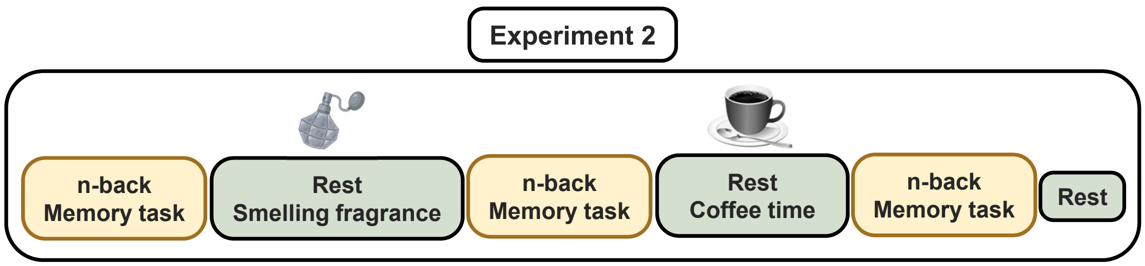

Figure 42: **Experiment 2 procedures.**

To design the experiments 1 and 2, we used E-Prime professional software (version 3.0) on a Dell Latitude 5580 DESKTOP-Q6TBA9H. Within E-Prime, E-Studio and E-Data Aid modules were used to design the presentation of multiple sessions of n-back tasks. To record the responses, we used Chronos. To have a more comfortable setting, we used a 50 inches LCD screen mounted on the wall in 2 meter distance of the subjects (see Figure 40). Participants were asked to sit in an armchair comfortably facing the screen with their dominant hand on the Chronos response device.

In the designed n-back experiments, subjects were shown trials of stimulus (500 ms)

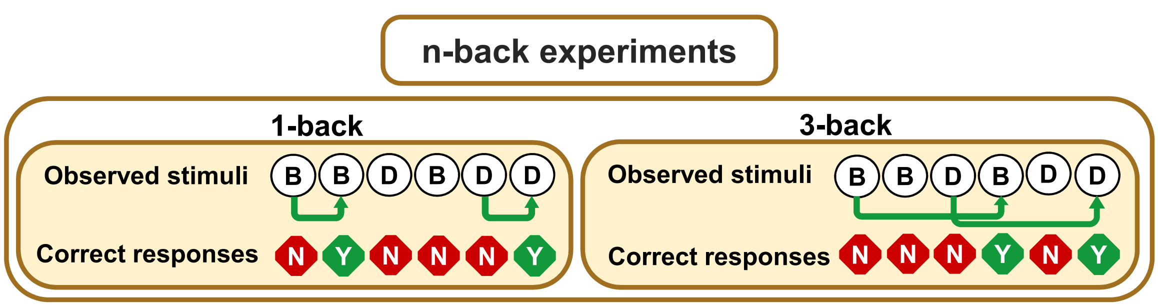

Figure 43: **Memory-related n-back tasks.**

along with a plus sign for their response (1500 ms). Each session consisted of an instruction that lasted for 5 s and 16 trials each of which includes 22 stimuli. There were 10 s breaks in between trials and 20 s relaxation in between the 16 trials. The total duration of each session was 964 s (i.e., $16 \times [5 + (22 \times 2) + 10] + 20 = 964$). To specify their response, participants had to press target (green) vs non-target (red) buttons on Chronos. Before the start of the experiment, they were provided explanation about the tasks and provided with a couple practice trials (i.e., one 1-back and one 3-back trials). In the 1-back task, the participants were asked to determine if the stimulus they saw is the same as they saw one steps before. Conversely, in the 3-back task, they were asked to indicate if the one they saw is the same as they observed three steps before (see bottom sub-panel in Figure 40). In session one of experiment 1, subjects perform n-back tasks with no music. In the second session, they are asked to repeat the tasks while listening to their choice of relaxing music. In the third session, they repeated the tasks while listening to their choice of exciting music. In the final session, they repeated the tasks while listening to the newly generated relaxing music. In what follows we illustrate the process of generating music based on their taste of relaxing music.

Music taste is a colloquial term to represent how different songs have distinct effects on each individual. Nowadays, there are multiple music genres and within each genre there are various bands producing a variety of content, in accordance with a wide range of preferences from their audiences. Musical preference is a very subjective matter, which usually encodes distinct auditory stimulation responses in the brain [270]. Moreover, music has been used to improve clinician-rated depressive symptoms [271], reduce stress levels and increase performance during exams [272, 273] and improve performance in non-complex cognitive tasks [274]. Artificially generated music is an interesting research topic that has the potential to automatically alter musical parameters and optimize the songs to achieve certain desired goals, such as relaxation, excitation or concentration [275]. In this research, we employ deep learning neural networks to generate new songs based on the subject's preference. More specifically, we use a long short-term memory (LSTM) neural network. LSTMs are capable of learning long-term and short-term dependencies and have been widely used in music generation [275, 276]. The LSTM architecture is comprised of various interconnected cell blocks that transfer the cell's hidden state to the next cell, after mathematical manipulations. Each cell block has a memory component that gets altered via the *Forget, Input and Output* gates. The Forget gate is responsible for removing unwanted information from the cell state, the Input gate selects relevant information to be stored in the cell's state and the Output gate filters information for the next cell, all based on the input data and previous cell's output. Each gate works by computing [276]

$$f_t = \sigma(w_f[h_{t-1}, u_t] + b_f), \tag{93}$$

$$i_t = \sigma(w_i[h_{t-1}, u_t] + b_i), \tag{94}$$

$$\text{and} \quad o_t = \sigma(w_o[h_{t-1}, u_t] + b_o), \tag{95}$$

where f_t, i_t, o_t represent forget, input, and output gates, respectively. σ stands for a Sigmoid function, w_x and b_x are weights and biases for a gate x respectively. h_{t-1} represents the output of the previous cell block at time-step $t-1$, u_t is the input at current time-step.

To generate the music in this study, we employ a neural network with three LSTM layers in succession, with a recurrent dropout parameter set to 0.3. With this parameter, at every update, a percentage of the input is dropped, preventing over-fitting. Next, a batch normalization layer is be added, followed by a fully connected layer, and an activation layer with a rectified linear activation function (ReLU). Subsequently, another batch normalization layer layer is added, a dropout layer, and a fully connected layer before the final activation layer with a "SoftMax" function. The "SoftMax" is a generalized logistic function. Finally, the loss metric is calculated during the training phase with a categorical cross entropy function.

The input songs for the training phase of the neural network need to be in textual format. For this, we use of the musical instrument digital interface (MIDI) format as there are plenty of songs available online [277]. This text-based musical format carries instructions on how to play the song, such as notation, pitch and tempo. With this format, the neural network is easily trained on the n-th sequence of notes of songs from a dataset. Once training is complete, each prediction of a future note considers the n-th previous notes and the neural network would be capable of generating new songs with a similar structure. We trained 3 separate networks in 3 different datasets of MIDI songs, obtained from [277]. The musical genres chosen were, (1) classical music with songs from Ludwig van Beethoven, Johann Sebastian Bach and Frédéric François Chopin; (2) fantasy music with video-game songs such as the various Final Fantasy and Mario theme songs; and (3) jazz music including songs from Frank Sinatra and various other authors. Prior to start of the experiment, samples of these types of music are played for the subjects and we asked them to choose their favorite one. Within the experiment newly generated music based on their selection is played for them in the last session. After each session, they sit and relaxed for three minutes (the relaxation time after the second session was six minutes). The entire duration of the experiment is about 80 minutes.

In experiment 2, in first session, they perform n-back tasks with no actuation (Figure 42). Before the second session, they are asked to smell their choice of fragrance. They have six minutes to apply this actuation. Next, they are asked to repeat the n-back tasks. In the third session, we propose to investigate the effects of drinking coffee as the actuation. They were provided with their regular coffee and were asked to sit down and drink their coffee during a 30-minute period while resting. Next, they repeat performing the memory tasks. The entire duration of the experiment is about 90 minutes.

In experiment 3, we incorporate three closed-loop sessions to analyze effects of each actuation separately (Figure 44). In the first and second sessions, effects of listening to relaxing music and newly generated music are analyzed. In the final session, we asked the subjects to start diaphragmatic breathing. In each session, they start with five minutes relaxation to measure their baseline. Next five minutes is dedicated to watching the clips to analyze the open-loop responses without any relaxing practices. In the third five minuets, subjects are asked to watch the clips and practice relaxing actuation (i.e., listening to relaxing music in the first and second sessions, and diaphragmatic breathing in the final

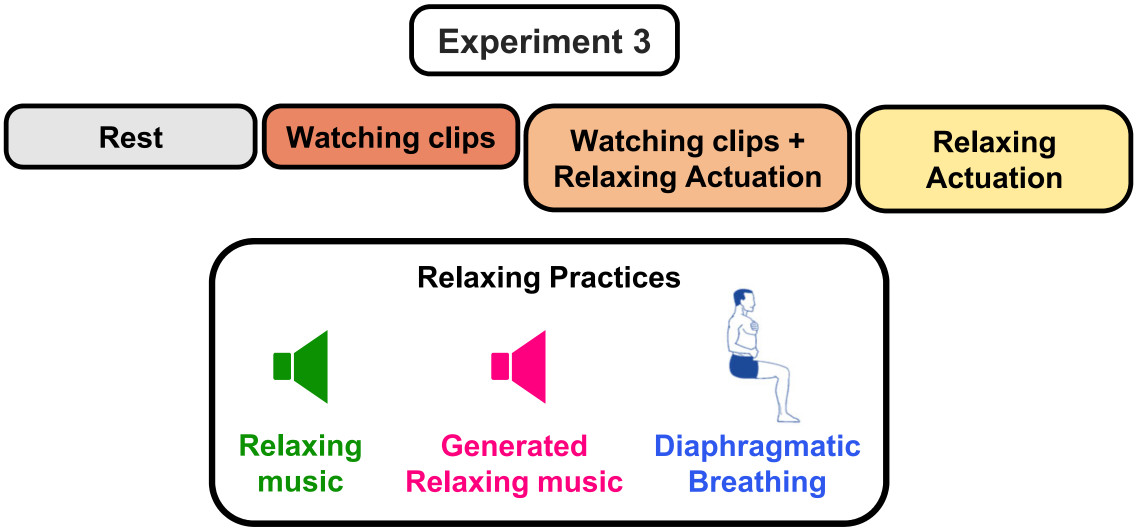

Figure 44: **Experiment 3 procedures.**

session). In the last five minutes of each session, subjects are supposed to continue relaxing practices to reach their baseline. After each session, we consider two minutes of relaxation prior to starting the next session. The overall duration of this experiment is around 70 minutes.

6.2.4 Data Analysis

To study the effectiveness of closing the loop in real-world situations, and investigate how changes in physiological signals affect internal brain states, we perform multiple analyses. These include physiological signal processing and internal cognitive performance estimation. In response to cognitive stress stimuli, we track subjects arousal state and engagement levels. Recording subjects' responses during the n-back experiments (experiments 1 and 2), we follow the goal of performance state estimation. Among the physiological signals collected via Empatica E4 devices, we analyze EDA signal to estimate cognitive arousal state.

Cognitive performance analysis

Analyzing correct/incorrect responses and recorded reaction times, we estimate the performance index to further evaluate the effect of listening to music on cognitive arousal and cognitive performance. Pursuing the state-space model in [65], we consider the cognitive performance state as

$$z_{k+1} = \rho z_k + w_k, \tag{96}$$

where z_k is the hidden performance state, $v_k \sim \mathcal{N}(0, \sigma_w^2)$ represents the process noise, ρ is the unknown coefficient; k stands for the trial number during each experiments. Assigning one binary observation (correct/incorrect response at k^{th} trial) and one continuous observation (reaction time of the corresponding trial) [65], we form the observation model

$$I_k = \log(t_k) = \alpha_0 + \alpha_1 z_k + \delta_k, \tag{97}$$

where $\delta_k \sim \mathcal{N}(0, \sigma_\delta^2)$, t_k displays the reaction time at each trial; α_0 and α_1 are the unknown parameters. The binary response is assumed to follow a Bernoulli distribution with the probability mass function $p_k^{m_k}(1 - p_k)^{1-m_k}$ where p_k stand for the probability of receiving response (i.e., $P(m_k = 1)$). To relate the performance state to the probability of having correct response, we apply the same Sigmoid transform function. Therefore,

$$p_k = \frac{1}{1 + e^{-(z_k + \mu)}}. \tag{98}$$

The constant term μ can be evaluated by $\mu \approx \log\left(\frac{p_0}{1-p_0}\right)$ where p_0 is the average probability of having a correct response over the experiment. Utilizing an expectation maximization (EM) approach, we estimate unknown parameters $\theta_P = \{\rho, \sigma_w^2, \alpha_0, \alpha_1, \sigma_\delta^2\}$ as well as the performance state z_k. The E-step formulation consists of the following prediction and update steps.

Prediction:

$$z_{k|k-1} = \rho z_{k-1|k-1} \tag{99}$$

$$\text{and} \quad s_{k|k-1}^2 = \rho^2 s_{k-1|k-1}^2 + \sigma_w^2. \tag{100}$$

Update:

$$z_{k|k} = z_{k|k-1} + \frac{s^2_{k|k-1}}{\alpha_1^2 s^2_{k|k-1} + \sigma^2_\delta}\left[\sigma^2_\delta(m_k - p_{k|k})] + \alpha_1(I_k - \alpha_0 - \alpha_1 z_{k|k-1})\right] \tag{101}$$

$$\text{and} \quad s^2_{k|k} = \left[\frac{1}{s^2_{k|k-1}} + p_{k|k}(1 - p_{k|k}) + \frac{\alpha_1^2}{\sigma^2_\delta}\right]^{-1}. \tag{102}$$

To achieve smoother results, we perform the following smoothing steps

$$B_k = \rho \frac{s^2_{k|k}}{s^2_{k+1|k}}, \tag{103}$$

$$z_{k|K} = z_{k|k} + B_k(z_{k+1|K} - z_{k+1|k}), \tag{104}$$

$$\text{and} \quad s^2_{k|K} = s^2_{k|k} + B_k^2(s^2_{k+1|K} - s^2_{k+1|k}). \tag{105}$$

The expected values of z_k^2, and $z_k z_{k-1}$ can be derived as,

$$\mathbb{E}[z_k^2] = z^2_{k|K} + s^2_{k|K} \tag{106}$$

$$\text{and} \quad \mathbb{E}[z_{k+1} z_k] = z_{k+1|K} z_{k|K} + B_k s^2_{k+1|K}. \tag{107}$$

At the M-step, the expected log-likelihood function can be formulated as

$$Q_2 = \sum_{k=1}^{K} \mathbb{E}[m_k(\mu + z_k) - \log(1 + e^{\mu + z_k})] \tag{108}$$
$$+ \frac{-K}{2}\log(2\pi\sigma^2_\delta) - \sum_{k=1}^{K} \frac{\mathbb{E}\left[(I_k - \alpha_0 - \alpha_1 z_k)^2\right]}{2\sigma^2_\delta} + \frac{-K}{2}\log(2\pi\sigma^2_w) - \sum_{k=1}^{K} \frac{\mathbb{E}\left[(z_k - z_{k-1})^2\right]}{2\sigma^2_w}.$$

Consequently, in response to the correct/incorrect responses and subject's reaction time, the cognitive performance state can be obtained.

Cognitive arousal analysis via EDA measurements

While main purpose of EDA or skin conductivity is the body's thermoregulation, it carries important information about internal cognitive arousal state. The human brain employs the autonomic nervous system to handle sweat gland activation and response to the internal and external stimuli. The skin conductance signal consists of two components: fast varying phasic and slow varying tonic [278]. By performing cvxEDA type approach we first separate phasic and tonic parts. By performing a deconvolution algorithm, similar to the ones presented in [50, 51, 168, 94], we obtain the underlying neural impulses. Next, we employ a state-space approach to relate the internal arousal state to the changes in SCR events. Since the internal cognitive arousal state is not directly measured, we utilize a marked pint process Bayesian-type filter to estimate the hidden arousal state [56]. In what follows, we review the steps.

In this study, we utilize the approach presented in [168]. SCR measurement as a function of time can be thought of as the summation of a slow varying (tonic) component and a fast varying (phasic) component. The SCR signal can be represented combining these three components as

$$y(t) = y_p(t) + y_s(t) + \nu(t), \tag{109}$$

where $y(t)$, $y_p(t)$, $y_s(t)$, and $\nu(t)$ represent the SCR signal, phasic component, tonic component, and noise process, respectively. The phasic responses can be written as the convolution operation between the autonomic nervous system activation $u(t)$ and the phasic response $h_{1,\boldsymbol{\tau}}(t)$, i.e. $y_p(t) = h_{1,\boldsymbol{\tau}}(t) * u(t)$. The phasic impulse response $h_{\boldsymbol{\tau}}(t)$ can be written as [168]

$$h_{\boldsymbol{\tau}}(t) = \begin{cases} \frac{1}{\tau_r - \tau_d}\left(e^{-\frac{t}{\tau_r}} - e^{-\frac{t}{\tau_d}}\right) & ; \quad \text{if } t \geq 0 \\ 0 & ; \quad \text{otherwise.} \end{cases} \tag{110}$$

Here, τ_r and τ_d are the rise time and decay time of a skin conductance response. On the other hand, the autonomic nervous system activation can be modeled as the weighted shifted some of the delta functions.

If SCR is periodically sampled with a period of T_y for M measurements, we can write the discrete observation equation as follows, i.e., $u(t) = \sum_{i=0}^{N-1} u_i \delta(t - iT_u)$. Here, N is the number of impulses in the input and T_u is the sampling frequency of the input

$$y[k] = y_p(kT_y) + y_s(kT_y) + \nu[k], \tag{111}$$

where $k \in \{1, 2, \cdots, M\}$ represents the k^{th} measurement with sampling frequency of T_y. One should note that here, $T_d = NT_u = MT_y$ is the sampled signal duration. Here, $\nu[k]$ represents the discretized measurement errors. We model $\nu[k]$ as a zero-mean independent and identically distributed (i.i.d) Gaussian random variable. We write the discrete model for $y[k]$ based on the tonic and phasic modeling

$$y[k] = \underbrace{h_{0,\boldsymbol{\tau}}[k]y_{p_0}}_{\text{initial condition}} + \underbrace{\mathbf{h}_{1,\boldsymbol{\tau}}[k]\mathbf{u}}_{\text{phasic}} + \underbrace{\mathbf{h}_2[k]\mathbf{q}}_{\text{tonic}} + \nu[k], \tag{112}$$

where $h_{0,\boldsymbol{\tau}}[k] = e^{-\frac{kT_y}{\tau_d}}$, $\mathbf{h}_{1,\boldsymbol{\tau}}[k] = \big[h_{1,\boldsymbol{\tau}}(kT_y)\ h_{1,\boldsymbol{\tau}}(kT_y - T_u)\ \cdots\ h_{1,\boldsymbol{\tau}}(T_u)\ \underbrace{0\ \cdots\ 0}_{N-\frac{kT_y}{T_u}}\big]^\top$, $\mathbf{h}_2[k] = \big[h_2(kT_y + \Lambda_s)\ \ h_2(kT_y)\ \ h_2(kT_y - \Lambda_s)\ \ \cdots\ \ h_2(kT_y - (P-1)\Lambda_s)\big]^\top$; $\mathbf{u} = [u_1 \quad u_2 \quad \cdots \quad u_N]^\top$ represents a sparse vector containing all the amplitudes of the impulses in the autonomic nervous system activation model over the entire signal duration and $\mathbf{q} = [q_1 \quad q_2 \quad \cdots \quad q_N]^\top$ represents all the coefficients of the cubic B-spline basis functions and $y_{p_0} = y_p(0)$. Here $h_2(t)$ represents the cubic B-spline basis functions and $\mathbf{h}_2[k]$ is the discretized version of a shifted cubic-spline basis function. Here the knot size for the cubic B-spline basis functions is selected similar to [168]. The overall vector matrix form becomes

$$\mathbf{y} = \underbrace{\mathbf{H}_{0,\boldsymbol{\tau}}y_{p_0} + \mathbf{H}_{1,\boldsymbol{\tau}}\mathbf{u}}_{\text{phasic}} + \underbrace{\mathbf{H}_2\mathbf{q}}_{\text{tonic}} + \boldsymbol{\nu}, \tag{113}$$

where $\mathbf{y} = [y[1] \quad y[2] \quad \cdots \quad y[M]]^\top$, $\mathbf{H}_{0,\boldsymbol{\tau}} = [h_{0,\boldsymbol{\tau}}[1] \quad h_{0,\boldsymbol{\tau}}[2] \quad \cdots \quad h_{0,\boldsymbol{\tau}}[M]^\top$, $\mathbf{H}_{1,\boldsymbol{\tau}} = [\mathbf{h}_{1,\boldsymbol{\tau}}[1] \quad \mathbf{h}_{1,\boldsymbol{\tau}}[2] \quad \cdots \quad \mathbf{h}_{1,\boldsymbol{\tau}}[M]]^\top$, $\mathbf{H}_2 = [\mathbf{h}_2[1] \quad \mathbf{h}_2[2] \quad \cdots \quad \mathbf{h}_2[M]]^\top$, and $\boldsymbol{\nu} = [\nu_1 \quad \nu_2 \quad \cdots \quad \nu_M]^\top$. Here y_{p_0} is assumed to be unknown and estimated during the deconvolution. During the deconvolution, all the unknowns, i.e., $\boldsymbol{\tau}$, $\mathbf{u}$, and $\mathbf{q}$ are identified by solving an optimization problem in a coordinate descent manner that utilizes physiological prior information and generalized-cross-validation. The details for the estimation is provided in [168]. For a long measurement, we split the data into multiple blocks of 200 seconds with a stride of 100 seconds to perform the deconvolution for each of these blocks. Later, all the results of $\mathbf{u}$ are concatenated by discarding 50 seconds of the start and end part of the results to avoid inaccuracies in the boundaries of the deconvolution. Only for the first block and last block, we keep the first 50 second and last 50 second parts, respectively, as they cannot be replaced by results from the adjacent blocks.

Following [56], we specify a first-order autoregressive model for hidden cognitive arousal state

$$x_{j+1} = x_j + \epsilon_j, \tag{114}$$

where x_j and $\epsilon_j \sim \mathcal{N}(0, \sigma_\epsilon^2)$ stand for internal cognitive arousal state and process noise at time j, respectively. Employing SCR events' timing and their amplitudes as the observation, we intend to estimate hidden arousal state using a marked point process Bayesian filter [56]. To this end, we consider the occurrence of a neural impulse n_j, as a Bernoulli-distributed random variable with probability mass function $a_j^{n_j}(1-a_j)^{1-n_j}$ where $a_j = P(n_j = 1)$. To relate relate x_j to a_j, we use Sigmoid transfer function [62]

$$a_j = \frac{1}{1 + e^{-(x_j + \beta)}}, \tag{115}$$

where β is a constant that can be calculated from $\beta \approx \log\left(\frac{a_0}{1-a_0}\right)$ and a_0 represents the average probability of observing an impulse during the experiment. Similar to [56], we define the continuous-valued amplitude r_j of each neural impulse as

$$r_j = \gamma_0 + \gamma_1 x_j + v_j, \tag{116}$$

where r_j is the amplitude of the observed neural impulse due to ANS activation, $v_j \sim \mathcal{N}(0, \sigma_v^2)$ describes the sensor noise, γ_0 and γ_1 are the unknown parameters to be determined.

Consequently, the joint density function for the observed neural stimuli is

$$p(n_j \cap r_j | x_j) = \begin{cases} 1 - a_j & \text{if } n_j = 0 \\ a_j \frac{1}{\sqrt{2\pi\sigma_v^2}} e^{\frac{-(r_j - \gamma_0 - \gamma_1 x_j)^2}{2\sigma_v^2}} & \text{if } n_j = 1 \end{cases}. \tag{117}$$

Applying the expectation-maximization framework, we estimate the unknown parameters $\theta_A = \{\sigma_\epsilon^2, \gamma_0, \gamma_1, \sigma_v^2\}$, and hidden state x_j, simultaneously. The E-step equations have been derived based on the observations $R^J = \{(n_1, r_1), ..., (n_J, r_J)\}$ up to time J. At the E-step, the main objective is to estimate x_j and its variance. The forward filter consist of the prediction and updates steps.

Prediction:

$$x_{j|j-1} = x_{j-1|j-1} \tag{118}$$

$$\text{and} \quad \sigma_{j|j-1}^2 = \sigma_{j-1|j-1}^2 + \sigma_\epsilon^2. \tag{119}$$

Update:

If $n_j = 0$

$$x_{j|j} = x_{j|j-1} + \sigma_{j|j-1}^2 (n_j - a_{j|j}) \tag{120}$$

$$\text{and} \quad \sigma_{j|j}^2 = \left[\frac{1}{\sigma_{j|j-1}^2} + a_{j|j}(1 - a_{j|j}) \right]^{-1}. \tag{121}$$

If $n_j = 1$

$$C_j = \frac{\sigma_{j|j-1}^2}{\gamma_1^2 \sigma_{j|j-1}^2 + \sigma_v^2}, \tag{122}$$

$$x_{j|j} = x_{j|j-1} + C_j \left[\sigma_v^2 (n_j - a_{j|j}) + \gamma_1 (r_j - \gamma_0 - \gamma_1 x_{j|j-1}) \right], \tag{123}$$

$$\text{and} \quad \sigma_{j|j}^2 = \left[\frac{1}{\sigma_{j|j-1}^2} + a_{j|j}(1 - a_{j|j}) + \frac{\gamma_1^2}{\sigma_v^2} \right]^{-1}. \tag{124}$$

To derive $x_{j|j}$ appears on both sides of (120) and (123), we use Newton-Raphson method.

Next we follow a smoother approach to derive s smooth estimate

$$A_j = \frac{\sigma^2_{j|j}}{\sigma^2_{j+1|j}}, \tag{125}$$

$$x_{j|J} = x_{j|j} + A_j(x_{j+1|J} - x_{j+1|j}), \tag{126}$$

$$\text{and} \quad \sigma^2_{j|J} = \sigma^2_{j|j} + A_j^2(\sigma^2_{j+1|J} - \sigma^2_{j+1|j}). \tag{127}$$

At the M-step, we define $\tilde{J} = \{j|n_j = 1\}$ to indicate the locations of neural impulse occurrences. Similar to [56] and [62], we compute the expected values of x_j^2 and $x_j x_{j-1}$ as

$$\mathbb{E}[x_j^2] = x^2_{j|J} + \sigma^2_{j|J} \quad \text{and} \quad \mathbb{E}[x_{j+1}x_j] = x_{j+1|J}x_{j|J} + A_j\sigma^2_{j+1|J}. \tag{128}$$

Thereafter, we derive the log-likelihood function Q_1 and, we estimate the unknown parameters such that they maximize it. The Q_1 function is

$$\begin{aligned} Q_1 = &\sum_{j=1}^{J} \mathbb{E}[n_j(\beta + x_j) - \log(1 + e^{\beta + x_j})] \qquad (129) \\ &+ \frac{-\tilde{J}}{2}\log(2\pi\sigma_v^2) - \sum_{j\in\tilde{J}} \frac{\mathbb{E}\left[(r_j - \gamma_0 - \gamma_1 x_j)^2\right]}{2\sigma_v^2} + \frac{-J}{2}\log(2\pi\sigma_\epsilon^2) - \sum_{j=1}^{J}\frac{\mathbb{E}\left[(x_j - x_{j-1})^2\right]}{2\sigma_\epsilon^2}. \end{aligned}$$

The algorithm iterates between the E-step and the M-step until convergence.

6.3 Results

In this section, we employ the physiological measurements and utilize state-space representation to model internal brain states. We then apply signal processing techniques to estimate hidden brain states. To demonstrate how incorporating safe actuation would affect subjects' performance state in experiments 1 and 2, we first present the changes in cognitive performance state in response to the recorded correct/incorrect responses and reaction times. Next, we present the cognitive arousal estimates in response to the changes in skin conductance signal. The results associated with selected subjects are presented in

Figures 45–73.

The results for experiment 1 are presented in Figures 45–54. In top panel of Figures 45–54, the first sup-panel shows the reaction time along with correct (black) and incorrect (red) responses. Second sub-panel shows cognitive performance state estimates. Bright and dark backgrounds present 1-back and 3-back tasks, respectively. In the bottom panel, sub-panels show in turn the skin conductance signal, underlying neural impulses, and estimated cognitive arousal state. The grey, green, purple, and blue background colors in turn represent the results associated with no music, relaxing music, exciting music, and newly generated relaxing music sessions, respectively.

The results for experiment 2 are presented in Figures 55–64. In top panel of Figures 55–64, the first sup-panel shows the reaction time along with correct (black) and incorrect (red) responses. Second sub-panel shows cognitive performance state estimates. Bright and dark backgrounds present 1-back and 3-back tasks, respectively. In the bottom panel, sub-panels show in turn the skin conductance signal, underlying neural impulses, and estimated cognitive arousal state. The grey, green, purple, and blue background colors in turn represent the results associated with no music, relaxing music, exciting music, and newly generated relaxing music sessions, respectively.

The results for experiment 3 are presented in Figures 65–73. In Figures 65–73, the sub-panels show in turn the skin conductance signal, underlying neural impulses, and estimated cognitive arousal state. The grey, red, orange, and yellow background colors in turn represent the results associated with rest, fear of heights with no actuation, fear of heights with relaxing actuation, relaxing periods, respectively. Left box is associated with relaxing music. Middle box is associated with newly generated relaxing music. Right box is corresponding to diaphragmatic breathing.

6.3.1 Cognitive Performance Analysis

We follow the methodology presented in [65] to decode latent performance state in experiments 1 and 2. We take correct/incorrect responses and reaction times as binary and continuous observations, respectively. The results of cognitive performance analysis in both experiments 1 and 2 are presented in top panels of Figures 45–64.

6.3.2 Cognitive Arousal and Engagement Analysis

To estimate internal arousal state, we analyze skin conductance signal collected via Empatica E4 wristbands. By applying deconvolution algorithm and inferring underlying neural impulses, we establish a marked point process Bayesian filter to estimate hidden cognitive arousal state. The results of cognitive arousal estimation in all three experiments are depicted in middle panels of Figures 45–64 (for experiments 1 and 2) and top panel of Figures 70–73 (for experiment3).

6.4 Discussion

As one of the very first attempts in closed-loop brain state regulation, we designed and performed novel human-subject experiments using wearable devices. We also proposed to use safe actuation to regulate brain states and enhance the productivity. More specifically, we designed two memory-related n-back experiments and proposed to take safe actuation (i.e., listening to music tracks in experiment 1, smelling perfumes, and drinking coffee in experiment 2) to close the loop. In experiment 3, we explored effects of safe actuation (i.e., relaxing music and diaphragmatic breathing) while watching the clips that induce fear of heights on individuals with levels of acrophobia. In what follows we discuss the results in each experiment. Next we elaborate on general findings and discuss the challenges.

6.4.1 Experiment 1

Analyzing the results for all subjects, we observe an enhancement in all subjects' performance state while listening to music. While the main goal of designing the closed-loop architectures is to keep the persons' performance state within a desired range and prevent them from feeling bored and unengaged, listening to music has further enhanced the performance state and helped them better concentrate on memory tasks. To further explain

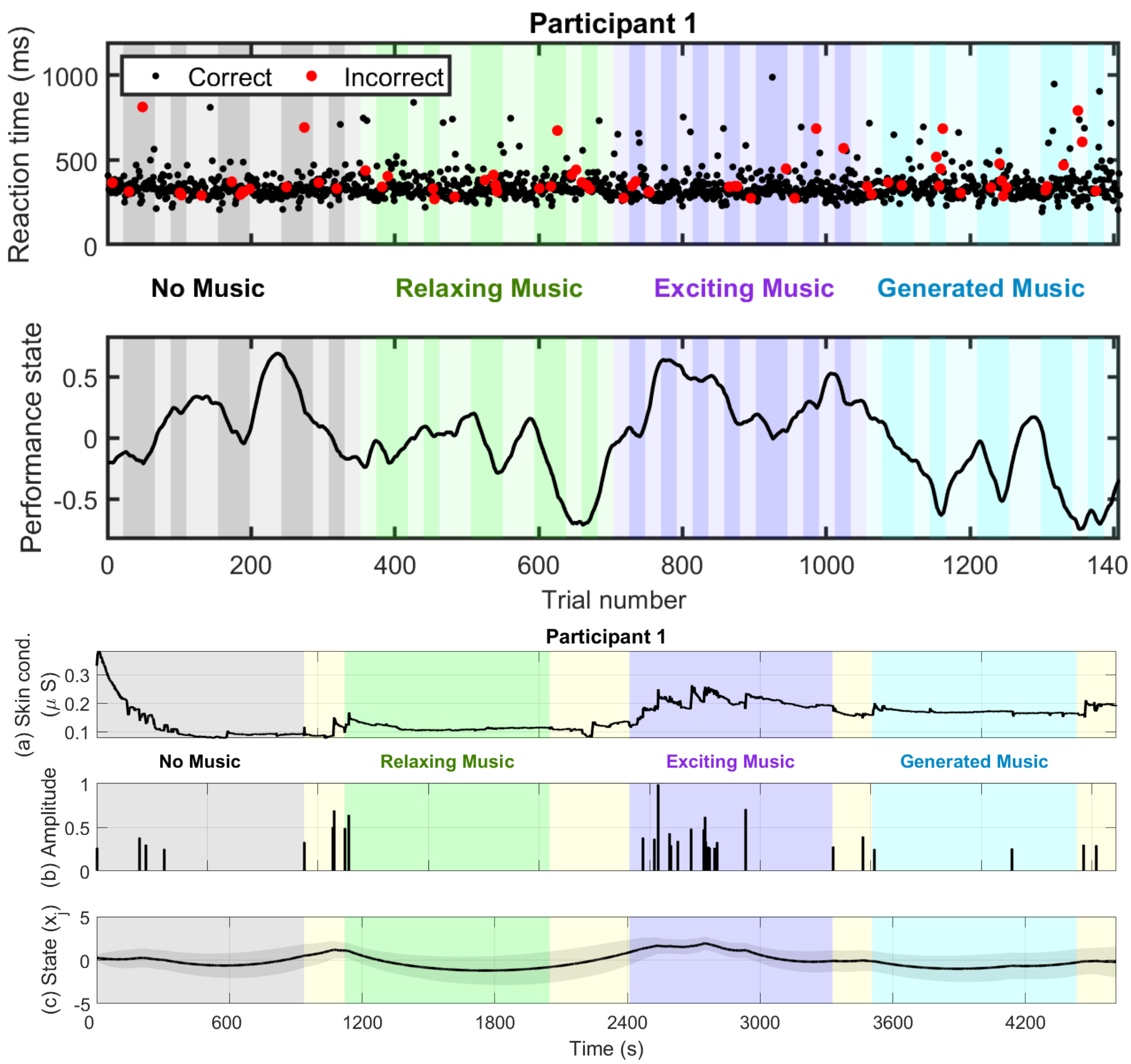

Figure 45: **Results of Experiment 1 (Subject 1).**

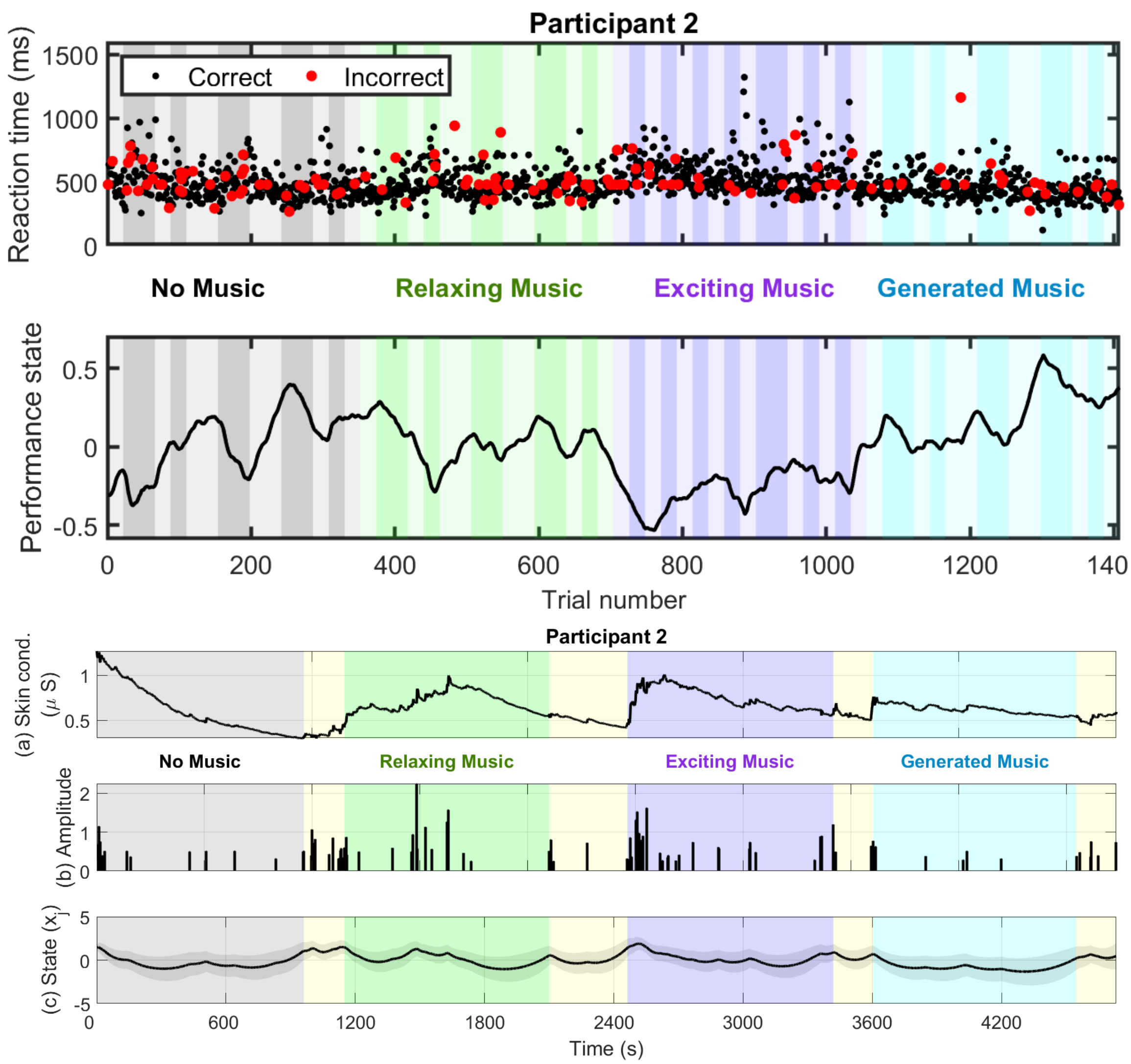

Figure 46: **Results of Experiment 1 (Subject 2).**

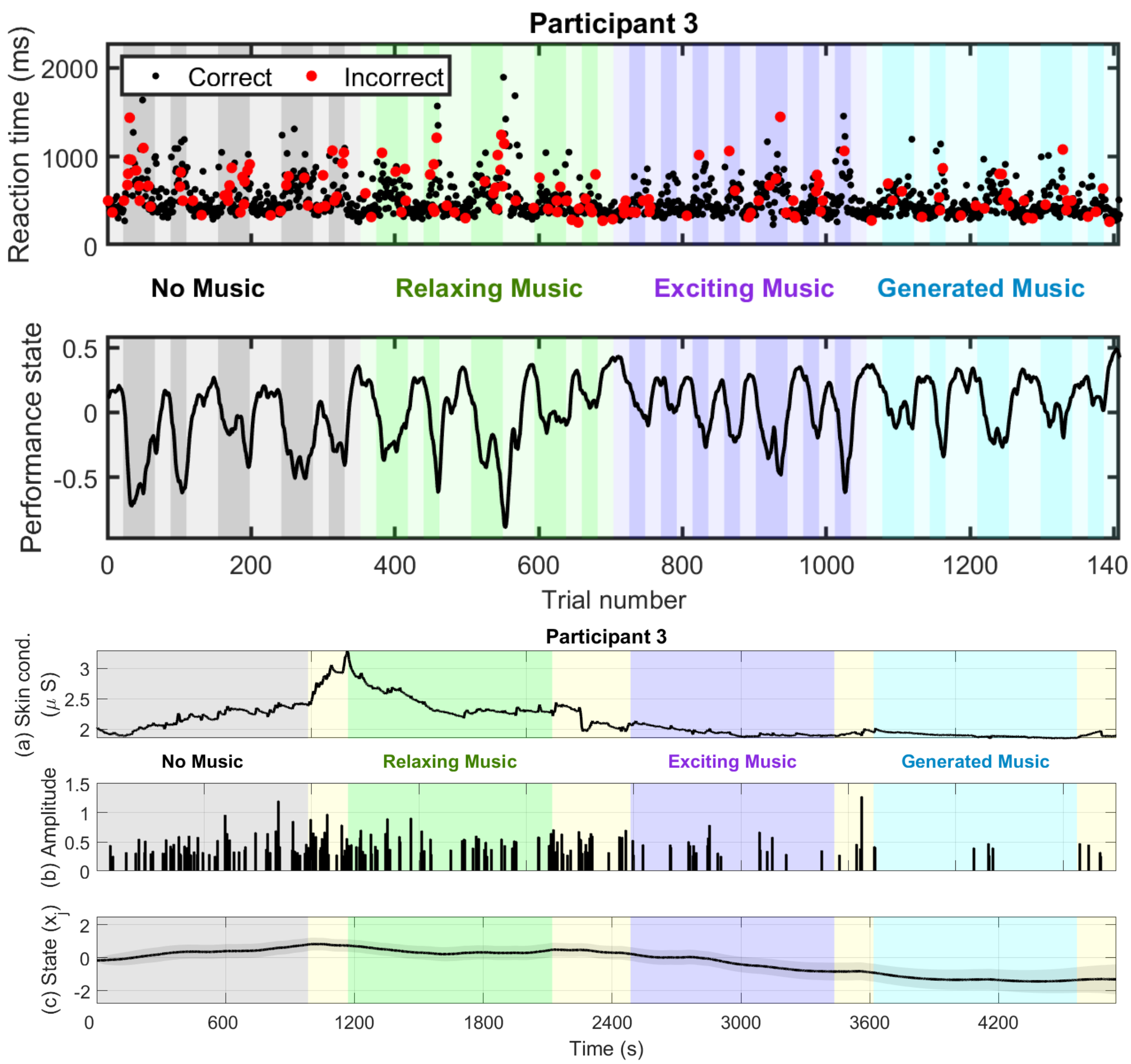

Figure 47: **Results of Experiment 1 (Subject 3).**

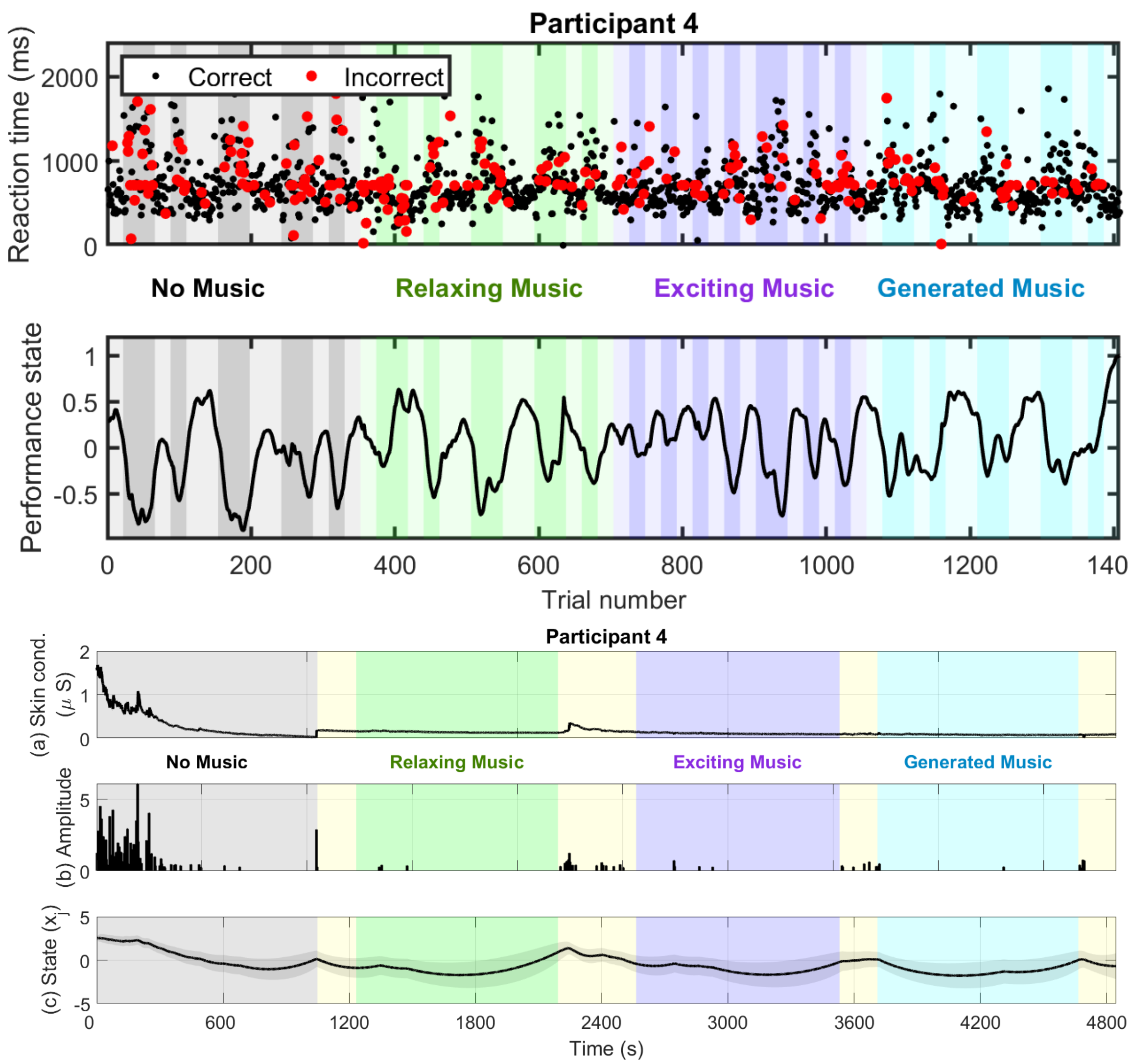

Figure 48: **Results of Experiment 1 (Subject 2).**

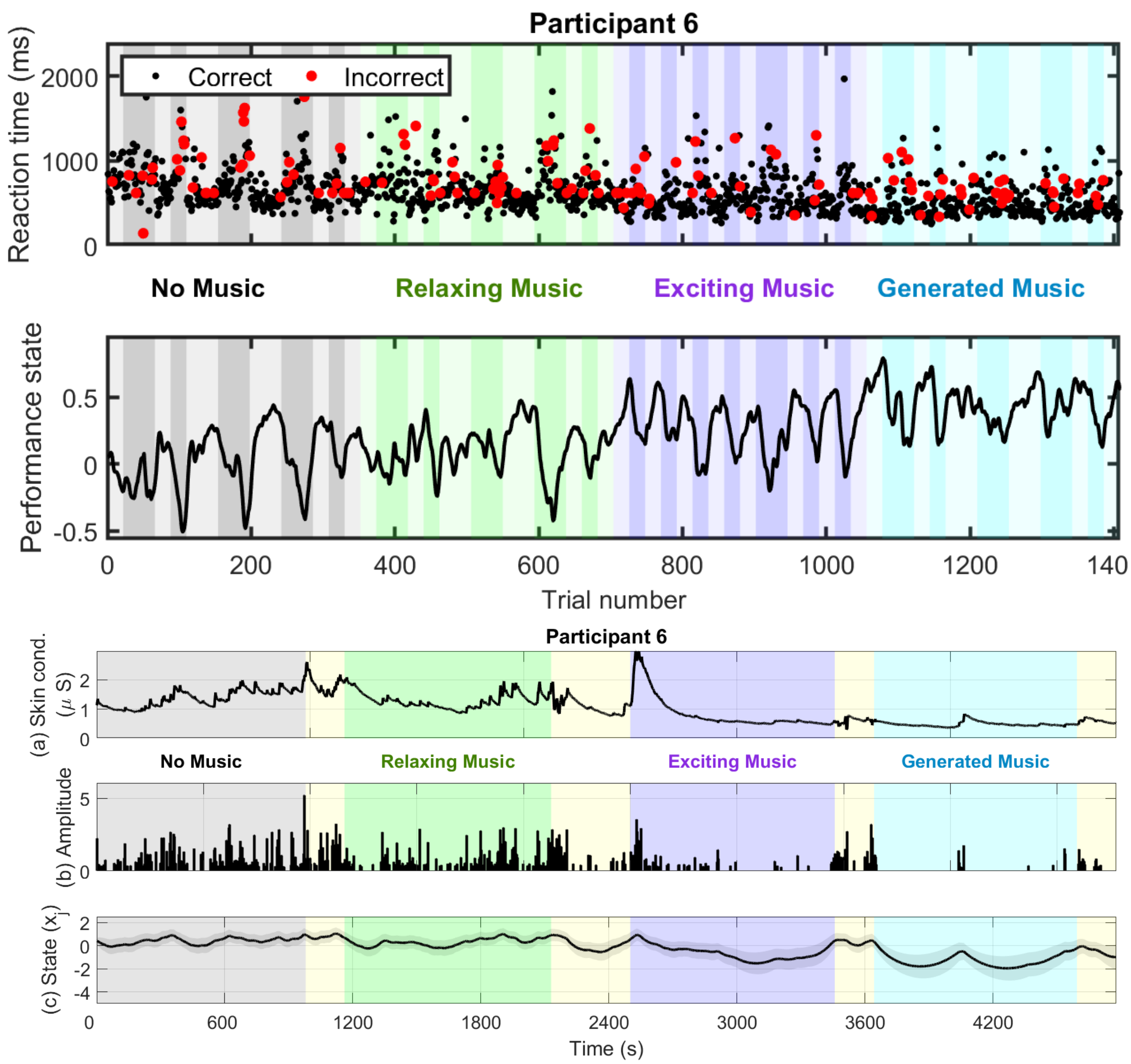

Figure 49: **Results of Experiment 1 (Subject 6).**

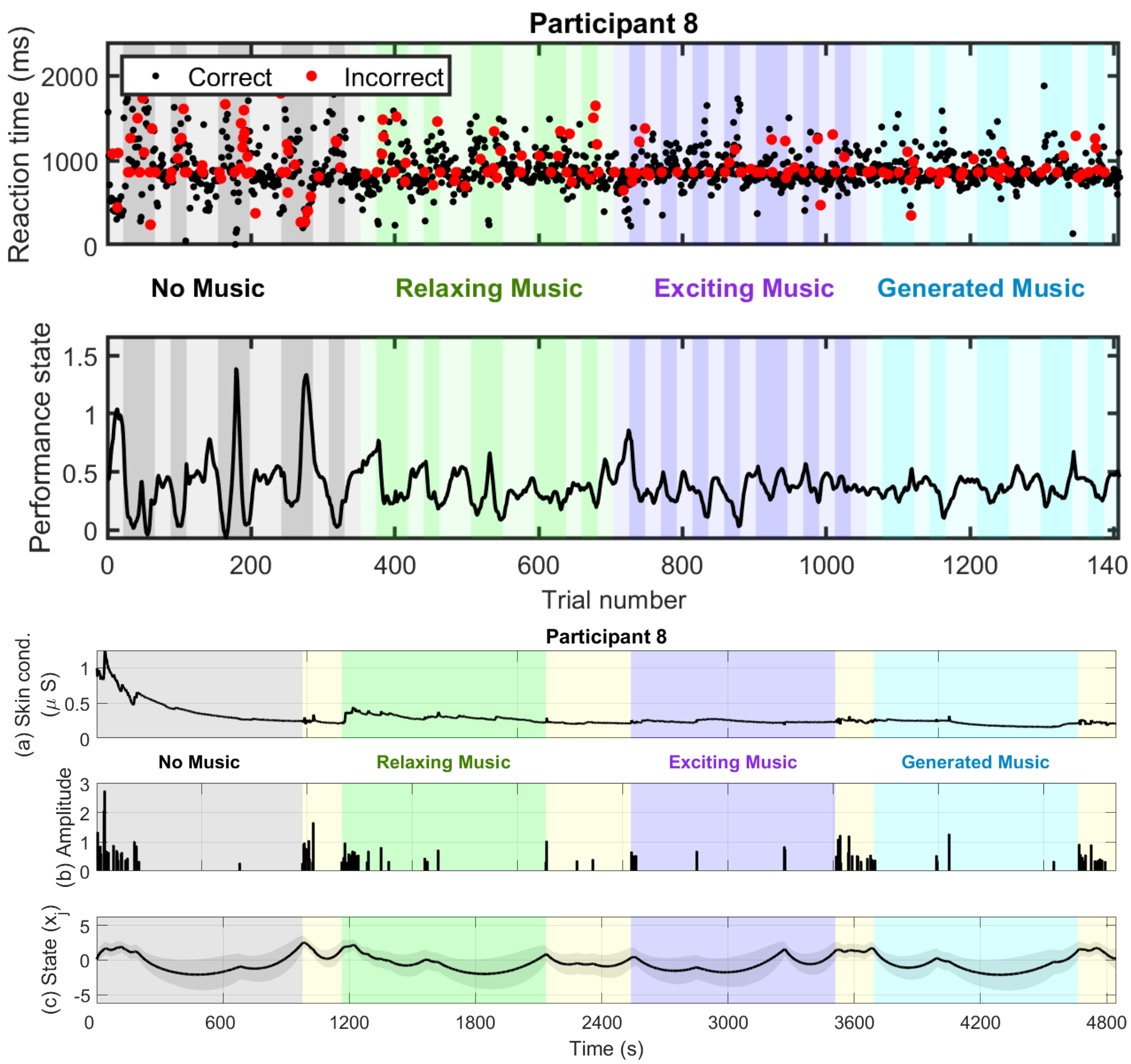

Figure 50: **Results of Experiment 1 (Subject 8).**

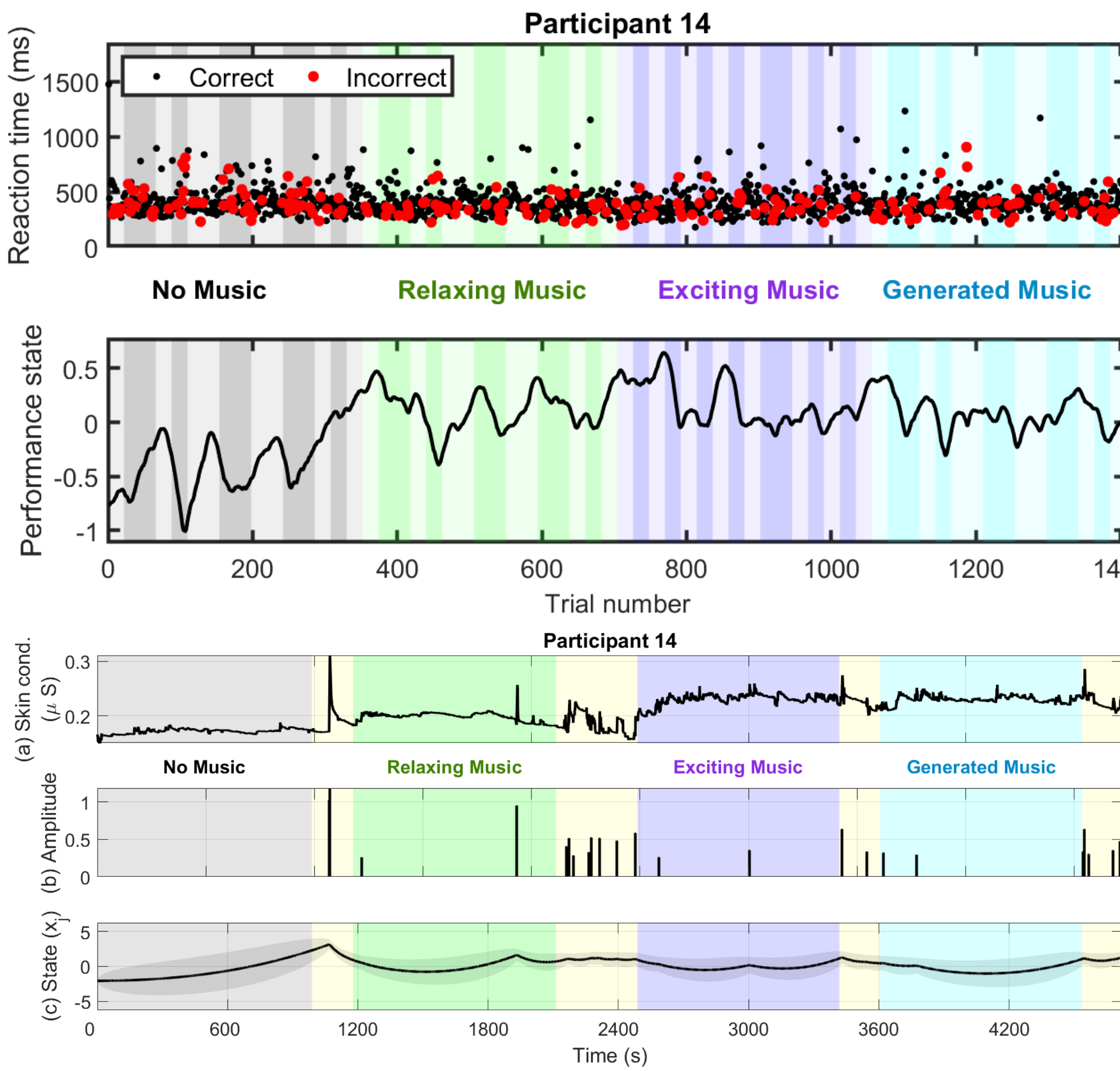

Figure 51: **Results of Experiment 1 (Subject 14).**

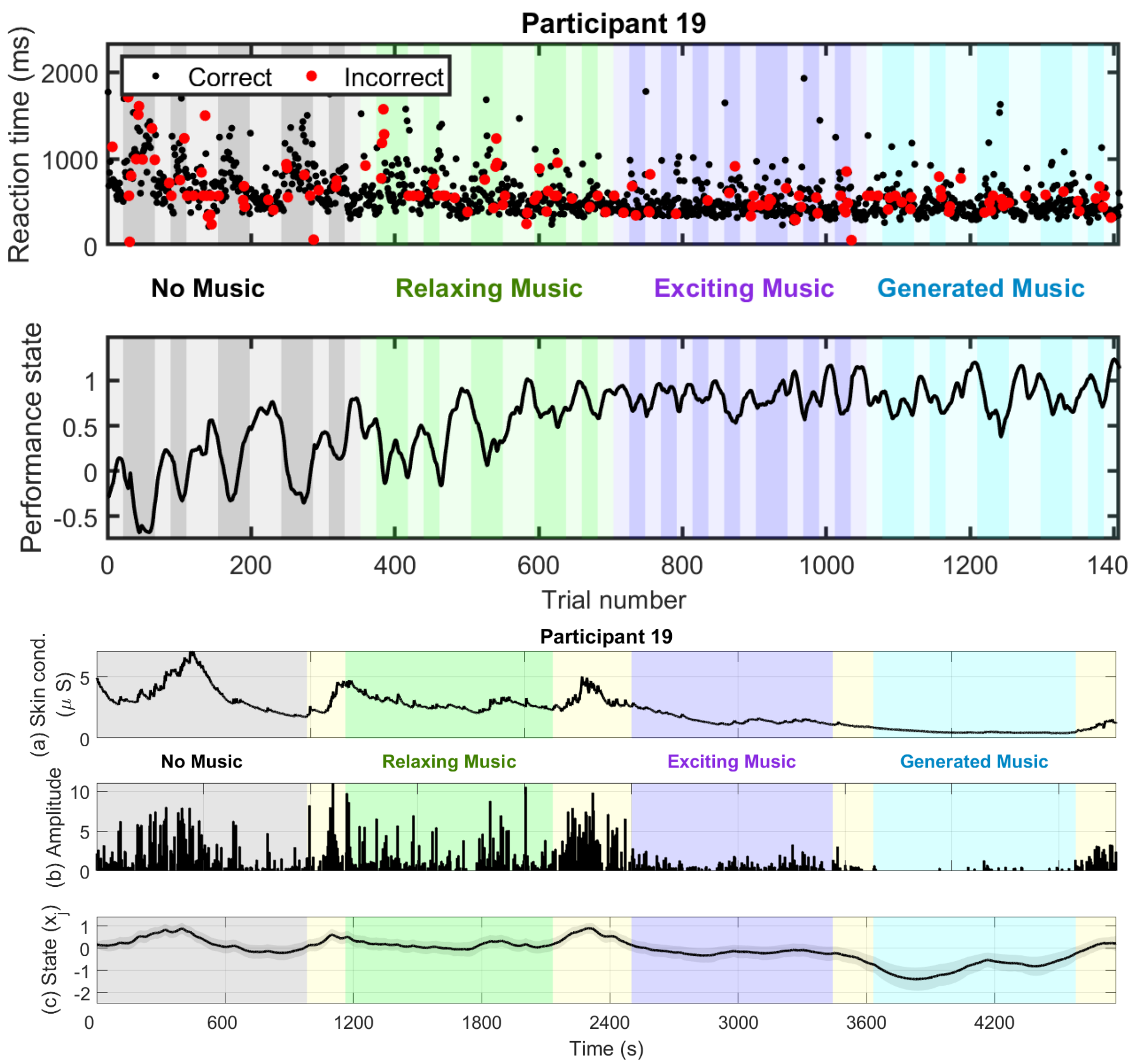

Figure 52: **Results of Experiment 1 (Subject 19).**

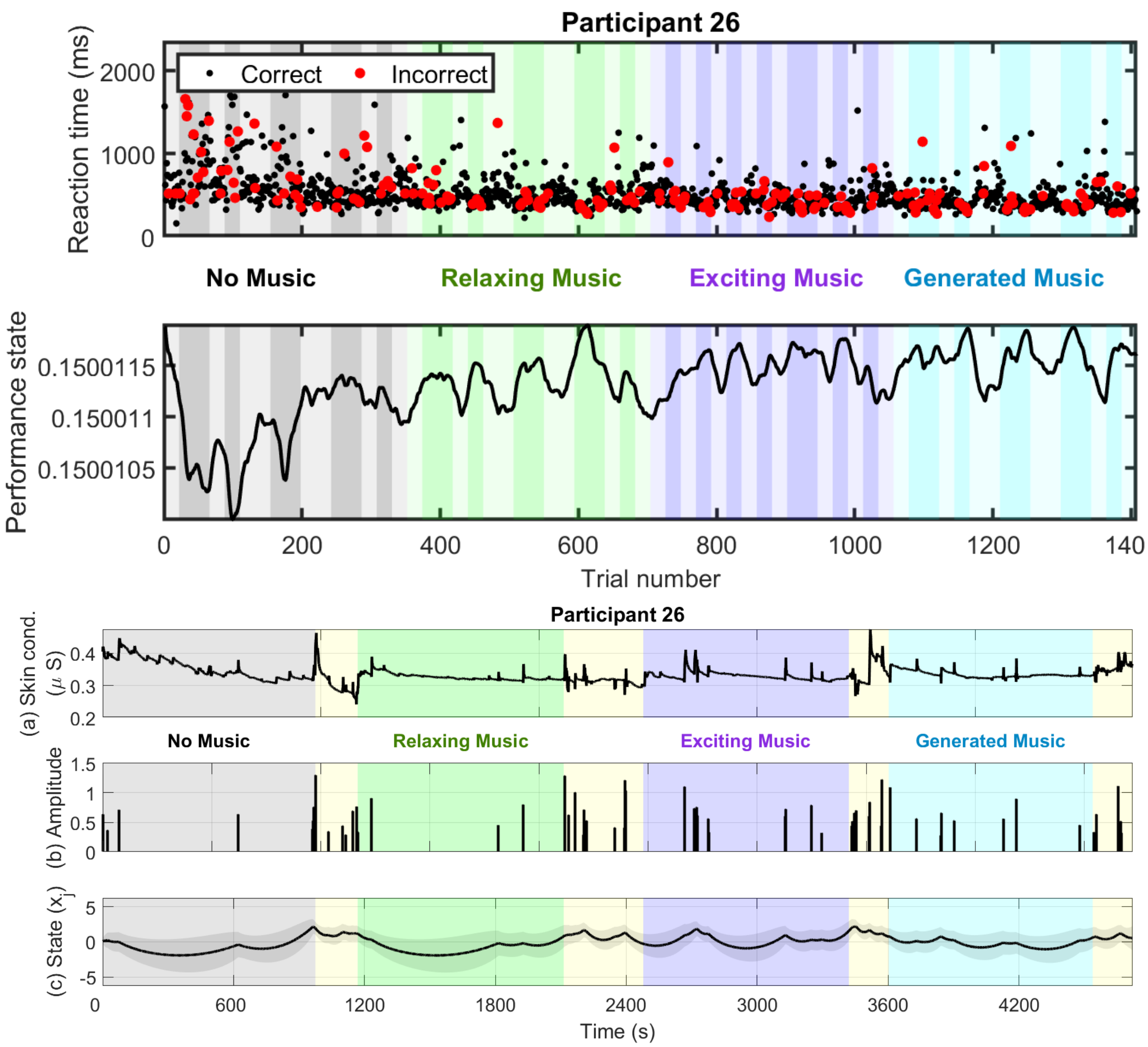

Figure 53: **Results of Experiment 1 (Subject 26).**

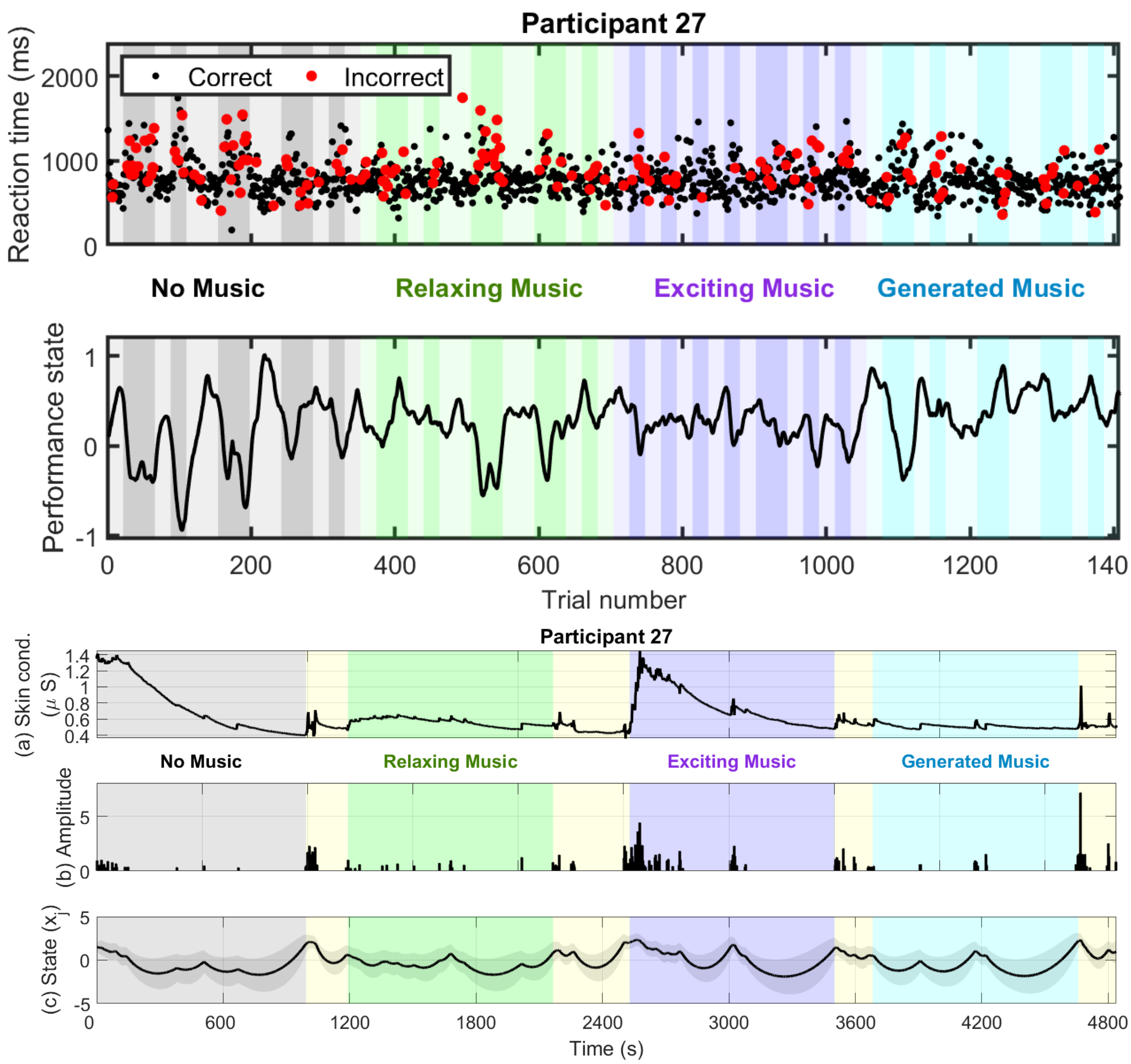

Figure 54: **Results of Experiment 1 (Subject 27).**

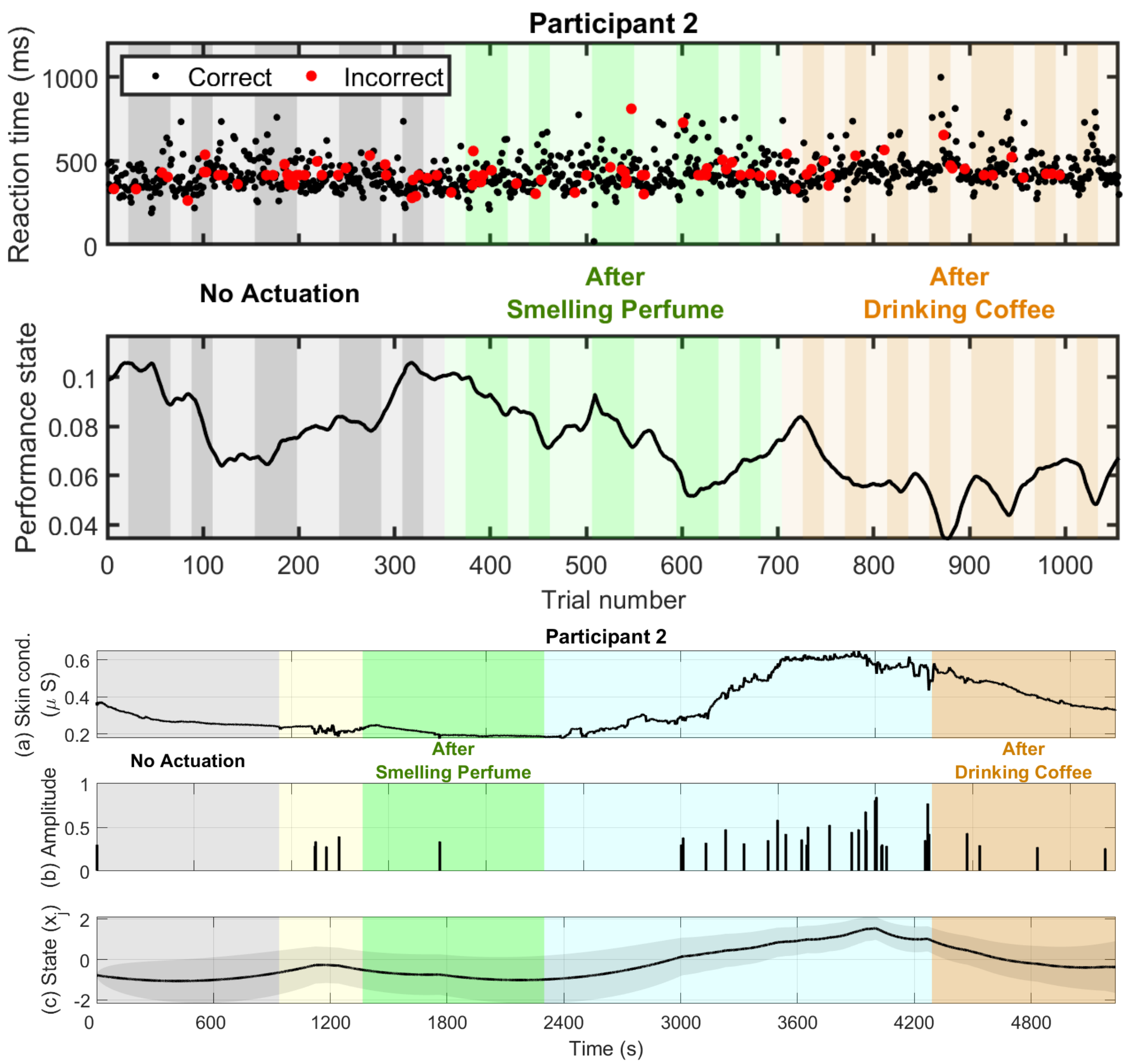

Figure 55: **Results of Experiment 2 (Subject 2).**

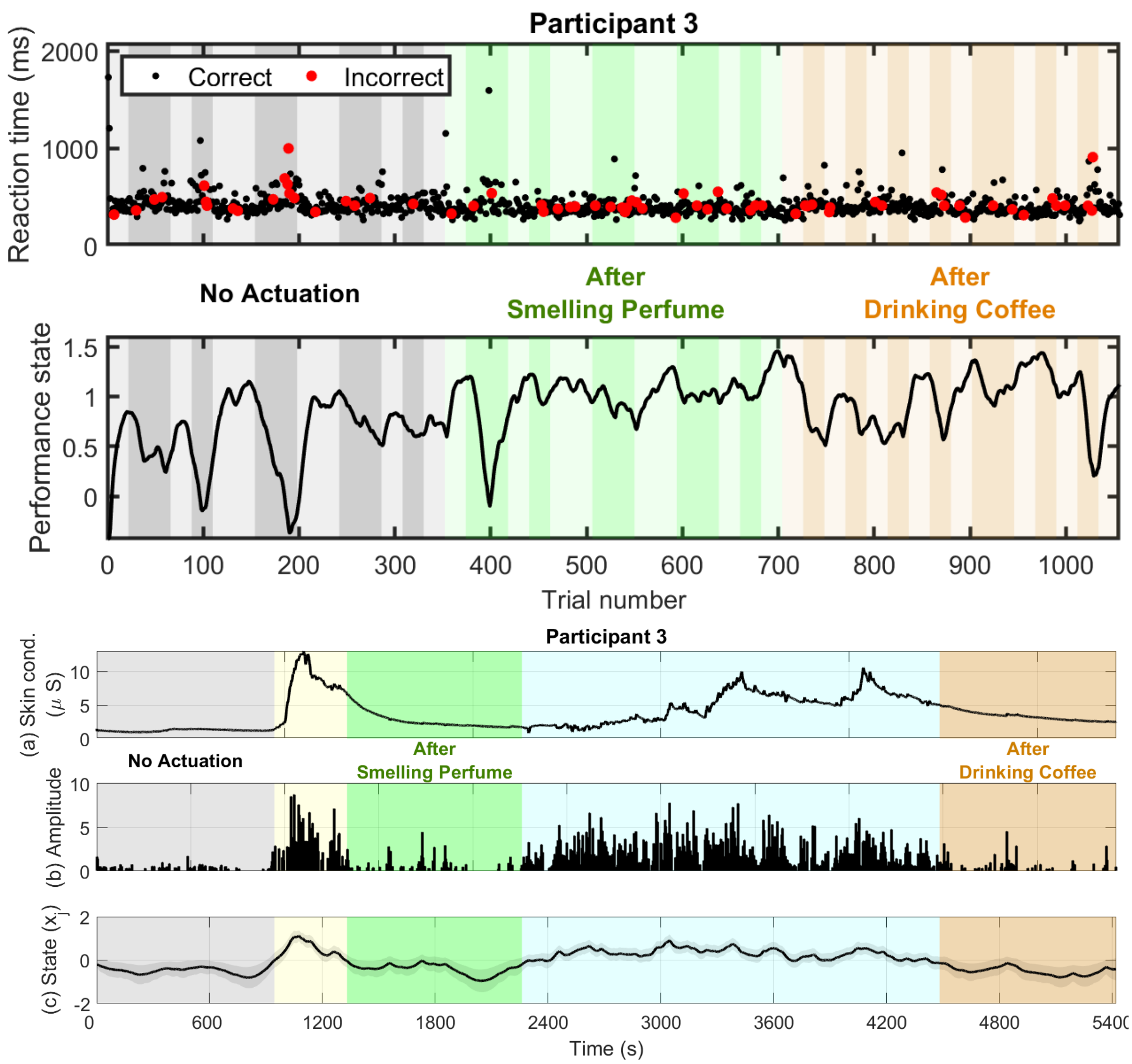

Figure 56: **Results of Experiment 2 (Subject 3).**

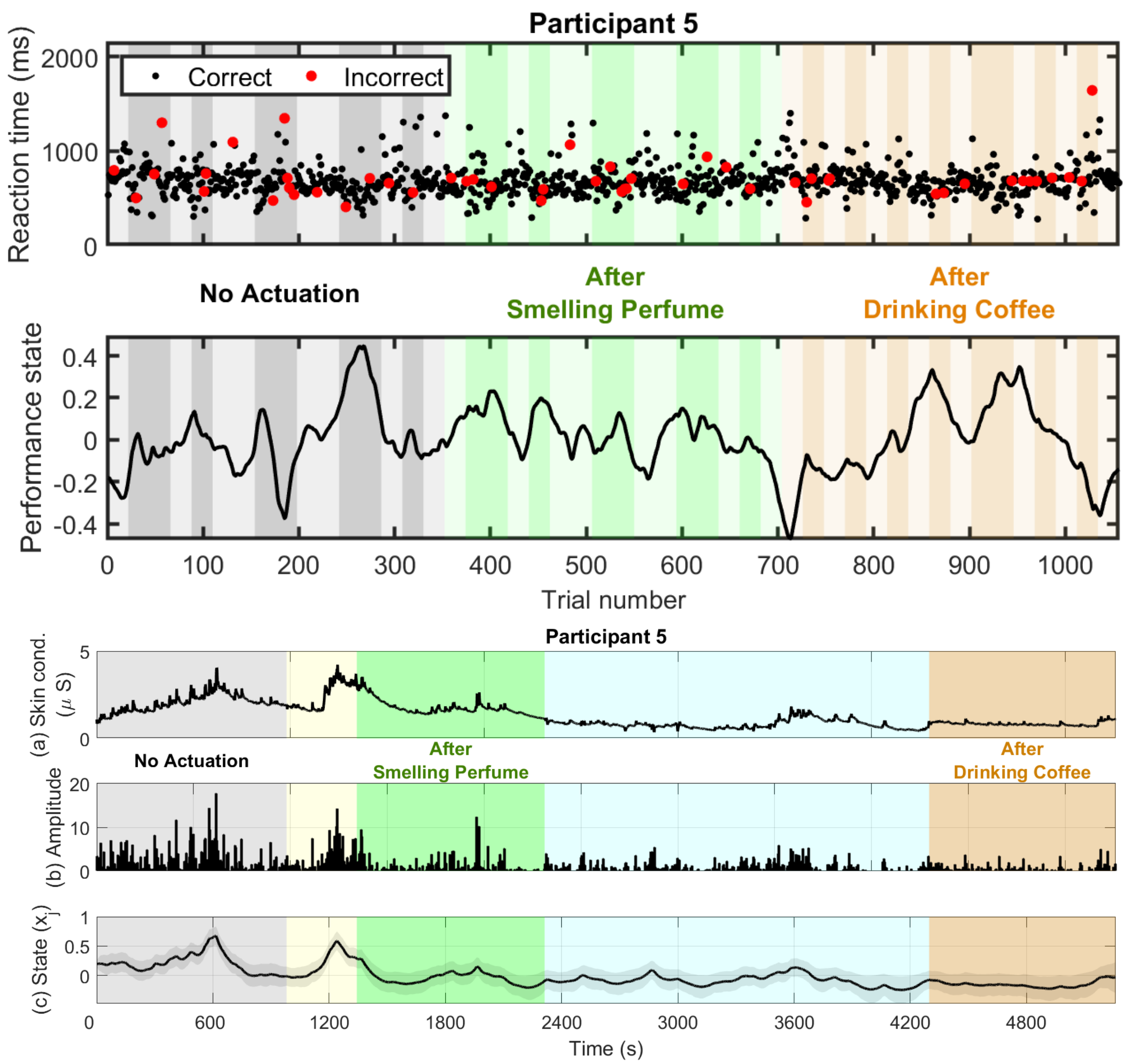

Figure 57: **Results of Experiment 2 (Subject 5).**

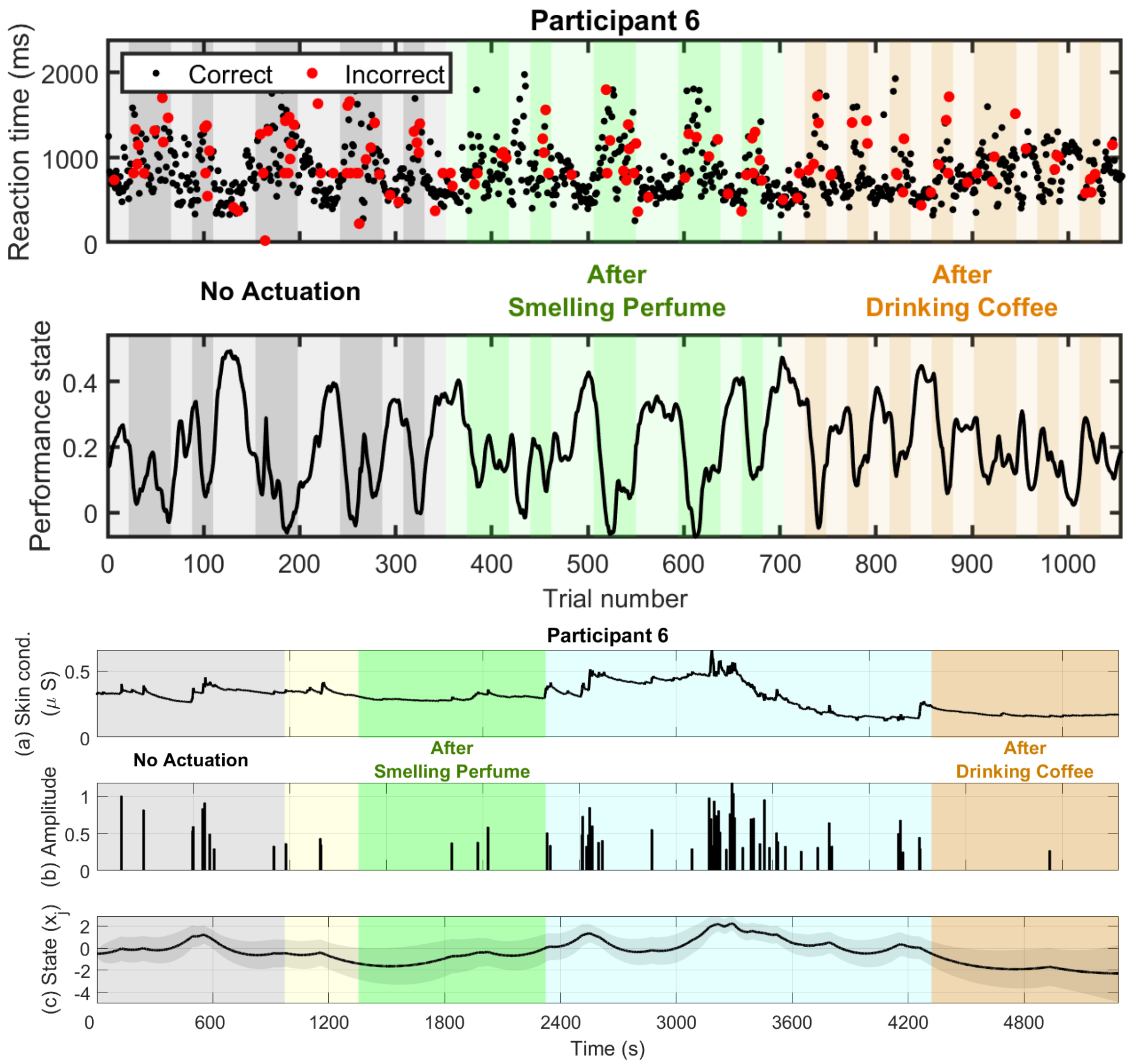

Figure 58: **Results of Experiment 2 (Subject 6).**

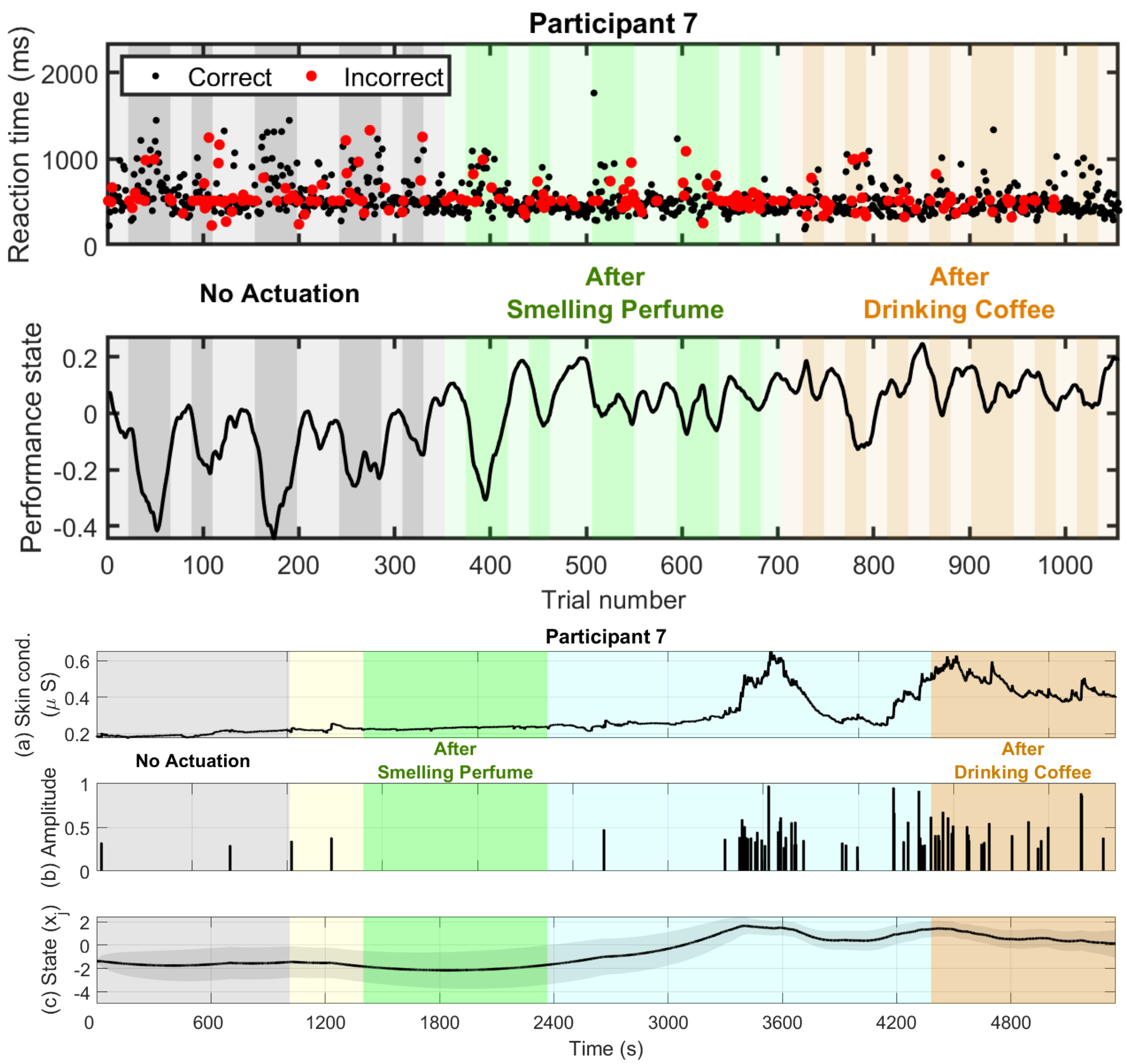

Figure 59: **Results of Experiment 2 (Subject 7).**

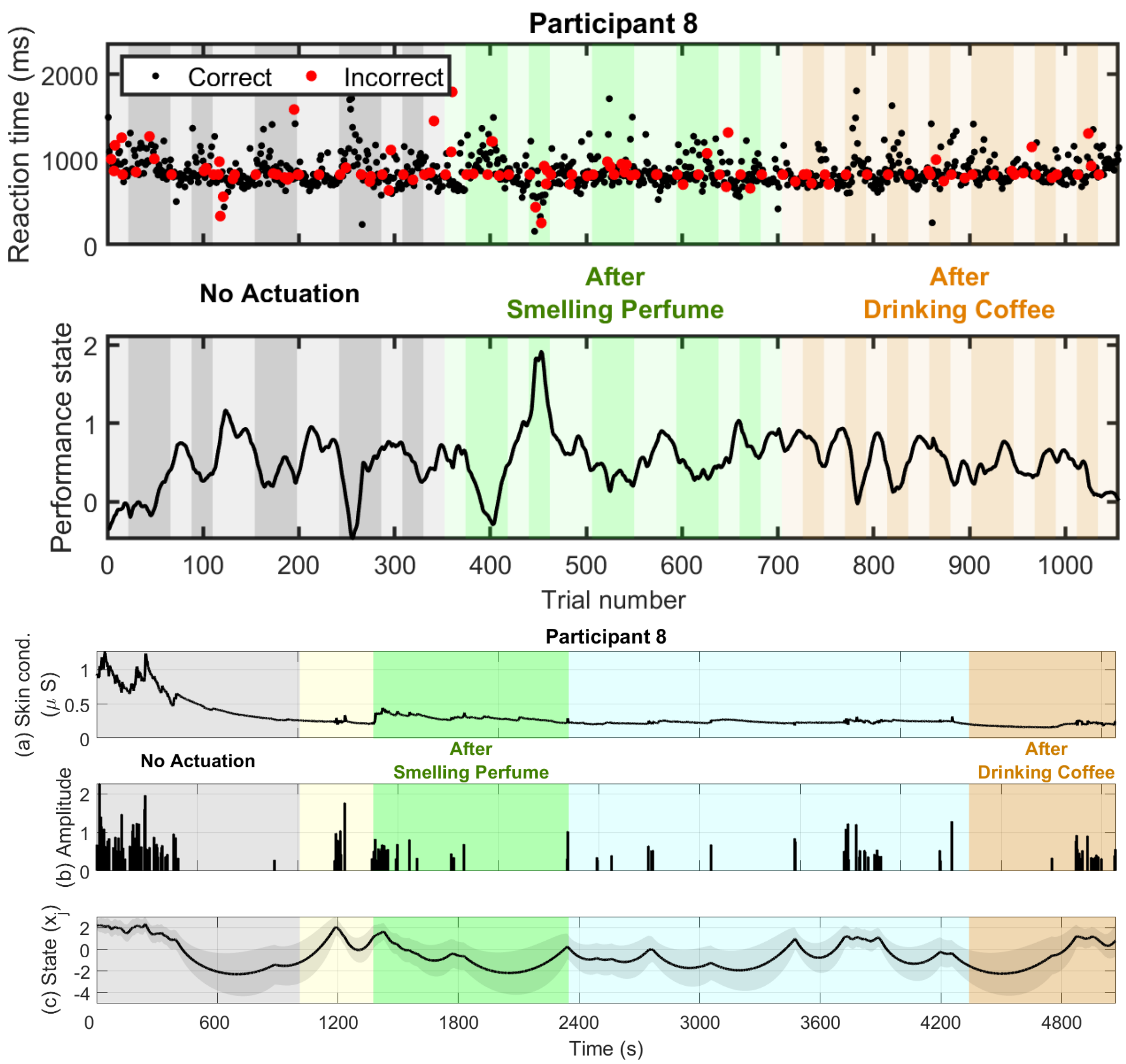

Figure 60: **Results of Experiment 2 (Subject 8).**

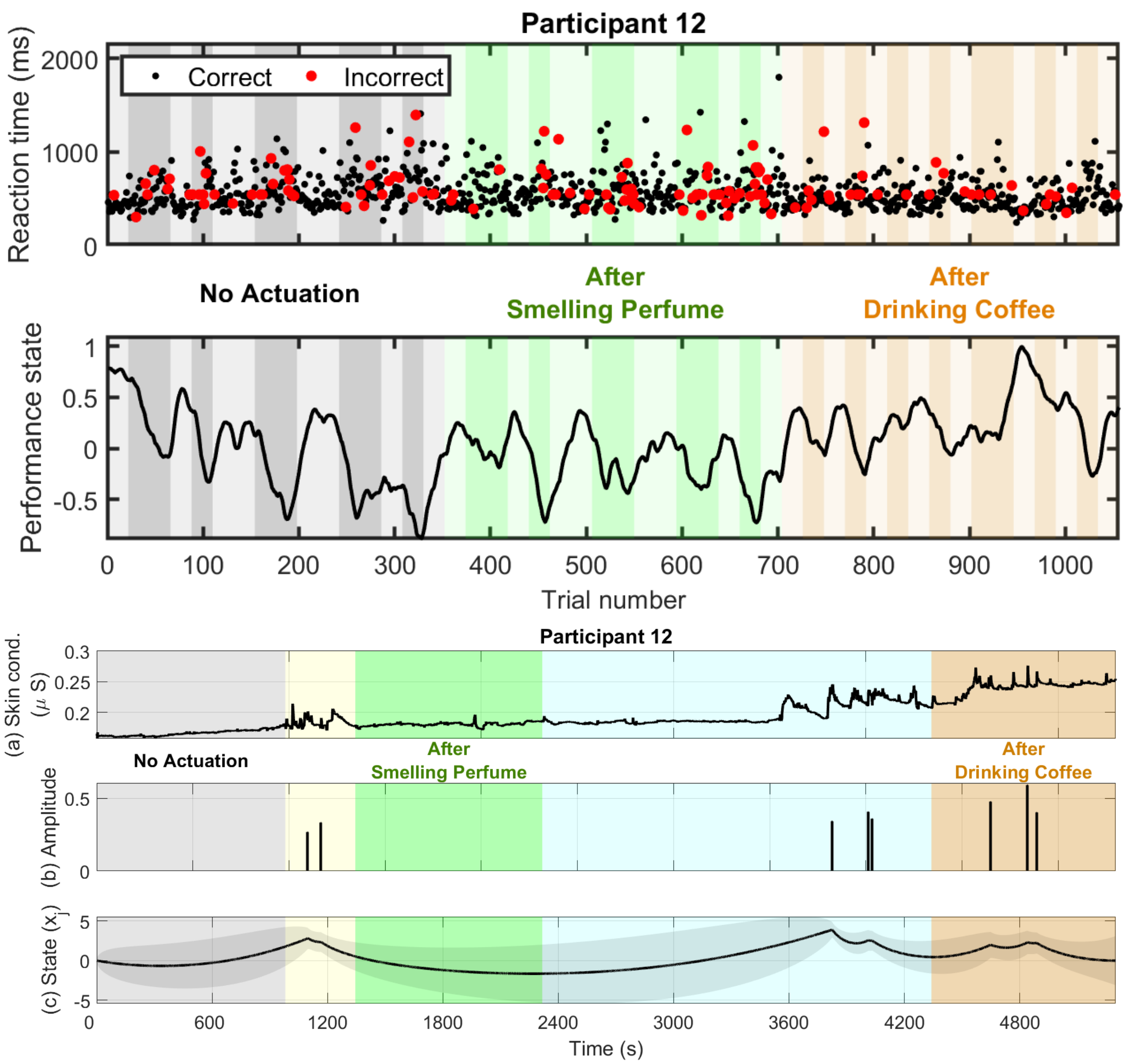

Figure 61: **Results of Experiment 2 (Subject 12).**

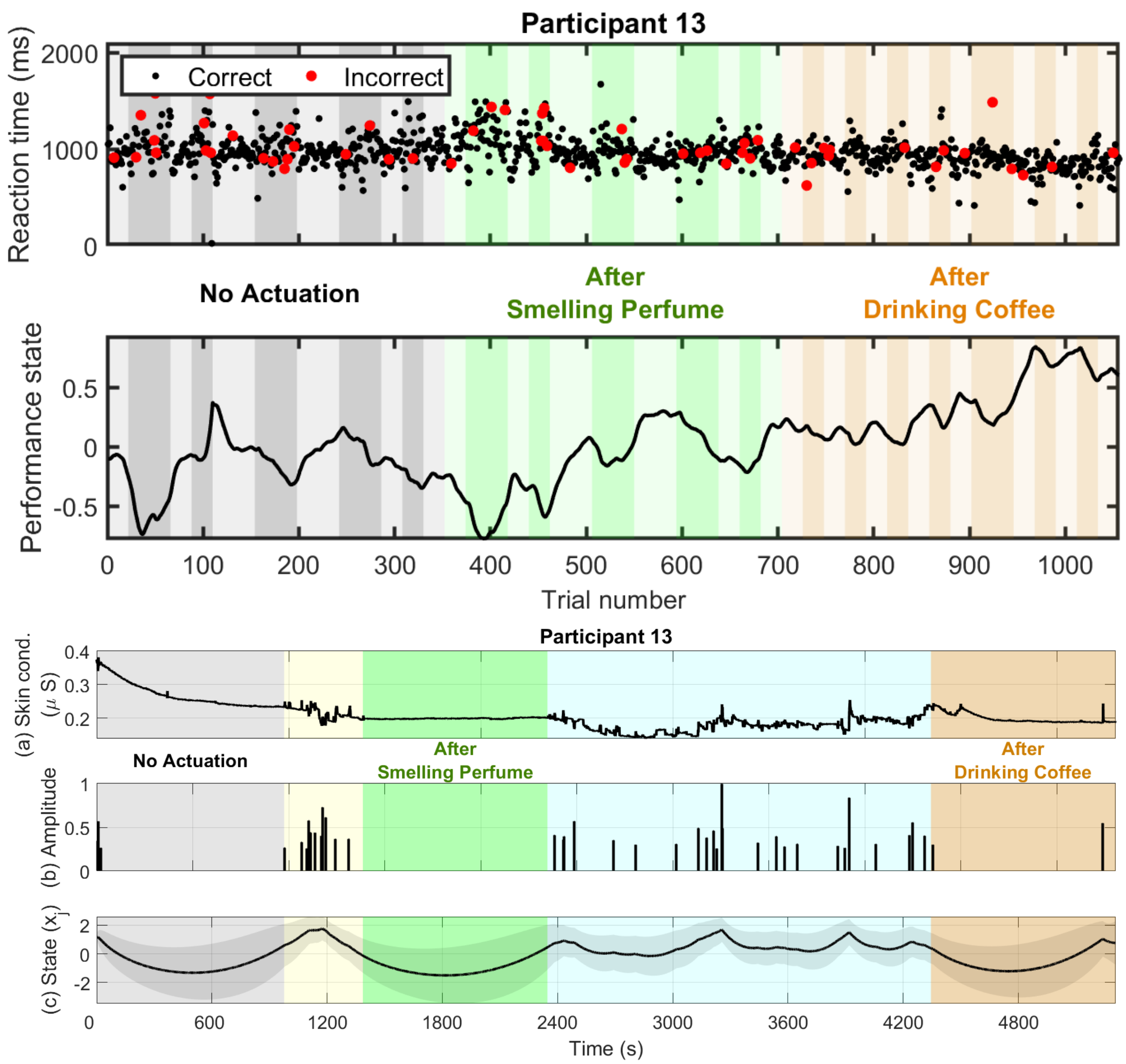

Figure 62: **Results of Experiment 2 (Subject 13).**

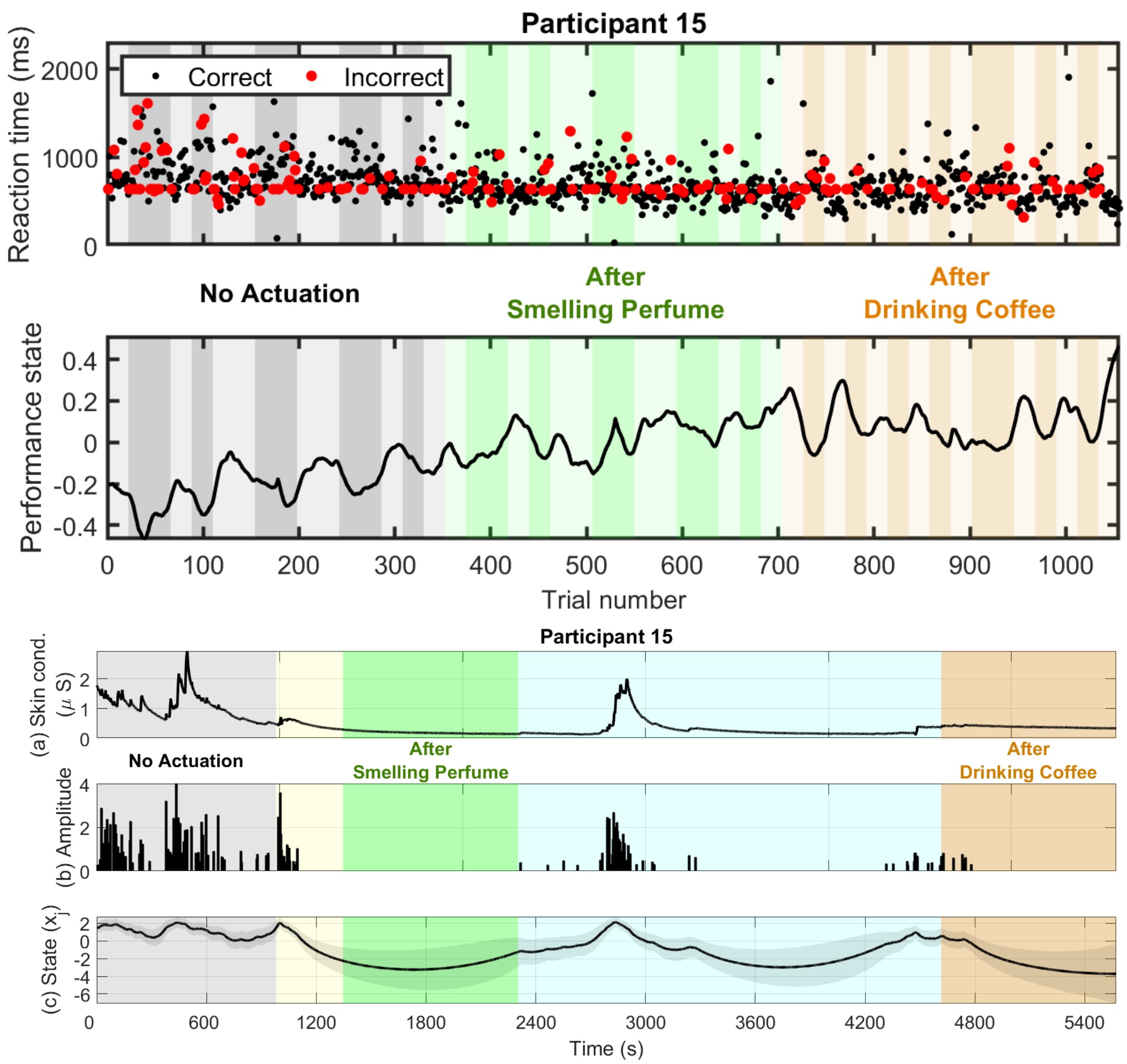

Figure 63: **Results of Experiment 2 (Subject 15).**

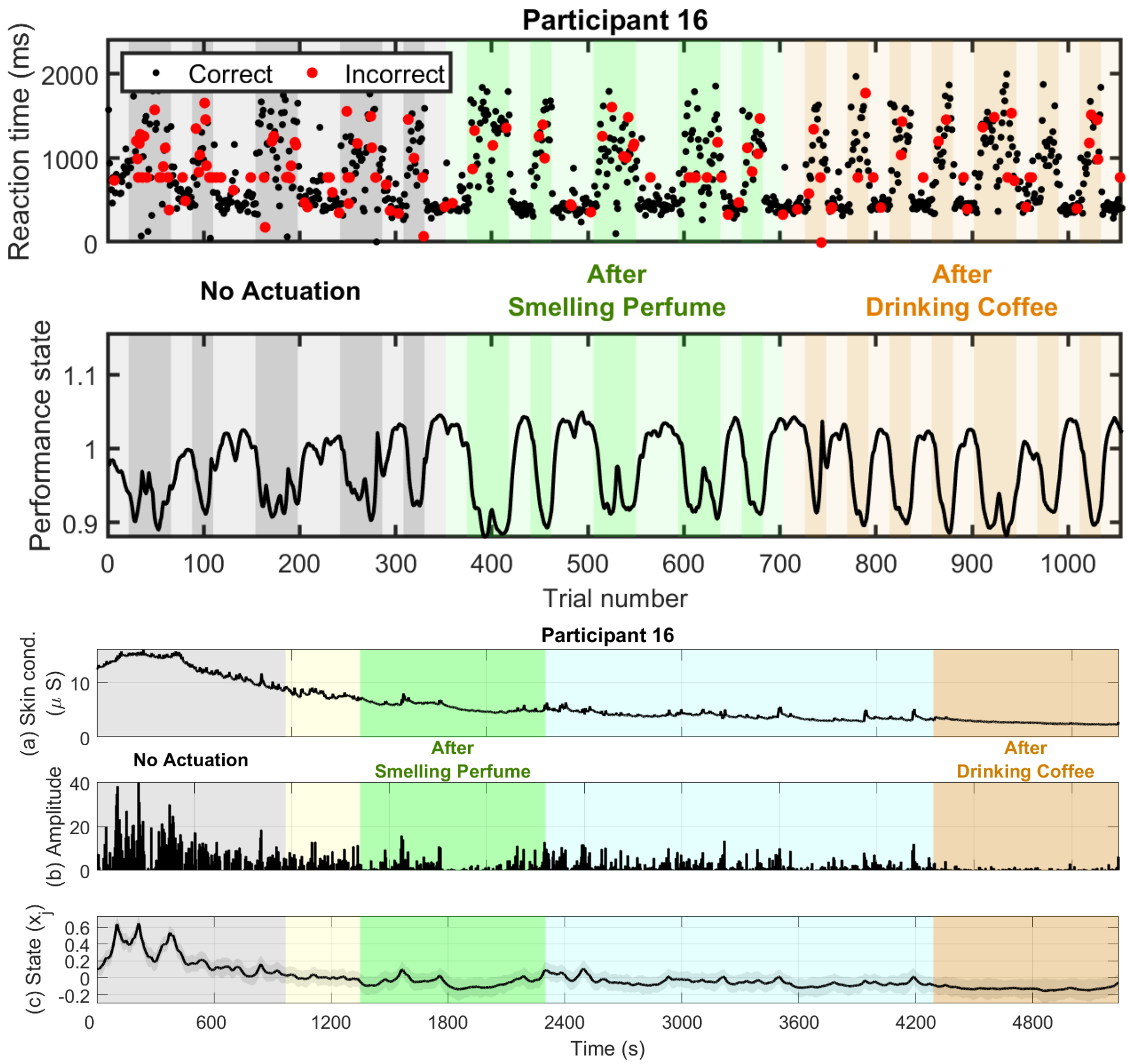

Figure 64: **Results of Experiment 2 (Subject 16).**

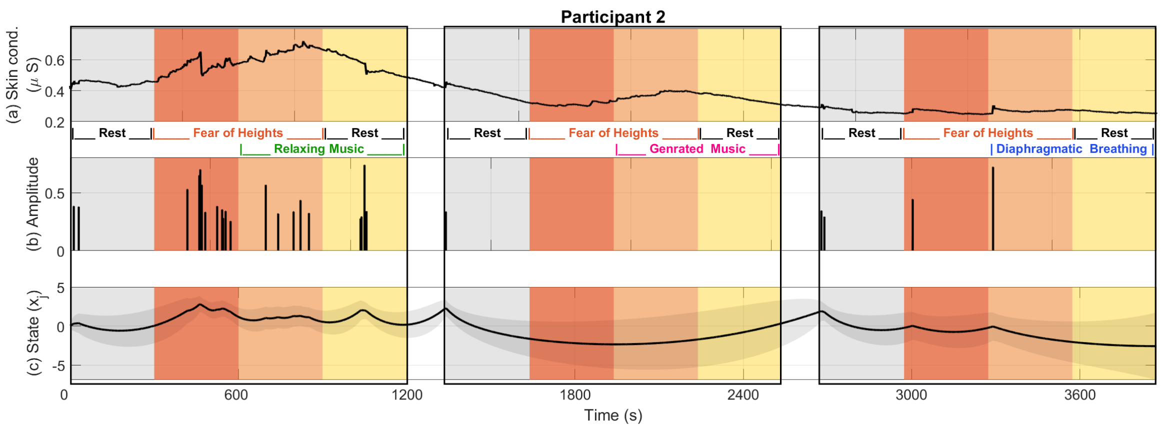

Figure 65: **Results of Experiment 3 (Subject 2).**

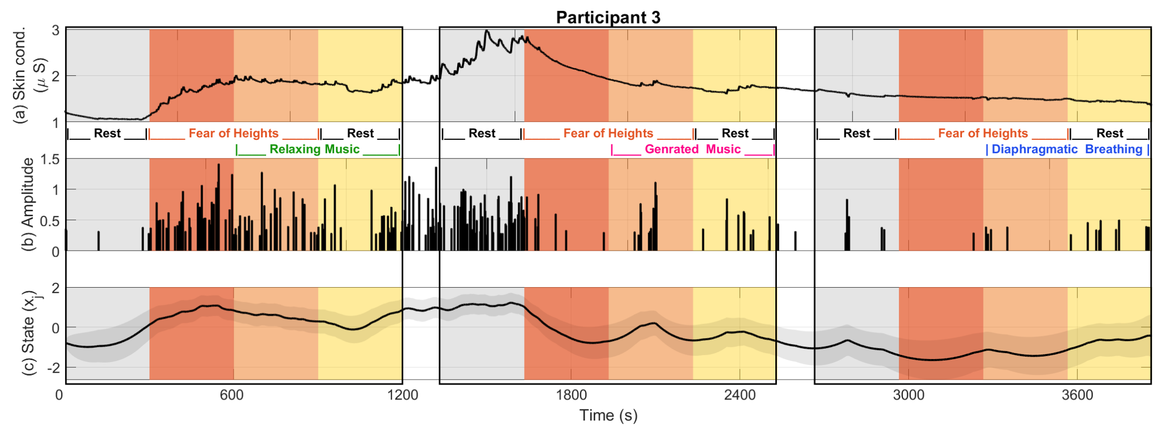

Figure 66: **Results of Experiment 3 (Subject 3).**

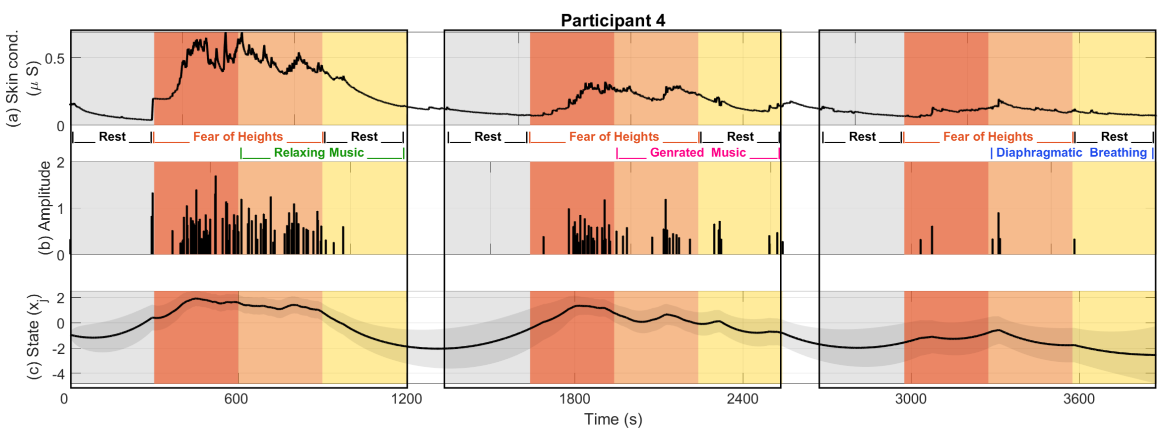

Figure 67: **Results of Experiment 3 (Subject 4).**

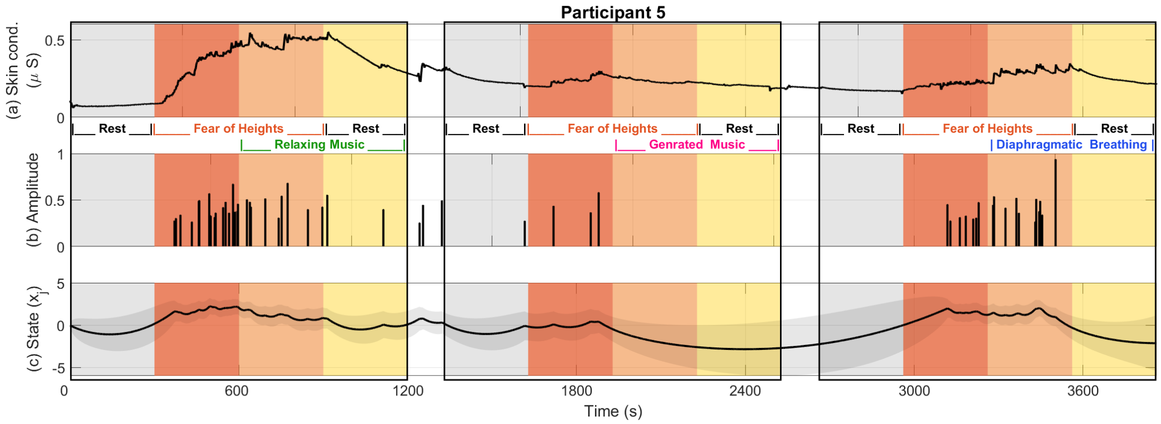

Figure 68: **Results of Experiment 3 (Subject 5).**

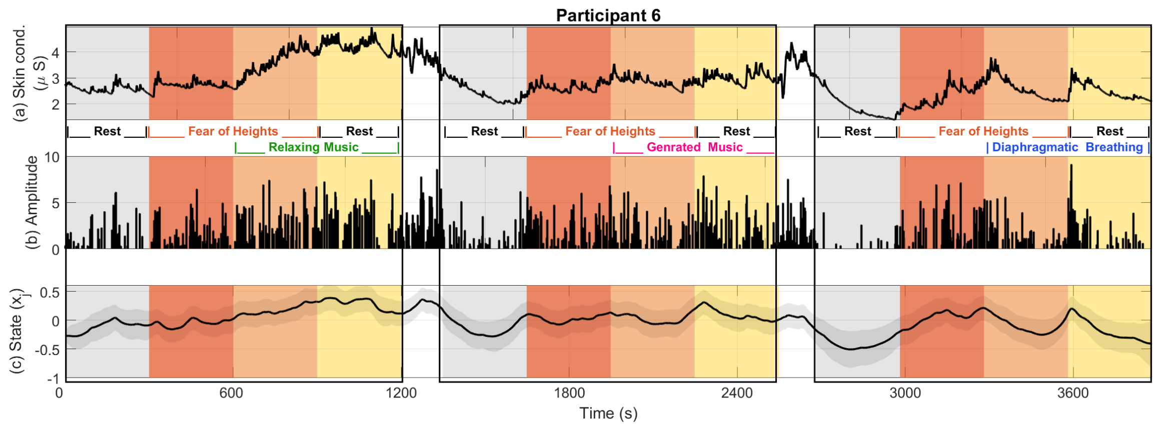

Figure 69: **Results of Experiment 3 (Subject 6).**

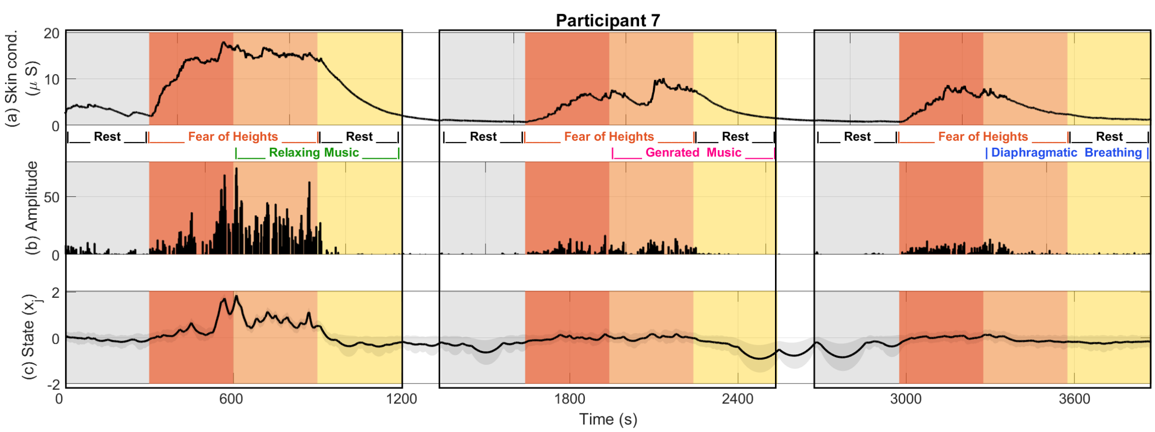

Figure 70: **Results of Experiment 3 (Subject 7).**

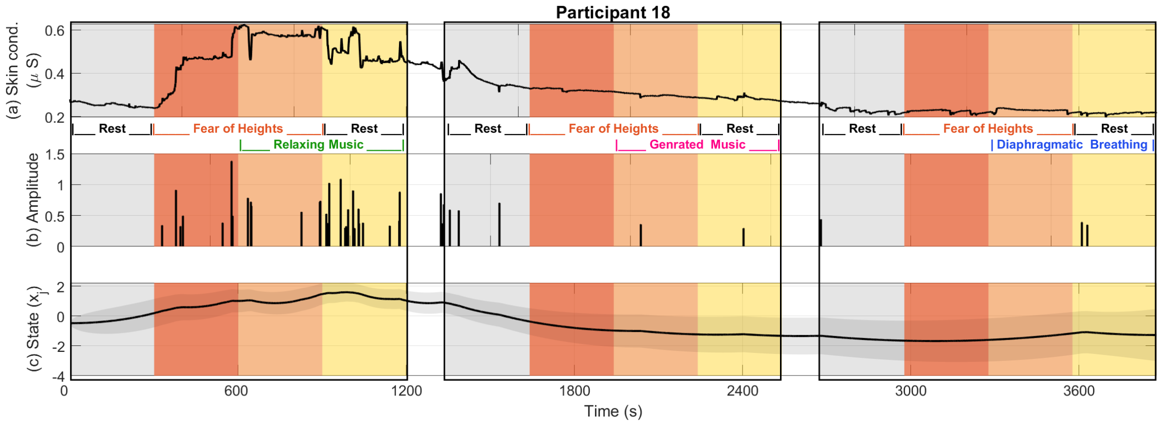

Figure 71: **Results of Experiment 3 (Subject 18).**

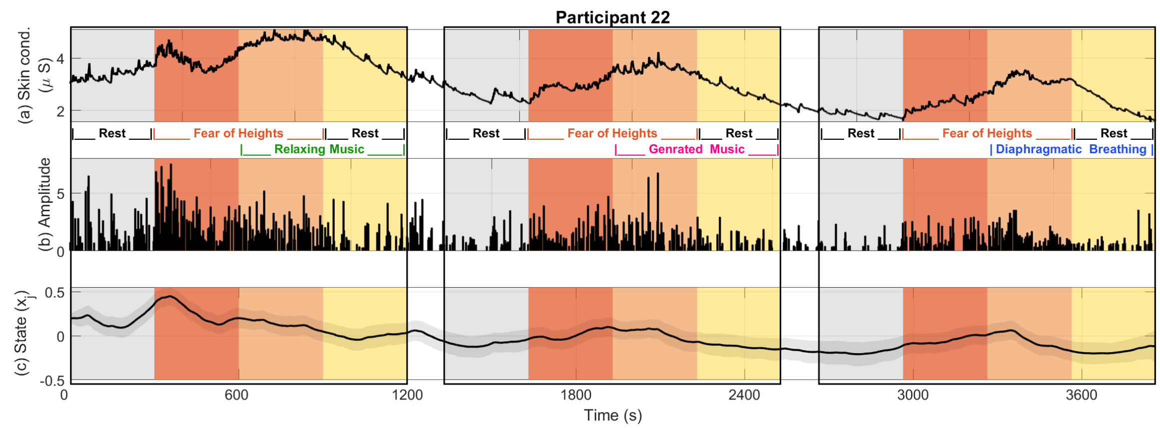

Figure 72: **Results of Experiment 3 (Subject 22).**

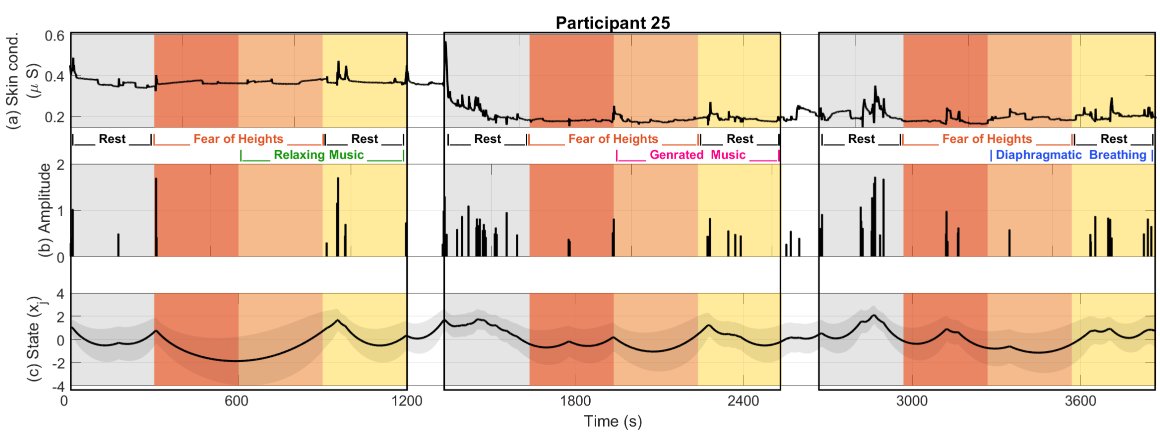

Figure 73: **Results of Experiment 3 (Subject 25).**

these results, we perform multiple analyses to compare the subjects' performance levels in open-loop case (i.e., baseline with no music) with closed-loop periods (i.e., while listening to different music). As it is presented in Table 16, listening to relaxing music has elevated the average levels of performance state from 0.12 and -0.08 to 0.15 and 0.04 in 1-back and 3-back tasks, respectively. In a similar manner, listening to exciting music has increased the performance state estimate from 0.12 and -0.08 in 1-back and 3-back tasks to 0.23 and 0.13, accordingly. In addition to these familiar types of music, we also played newly generated relaxing music in the fourth session of the experiment, which they had never heard before and was created by using deep learning. In response to this new music, subjects show improved performance state levels (i.e., reaching 0.25 and 0.145 performance levels in 1-back and 3-back tasks, respectively).

It is also worth mentioning that this enhancement in levels of estimated performance state is because of receiving more correct responses and/or the improved reaction times. The Bayesian filter incorporates this recorded information and results in cognitive performance state estimation. To further illustrate effects of listening to music while performing cognitive stress tasks, we perform corresponding statistical analysis. As presented in Table 16, listening to different music in all sections have not affected the reaction times in 1-back tasks. However, relaxing, exciting, and newly generated relaxing music have improved the reaction times in 1-back task by 0.3%, 5.2%, and 5.9%, respectively. Interestingly, listening to music in all three sessions brought about enhancement in receiving more correct responses in less reaction times 3-back tasks. Relaxing, exciting, and newly generated relaxing music have improved the rate of correct responses by 2.5%, 4.3%, and 3.4% in 3-back tasks, respectively. These improvements in correct responses are achieved with enhancements in reaction times; 10.5%, 13.7%, and 17.2% in relaxing, exciting, and newly generated relaxing music, respectively.

These comparisons demonstrate how listening to music has improved subjects' performance state with both reducing reaction times and increasing correct responses. It should be also noted that this experiment lasted for more than 70 minutes and it is more probable

Table 16: Experiment 1 - closed-loop analysis.

Performance criteria	**Baseline (No Music)**		**Relaxing Music**		**Exciting Music**		**New Music**	
	1-back	3-back	1-back	3-back	1-back	3-back	1-back	3-back
Correct responses (%)	93.8	81.7	93.6	84.2	92.87	85.98	93.7	85.1
Reaction time (ms)	606	743	604	665	574	641	570	615
Performance state	0.12	-0.08	0.15	0.04	0.23	0.13	0.25	0.145

that without this music, subjects' performance state would be dropped due to tiredness. Hence, we can conclude that listening to music while performing memory-related tasks would enhance subjects' productivity.

6.4.2 Experiment 2

Analyzing the results of all subjects in experiment 2 (i.e., perfume smelling and coffee drinking), we observe an enhancement on average levels of performance state after taking safe actuation. Similar to experiment 1, taking these safe actuation not only prevent the participants to feel bored and unengaged, but also they helped the subjects to show higher performance levels. To further describe the outcome of this closed-loop experiment, we execute multiple analyses to compare the performance levels in open-loop case (i.e., baseline with no actuation) with closed-loop periods (i.e., after smelling fragrance and drinking coffee). As it is presented in Table 17, smelling fragrances has increased the average levels of performance state from 0.27 and 0.11 to 0.36 and 0.27 in 1-back and 3-back tasks, respectively. In a similar manner, drinking coffee has increased the performance state estimate from 0.27 and 0.11 in 1-back and 3-back tasks to 0.42 and 0.37, accordingly. It should also be noted that this enhancement in levels of estimated performance state is due to receiving more correct responses and shorter reaction times. To further demonstrate effects of olfactory stimulation and caffeine intake in improving brain cognitive performance levels, we present corresponding statistical analyses.

As presented in Table 17, smelling perfumes results in an improvement in the rate of correct responses by 0.6% and 1.1% in 1-back and 3-back tasks, respectively. These improvements in correct responses are achieved with enhancements in reaction times; 4.4% and 8.2% in 1-back and 3-back tasks, respectively. Similarly, in response to drinking coffee,

Table 17: Experiment 2 - closed-loop analysis.

Performance criteria	Baseline (No Actuation)		After smelling Perfume		After Drinking Coffee	
	1-back	3-back	1-back	3-back	1-back	3-back
Correct responses (%)	92.9	84.0	93.5	85.1	93.9	88.8
Reaction time (ms)	617	766	590	708	570	678
Performance state	0.27	0.11	0.36	0.27	0.42	0.37

subjects showed 1% and 4.8 enhancement in the rate of correct responses in 1-back and 3-back tasks, respectively. After Drinking coffee, more correct responses are achieved with shorter reaction times (i.e., 7.6% and 11.5% improvement in 1-back and 3-back tasks, respectively). This comparison further shows how these safe actuation have improved subjects' performance state by both reducing reaction times and receiving more correct responses. Hence, we may conclude that performing memory-related tasks after smelling perfume and drinking coffee would enhance subjects' productivity.

6.4.3 Experiment 3

The outcome in experiment 3 further validates our hypothesis. In this experiment, we recorded physiological data to analyze how listening to music and diaphragmatic breathing would alleviate subjects with fear of heights. While we derive the results for all 18 participants, due to the potential variations in subjects' responses and different levels of skin conductance levels in different subjects, we mainly discuss the subjects with significant levels of skin conductance signal. Hence we select eight subjects with sufficient responses (Table 18). On average, we observe that listening to music has lead them to have lower levels of cognitive arousal states from 0.83 in open-loop with no actuation to 0.75 while listening to relaxing music. In a similar manner, listening to newly generated relaxing music, based on their specific taste of relaxing music, has lead the average levels of arousal state to reach -0.62 compared to the average levels of -0.3 in open-loop period with no actuation. As the third relaxing actuation, we asked the subjects to practice diaphragmatic breathing. In response to this relaxing exercises, they demonstrate lower levels of arousal state (i.e., -0.54 while performing diaphragmatic breathing compared to -0.46 over open-loop period with no actuation). While we only analyzed skin conductance signal and EEG measurements, further analysis could consider different features from other recorded physiological signals.

Table 18: Experiment 3 - closed-loop analysis.

Selected Subject id	**Relaxing Music**		**Generated Music**		**Diaphragmatic Breathing**	
	open-loop	closed-loop	open-loop	closed-loop	open-loop	closed-loop
2	1.6160	0.9766	-2.1187	-2.1532	-0.4974	-1.1883
3	0.7619	0.5436	-0.2574	-0.2898	-1.5040	-1.3018
4	1.3724	1.2499	0.7566	0.3154	-1.2026	-1.3184
5	1.5824	1.0817	-0.0528	-1.7936	1.2058	1.1387
6	-0.0540	0.1731	0.0281	0.0262	0.0481	-0.0850
7	0.4228	0.8024	-0.0212	0.0204	0.0091	-0.0775
18	0.6464	1.0378	-0.7358	-1.0886	-1.6532	-1.4108
22	0.2743	0.1341	0.0149	0.0283	-0.0507	-0.0474

7 Conclusion and Future Work

Inspired by recent advances in wearable technologies, we proposed wearable-machine interface (WMI) architectures for controlling internal brain states. The WMI architecture encompasses collecting physiological data using wearable devices, inferring neural stimuli underlying pulsatile signals, estimating an unobserved state based on the underlying stimuli, designing the controller, and closing the loop in real-time. In the proposed architectures, we approach the human-in-the-loop problems in a system theoretic framework. Relying on physiological signals that are collected via wearable devices and employing signal processing and control system techniques to infer internal brain state(s) would enhance current medical practices.

7.1 Energy Regulation in Patients with Hypercortisolism

In chapter 2, by implementing the proposed WMI architecture on multiple simulated cortisol profiles, we demonstrated that we can reach energy regulation in hypercortisolism. Simulated results verify that the proposed closed-loop approach has great potential to be utilized in real life. In the prospective practical system, a real-time deconvolution algorithm should be utilized to derive the corticotrophin-releasing hormone (CRH) secretion times. With future generations of wearable devices that could monitor cortisol data in real-time, the time and dosage of the required medications would be regulated in a closed-loop automated manner. With the goal of real implementation of the proposed WMI architectures and due to the lack of technologies for real-time monitoring of cortisol data, we explored cognitive stress regulation in chapters 3–6.

7.2 Closed-loop Cognitive Stress Management

In chapter 3, utilizing the experimental data, we followed the goal of designing a simulation environment by monitoring subjects' skin conductance variations (as a validated stress indicator). In the developed simulation system, we designed a knowledge-based fuzzy control system to close the loop and regulate the internal cognitive stress-related state in real-time. The results in this simulation study validate the performance of our proposed WMI architectures in accomplishing the tasks of (1) tracking the cognitive stress state, (2) lowering the levels of cognitive stress-related state by applying inhibitory control in high cognitive arousal environments, and (3) elevating the cognitive stress-related state levels by applying excitatory control in low cognitive arousal environments. All of these tasks are accomplished in an automatic closed-loop manner. This work is an important first step which will ultimately lead to help patients suffering from stress and anxiety disorders.

7.3 Supervised Control Architectures in Cognitive Stress Management

In chapter 4, influenced by the fact that skin conductance carries important information regarding the internal arousal state, we first developed novel closed-loop architectures to enhance the cognitive stress estimation and regulation. To this end, we further expanded the estimation algorithm to incorporate amplitudes associated with SCR events. Hence, we implemented a marked point process filtering approach and included both amplitude and timing of SCR events while estimating the hidden state. To close the loop, by taking advantages of state-space representation, we first implemented model-based LQR and MPC. Using these methods, we overcame the heuristic nature of fuzzy control design in chapter 3. Since the performance of model-based LQR and MPC approaches rely on defining appropriate objective functions, we next utilized our novel supervised control techniques to take advantage of both model-based and knowledge-based methods. Hence, we established supervised LQR and supervised MPC architectures for regulating the cognitive arousal state. We investigated the efficiency of the proposed architectures in two classes of closed-loop scenarios: inhibition and excitation. The results verify the effectiveness of proposed architectures in keeping the estimated stress state within a target range with more optimal control efforts. The idea of applying a supervised layer on top of the model-based control systems would result in performance improvement in closed-loop systems. It can also provide an excellent structure to incorporate medical expertise while designing the control. As we are dealing with a human-in-the-loop system, it is highly crucial to supervise the control systems. In the proposed supervised architectures, with respect to the nature of model-based control approaches, we ensure that the essential control system design criteria, such as stability and optimality, would be guaranteed. In fact, the supervised knowledge-based network would further enhance their efficiency by adjusting the control tune parameters in real-time. The proposed supervised methodologies are well-aligned to the human physiology basis and could be further investigated in similar closed-loop disorder treatments.

7.4 Adaptive and Robust Control Systems for Closed-loop Stress Management

As uncertainty in model parameters, presented in the state-space representation, is unavoidable, we followed the goal of designing adaptive control systems to handle it in chapter 5. Considering potential disturbance inputs while implementing the WMI architectures, we performed research in robust state estimation and control design. In chapter 5, we expanded the state-space model and considered uncertainty in model parameters as well as undesired disturbance input. These state-space model extension would capture inter- and intra-subject variation. To handle the added parameters and establish robust and adaptive control architectures, we first defined augmented states and estimated them using a Bayesian filtering approach. We next designed and implemented adaptive LQR and Robust LQR to handle uncertainty in model parameters and additional disturbance input, respectively. The simulation results verify the effectiveness of adaptive and robust control design in regulating cognitive arousal. Considering inter- and intra-subject variation in human subject responses, corresponding adaptive and robust control approaches should be utilized while designing control action and incorporating experimental actuation.

7.5 Closed-loop Human-Subject Experiments with Incorporating Safe Actuation

In the last chapter of this research, we followed the goal of investigating effects of possible safe actuation effective in regulating internal brain states to be implemented in real-world settings. In chapter 6, we designed and performed three sets of closed-loop experiments. To this end, we employed wearable devices to collect human physiological data. Using only the wearable devices provides us with an excellent opportunity to implement the proposed architectures in real-life. In the first experiment, we proposed to apply music while performing memory-related n-back tasks. In the second experiment, we suggested to apply olfactory stimuli (i.e., smell perfume) and coffee to further explore their effects on internal brain states while performing memory-related tasks. To validate our hypothesis about effectiveness of listening to music, smelling fragrance, and drinking coffee in regulating brain states, we performed multiple analyses. To estimate cognitive performance, we analyzed correct/incorrect responses as well as their reaction times. To explore effects of safe actuation in cognitive arousal, we analyzed changes in electrodermal activity. The experimental results verify our hypothesis about effectiveness of the proposed safe actuation in regulating internal brain states. In the third experiment, we explored the influence of listening to relaxing music and diaphragmatic breathing while watching clips that might induce a fear of heights on the subjects with acrophobia. The hypothesis about the impacts of the proposed relaxing actuation is confirmed in the experimental data. Listening to relaxing music and newly generated music and practicing diaphragmatic breathing caused the subjects feel more relaxed.

7.6 Future Directions

In the simulation study of closed-loop energy regulation, we showed the feasibility of the proposed algorithms to be implemented in real life. With respect to future advances in wearable technologies, which could monitor cortisol data in real-time, one should apply the proposed architectures and implement it in real-world settings. By performing human-subject experiments, we could better understand how a specific medication would affect cortisol profiles and internal energy state in real-time. Since cortisol variations are influenced by a variety of physiological and psychological factors, a future direction of this research could be including additional information from multiple sources while designing the closed-loop system. In the prospective architectures, a multi-input multi-output system will take the information from multiple sources and make the required decisions about taking the medications (i.e., dosage and time). It results in an enhancement in medications' efficiency and minimizes their possible side effects. Future directions of this research could also include incorporating all possible medications and designing the control algorithms with the capability to choose among them. Similar to what is presented in cognitive stress regulation, one may explore more advanced control strategies (e.g., supervised, adaptive, and robust control methods) to close the loop. Another possible future direction could be including the system identification process for each medication inside the real-time system. As a result, the way that each specific individual responds to a particular medication will be monitored to update the medication dynamics in real-time. Consequently, the personalized control design would be more efficient.

In cognitive stress regulation, as skin conductance could also be affected in response to other types of stimuli, it would be beneficial to analyze variations in valence state. As emotional valence is another important aspect of the emotional state, exploring valence state regulation could be another future direction of this research. By analyzing more physiological measurements, we are able to differentiate between excitement and nervousness as well. While the proposed fuzzy control system is designed in a simple single-input single-output structure, it has the capability to be further expanded and incorporates multiple physiological measurements from wearable devices. Accordingly, the expanded multi-input multi-output system would be expanded to receive data from multiple sources, perform appropriate analysis, and govern the control action to regulate corresponding internal states. Furthermore, investigating more advanced control approaches such as genetic algorithm on top of fuzzy structure could further enable us to optimize the actuation design and achieve the ultimate goal of practically employing the WMI architectures to manage individuals' internal states.

The supervised control architectures discussed in chapter 4 could be further expanded to result in adaptive, robust, and person-specific closed-loop tools. While we designed and implemented separate adaptive and robust control systems in chapter 5, a future direction of this research would be combining them to establish a unified system that could handle both mode uncertainty and disturbance input simultaneously. In the prospective system, terms associated with model uncertainty and disturbance input would be considered together and we should consider a more expanded augmented state while estimating the hidden state. To design the control system, one might also apply the supervised architectures presented in chapter 4 and establish an advance supervised adaptive and robust control architecture. Exploring artificial intelligence-based decision making approaches such as deep learning and reinforcement learning could also considered as alternative approaches while designing the control and closing the loop.

As a result of the human subject experiments presented in chapter 6, we collected and published multiple physiological data (i.e., EDA, BVP, PPG, 3-axis accelerometer data, skin temperature, EEG). An important future direction of this research could be exploring the dynamic effects of each safe actuation in humans' responses. One important aspect that should be considered while analyzing these dataset is to explore pharmacokinetics and pharmacodynamics of each actuation. To further evaluate effects of the proposed safe actuation, performing more experiments on more subjects would enhance the conclusion. To further evaluate our hypothesis, we propose to repeat experiments and shuffle open-loop and closed-loop (i.e., performing the tasks while taking the actuation) periods. It would enhance our understanding of each safe actuation's dynamics. Considering subject-specific reactions and possible latency in physiological responses to any actuation, one may model the actuation dynamics and include them in the real-world implementation of WMI architectures. In such practical WMI architectures, a wearable device collects physiological data from human in the loop, a decoder estimates the cognitive stress state, and a controller brings the cognitive stress to the desired range by incorporating modeled safe actuation in a closed-loop manner. Another future direction of this research includes performing more experiments with more subjects to achieve a more diverse dataset.

With ongoing recent advances in wearable technologies, the proposed research could open avenues of opportunities addressing mental and hormone-related disorders within the remote monitoring properties. The proposed architecture could provide an excellent infrastructure to incorporate medical expertise while designing the actuation and closing the loop. Humankind would derive a benefit from the proposed real-time monitoring and regulation toolsets by receiving the personalized effective suggestions and medications with minimized side-effects to enhance their overall quality of life.

References

[1] Celso Arango, Covadonga M Diaz-Caneja, Patrick D McGorry, Judith Rapoport, Iris E Sommer, Jacob A Vorstman, David McDaid, Oscar Marin, Elena Serrano-Drozdowskyj, Robert Freedman, and William Carpenter. Preventive strategies for mental health. *The Lancet Psychiatry*, 5(7):591–604, 2018.

[2] Chris Gibbons, Martin Dempster, and Marianne Moutray. Stress and eustress in nursing students. *Journal of Advanced Nursing*, 61(3):282–290, 2008.

[3] Hamid Fekri Azgomi, Iahn Cajigas, and Rose T Faghih. Closed-loop cognitive stress regulation using fuzzy control in wearable-machine interface architectures. *IEEE Access*, 9:106202–106219, 2021.

[4] Hamid Fekri Azgomi, Jin-Oh Hahn, and Rose T Faghih. Closed-loop fuzzy energy regulation in patients with hypercortisolism via inhibitory and excitatory intermittent actuation. *Frontiers in Neuroscience*, 15:909, 2021.

[5] Hamid Fekri Azgomi and Rose T Faghih. A wearable brain machine interface architecture for regulation of energy in hypercortisolism. In *2019 53rd Asilomar Conference on Signals, Systems, and Computers*, pages 254–258, (Pacific Grove, CA). IEEE, 2019.

[6] Hamid Fekri Azgomi, Dilranjan S Wickramasuriya, and Rose T Faghih. State-space modeling and fuzzy feedback control of cognitive stress. In *2019 41st Annual International Conference of the IEEE Engineering in Medicine and Biology Society (EMBC)*, pages 6327–6330, (Berlin). IEEE, 2019.

[7] Richard J McNally, Donald J Robinaugh, Gwyneth WY Wu, Li Wang, Marie K Deserno, and Denny Borsboom. Mental disorders as causal systems: A network

approach to posttraumatic stress disorder. *Clinical psychological science*, 3(6):836–849, 2015.

[8] Suzanne M Waddill-Goad. Stress, fatigue, and burnout in nursing. *Journal of Radiology Nursing*, 38(1):44–46, 2019.

[9] Julia Thom, Julia Bretschneider, Nils Kraus, Josua Handerer, and Frank Jacobi. Healthcare epidemiology of mental disorders: why is the prevalence not declining despite growing provision of care? *Bundesgesundheitsblatt, Gesundheitsforschung, Gesundheitsschutz*, 2019.

[10] Divesh Deepak Pednekar, Md Rafiul Amin, Hamid Fekri Azgomi, Kirstin Aschbacher, Leslie J Crofford, and Rose T Faghih. Characterization of cortisol dysregulation in fibromyalgia and chronic fatigue syndromes: a state-space approach. *IEEE Transactions on Biomedical Engineering*, 67(11):3163–3172, 2020.

[11] Lisa R Starr, Kimberly Dienes, Y Irina Li, and Zoey A Shaw. Chronic stress exposure, diurnal cortisol slope, and implications for mood and fatigue: Moderation by multilocus hpa-axis genetic variation. *Psychoneuroendocrinology*, 100:156–163, 2019.

[12] Amparo Güemes Gonzalez, Ralph Etienne-Cummings, and Pantelis Georgiou. Closed-loop bioelectronic medicine for diabetes management. *Bioelectronic Medicine*, 6:1–7, 2020.

[13] Theresa M Buckley and Alan F Schatzberg. On the interactions of the hypothalamic-pituitary-adrenal (HPA) axis and sleep: normal HPA axis activity and circadian rhythm, exemplary sleep disorders. *The Journal of Clinical Endocrinology & Metabolism*, 90(5):3106–3114, 2005.

[14] Swati Chopra, Aman Rathore, Haris Younas, Luu V Pham, Chenjuan Gu, Aleksandra Beselman, Il-Young Kim, Robert R Wolfe, Jamie Perin, Vsevolod Y Polotsky, and Jonathan C Jun. Obstructive sleep apnea dynamically increases nocturnal plasma free fatty acids, glucose, and cortisol during sleep. *The Journal of Clinical Endocrinology & Metabolism*, 102(9):3172–3181, 2017.

[15] Osamah A Hakami, Shahzada Ahmed, and Niki Karavitaki. Epidemiology and mortality of cushing's syndrome. *Best Practice & Research Clinical Endocrinology & Metabolism*, page 101521, 2021.

[16] Natacha Driessens, Dominique Maiter, Pascale Borensztein, Amelie Jaspart, Martine Bostnavaron, and Albert Beckers. Long-term treatment with metyrapone in four patients with cushing's disease. 2018.

[17] Rosario Pivonello, Monica De Leo, Alessia Cozzolino, and Annamaria Colao. The treatment of cushing's disease. *Endocrine Reviews*, 36(4):385–486, 2015.

[18] Martin Hatzinger, Serge Brand, Sonja Perren, Anges von Wyl, Stephanie Stadelmann, Kai von Klitzing, and Edith Holsboer-Trachsler. Pre-schoolers suffering from psychiatric disorders show increased cortisol secretion and poor sleep compared to healthy controls. *Journal of Psychiatric Research*, 46(5):590–599, 2012.

[19] Etsuo Niki. Oxidative stress and antioxidants: distress or eustress? *Archives of Biochemistry and Biophysics*, 595:19–24, 2016.

[20] Federica Pallavicini, Luca Argenton, Nicola Toniazzi, Luciana Aceti, and Fabrizia Mantovani. Virtual reality applications for stress management training in the military. *Aerospace Medicine and Human Performance*, 87(12):1021–1030, 2016.

[21] Anastasia Bougea, Nikolaos Spantideas, and George P Chrousos. Stress management for headaches in children and adolescents: a review and practical recommendations for health promotion programs and well-being. *Journal of Child Health Care*, 22(1):19–33, 2018.

[22] Nina Smyth, Elena Rossi, and Carly Wood. Effectiveness of stress-relieving strategies in regulating patterns of cortisol secretion and promoting brain health. *International Review of Neurobiology*, 150:219–246, 2020.

[23] Dilranjan S Wickramasuriya and Rose T Faghih. A cortisol-based energy decoder for investigation of fatigue in hypercortisolism. In *2019 41st Annual International Conference of the IEEE Engineering in Medicine and Biology Society (EMBC)*, pages 11–14, (Berlin). IEEE, 2019.

[24] Hadi Taghvafard, Ming Cao, Yu Kawano, and Rose T Faghih. Design of intermittent control for cortisol secretion under time-varying demand and holding cost constraints. *IEEE Transactions on Biomedical Engineering*, 67(2):556–564, 2019.

[25] Rose T Faghih. From physiological signals to pulsatile dynamics: a sparse system identification approach. In *Dynamic Neuroscience*, pages 239–265. Springer, 2018.

[26] Yuko Hakamata, Shotaro Komi, Yoshiya Moriguchi, Shuhei Izawa, Yuki Motomura, Eisuke Sato, Shinya Mizukami, Yoshiharu Kim, Takashi Hanakawa, Yusuke Inoue, and Hirokuni Tagaya. Amygdala-centred functional connectivity affects daily cortisol concentrations: a putative link with anxiety. *Scientific Reports*, 7(1):1–11, 2017.

[27] Divesh Deepak Pednekar, Md Rafiul Amin, Hamid Fekri Azgomi, Kirstin Aschbacher, Leslie J Crofford, and Rose T Faghih. A system theoretic investigation of cortisol

dysregulation in fibromyalgia patients with chronic fatigue. In *2019 41st Annual International Conference of the IEEE Engineering in Medicine and Biology Society (EMBC)*, pages 6896–6901, (Pacific Grove, CA). IEEE, 2019.

[28] Rose T Faghih, Munther A Dahleh, Gail K Adler, Elizabeth B Klerman, and Emery N Brown. Deconvolution of serum cortisol levels by using compressed sensing. *PloS one*, 9(1), 2014.

[29] Rose T Faghih. *System identification of cortisol secretion: Characterizing pulsatile dynamics*. PhD thesis, Massachusetts Institute of Technology, 2014.

[30] Anette Harris, Silje Endresen Reme, Tone Tangen, Åse Marie Hansen, Anne Helene Garde, and Hege Randi Eriksen. Diurnal cortisol rhythm: Associated with anxiety and depression, or just an indication of lack of energy? *Psychiatry Research*, 228(2):209–215, 2015.

[31] Lesley M Arnold. Understanding fatigue in major depressive disorder and other medical disorders. *Psychosomatics*, 49(3):185–190, 2008.

[32] Valentina D'Angelo, Guglielmo Beccuti, Rita Berardelli, Ioannis Karamouzis, Clizia Zichi, Roberta Giordano, Marco Alessandro Minetto, Mauro Maccario, Ezio Ghigo, and Emanuela Arvat. Cushing's syndrome is associated with sleep alterations detected by wrist actigraphy. *Pituitary*, 18(6):893–897, 2015.

[33] ML Vance. Physical presentation of cushing's syndrome: Typical and atypical presentations. In *Cushing's Disease*, pages 57–65. Elsevier, 2017.

[34] Tobias Stalder, Clemens Kirschbaum, Brigitte M Kudielka, Emma K Adam, Jens C Pruessner, Stefan Wüst, Samantha Dockray, Nina Smyth, Phil Evans, Dirk H Hellhammer, Robert Miller, Mark A. Wetherell, Sonia J. Lupieni, and Angela Clow. Assessment of the cortisol awakening response: expert consensus guidelines. *Psychoneuroendocrinology*, 63:414–432, 2016.

[35] Robert T Dwyer, René H Gifford, Fred H Bess, Michael Dorman, Anthony Spahr, and Benjamin WY Hornsby. Diurnal cortisol levels and subjective ratings of effort and fatigue in adult cochlear implant users: A pilot study. *American Journal of Audiology*, 28(3):686–696, 2019.

[36] Nicholas A Tritos and Beverly MK Biller. Medical therapies in cushing's syndrome. In *The Hypothalamic-Pituitary-Adrenal Axis in Health and Disease*, pages 165–179. Springer, 2017.

[37] Arie G Nieuwenhuizen and Femke Rutters. The hypothalamic-pituitary-adrenal-axis in the regulation of energy balance. *Physiology & behavior*, 94(2):169–177, 2008.

[38] Per Björntorp and Roland Rosmond. Obesity and cortisol. *Nutrition*, 16(10):924–936, 2000.

[39] Leslie J Crofford, Elizabeth A Young, N Cary Engleberg, Ania Korszun, Christine B Brucksch, Leslie A McClure, Morton B Brown, and Mark A Demitrack. Basal circadian and pulsatile acth and cortisol secretion in patients with fibromyalgia and/or chronic fatigue syndrome. *Brain, Behavior, and Immunity*, 18(4):314–325, 2004.

[40] Nava Zisapel, Ricardo Tarrasch, and Moshe Laudon. The relationship between melatonin and cortisol rhythms: clinical implications of melatonin therapy. *Drug Development Research*, 65(3):119–125, 2005.

[41] Francine O James, Nicolas Cermakian, and Diane B Boivin. Circadian rhythms of melatonin, cortisol, and clock gene expression during simulated night shift work. *Sleep*, 30(11):1427–1436, 2007.

[42] Daniel Blockmans, Philippe Persoons, Boudewijn Van Houdenhove, and Herman Bobbaers. Does methylphenidate reduce the symptoms of chronic fatigue syndrome? *The American Journal of Medicine*, 119(2):167–e23, 2006.

[43] Abhijit Chaudhuri and Peter O Behan. Fatigue in neurological disorders. *The Lancet*, 363(9413):978–988, 2004.

[44] Maria Fleseriu, Stephan Petersenn, Beverly MK Biller, Pinar Kadioglu, Christophe De Block, Guy T'Sjoen, Marie-Christine Vantyghem, Libuse Tauchmanova, Judi Wojna, Michael Roughton, André Lacroix, and John Newell-Price. Long-term efficacy and safety of once-monthly pasireotide in cushing's disease: A phase iii extension study. *Clinical Endocrinology*, 91(6):776–785, 2019.

[45] Joseph Rinehart, Brenton Alexander, Yannick Le Manach, Christoph K Hofer, Benoit Tavernier, Zeev N Kain, and Maxime Cannesson. Evaluation of a novel closed-loop fluid-administration system based on dynamic predictors of fluid responsiveness: an in silico simulation study. *Critical Care*, 15(6):1–12, 2011.

[46] Behnood Gholami, James M Bailey, Wassim M Haddad, and Allen R Tannenbaum. Clinical decision support and closed-loop control for cardiopulmonary management

and intensive care unit sedation using expert systems. *IEEE Transactions on Control Systems Technology*, 20(5):1343–1350, 2011.

[47] Xin Jin, Ramin Bighamian, and Jin-Oh Hahn. Development and in silico evaluation of a model-based closed-loop fluid resuscitation control algorithm. *IEEE Transactions on Biomedical Engineering*, 66(7):1905–1914, 2019.

[48] Yuxiao Yang and Maryam M Shanechi. An adaptive and generalizable closed-loop system for control of medically induced coma and other states of anesthesia. *Journal of Neural Engineering*, 13(6):066019, 2016.

[49] Max Y Liberman, ShiNung Ching, Jessica Chemali, and Emery N Brown. A closed-loop anesthetic delivery system for real-time control of burst suppression. *Journal of Neural Engineering*, 10(4):046004, 2013.

[50] Md Rafiul Amin and Rose T Faghih. Sparse deconvolution of electrodermal activity via continuous-time system identification. *IEEE Transactions on Biomedical Engineering*, 66(9):2585–2595, 2019.

[51] MD Rafiul Amin and Rose T Faghih. Robust inference of autonomic nervous system activation using skin conductance measurements: A multi-channel sparse system identification approach. *IEEE Access*, 7:173419–173437, 2019.

[52] Md Rafiul Amin and Rose T Faghih. Tonic and phasic decomposition of skin conductance data: A generalized-cross-validation-based block coordinate descent approach. In *2019 41st Annual International Conference of the IEEE Engineering in Medicine and Biology Society (EMBC)*, pages 745–749, (Berlin). IEEE, 2019.

[53] Md Rafiul Amin and Rose T Faghih. Inferring autonomic nervous system stimulation from hand and foot skin conductance measurements. In *2018 52nd Asilomar Conference on Signals, Systems, and Computers*, pages 655–660, (Pacific Grove, CA). IEEE, 2018.

[54] Emery N Brown, Patricia M Meehan, and Arthur P Dempster. A stochastic differential equation model of diurnal cortisol patterns. *American Journal of Physiology-Endocrinology And Metabolism*, 280(3):E450–E461, 2001.

[55] Rose T Faghih, Munther A Dahleh, and Emery N Brown. An optimization formulation for characterization of pulsatile cortisol secretion. *Frontiers in Neuroscience*, 9:228, 2015.

[56] Dilranjan S Wickramasuriya and Rose T Faghih. A marked point process filtering approach for tracking sympathetic arousal from skin conductance. *IEEE Access*, 8:68499–68513, 2020.

[57] Onur Parlak. Portable and wearable real-time stress monitoring: A critical review. *Sensors and Actuators Reports*, 3:100036, 2021.

[58] Manju Venugopal, Sunil K Arya, Ganna Chornokur, and Shekhar Bhansali. A realtime and continuous assessment of cortisol in isf using electrochemical impedance spectroscopy. *Sensors and Actuators A: Physical*, 172(1):154–160, 2011.

[59] Onur Parlak, Scott Tom Keene, Andrew Marais, Vincenzo F Curto, and Alberto Salleo. Molecularly selective nanoporous membrane-based wearable organic electrochemical device for noninvasive cortisol sensing. *Science Advances*, 4(7):eaar2904, 2018.

[60] Michael A Lee, Naveed Bakh, Gili Bisker, Emery N Brown, and Michael S Strano. A pharmacokinetic model of a tissue implantable cortisol sensor. *Advanced Healthcare Materials*, 5(23):3004–3015, 2016.

[61] G Van den Berg, M Frölich, Johannes D Veldhuis, and F Roelfsema. Combined amplification of the pulsatile and basal modes of adrenocorticotropin and cortisol secretion in patients with cushing's disease: evidence for decreased responsiveness of the adrenal glands. *The Journal of Clinical Endocrinology & Metabolism*, 80(12):3750–3757, 1995.

[62] Anne C Smith, Loren M Frank, Sylvia Wirth, Marianna Yanike, Dan Hu, Yasuo Kubota, Ann M Graybiel, Wendy A Suzuki, and Emery N Brown. Dynamic analysis of learning in behavioral experiments. *Journal of Neuroscience*, 24(2):447–461, 2004.

[63] Dilranjan S Wickramasuriya and Rose T Faghih. A mixed filter algorithm for sympathetic arousal tracking from skin conductance and heart rate measurements in pavlovian fear conditioning. *Plos one*, 15(4):e0231659, 2020.

[64] Todd P Coleman, Marianna Yanike, Wendy A Suzuki, and Emery N Brown. A mixed-filter algorithm for dynamically tracking learning from multiple behavioral and neurophysiological measures. *The Dynamic Brain: An Exploration of Neuronal Variability and Its Functional Significance*, pages 1–16, 2011.

[65] Michael J Prerau, Anne C Smith, Uri T Eden, Yasuo Kubota, Marianna Yanike, Wendy Suzuki, Ann M Graybiel, and Emery N Brown. Characterizing learning by simultaneous analysis of continuous and binary measures of performance. *Journal of Neurophysiology*, 102(5):3060–3072, 2009.

[66] Dilranjan S Wickramasuriya and Rose T Faghih. A bayesian filtering approach for tracking arousal from binary and continuous skin conductance features. *IEEE Transactions on Biomedical Engineering*, 67(6):1749–1760, 2019.

[67] Rose T Faghih, Munther A Dahleh, Gail K Adler, Elizabeth B Klerman, and Emery N Brown. Quantifying pituitary-adrenal dynamics and deconvolution of concurrent cortisol and adrenocorticotropic hormone data by compressed sensing. *IEEE Transactions on Biomedical Engineering*, 62(10):2379–2388, 2015.

[68] Mohammed Dahleh, Munther A Dahleh, and George Verghese. Lectures on dynamic systems and control. *A+ A*, 4(100):1–100, 2004.

[69] Jonathan M Garibaldi and Turhan Ozen. Uncertain fuzzy reasoning: a case study in modelling expert decision making. *IEEE Transactions on Fuzzy Systems*, 15(1):16–30, 2007.

[70] Willians Ribeiro Mendes, Fábio Meneghetti U Araújo, Ritaban Dutta, and Derek M Heeren. Fuzzy control system for variable rate irrigation using remote sensing. *Expert Systems with Applications*, 124:13–24, 2019.

[71] Xinbo Yu, Wei He, Hongyi Li, and Jian Sun. Adaptive fuzzy full-state and output-feedback control for uncertain robots with output constraint. *IEEE Transactions on Systems, Man, and Cybernetics: Systems*, 52:1–14, 2020.

[72] Hao-Ran Lin, Bing-Yuan Cao, and Yun-zhang Liao. Fuzzy control. In *Fuzzy Sets Theory Preliminary*, pages 73–108. Springer, 2018.

[73] Ahmed Zoukit, Hicham El Ferouali, Issam Salhi, Said Doubabi, and Naji Abdenouri. Design of mamdani type fuzzy controller for a hybrid solar-electric dryer: case study

of clay drying. In *2019 6th International Conference on Control, Decision and Information Technologies (CoDIT)*, pages 1332–1337, (Paris). IEEE, 2019.

[74] Richard A Feelders, John Newell-Price, Rosario Pivonello, Lynnette K Nieman, Leo J Hofland, and Andre Lacroix. Advances in the medical treatment of cushing's syndrome. *The Lancet Diabetes & Endocrinology*, 7(4):300–312, 2019.

[75] Hamid Fekri Azgomi, Javad Poshtan, and Majid Poshtan. Experimental validation on stator fault detection via fuzzy logic. In *2013 3rd International Conference on Electric Power and Energy Conversion Systems (EPECS)*, pages 1–6. IEEE, 2013.

[76] WB Zulfikar, PK Prasetyo, and MA Ramdhani. Implementation of mamdani fuzzy method in employee promotion system. In *IOP Conference Series: Materials Science and Engineering*, volume 288, page 012147. IOP Publishing, 2018.

[77] Colin Bouwer, Johann Claassen, Timothy G Dinan, and Charles B Nemeroff. Prednisone augmentation in treatment-resistant depression with fatigue and hypocortisolaemia: A case series. *Depression and Anxiety*, 12(1):44–50, 2000.

[78] Carolina Inda, Natalia G Armando, Paula A dos Santos Claro, and Susana Silberstein. Endocrinology and the brain: corticotropin-releasing hormone signaling. *Endocrine Connections*, 6(6):R99–R120, 2017.

[79] Lynnette K Nieman, Beverly MK Biller, James W Findling, M Hassan Murad, John Newell-Price, Martin O Savage, and Antoine Tabarin. Treatment of cushing's syndrome: an endocrine society clinical practice guideline. *The Journal of Clinical Endocrinology & Metabolism*, 100(8):2807–2831, 2015.

[80] A Janet Tomiyama. Stress and obesity. *Annual Review of Psychology*, (0), 2019.

[81] Rajitha K Pradeep. Stress management of women managers a comparative study of public sector and private sector banks in kerala. 2016.

[82] FM Al-Shargie, Tong Boon Tang, Nasreen Badruddin, and Masashi Kiguchi. Mental stress quantification using eeg signals. In *International Conference for Innovation in Biomedical Engineering and Life Sciences*, pages 15–19. Springer, 2015.

[83] Javad Birjandtalab, Diana Cogan, Maziyar Baran Pouyan, and Mehrdad Nourani. A non-eeg biosignals dataset for assessment and visualization of neurological status. In *Signal Processing Systems (SiPS), 2016 IEEE International Workshop on*, pages 110–114. IEEE, 2016.

[84] Shih-Sung Lin, Chien-Wu Lan, Hao-Yen Hsu, and Sheng-Tao Chen. Data analytics of a wearable device for heat stroke detection. *Sensors*, 18(12):4347, 2018.

[85] Yekta Said Can, Bert Arnrich, and Cem Ersoy. Stress detection in daily life scenarios using smart phones and wearable sensors: A survey. *Journal of Biomedical Informatics*, 92:103139, 2019.

[86] Sumit Majumder, Tapas Mondal, and M. Jamal Deen. Wearable sensors for remote health monitoring. *Sensors*, 17(1):130, 2017.

[87] Akane Sano and Rosalind W Picard. Stress recognition using wearable sensors and mobile phones. In *Affective Computing and Intelligent Interaction (ACII), 2013 Humaine Association Conference on*, pages 671–676. IEEE, 2013.

[88] Bill Byrom, Marie McCarthy, Peter Schueler, and Willie Muehlhausen. Brain monitoring devices in neuroscience clinical research: the potential of remote monitoring

using sensors, wearables, and mobile devices. *Clinical Pharmacology & Therapeutics*, 104(1):59–71, 2018.

[89] Vivekanand Jha, Nupur Prakash, and Sweta Sagar. Wearable anger-monitoring system. *ICT Express*, 4(4):194–198, 2018.

[90] Himanshu Thapliyal, Vladislav Khalus, and Carson Labrado. Stress detection and management: A survey of wearable smart health devices. *IEEE Consumer Electronics Magazine*, 6(4):64–69, 2017.

[91] Cornelia Setz, Bert Arnrich, Johannes Schumm, Roberto La Marca, Gerhard Tröster, and Ulrike Ehlert. Discriminating stress from cognitive load using a wearable eda device. *IEEE Transactions on Information Technology in Biomedicine*, 14(2):410–417, 2009.

[92] Rose T Faghih, Patrick A Stokes, Marie-France Marin, Rachel G Zsido, Sam Zorowitz, Blake L Rosenbaum, Huijin Song, Mohammed R Milad, Darin D Dougherty, Emad N Eskandar, Alik S. Widge, Emery N. Brown, and Riccardo Barbieri. Characterization of fear conditioning and fear extinction by analysis of electrodermal activity. In *2015 37th Annual International Conference of the IEEE Engineering in Medicine and Biology Society (EMBC)*, pages 7814–7818. IEEE, 2015.

[93] Xinyi Deng, Rose T Faghih, Riccardo Barbieri, Angelique C Paulk, Wael F Asaad, Emery N Brown, Darin D Dougherty, Alik S Widge, Emad N Eskandar, and Uri T Eden. Estimating a dynamic state to relate neural spiking activity to behavioral signals during cognitive tasks. In *Engineering in Medicine and Biology Society (EMBC), 2015 37th Annual International Conference of the IEEE*, pages 7808–7813. IEEE, 2015.

[94] Dilranjan S Wickramasuriya, Md Amin, and Rose T Faghih. Skin conductance as a viable alternative for closing the deep brain stimulation loop in neuropsychiatric disorders. *Frontiers in Neuroscience*, 13:780, 2019.

[95] Dilranjan S Wickramasuriya, Chaoxian Qi, and Rose T Faghih. A state-space approach for detecting stress from electrodermal activity. In *2018 40th Annual International Conference of the IEEE Engineering in Medicine and Biology Society (EMBC)*, pages 3562–3567. IEEE, 2018.

[96] Hugo D Critchley. Electrodermal responses: what happens in the brain. *The Neuroscientist*, 8(2):132–142, 2002.

[97] Hugo F Posada-Quintero, John P Florian, Alvaro D Orjuela-Cañón, and Ki H Chon. Electrodermal activity is sensitive to cognitive stress under water. *Frontiers in Physiology*, 8:1128, 2018.

[98] Alexandros Liapis, Christos Katsanos, Dimitris Sotiropoulos, Michalis Xenos, and Nikos Karousos. Recognizing emotions in human computer interaction: studying stress using skin conductance. In *IFIP Conference on Human-Computer Interaction*, pages 255–262. Springer, 2015.

[99] M Mestanlk, Z Vlsnovcova, and I Tonhajzerova. The assessment of the autonomic response to acute stress using electrodermal activity. *Acta Medica Martiniana*, 14(2):5–9, 2014.

[100] David J Clark, Sudeshna A Chatterjee, Theresa E McGuirk, Eric C Porges, Emily J Fox, and Chitralakshmi K Balasubramanian. Sympathetic nervous system activity

measured by skin conductance quantifies the challenge of walking adaptability tasks after stroke. *Gait & Posture*, 60:148–153, 2018.

[101] Michael E Dawson, Anne M Schell, and Diane L Filion. The electrodermal system. *Handbook of Psychophysiology*, 2:200–223, 2007.

[102] Yasuaki Ohtaki, Akihiro Suzuki, and Georgios Papastefanou. Integration of psychophysiological and behavioral indicators with ambulatory tracking for momentary indoor activity assessment. In *2009 ICCAS-SICE*, pages 499–502. IEEE, 2009.

[103] Rose T Faghih. From physiological signals to pulsatile dynamics: a sparse system identification approach. In *Dynamic Neuroscience*, pages 239–265. Springer, 2018.

[104] Hugo Silva, Ana Fred, and André Lourenço. Electrodermal response propagation time as a potential psychophysiological marker. In *2012 Annual International Conference of the IEEE Engineering in Medicine and Biology Society*, pages 6756–6759. IEEE, 2012.

[105] Aniket Vartak, Cali Fidopiastis, Denise Nicholson, and Wasfy Mikhael. Estimation of arousal using decomposed skin conductance features-biomed 2009. *Biomedical Sciences Instrumentation*, 45:77–82, 2009.

[106] Joshua D Isen, William G Iacono, and Stephen M Malone. Characterizing electrodermal response habituation: A latent class approach with application to psychopathology. *Psychophysiology*, 50(10):954–962, 2013.

[107] Boon-Giin Lee and Wan-Young Chung. Wearable glove-type driver stress detection using a motion sensor. *IEEE Transactions on Intelligent Transportation Systems*, 18(7):1835–1844, 2016.

[108] Tekla S Perry. Wearable sensor detects stress in sweat: Cortisol is key to tracking stress, but it's tough to measure in an instant-[news]. *IEEE Spectrum*, 55(9):14–15, 2018.

[109] F Lebepe, G Niezen, Gerhard P Hancke, and TD Ramotsoela. Wearable stress monitoring system using multiple sensors. In *2016 IEEE 14th International Conference on Industrial Informatics (INDIN)*, pages 895–898. IEEE, 2016.

[110] Naoki Tateyama, Kazutaka Ueda, and Masayuki Nakao. Development of an active sensing system for distress detection using skin conductance response. In *2019 8th International Conference on Affective Computing and Intelligent Interaction (ACII)*, pages 1–6. IEEE, 2019.

[111] Laavanya Rachakonda, Prabha Sundaravadivel, Saraju P Mohanty, Elias Kougianos, and Madhavi Ganapathiraju. A smart sensor in the iomt for stress level detection. In *2018 IEEE International Symposium on Smart Electronic Systems (iSES)(Formerly iNiS)*, pages 141–145. IEEE, 2018.

[112] Akane Sano and Rosalind W Picard. Stress recognition using wearable sensors and mobile phones. In *2013 Humaine Association Conference on Affective Computing and Intelligent Interaction*, pages 671–676. IEEE, 2013.

[113] Yekta Said Can, Niaz Chalabianloo, Deniz Ekiz, and Cem Ersoy. Continuous stress detection using wearable sensors in real life: Algorithmic programming contest case study. *Sensors*, 19(8):1849, 2019.

[114] Tejaswini Panure and Shilpa Sonawani. Novel approach for stress detection using

smartphone and e4 device. In *International Conference on Sustainable Communication Networks and Application*, pages 736–745. Springer, 2019.

[115] Minho Choi, Gyogwon Koo, Minseok Seo, and Sang Woo Kim. Wearable device-based system to monitor a driver's stress, fatigue, and drowsiness. *IEEE Transactions on Instrumentation and Measurement*, 67(3):634–645, 2017.

[116] Victoria Branson, Deborah Turnbull, Matthew J Dry, and Edward Palmer. How do young people experience stress? a qualitative examination of the indicators of distress and eustress in adolescence. *International Journal of Stress Management*, 26(3):321, 2019.

[117] Kevin McKee, Michael Russell, Jeremy Mennis, Michael Mason, and Michael Neale. Emotion regulation dynamics predict substance use in high-risk adolescents. *Addictive Behaviors*, page 106374, 2020.

[118] Zhen-hao Wang, Yi Wang, Bing-qian Liu, Dong-ni Pan, and Xuebing Li. Neurological foundations of the brain in the automatic emotion regulation of anger and fear. In *2018 IEEE 17th International Conference on Cognitive Informatics & Cognitive Computing (ICCI* CC)*, pages 228–233. IEEE, 2018.

[119] Pedro Alves Nogueira, Rui Rodrigues, Eugénio Oliveira, and Lennart E Nacke. Guided emotional state regulation: understanding and shaping players' affective experiences in digital games. In *Ninth Artificial Intelligence and Interactive Digital Entertainment Conference*, 2013.

[120] Jin-Xi Zhang and Guang-Hong Yang. Robust adaptive fault-tolerant control for a class of unknown nonlinear systems. *IEEE Transactions on Industrial Electronics*,

64(1):585–594, 2016.

[121] Xuefeng Zhang and YangQuan Chen. Admissibility and robust stabilization of continuous linear singular fractional order systems with the fractional order α: the 0¡ α¡ 1 case. *ISA Transactions*, 82:42–50, 2018.

[122] Carina Benigna Walter. *EEG workload prediction in a closed-loop learning environment*. PhD thesis, Doctoral dissertation, Universität Tübingen, 2015.

[123] Jin-Xi Zhang and Guang-Hong Yang. Prescribed performance fault-tolerant control of uncertain nonlinear systems with unknown control directions. *IEEE Transactions on Automatic Control*, 62(12):6529–6535, 2017.

[124] Hamid Fekri Azgomi and Javad Poshtan. Induction motor stator fault detection via fuzzy logic. In *2013 21st Iranian Conference on Electrical Engineering (ICEE)*, pages 1–5. IEEE, 2013.

[125] Jin-Xi Zhang and Guang-Hong Yang. Fuzzy adaptive output feedback control of uncertain nonlinear systems with prescribed performance. *IEEE transactions on Cybernetics*, 48(5):1342–1354, 2017.

[126] Anne C Smith, Loren M Frank, Sylvia Wirth, Marianna Yanike, Dan Hu, Yasuo Kubota, Ann M Graybiel, Wendy A Suzuki, and Emery N Brown. Dynamic analysis of learning in behavioral experiments. *Journal of Neuroscience*, 24(2):447–461, 2004.

[127] Ary L Goldberger, Luis AN Amaral, Leon Glass, Jeffrey M Hausdorff, Plamen Ch Ivanov, Roger G Mark, Joseph E Mietus, George B Moody, Chung-Kang Peng, and H Eugene Stanley. Physiobank, physiotoolkit, and physionet: components of a new

research resource for complex physiologic signals. *Circulation*, 101(23):e215–e220, 2000.

[128] Rachel Atchley, Roger Ellingson, Daniel Klee, Tabatha Memmott, and Barry Oken. A cognitive stressor for event-related potential studies: the portland arithmetic stress task. *Stress*, 20(3):277–284, 2017.

[129] Siddharth Sharma, Shreya Rewadkar, Harshada Pawar, Vaibhav Deokar, and Vina M Lomte. Survey on binaural beats and background music for increased focus and relaxation. In *2017 International Conference on Emerging Trends & Innovation in ICT (ICEI)*, pages 98–103. IEEE, 2017.

[130] Rab Nawaz, Humaira Nisar, and Yap Vooi Voon. The effect of music on human brain; frequency domain and time series analysis using electroencephalogram. *IEEE Access*, 6:45191–45205, 2018.

[131] Wolfram Boucsein. *Electrodermal activity*. Springer Science & Business Media, 2012.

[132] Alberto Greco, Gaetano Valenza, and Enzo Pasquale Scilingo. Evaluation of cda and cvxeda models. In *Advances in Electrodermal Activity Processing with Applications for Mental Health*, pages 35–43. Springer, 2016.

[133] David M Alexander, Chris Trengove, P Johnston, Tim Cooper, JP August, and Evian Gordon. Separating individual skin conductance responses in a short interstimulus-interval paradigm. *Journal of Neuroscience Methods*, 146(1):116–123, 2005.

[134] Mathias Benedek and Christian Kaernbach. Decomposition of skin conductance data by means of nonnegative deconvolution. *Psychophysiology*, 47(4):647–658, 2010.

[135] Jerry M Mendel. *Lessons in estimation theory for signal processing, communications, and control*. Pearson Education, 1995.

[136] Paul Geladi and Bruce R Kowalski. Partial least-squares regression: a tutorial. *Analytica Chimica Acta*, 185:1–17, 1986.

[137] Gang Feng. A survey on analysis and design of model-based fuzzy control systems. *IEEE Transactions on Fuzzy systems*, 14(5):676–697, 2006.

[138] Matthias Neumann-Brosig, Alonso Marco, Dieter Schwarzmann, and Sebastian Trimpe. Data-efficient autotuning with bayesian optimization: An industrial control study. *IEEE Transactions on Control Systems Technology*, 28(3):730–740, 2019.

[139] Julia Vinogradska, Bastian Bischoff, Duy Nguyen-Tuong, Anne Romer, Henner Schmidt, and Jan Peters. Stability of controllers for gaussian process forward models. In *International Conference on Machine Learning*, pages 545–554. PMLR, 2016.

[140] Jacob Steinhardt and Russ Tedrake. Finite-time regional verification of stochastic non-linear systems. *The International Journal of Robotics Research*, 31(7):901–923, 2012.

[141] Franco Blanchini. Set invariance in control. *Automatica*, 35(11):1747–1767, 1999.

[142] Jennie Ponsford, Nicole Kathleen Lee, D Wong, A McKay, K Haines, Y Alway, M Downing, Christina Furtado, and Meaghan L O'Donnell. Efficacy of motivational interviewing and cognitive behavioral therapy for anxiety and depression symptoms following traumatic brain injury. *Psychological Medicine*, 46(5):1079–1090, 2016.

[143] Dan Nie, Xiao-Wei Wang, Li-Chen Shi, and Bao-Liang Lu. Eeg-based emotion recognition during watching movies. In *2011 5th International IEEE/EMBS Conference on Neural Engineering*, pages 667–670. IEEE, 2011.

[144] Xiyuan Hou, Yisi Liu, Olga Sourina, Yun Rui Eileen Tan, Lipo Wang, and Wolfgang Mueller-Wittig. Eeg based stress monitoring. In *2015 IEEE International Conference on Systems, Man, and Cybernetics*, pages 3110–3115. IEEE, 2015.

[145] Päivi Pohjavaara, Timo Telaranta, and Erkki Väisänen. The role of the sympathetic nervous system in anxiety: is it possible to relieve anxiety with endoscopic sympathetic block? *Nordic Journal of Psychiatry*, 57(1):55–60, 2003.

[146] Tom Hollenstein, Adrian McNeely, Jenny Eastabrook, Allison Mackey, and Jessica Flynn. Sympathetic and parasympathetic responses to social stress across adolescence. *Developmental Psychobiology*, 54(2):207–214, 2012.

[147] Benny van der Vijgh, Robbert J Beun, Maarten van Rood, and Peter Werkhoven. Gasica: generic automated stress induction and control application design of an application for controlling the stress state. *Frontiers in Neuroscience*, 8:400, 2014.

[148] Annie Bernier, Stephanie M. Carlson, Stéphanie Bordeleau, and Julie Carrier. Relations between physiological and cognitive regulatory systems: Infant sleep regulation and subsequent executive functioning. *Child Development*, 81(6):1739–1752, 2010.

[149] Jonas Umlauft, Lukas Pöhler, and Sandra Hirche. An uncertainty-based control lyapunov approach for control-affine systems modeled by gaussian process. *IEEE Control Systems Letters*, 2(3):483–488, 2018.

[150] Shi Li, Choon Ki Ahn, and Zhengrong Xiang. Command filter based adaptive fuzzy finite-time control for switched nonlinear systems using state-dependent switching method. *IEEE Transactions on Fuzzy Systems*, 2020.

[151] Melisa Bubonya, Deborah A Cobb-Clark, and Mark Wooden. Mental health and productivity at work: Does what you do matter? *Labour Economics*, 46:150–165, 2017.

[152] Gulzhaina Kassymova, Oksana V Tokar, Anna I Tashcheva, Galina V Slepukhina, Svetlana V Gridneva, Natalya G Bazhenova, ElenaYu Shpakovskaya, and Mariam R Arpentieva. Impact of stress on creative human resources and psychological counseling in crises. *International Journal of Education and Information Technologies*, 13(1):26–32, 2019.

[153] Sara Simblett, Jennifer Birch, Faith Matcham, Lidia Yaguez, and Robin Morris. A systematic review and meta-analysis of e-mental health interventions to treat symptoms of posttraumatic stress. *JMIR Mental Health*, 4(2):e14, 2017.

[154] Carol L Mackersie and Natalie Calderon-Moultrie. Autonomic nervous system reactivity during speech repetition tasks: Heart rate variability and skin conductance. *Ear and Hearing*, 37:118S–125S, 2016.

[155] Roman Kupriyanov and Renad Zhdanov. The eustress concept: problems and outlooks. *World Journal of Medical Sciences*, 11(2):179–185, 2014.

[156] Cornelius T Leondes. *Advances in Control Systems: Theory and Applications*. Elsevier, 2014.

[157] Mohammad Javad Khodaei, Nicholas Candelino, Amin Mehrvarz, and Nader Jalili. Physiological closed-loop control (pclc) systems: review of a modern frontier in automation. *IEEE Access*, 8:23965–24005, 2020.

[158] David A Copp, Ravi Gondhalekar, and Joao P Hespanha. Simultaneous model predictive control and moving horizon estimation for blood glucose regulation in type 1 diabetes. *Optimal Control Applications and Methods*, 39(2):904–918, 2018.

[159] Ankush Chakrabarty, Stamatina Zavitsanou, Francis J Doyle, and Eyal Dassau. Event-triggered model predictive control for embedded artificial pancreas systems. *IEEE Transactions on Biomedical Engineering*, 65(3):575–586, 2017.

[160] Thomas Seel, Cordula Werner, Jörg Raisch, and Thomas Schauer. Iterative learning control of a drop foot neuroprosthesis—generating physiological foot motion in paretic gait by automatic feedback control. *Control Engineering Practice*, 48:87–97, 2016.

[161] Adriana Savoca and Davide Manca. A physiologically-based approach to model-predictive control of anesthesia and analgesia. *Biomedical Signal Processing and Control*, 53:101553, 2019.

[162] Alexandra Krieger and Efstratios N Pistikopoulos. Model predictive control of anesthesia under uncertainty. *Computers & Chemical Engineering*, 71:699–707, 2014.

[163] Hugh J McDermott and Nicholas C Sinclair. Feedback control for deep brain stimulation for motor disorders. *Healthcare Technology Letters*, 7(3):72–75, 2020.

[164] Jon X Genty, Md Rafiul Amin, Natalie D Shaw, Elizabeth Klerman, and Rose T Faghih. Sparse deconvolution of pulsatile growth hormone secretion in adolescents. *IEEE/ACM Transactions on Computational Biology and Bioinformatics*, 2021.

[165] Laina E Rosebrock, Denada Hoxha, Catherine Norris, John T Cacioppo, and Jackie K Gollan. Skin conductance and subjective arousal in anxiety, depression, and comorbidity. *Journal of Psychophysiology*, 2016.

[166] Kristin A Buss, Sara Jaffee, Martha E Wadsworth, and Wendy Kliewer. Impact of psychophysiological stress-response systems on psychological development: Moving beyond the single biomarker approach. *Developmental Psychology*, 54(9):1601, 2018.

[167] Jue Huang, Christine Ulke, Christian Sander, Philippe Jawinski, Janek Spada, Ulrich Hegerl, and Tilman Hensch. Impact of brain arousal and time-on-task on autonomic nervous system activity in the wake-sleep transition. *BMC Neuroscience*, 19(1):18, 2018.

[168] Md Rafiul Amin and Rose T Faghih. Identification of sympathetic nervous system activation from skin conductance: A sparse decomposition approach with physiological priors. *IEEE Transactions on Biomedical Engineering*, 2020.

[169] Yi-Yuan Tang, Yinghua Ma, Yaxin Fan, Hongbo Feng, Junhong Wang, Shigang Feng, Qilin Lu, Bing Hu, Yao Lin, Jian Li, Ye Zhanga, Yan Wanga, Li Zhoua, and Ming Fan. Central and autonomic nervous system interaction is altered by short-term meditation. *Proceedings of the national Academy of Sciences*, 106(22):8865–8870, 2009.

[170] Luca Menghini, Evelyn Gianfranchi, Nicola Cellini, Elisabetta Patron, Mariaelena Tagliabue, and Michela Sarlo. Stressing the accuracy: Wrist-worn wearable sensor validation over different conditions. *Psychophysiology*, 56(11):e13441, 2019.

[171] O Nepal, RK Jha, A Bhattarai, P Khadka, and BK Kapoor. Galvanic skin response as a simple physiology lab teaching tool-an alternative indicator of sympathetic arousal.

Kathmandu Univ Med J, 62(2):156–60, 2018.

[172] Matteo Vissani, Ioannis U Isaias, and Alberto Mazzoni. Deep brain stimulation: a review of the open neural engineering challenges. *Journal of Neural Engineering*, 17(5):051002, 2020.

[173] Wei He, Tingting Meng, Xiuyu He, and Shuzhi Sam Ge. Unified iterative learning control for flexible structures with input constraints. *Automatica*, 96:326–336, 2018.

[174] Wei He, Tingting Wang, Xiuyu He, Lung-Jieh Yang, and Okyay Kaynak. Dynamical modeling and boundary vibration control of a rigid-flexible wing system. *IEEE/ASME Transactions on Mechatronics*, 25(6):2711–2721, 2020.

[175] Wei He, Tingting Meng, Xiuyu He, and Changyin Sun. Iterative learning control for a flapping wing micro aerial vehicle under distributed disturbances. *IEEE Transactions on Cybernetics*, 49(4):1524–1535, 2018.

[176] Iman Hajizadeh, Sediqeh Samadi, Mert Sevil, Mudassir Rashid, and Ali Cinar. Performance assessment and modification of an adaptive model predictive control for automated insulin delivery by a multivariable artificial pancreas. *Industrial & Engineering Chemistry Research*, 58(26):11506–11520, 2019.

[177] Valarmathi Ramasamy, Rakesh Kumar Sidharthan, Ramkumar Kannan, and Guruprasath Muralidharan. Optimal tuning of model predictive controller weights using genetic algorithm with interactive decision tree for industrial cement kiln process. *Processes*, 7(12):938, 2019.

[178] Jose Eduardo W Santos, Jorge Otavio Trierweiler, and Marcelo Farenzena. Robust tuning for classical mpc through the multi-scenarios approach. *Industrial & Engineering Chemistry Research*, 58(8):3146–3158, 2019.

[179] JH Van der Lee, WY Svrcek, and BR Young. A tuning algorithm for model predictive controllers based on genetic algorithms and fuzzy decision making. *ISA Transactions*, 47(1):53–59, 2008.

[180] RC Zhao, PK Wong, ZC Xie, and Jingyao Zhao. Real-time weighted multi-objective model predictive controller for adaptive cruise control systems. *International Journal of Automotive Technology*, 18(2):279–292, 2017.

[181] Emad Ali and Ashraf Al-Ghazzawi. On-line tuning of model predictive controllers using fuzzy logic. *The Canadian Journal of Chemical Engineering*, 81(5):1041–1051, 2003.

[182] Hee-Sang Ko and Juri Jatskevich. Power quality control of wind-hybrid power generation system using fuzzy-lqr controller. *IEEE Transactions on Energy Conversion*, 22(2):516–527, 2007.

[183] Michaela Killian, Barbara Mayer, and Martin Kozek. Hierachical fuzzy mpc concept for building heating control. *IFAC Proceedings Volumes*, 47(3):12048–12055, 2014.

[184] Peter McCullagh and John A Nelder. *Generalized linear models*. Routledge, 2019.

[185] Alberto Zenere and Mattia Zorzi. Model predictive control meets robust kalman filtering. *IFAC-PapersOnLine*, 50(1):3774–3779, 2017.

[186] Alberto Bemporad, WP Maurice H Heemels, and Bart De Schutter. On hybrid systems and closed-loop mpc systems. *IEEE Transactions on Automatic Control*, 47(5):863–869, 2002.

[187] W Kwon and A Pearson. A modified quadratic cost problem and feedback stabilization of a linear system. *IEEE Transactions on Automatic Control*, 22(5):838–842, 1977.

[188] SSa Keerthi and Elmer G Gilbert. Optimal infinite-horizon feedback laws for a general class of constrained discrete-time systems: Stability and moving-horizon approximations. *Journal of Optimization Theory and Applications*, 57(2):265–293, 1988.

[189] Karl Worthmann. *Stability analysis of unconstrained receding horizon control schemes.* PhD thesis, 2011.

[190] Michael F Bolus, Adam A Willats, Christopher J Rozell, and Garrett B Stanley. State-space optimal feedback control of optogenetically driven neural activity. *Journal of Neural Engineering*, 18(3):036006, 2021.

[191] Yuxiao Yang, Parima Ahmadipour, and Maryam M Shanechi. Adaptive latent state modeling of brain network dynamics with real-time learning rate optimization. *Journal of Neural Engineering*, 18(3):036013, 2021.

[192] Dilranjan S Wickramasuriya and Rose T Faghih. A novel filter for tracking real-world cognitive stress using multi-time-scale point process observations. In *2019 41st Annual International Conference of the IEEE Engineering in Medicine and Biology Society (EMBC)*, pages 599–602. IEEE, 2019.

[193] Hamid Fekri Azgomi, Iahn Cajigas, and Rose T. Faghih. Closed-Loop Cognitive Stress Regulation Using Fuzzy Control in Wearable-Machine Interface Architectures. *IEEE Access*, 9:106202–106219, 2021.

[194] Yuxiao Yang and Maryam M. Shanechi. An adaptive and generalizable closed-loop system for control of medically induced coma and other states of anesthesia. *Journal of Neural Engineering*, 13(6), 2016.

[195] Maryam M. Shanechi, Jessica J. Chemali, Max Liberman, Ken Solt, and Emery N. Brown. A Brain-Machine Interface for Control of Medically-Induced Coma. *PLoS Computational Biology*, 9(10), 2013.

[196] Jermaine M Ravalier, Andrew McVicar, and Charlotte Boichat. Work stress in nhs employees: A mixed-methods study. *International Journal of Environmental Research and Public Health*, 17(18):6464, 2020.

[197] MK Anniko, Katja Boersma, and Maria Tillfors. Sources of stress and worry in the development of stress-related mental health problems: A longitudinal investigation from early-to mid-adolescence. *Anxiety, Stress, & Coping*, 32(2):155–167, 2019.

[198] Maria Strauß, Christine Ulke, Madlen Paucke, Jue Huang, Nicole Mauche, Christian Sander, Tetyana Stark, and Ulrich Hegerl. Brain arousal regulation in adults with attention-deficit/hyperactivity disorder (adhd). *Psychiatry Research*, 261:102–108, 2018.

[199] Josef Faller, Jennifer Cummings, Sameer Saproo, and Paul Sajda. Regulation of arousal via online neurofeedback improves human performance in a demanding

sensory-motor task. *Proceedings of the National Academy of Sciences*, 116(13):6482–6490, 2019.

[200] Andrius Dzedzickis, Artūras Kaklauskas, and Vytautas Bucinskas. Human emotion recognition: Review of sensors and methods. *Sensors*, 20(3):592, 2020.

[201] Frank M Schmidt, Christian Sander, Marie-Elisa Dietz, Claudia Nowak, Thomas Schröder, Roland Mergl, Peter Schönknecht, Hubertus Himmerich, and Ulrich Hegerl. Brain arousal regulation as response predictor for antidepressant therapy in major depression. *Scientific Reports*, 7(1):1–10, 2017.

[202] David M Diamond, Adam M Campbell, Collin R Park, Joshua Halonen, and Phillip R Zoladz. The temporal dynamics model of emotional memory processing: a synthesis on the neurobiological basis of stress-induced amnesia, flashbulb and traumatic memories, and the yerkes-dodson law. *Neural Plasticity*, 2007, 2007.

[203] Lucy Morrish, Nikki Rickard, Tan Chyuan Chin, and Dianne Anne Vella-Brodrick. Emotion regulation in adolescent well-being and positive education. *Journal of Happiness Studies*, 19(5):1543–1564, 2018.

[204] Anna Lekova, Maya Dimitrova, Snezhanka Kostova, Omar Bouattane, and Leire Ozaeta. Bci for assessing the emotional and cognitive skills of children with special educational needs. In *2018 IEEE 5th International Congress on Information Science and Technology (CiSt)*, pages 400–403. IEEE, 2018.

[205] M Ottonello, E Fiabane, C Pistarini, P Spigno, and E Torselli. Difficulties in emotion regulation during rehabilitation for alcohol addiction: correlations with metacognitive

beliefs about alcohol use and relapse risk. *Neuropsychiatric Disease and Treatment*, 15:2917, 2019.

[206] Christian E Salas, James J Gross, and Oliver H Turnbull. Using the process model to understand emotion regulation changes after brain injury. *Psychology & Neuroscience*, 12(4):430, 2019.

[207] Stefan K Ehrlich, Kat R Agres, Cuntai Guan, and Gordon Cheng. A closed-loop, music-based brain-computer interface for emotion mediation. *PloS one*, 14(3), 2019.

[208] Nikolai von Janczewski, Jennifer Wittmann, Arnd Engeln, Martin Baumann, and Lutz Krauß. A meta-analysis of the n-back task while driving and its effects on cognitive workload. *Transportation Research Part F: Traffic Psychology and Behaviour*, 76:269–285, 2021.

[209] Sebastian Grissmann, Josef Faller, Christian Scharinger, Martin Spüler, and Peter Gerjets. Electroencephalography based analysis of working memory load and affective valence in an n-back task with emotional stimuli. *Frontiers in Human Neuroscience*, 11:616, 2017.

[210] Anirudh Unni, Klas Ihme, Meike Jipp, and Jochem W Rieger. Assessing the driver's current level of working memory load with high density functional near-infrared spectroscopy: a realistic driving simulator study. *Frontiers in Human Neuroscience*, 11:167, 2017.

[211] Michael K Yeung, Tsz L Lee, Yvonne MY Han, and Agnes S Chan. Prefrontal activation and pupil dilation during n-back task performance: A combined fnirs and pupillometry study. *Neuropsychologia*, 159:107954, 2021.

[212] Yuan-Pin Lin, Chi-Hong Wang, Tzyy-Ping Jung, Tien-Lin Wu, Shyh-Kang Jeng, Jeng-Ren Duann, and Jyh-Horng Chen. Eeg-based emotion recognition in music listening. *IEEE Transactions on Biomedical Engineering*, 57(7):1798–1806, 2010.

[213] Xiao-Wei Wang, Dan Nie, and Bao-Liang Lu. Emotional state classification from eeg data using machine learning approach. *Neurocomputing*, 129:94–106, 2014.

[214] WOAS Wan Ismail, M Hanif, SB Mohamed, Noraini Hamzah, and Zairi Ismael Rizman. Human emotion detection via brain waves study by using electroencephalogram (eeg). *International Journal on Advanced Science, Engineering and Information Technology*, 6(6):1005–1011, 2016.

[215] Monika Lohani, Brennan R Payne, and David L Strayer. A review of psychophysiological measures to assess cognitive states in real-world driving. *Frontiers in Human Neuroscience*, 13:57, 2019.

[216] Srinidhi Parshi, Rafiul Amin, Hamid Fekri Azgomi, and Rose T Faghih. Mental workload classification via hierarchical latent dictionary learning: A functional near infrared spectroscopy study. In *2019 IEEE EMBS International Conference on Biomedical & Health Informatics (BHI)*, pages 1–4. IEEE, 2019.

[217] Goran Udovičić, Jurica erek, Mladen Russo, and Marjan Sikora. Wearable emotion recognition system based on gsr and ppg signals. In *Proceedings of the 2nd International Workshop on Multimedia for Personal Health and Health Care*, pages 53–59, 2017.

[218] Andrea Giorgi, Vincenzo Ronca, Alessia Vozzi, Nicolina Sciaraffa, Antonello Di Florio, Luca Tamborra, Ilaria Simonetti, Pietro Aricò, Gianluca Di Flumeri, Dario Rossi, and

Gianluca Borghini. Wearable technologies for mental workload, stress, and emotional state assessment during working-like tasks: a comparison with laboratory technologies. *Sensors*, 21(7):2332, 2021.

[219] Martin Ragot, Nicolas Martin, Sonia Em, Nico Pallamin, and Jean-Marc Diverrez. Emotion recognition using physiological signals: laboratory vs. wearable sensors. In *International Conference on Applied Human Factors and Ergonomics*, pages 15–22. Springer, 2017.

[220] Philip Schmidt, Attila Reiss, Robert Dürichen, and Kristof Van Laerhoven. Wearable-based affect recognition—a review. *Sensors*, 19(19):4079, 2019.

[221] Ifigeneia Mavridou, Ellen Seiss, Theodoros Kostoulas, Charles Nduka, and Emili Balaguer-Ballester. Towards an effective arousal detection system for virtual reality. In *Proceedings of the Workshop on Human-Habitat for Health (H3): Human-Habitat Multimodal Interaction for Promoting Health and Well-Being in the Internet of Things Era*, pages 1–6, 2018.

[222] Stanisław Saganowski, Anna Dutkowiak, Adam Dziadek, Maciej Dzieżyc, Joanna Komoszyńska, Weronika Michalska, Adam Polak, Michał Ujma, and Przemysław Kazienko. Emotion recognition using wearables: A systematic literature review-work-in-progress. In *2020 IEEE International Conference on Pervasive Computing and Communications Workshops (PerCom Workshops)*, pages 1–6. IEEE, 2020.

[223] Arturo Martínez-Rodrigo, Roberto Zangróniz, José Manuel Pastor, and Antonio Fernández-Caballero. Arousal level classification in the ageing adult by measuring electrodermal skin conductivity. In *Ambient Intelligence for Health*, pages 213–223. Springer, 2015.

[224] Lucas Paletta, NM Pittino, Michael Schwarz, Verena Wagner, and K Wolfgang Kallus. Human factors analysis using wearable sensors in the context of cognitive and emotional arousal. *Procedia Manufacturing*, 3:3782–3787, 2015.

[225] Cameron McCarthy, Nikhilesh Pradhan, Calum Redpath, and Andy Adler. Validation of the empatica e4 wristband. In *2016 IEEE EMBS international Student Conference (ISC)*, pages 1–4. IEEE, 2016.

[226] Olave E Krigolson, Chad C Williams, Angela Norton, Cameron D Hassall, and Francisco L Colino. Choosing muse: Validation of a low-cost, portable eeg system for erp research. *Frontiers in Neuroscience*, 11:109, 2017.

[227] Adam R Clarke, Robert J Barry, Diana Karamacoska, and Stuart J Johnstone. The eeg theta/beta ratio: a marker of arousal or cognitive processing capacity? *Applied Psychophysiology and Biofeedback*, 44(2):123–129, 2019.

[228] Daniel Szafir and Bilge Mutlu. Pay attention! designing adaptive agents that monitor and improve user engagement. In *Proceedings of The SIGCHI Conference on Human Factors in Computing Systems*, pages 11–20, 2012.

[229] Konstantinos Tsiakas, Maher Abujelala, and Fillia Makedon. Task engagement as personalization feedback for socially-assistive robots and cognitive training. *Technologies*, 6(2):49, 2018.

[230] Athanasios Gkaintatzis, Rob Van Der Lubbe, Kalipso Karantinou, and Efthymios Constantinides. Consumers' cognitive, emotional and behavioral responses towards background music: An eeg study. In *WEBIST*, pages 314–318, 2019.

[231] Arthur Abia and Loïc Caroux. Effects of self-selected music and the arousal level of music on user experience and performance in video games. In *Congress of the International Ergonomics Association*, pages 3–12. Springer, 2018.

[232] Andrea Valenzuela Ramírez, Gemma Hornero, Daniel Royo, Angel Aguilar, and Oscar Casas. Assessment of emotional states through physiological signals and its application in music therapy for disabled people. *IEEE Access*, 8:127659–127671, 2020.

[233] Garry Kuan, Tony Morris, Yee Cheng Kueh, and Peter C Terry. Effects of relaxing and arousing music during imagery training on dart-throwing performance, physiological arousal indices, and competitive state anxiety. *Frontiers in Psychology*, 9:14, 2018.

[234] Janina AM Lehmann and Tina Seufert. The influence of background music on learning in the light of different theoretical perspectives and the role of working memory capacity. *Frontiers in Psychology*, 8:1902, 2017.

[235] Meng Du, Jun Jiang, Zhemin Li, Dongrui Man, and Cunmei Jiang. The effects of background music on neural responses during reading comprehension. *Scientific Reports*, 10(1):1–10, 2020.

[236] John A Caldwell, J Lynn Caldwell, Lauren A Thompson, and Harris R Lieberman. Fatigue and its management in the workplace. *Neuroscience & Biobehavioral Reviews*, 96:272–289, 2019.

[237] Tom M McLellan, Lyndon A Riviere, Kelly W Williams, Dennis McGurk, and Harris R Lieberman. Caffeine and energy drink use by combat arms soldiers in afghanistan as a countermeasure for sleep loss and high operational demands. *Nutritional Neuroscience*, 22(11):768–777, 2019.

[238] Bernard J Fine, John L Kobrick, Harris R Lieberman, Brent Marlowe, Robert H Riley, and William J Tharion. Effects of caffeine or diphenhydramine on visual vigilance. *Psychopharmacology*, 114(2):233–238, 1994.

[239] Craig Pickering and John Kiely. What should we do about habitual caffeine use in athletes? *Sports Medicine*, 49(6):833–842, 2019.

[240] Robert J Barry, Adam R Clarke, Rory McCarthy, Mark Selikowitz, Brett MacDonald, and Franca E Dupuy. Caffeine effects on resting-state electrodermal levels in ad/hd suggest an anomalous arousal mechanism. *Biological Psychology*, 89(3):606–608, 2012.

[241] Tom M McLellan, John A Caldwell, and Harris R Lieberman. A review of caffeine's effects on cognitive, physical and occupational performance. *Neuroscience & Biobehavioral Reviews*, 71:294–312, 2016.

[242] Youssef Souissi, Makram Souissi, and Hamdi Chtourou. Effects of caffeine ingestion on the diurnal variation of cognitive and repeated high-intensity performances. *Pharmacology Biochemistry and Behavior*, 177:69–74, 2019.

[243] M Saifudinova, M Bachmann, J Lass, and H Hinrikus. Effect of coffee on eeg spectral assymmetry. In *World Congress on Medical Physics and Biomedical Engineering, June 7-12, 2015, Toronto, Canada*, pages 1030–1033. Springer, 2015.

[244] Amanda Sargent, Jan Watson, Hongjun Ye, Rajneesh Suri, and Hasan Ayaz. Neuroergonomic assessment of hot beverage preparation and consumption: an eeg and eda study. *Frontiers in Human Neuroscience*, 14:175, 2020.

[245] Amanda Sargent, Jan Watson, Yigit Topoglu, Hongjun Ye, Rajneesh Suri, and Hasan Ayaz. Impact of tea and coffee consumption on cognitive performance: an fnirs and eda study. *Applied Sciences*, 10(7):2390, 2020.

[246] Jianjun Meng, John H Mundahl, Taylor D Streitz, Kaitlin Maile, Nicholas S Gulachek, Jeffrey He, and Bin He. Effects of soft drinks on resting state eeg and brain–computer interface performance. *IEEE Access*, 5:18756–18764, 2017.

[247] Kandhasamy Sowndhararajan and Songmun Kim. Influence of fragrances on human psychophysiological activity: With special reference to human electroencephalographic response. *Scientia Pharmaceutica*, 84(4):724–751, 2016.

[248] Nidal Amin Jaradat, Hamzeh Al Zabadi, Belal Rahhal, Azmi Mahmoud Ali Hussein, Jamal Shaker Mahmoud, Basel Mansour, Ahmad Ibrahim Khasati, and Abdelkhaleq Issa. The effect of inhalation of citrus sinensis flowers and mentha spicata leave essential oils on lung function and exercise performance: a quasi-experimental uncontrolled before-and-after study. *Journal of the International Society of Sports Nutrition*, 13(1):1–8, 2016.

[249] Morteza Nasiri, Mahya Torkaman, Shahoo Feizi, and Marzieh Beigom Bigdeli Shamloo. Effect of aromatherapy with damask rose on alleviating adults' acute pain severity: A systematic review and meta-analysis of randomized controlled trials. *Complementary Therapies in Medicine*, 56:102596, 2021.

[250] Mansooreh Aliasgharpour, Reyhaneh Abbaszadeh, Nooredin Mohammadi, and Anoshirvan Kazemnejad. Effect of lavender aromatherapy on the pain of arteriovenous fistula puncture in patients on hemodialysis. *Nursing Practice Today*, 3(1):26–30, 2016.

[251] Sun Ae Moon, Jisub Bae, Kwangsu Kim, Si Young Cho, Gusang Kwon, Ran Lee, Seung Ho Ko, Soyeon Lim, and Cheil Moon. Eeg revealed that fragrances positively affect menopausal symptoms in mid-life women. *Experimental Neurobiology*, 29(5):389, 2020.

[252] Christelle Porcherot, Sophie Raviot-Derrien, Marie-Pierre Beague, Sven Henneberg, Michelle Niedziela, Kathryn Ambroze, and Jean A McEwan. Effect of context on fine fragrance-elicited emotions: Comparison of three experimental methodologies. *Food Quality and Preference*, 95:104342, 2022.

[253] Helene M Loos, Linda Schreiner, and Brid Karacan. A systematic review of physiological responses to odours with a focus on current methods used in event-related study designs. *International Journal of Psychophysiology*, 2020.

[254] Hilmar Gudziol and Orlando Guntinas-Lichius. Electrophysiologic assessment of olfactory and gustatory function. *Handbook of Clinical Neurology*, 164:247–262, 2019.

[255] Manuel S Seet, Md Rafiul Amin, Nida I Abbasi, Junji Hamano, Anumita Chaudhury, Anastasios Bezerianos, Rose T Faghih, Nitish V Thakor, and Andrei Dragomir. Olfactory-induced positive affect and autonomic response as a function of hedonic and intensity attributes of fragrances. In *2020 42nd Annual International Conference of the IEEE Engineering in Medicine & Biology Society (EMBC)*, pages 3170–3173. IEEE, 2020.

[256] Takashi AOKI and Yoshinori ADACHI. Influence of jasmine fragrance on heartbeat fluctuation (research report, the 21st symposium on life information science). *Journal of International Society of Life Information Science*, 24(1):121–125, 2006.

[257] Girija Kaimal, Katrina Carroll-Haskins, Yigit Topoglu, Arun Ramakrishnan, Asli Arslanbek, and Hasan Ayaz. Exploratory fnirs assessment of differences in activation in virtual reality visual self-expression including with a fragrance stimulus. *Art Therapy*, pages 1–10, 2021.

[258] Y Saeki and YL Tanaka. Effect of inhaling fragrances on relieving pricking pain. *International Journal of Aromatherapy*, 15(2):74–80, 2005.

[259] Shaheen E Lakhan, Heather Sheafer, and Deborah Tepper. The effectiveness of aromatherapy in reducing pain: a systematic review and meta-analysis. *Pain Research and Treatment*, 2016.

[260] Takuya Onuma and Nobuyuki Sakai. Fabric softener fragrances modulate the impression toward female faces and frontal brain activity. *Japanese Psychological Research*, 60(4):276–287, 2018.

[261] Mark Moss, Steven Hewitt, Lucy Moss, and Keith Wesnes. Modulation of cognitive performance and mood by aromas of peppermint and ylang-ylang. *International Journal of Neuroscience*, 118(1):59–77, 2008.

[262] Brenda K Wiederhold and Stéphane Bouchard. Fear of heights (acrophobia): Efficacy and lessons learned from psychophysiological data. In *Advances in Virtual Reality and Anxiety Disorders*, pages 119–144. Springer, 2014.

[263] Julia Diemer, Nora Lohkamp, Andreas Mühlberger, and Peter Zwanzger. Fear and physiological arousal during a virtual height challenge—effects in patients with acrophobia and healthy controls. *Journal of Anxiety Disorders*, 37:30–39, 2016.

[264] Oana Bălan, Gabriela Moise, Alin Moldoveanu, Marius Leordeanu, and Florica Moldoveanu. An investigation of various machine and deep learning techniques applied in automatic fear level detection and acrophobia virtual therapy. *Sensors*, 20(2):496, 2020.

[265] Jacob Kritikos, Giannis Tzannetos, Chara Zoitaki, Stavroula Poulopoulou, and Dimitris Koutsouris. Anxiety detection from electrodermal activity sensor with movement & interaction during virtual reality simulation. In *2019 9th International IEEE/EMBS Conference on Neural Engineering (NER)*, pages 571–576. IEEE, 2019.

[266] Sofia Seinfeld, Ilias Bergstrom, Ausias Pomes, Jorge Arroyo-Palacios, Francisco Vico, Mel Slater, and Maria V Sanchez-Vives. Influence of music on anxiety induced by fear of heights in virtual reality. *Frontiers in Psychology*, 6:1969, 2016.

[267] Susan I Hopper, Sherrie L Murray, Lucille R Ferrara, and Joanne K Singleton. Effectiveness of diaphragmatic breathing for reducing physiological and psychological stress in adults: a quantitative systematic review. *JBI Evidence Synthesis*, 17(9):1855–1876, 2019.

[268] Youssef Shiban, Julia Diemer, Jana Müller, Johanna Brütting-Schick, Paul Pauli, and Andreas Mühlberger. Diaphragmatic breathing during virtual reality exposure therapy for aviophobia: functional coping strategy or avoidance behavior? a pilot study. *BMC Psychiatry*, 17(1):1–10, 2017.

[269] Rosalind W Picard, Szymon Fedor, and Yadid Ayzenberg. Multiple arousal theory and daily-life electrodermal activity asymmetry. *Emotion Review*, 8(1):62–75, 2016.

[270] Gregory S Berns, C Monica Capra, Sara Moore, and Charles Noussair. Neural mechanisms of the influence of popularity on adolescent ratings of music. *Neuroimage*, 49(3):2687–2696, 2010.

[271] S Aalbers, L Fusar-Poli, RE Freeman, M Spreen, JC Ket, AC Vink, A Maratos, M Crawford, XJ Chen, and C Gold. Music therapy for depression. *In Cochrane Database of Systematic Reviews*, 2017.

[272] Juana Inés Gallego-Gómez, Serafín Balanza, Jesús Leal-Llopis, Juan Antonio García-Méndez, José Oliva-Pérez, Javier Doménech-Tortosa, María Gómez-Gallego, Agustín Javier Simonelli-Muñoz, and José Miguel Rivera-Caravaca. Effectiveness of music therapy and progressive muscle relaxation in reducing stress before exams and improving academic performance in nursing students: A randomized trial. *Nurse Education Today*, 84:104217, 2020.

[273] Martina de Witte, Ana da Silva Pinho, Geert-Jan Stams, Xavier Moonen, Arjan ER Bos, and Susan van Hooren. Music therapy for stress reduction: a systematic review and meta-analysis. *Health Psychology Review*, pages 1–26, 2020.

[274] Manuel F Gonzalez and John R Aiello. More than meets the ear: Investigating how music affects cognitive task performance. *Journal of Experimental Psychology: Applied*, 25(3):431, 2019.

[275] Falak Shah, Twisha Naik, and Nisarg Vyas. Lstm based music generation. In *2019 International Conference on Machine Learning and Data Engineering (iCMLDE)*, pages 48–53. IEEE, 2019.

[276] Zachary C Lipton, John Berkowitz, and Charles Elkan. A critical review of recurrent neural networks for sequence learning. *arXiv preprint arXiv:1506.00019*, 2015.

[277] Midkar.com. `https://midkar.com/`, 2019. Accessed: 2021-03-15.

[278] Hugo F Posada-Quintero and Ki H Chon. Phasic component of electrodermal activity is more correlated to brain activity than tonic component. In *2019 IEEE EMBS International Conference on Biomedical & Health Informatics (BHI)*, pages 1–4. IEEE, 2019.